A genetically-encoded biosensor and a conditional gene expression system for investigating Notch activity *in vivo*

Justin Matthew Shaffer

Submitted in partial fulfillment of the
requirements for the degree of
Doctor of Philosophy
under the Executive Committee
of the Graduate School of Arts and Sciences

COLUMBIA UNIVERSITY

2022

Abstract

A genetically-encoded biosensor and a conditional gene expression system for investigating Notch activity *in vivo*

Justin Matthew Shaffer

Intercellular communication is crucial during animal development and tissue maintenance to ensure that correct patterns of cell types are generated to meet the needs of the organism. During lateral specification, intercellular communication resolves cell fate decisions between equipotent cells, creating fate patterns that are biased by external factors in some contexts, but appear stochastic in others. The Notch signaling pathway mediates lateral specification; small differences in Notch activity are amplified by regulatory feedback loops to robustly differentiate cell fates based on relative levels of Notch activity. It is often unclear how noise in the environment is processed by cells to generate differences in Notch activity that can be translated into stochastic, but robust, cell fate outcomes.

The nematode *Caenorhabditis elegans* contains a simple, Notch-mediated, stochastic lateral specification event; a small, random difference in Notch activity between two cells, the α cells, is amplified so that one α cell assumes Anchor Cell (AC) fate and the other assumes Ventral Uterine precursor cell (VU) fate. Two upstream factors bias the outcome of the AC/VU decision depending on the length of the time interval between the births of the α cells: the relative birth order of the α cells and the onset of expression of the transcription factor HLH-2. It is unknown how these factors create a difference in the relative Notch activity level between the two α cells, and limitations of existing Notch reporters have prevented the direct observation of Notch activity levels required for determining the relationships.

In this thesis, I describe a genetically-encoded Sensor Able to detect Lateral Signaling Activity, or SALSA, which uses changes in nuclear Red:Green fluorescence to indicate Notch activity. I demonstrated that SALSA captures expected Notch activity patterns in four paradigms in *C. elegans*, encompassing both Notch homologs, and reports low levels of Notch activity that were predicted but undetectable with other Notch activity reporters. Using SALSA, I showed that the first-born α cell is able to develop an advantage in Notch activity prior to the birth of the other α cell when the time interval between α cell births is long, but the α cell that gains the Notch activity advantage is random with respect to birth order when the time interval between α cell births is short. These results agree with the current model of the AC/VU decision.

I also describe Flexon, a method for the conditional activation of strong gene expression in specific cell lineages using a lox-stop-lox cassette encoded into an artificial exon flanked by two artificial introns. A *flexon* can be placed into the coding region of a gene to prevent translation of a functional gene product; gene expression is restored to specific lineages through expression of a tissue-specific Cre driver that excises the *flexon*. I show that *flexon* can be used to make bright, long-lasting, tissue-specific fluorescent lineage markers. I also showed that the *flexon* could be used for conditional activation of an endogenous gene by inserting a *flexon* into *rde-1* to severely reduce RNAi activity and restore gene function in specific tissues using Cre drivers.

Table of Contents

List of Figures and Tables

Chapter 1

Chapter 2

Chapter 3

Appendix A

Appendix B

Appendix C

Acknowledgments

Dr. Iva Greenwald was the first professor I talked to at my first graduate school interview. It is absolutely perplexing that she was able to guide that remarkably clueless prospective student to complete a doctoral thesis. Her ridiculously sharp scientific intellect and immense curiosity are enviable. She has the uncanny ability to ask the right questions, and an innate sense of when to push her students and when to give them emotional support. I am extremely privileged to have learned from the best and deeply grateful for her mentorship. I would not be the scientist I am today without her as an advisor.

I would like to thank Dr. Raju Tomer for serving on my thesis committee, Dr. Oliver Hobert for serving on my qualifying committee, and Dr. Gary Struhl for serving on both. Their scientific and career guidance over the years was invaluable. I would also like to thank Dr. Kelly Liu and Dr. Luisa Cochella for reading my dissertation and serving on my thesis committee.

There are no warmer, more supportive, or more enthusiastic people than those in the Greenwald lab. Special thanks to Dr. Michelle Attner; not only is her prowess for science and education unmatched, but she also made the suggestion in lab meeting that literally saved my project from the brink of failure. Thank you to Dr. Claire de la Cova, who continued to give me excellent advice even after she left and started up her own lab. I am grateful to Dr. Dan Shaye and Dr. Yuting Deng for the support while our paths briefly crossed; to the old guard of Dr. Ryan Underwood, Dr. Jessica Chan, Dr. Hana Littleford, Dr. Rob Townley, and Dr. Katherine Luo for modeling what it means to be a curious, rigorous researcher and kind, helpful labmate; and to my current lab mates Dr. Julia Wittes, Jee Hun “Henry” Kim, and Dr. Ali Ketcham for always being equally ready to dive into technical experimental details or share a laugh. It was a total pleasure to work with Matt Johnson for a semester, and with Alex Garcia Diaz a little longer than that. I’d

also like to thank Gleniza Gomez, who kept the lab running like a well-oiled machine, and whose positive energy brightened up the room every morning.

I would like to give a huge thank you to the best group of friends one could find in graduate school: Catherine O'Keeffe, who has sat back-to-back with me, and had my back, since the day we both joined the lab; Dr. Justin Benavidez, who is always down for a sidebar on pop culture or politics; Sarah Finkelstein, who is a limitless source of optimism when things look dreary; and Gillie Benchorin, who always has something fun up her sleeve when you need to get off the research rollercoaster. I have to thank my Millstone friends for supporting me from the beginning, and my college friends for perennially being prepared for sports, a dance party, or a deep conversation. Finally, I am so grateful to have a brother-in-all-but-blood, Jordan Disick, whose confidence is inspirational and dependability is second to none.

Thank you to my sister, Hannah, for never failing to pull me out of a spiral and set me on my feet again, and to my mom, Karen, for giving me the best guidance when she could and overwhelming support when she could not. The hustle from both of them is humbling, and they are my role models for diligence and perseverance. I'd like to thank the Menakis family for taking care of me and feeding me more weekends than I can count. And finally, I could not have done anything without my amazing fiancé Steph Menakis, who served as an emotional anchor, a paragon of hard-work, a boundless spring of assurance, and an always welcome distraction over these many years. Thank you for selflessly supporting me through this leg of the journey, and sticking around for the next.

Dedication

For John Shaffer, my father, coach, role model, and best friend.

Chapter 1: Introduction

Growth and development are two of the defining characteristics of living beings. Robust coordination between cell fate specification programs is required to ensure that all necessary cell types arise in proper balance. In this thesis, I use a model organism, the nematode *Caenorhabditis elegans*, to investigate how the relative levels of Notch signaling activity affect a stochastic fate decision called the AC/VU decision between two cells that are involved in gonadal development. In order to visualize and quantify Notch activity *in* vivo over time, I developed a genetically-encoded Sensor Able to detect Lateral Signaling Activity (SALSA), and Flexon, a method of conditional gene expression to express sensor components strongly in specific tissues. I will show examples of the use of SALSA and Flexon in *C. elegans* as proof of concept, as well as how they were applied to confirm a model of the role of Notch activity in translating stochastic events into deterministic fate outcomes during the AC/VU decision. Finally, I will discuss potential applications and adaptations of SALSA and Flexon in *C. elegans* and other model organisms.

1.1 An overview of Notch signaling in *C. elegans*

C. elegans is an excellent model for studying cell interactions during development. *C. elegans* is transparent, so cell divisions and fates can be tracked visually over time *in vivo* using Nomarski microscopy and genetically-encoded fluorescent markers. The cell lineages are largely invariant throughout embryonic development, the four larval stages (called L1-L4), and into adulthood (Sulston and Horvitz, 1977); therefore, cell fate outcomes during normal development and mutant analysis are robust and easily detectable (Horvitz et al., 1983).

The Notch signaling pathway is a conserved mechanism for intercellular communication between adjacent cells. Notch signaling is spatially and temporally widespread during mammalian, *Drosophila*, and *C. elegans* development. Notch signaling events can be divided into two broad categories. Inductive signaling generally involves unidirectional signaling from cells of one type to cells of another type. Lateral signaling involves cells with similar developmental potential, between which differences in Notch activity are amplified by feedback loops to generate robust cell fate outcomes. This section will explore multiple Notch events in the *C. elegans* in which SALSA was tested or used to study Notch activity over time.

1.1.1 *lin-12/Notch* in the mesodermal M lineage

C. elegans hatch with a single M mesoblast cell (Sulston and Horvitz, 1977; Fig. 1A). The M cell divides first along the dorsal-ventral axis during the first larval phase (L1), creating distinct dorsal and ventral cell lineages with different fate trajectories. The dorsal lineage will give rise to eight cells, two of which become non-muscle coelomocytes (CCs), while the ventral lineage produces 10 cells, two of which become sex myoblasts (SMs); the remaining cells of both lineages assume body wall muscle fates. *lin-12* is required for SM fate; in *lin-12(0)* animals the ventral parent cells of the SMs instead become CCs and fail to divide, while in *lin-12(d)* animals the dorsal cells that in wild-type become the CCs instead divide to give rise to SMs (Greenwald et al., 1983). A *lin-12::gfp* fusion transgene confirmed that *lin-12* is expressed in cells of the M lineage from the second division onward (Foehr and Liu, 2008). Transcriptional reporters of the ligands *lag-2, apx-1,* and *dsl-1* are expressed in cells adjacent to the ventral M descendants.

GFP fluorescence from the *lin-12::gfp* translational reporter was only visible on the membrane and not in the nucleus, so it was not possible to determine the timing of LIN-12 activity onset using this reporter (Foehr and Liu, 2008). Therefore, temperature shift experiments using a temperature-sensitive allele of *lin-12* determined that activity is not required prior to the second division of the M lineages, or the 4-M stage (Fig. 1A). Mutant and RNAi analysis indicated that *lin-12* is the sole *Notch* homolog involved in this decision and it acts through the canonical downstream pathway; *lag-2* was also shown to be the primary ligand in this paradigm, with redundant roles for *apx-1* and *dsl-1*. A model based on analysis of single and double mutants in the *lin-12* and TGFβ signaling pathways proposes that the two pathways work in concert to promote robust fate outcomes (Foehr et al., 2006; Foehr and Liu, 2008; Fig. 1B). The TGFβ pathway promotes SM fate in both the ventral and dorsal cell lineages, but *sma-9/Schnurri* promotes CC fate by antagonizing the TGFβ pathway. In the ventral descendants, *lin-12* activity bypasses *sma-9* to promote SM fate.

1.1.2 *glp-1/Notch* in the germline

During development, the *C. elegans* germline expands from two germline precursor cells that are present in the L1 at hatching to about 1000 cells present in each of two U-shaped gonad arms (Kimble and Hirsh, 1979). Within each arm, the germline forms an "assembly line" of germ cell progression, with a pool of germline stem cells (GCSs) at the distal end and mature oocytes at the proximal end (Fig. 2). The distal pool of GSCs proliferates mitotically, and as cells are displaced in a proximal direction, they enter meiosis and progress through the stages of oogenesis, ovulation, and fertilization. *glp-1/Notch* activity is required to maintain mitotic proliferation within the pool of GSCs through repression of the GLD-1, GLD-2, and SCF^{PROM-1}

pathways (reviewed in Hubbard and Schedl, 2019). *glp-1(0)* mutants produce very few germ cells, and shifting *glp-1(ts)* alleles from the permissive to restrictive temperature at any time during larval development or adulthood causes all of the germ cells to enter meiosis (Austin and Kimble, 1987). Additionally, *glp-1(d)* alleles result in excessive mitotic proliferation and germline tumors (Berry et al., 1997). The Distal Tip Cell (DTC), a somatic cell that caps the distal end of each gonad arm, expresses the ligands *lag-2* and *apx*-1 that interact with *glp-1* in the GSCs (Henderson et al., 1994; Nadarajan et al., 2009).

The DTC reaches the cells of the GSC niche through a web of cellular projections. Short projections from the DTC encompass the most distal cells and form the GSC niche which extends approximately 10 cd from the distal end (Byrd et al., 2014). Longer external projections can contact cells up to 20 cell diameters away (Byrd et al., 2014; Fitzgerald and Greenwald, 1995), coinciding with the end of the proliferative zone and the entry of the germline cells into meiosis (Crittenden et al., 2006; Hansen et al., 2004). While GLP-1 is expressed throughout the proliferative zone (Crittenden et al., 1994), evidence of GLP-1 activity is restricted to the niche. LST-1 and SYGL-1 are two direct transcriptional targets of GLP-1 that are required for maintaining stemness in the niche (Kershner et al., 2014; Shin et al., 2017). LST-1 expression ceases after about 5 cell diameters from the distal end but SYGL-1 expression reaches 8-10 cell diameters from the distal end, according to protein staining, RNA *in situ* hybridization, and nascent transcript reporters (Chen et al., 2020a; Kershner et al., 2014; Lee et al., 2019; Lee et al., 2016). LAG-1 expression is also restricted to 10 cell diameters from the distal end by positive regulation from GLP-1 activity and negative regulation by GLD-1/GLD-2 (Chen et al., 2020a). Nuclear fluorescence from active GLP-1 using an endogenous GLP-1::GFP tag was visible in the

distal cells of the germline in L3 and L4 but not in adults, suggesting there may be differences in nuclear accumulation in different developmental stages (Gutnik et al., 2018).

1.1.3 *lin-12/Notch* in the Vulval Precursor Cells

The vulva is made of 22 cells from two distinct vulval lineages, 1° and 2° (Sulston and Horvitz, 1977). Vulval Precursor Cells (VPCs) are six ectodermal cells, named P3.p-P8.p, that are born during L1 and are competent for both vulval lineages (Kimble, 1981; Sternberg and Horvitz, 1986; Sulston and White, 1980). In wild-type animals, P6.p assumes 1° fate, P5.p and P7.p assume 2° fate; all other VPCs assume 3° fate and do not contribute to the vulva, but the daughter cells fuse with the hypodermis after one division (Fig. 3). LIN-12/Notch is expressed in all of the VPCs (Chan, 2020; Levitan and Greenwald, 1995; Wilkinson and Greenwald, 1995), and *lin-12* activity is necessary and sufficient for 2° fate.

VPC fates are specified by the EGFR and LIN-12 signaling pathways. A LIN-3/EGF-like signal from the anchor cell of the somatic gonad activates a canonical Ras-Raf-MEK-ERK MAPK phosphorylation cascade through LET-23/EGFR in P6.p to induce 1° fate (reviewed in Sternberg, 2005; Sundaram, 2006). Low levels of EGFR signal pathway activity are also seen in P5.p and P7.p (Yoo et al., 2004). P6.p then sends a lateral signal composed of Notch ligands to the adjacent cells P5.p and P7.p (Chen and Greenwald, 2004), activating Notch and promoting 2°fate (Greenwald et al., 1983; Sternberg, 1988). VPC cell fates are specified in L3 (Greenwald et al., 1983), but there is evidence for pulses of LIN-3 signaling and MAPK signal transduction in P6.p in L2 (de la Cova et al., 2017).

Crosstalk between the LIN-12 and LET-23/EGFR pathways ensure a robust cell fate decision in the VPCs. The crosstalk model involves interaction between the EGFR pathway

target LIN-1/ELK1 (Beitel et al., 1995; Jacobs et al., 1998) and several components of Mediator, a large multiunit protein complex that couples transcription factors with basal transcription machinery (Allen and Taatjes, 2015). In all VPCs, unphosphorylated LIN-1 represses transcription of *lag-2* (Zhang and Greenwald, 2011), while the CKM subunit of Mediator sets a threshold for LIN-12 activity through the kinase function of *cdk-8* (Underwood et al., 2017). Activation of LET-23 in P6.p leads to phosphorylation of LIN-1, relieving *lag-2* repression and allowing transcription to be promoted by a Hox protein, most likely LIN-39, in conjunction with SUR-2/Med23 and LIN-25/Med24 independently of their roles with the Mediator complex (Takács-Vellai et al., 2007; Underwood et al., 2017; Zhang and Greenwald, 2011). SUR-2, LIN-1, and the CKM complex resist ectopic LIN-12 activity in P6.p, while SUR-2 and LIN-25 downregulate LIN-12 expression independent of the CKM (Shaye and Greenwald, 2002; Underwood et al., 2017). Meanwhile in P5.p and P7.p, Notch signal transduction activates feedback loops in which the Notch transcriptional targets *dpy-23, lst-1, lst-2, lst-3, lst-4,* and *lip-1* negatively regulate the EGFR pathway (Berset et al., 2001; Yoo et al., 2004), while the Notch target microRNA *mir-61* downregulates the LIN-12 negative regulator *vav-1* (Yoo and Greenwald, 2005). LAG-1 also undergoes positive autoregulation in a manner dependent LIN-12 activity and LAG-1 binding sites in an enhancer region in the first intron of isoforms A and B (Luo et al., 2020).

1.1.4 *lin-12/Notch* signaling during somatic gonad primordium development

C. elegans larva hatch with two somatic gonad precursor cells, Z1 and Z4 (Kimble and Hirsh, 1979). These cells produce 12 cells in hermaphrodites by the end of L1 (Fig. 4A). Specification of key cell types occurs during the L2 larval stage as cells temporarily halt division

and undergo a rearrangement to form the somatic gonad primordium. One cell type specified during primordium formation is the Anchor Cell (AC), a terminally differentiated cell that directs the patterning of the vulva and uterus through intercellular signaling, and eventually fuses with other cells at the interface of the vulva and uterus to form the vulval-uterine connection called the utse.

The cells Z1.ppp and Z4.aaa, referred to as the α cells, undergo a stochastic, Notch-mediated, lateral cell fate decision in which one AC and one Ventral Uterine precursor cell (VU) are specified (Greenwald et al., 1983; Kimble and Hirsh, 1979; Fig. 4B). LIN-12 acts as a genetic switch in the AC/VU decision: both α cells become ACs in *lin-12(0)* animals and both become VUs in *lin-12(d)* animals. (Greenwald and Seydoux, 1990; Greenwald et al., 1983). The transcription factor HLH-2 is required for AC competence and initial expression of *lin-12* and *lag-2* in the α cells (Attner et al., 2019; Karp and Greenwald, 2003). A stochastic difference in *lin-12* activity between the α cells is amplified by autoregulatory feedback loops so that the cell with higher *lin-12* activity becomes the VU, while the cell with lower *lin-12* activity becomes the AC (Seydoux and Greenwald, 1989; Fig. 4C). In the pre-VU, *lin-12* expression is amplified and maintained via positive autoregulation. A reporter of *lin-12* transcription suggested that positive autoregulation required a specific 5' regulatory sequence (Wilkinson et al., 1994); however, this has not been shown at the endogenous locus (see Appendix C). The Notch core nuclear complex component *lag-1* is also positively autoregulated in the pre-VU, which requires an intronic region containing multiple LAG-1 binding sites (Luo et al., 2020). Simultaneously, *lin-12* activity downregulates HLH-2 through proteosome-dependent degradation of HLH-2 dimers and additional mechanisms (Benavidez et al., 2022; Sallee and Greenwald, 2015), thereby downregulating *lag-2* transcription. Lower levels of *lin-12* activity in the pre-AC fail to

downregulate HLH-2 and LAG-2 or maintain LIN-12 expression. Ultimately, the AC/VU decision is resolved so that the AC expresses only HLH-2 and LAG-2, which are required for proper AC function (Karp and Greenwald, 2004), and the VU expresses only LIN-12.

Two independent but related stochastic differences upstream of the AC/VU decision bias the cell fate outcome: the relative birth order of the α cells, and the relative onset of HLH-2 expression in the parents of the α cells (Attner et al., 2019; Fig. 5). The α cells are not of the same lineage and are often born some time difference apart; the relative birth order between these cells is usually reflected by differences in the times of division of their predecessors, all the way up the lineage to Z1 and Z4. When there is a "long" time interval between the births of the α cells (>40-45 minutes), the first-born cell always becomes the VU. However, when the time interval between the α cell births is short, the α cell that assumes VU fate is random with respect to birth order. Instead, VU fate can be predicted by the relative order of HLH-2 expression in the parents, so that the first parent to express HLH-2 almost always gives rise to the VU. HLH-2 expression begins in the parent cells about 100 minutes after cell birth within approximately a 30-minute window; for cells born >40-45 minutes apart, the first parent cell to divide always has earlier onset of HLH-2 expression.

The sister cells of the α cells, called the β cells, are also competent for AC fate (Greenwald et al., 1983; Kimble, 1981; Seydoux et al., 1990). The β cells initially express *lin-12, lag-2,* and *hlh-2,* but quickly lose expression of the latter two genes and invariably become VUs (Kimble and Hirsh, 1979; Fig. 4B). Although LIN-12 activity promotes HLH-2 degradation in β cells, it is not required for downregulation of *hlh-2* transcription nor strictly required for VU fate assumption (Benavidez et al., 2022; Sallee et al., 2015; Sallee and Greenwald, 2015).

1.2 Notch structure and mechanism

Notch homologs include *C. elegans* LIN-12 and GLP-1, Notch in *Drosophila*, and NOTCH1-4 in mammals; the structure and mechanism of signaling is well conserved across all Notch homologs with some notable differences (reviewed in Gordon et al., 2008; Kovall and Blacklow, 2010), a few of which are discussed here. Notch is essentially a membrane-tethered, ligand-activated transcriptional co-activator (Figs. 6, 7A). Interaction with a ligand leads to proteolytic cleavage events in the ectodomain and transmembrane domain to release the intracellular domain from the membrane. The active intracellular domain translocates to the nucleus, where it joins with the Notch core nuclear complex to activate transcription of target genes.

1.2.1 Notch activation by canonical ligands

The Notch ectodomain can be divided into two sub-regions. The ligand binding region is at the N-terminus of the protein, and contains a series of EGF-like repeats, the number and pattern of which are not conserved across homologs (Gordon et al., 2008). Canonical ligands are members of the DSL (Delta, Serrate, LAG-2) family of transmembrane proteins, and include Delta and Serrate in *Drosophila*, Jagged1-2 and Dll1-4 in mammals, and LAG-2 and APX-1 in *C. elegans*. There are many other predicted *C. elegans* DSL proteins, but those that have been characterized have modest or redundant roles in development (Chen and Greenwald, 2004). All ligands contain EGF-like repeats and the eponymous DSL domain, which interact with the Notch ligand binding domain (Gordon et al., 2008).

The Notch Regulatory Region (NRR) falls between the ligand binding and transmembrane domains, and contains highly conserved LIN-12/Notch repeats and

heterodimerization domains. The NRR contains a cleavage site, S2, that is a target for ADAM metalloproteases such as SUP-17/Kuzbanian and ADM-4/TACE (Brou et al., 2000; Jarriault and Greenwald, 2005; Pan and Rubin, 1997; Rooke et al., 1996; Sotillos et al., 1997; Tax et al., 1997; Wen et al., 1997). Cleavage at the S2 site is activated by interaction with a ligand and required for Notch signal transduction (Mumm et al., 2000). The S2 cleavage site is hidden by the structure of the NRR (Gordon et al., 2009a; Gordon et al., 2007; Sanchez-Irizarry et al., 2004), but sufficient force can unfold the NRR and expose the S2 site for cleavage (Gordon et al., 2015; Langridge et al., 2021; Langridge and Struhl, 2017; Luca Vincent et al., 2017; Seo et al., 2016; Stephenson and Avis, 2012). In *Drosophila* and mammalian systems, Epsin-mediated endocytosis of the ligand is required to generate the pulling force to disrupt the NRR and relieve the inhibition of the cleavage site (Chen et al., 2009; Langridge and Struhl, 2017; Meloty-Kapella et al., 2012; Overstreet et al., 2004; Wang and Struhl, 2004, 2005). *C. elegans* LIN-12 and GLP-1 require lower force to expose the cleavage site, and do not require Epsin for activation; rather, the force threshold may be met by nonspecific endocytic processes or by the mechanical tension of physical interaction while being tethered to relatively rigid membranes (Langridge et al., 2021; Langridge and Struhl, 2017).

A second cleavage event within the transmembrane domain is mediated by the presenilin subunit of γ-secretase, which also includes APH-2/nicastrin, PEN-2, and APH-1 (reviewed in Greenwald and Kovall, 2013). In *C. elegans,* the presenilin subunit is SEL-12 or HOP-1 (Levitan and Greenwald, 1995; Li and Greenwald, 1997). Presenilin indiscriminately cleaves transmembrane domains with small ectodomains, like Notch after the ectodomain has been shed following the first cleavage event (Mumm et al., 2000; Struhl and Adachi, 2000).

Cleavage of the heterodimerization domain by furin at the S1 site during maturation of the protein occurs in mammals and can influence the folding and trafficking (Gordon et al., 2009b; Logeat et al., 1998). However, S1 cleavage is not required in *Drosophila* (Kidd and Lieber, 2002) and there is no evidence for it in *C. elegans*.

1.2.2 The intracellular domain of Notch as a transcriptional co-activator

Once released from membrane, the intracellular domain translocates to the nucleus and acts as a transcriptional co-activator (Schroeter et al., 1998; Struhl and Adachi, 1998; Struhl et al., 1993; Struhl and Greenwald, 1999, 2001). The intracellular domain contains RAM, Ank, and TAD protein-interacting domains, which facilitate formation of the Notch nuclear complex (reviewed in Greenwald and Kovall, 2013). A CSL (CBF1/RBP-J, Su(H), LAG-1) DNA-binding transcription factor and a Mastermind family transcriptional co-activator are required for Notch activity as part of the Notch core nuclear complex (Christensen et al., 1996; Doyle et al., 2000; Petcherski and Kimble, 2000; Wu et al., 2000); other transcriptional coactivators and chromatin modifiers are recruited on a context-specific basis (Oswald et al., 2001; Wallberg et al., 2002). Interestingly, CSL proteins are also found at Notch targets in a transcriptional repressor complex in the absence of Notch activity (reviewed in Lai, 2002; Luo et al., 2020). It is unclear whether nuclear Notch intracellular domain directly displaces co-repressors of the negative regulatory complex or whether pre-formed Notch core nuclear complexes replace the negative regulatory complex; while the latter model is currently favored, it is likely that both mechanisms occur at different levels (Bray, 2016; Bray and Gomez-Lamarca, 2018; Falo-Sanjuan and Bray, 2020).

The Notch intracellular domain includes a PEST degradation domain, which facilitates rapid turnover of active Notch. The PEST domain is phosphorylated by CDK-8, which is a part

of the mediator complex that is recruited by SEL-8/Mastermind (Fryer et al., 2004; Underwood et al., 2017). CK2 also has a role in the downregulation of Notch activity, while other kinases may contribute to Notch downregulation in specific contexts (Deng et al., 2019; Wang et al., 2014). The active Notch intracellular domain is ultimately ubiquitinated and tagged for degradation by the E3 ubiquitin ligase SEL-10/Fbw7 (Hubbard et al., 1997; Öberg et al., 2001; Sundaram and Greenwald, 1993; Wu et al., 2001).

1.3 Notch reporters

Active Notch is difficult to directly observe, due to the instability and short half-life of the free intracellular domain, and that a very low level of Notch activity is required for function (Lieber et al., 1993; Schroeter et al., 1998; Struhl and Adachi, 1998; Struhl et al., 1993). Many types of Notch transcriptional and translational reporters have been developed, each with upsides and downsides based upon the nature of the reporter. In this section, I will review Notch reporters that have been used in *C. elegans, Drosophila,* mammals, and mammalian cell lines.

1.3.1 Notch target gene transcriptional reporters

The most commonly used Notch activity reporters are knock-ins or transgenes of fluorescent or bioluminescent protein markers controlled by native regulatory information of Notch transcriptional targets (Fig. 7B). Common targets include the *Hes* genes in vertebrates (Masamizu et al., 2006; Ohtsuka et al., 2006; Vilas-Boas et al., 2011) and genes of the *E(spl)* locus in *Drosophila* (reviewed in Zacharioudaki and Bray, 2014), both which encode bHLH proteins involved in regulatory feedback loops during signaling events. Some *Hes* and *E(spl)* genes are expressed in many cell types in response to Notch activity, while others have more

spatiotemporally restricted expression patterns (Couturier et al., 2019; Imayoshi et al., 2013; Zacharioudaki and Bray, 2014). Regulatory sequences from other Notch target genes are commonly used to drive reporters of Notch activity in specific developing tissues in *Drosophila*, such as *cut* and *wg* in the wing disc and *bib* in the leg disc (Zacharioudaki and Bray, 2014)

Several transcriptional targets have been identified in *C. elegans,* but there are no broadly expressed native gene regulatory sequences that may be used for transcriptional reporters. Common promoter fusion transgenes of Notch targets include *lst-5p::YFP*, which has been used as a 2° fate reporter in VPCs (Choi, 2009; Karp and Greenwald, 2013; Keil et al., 2017; Li and Greenwald, 2010; Underwood et al., 2017) and *sygl-1p::GFP,* which indicates GLP-1 activity in the germline (Kershner et al., 2014). Some of the *C. elegans* Notch target gene transcriptional reporters have been shown to be susceptible to regulation from other inputs. For example, transcriptional reporters for LIN-12 targets *lst1, lst-2,* and *lst-4* are expressed at high levels in all VPCs before inductive or lateral signaling, a pattern which does not rely on the LAG-1 binding sites (Yoo et al., 2004). The reporters are then downregulated in P5.p and P7.p by low, graded levels of EGFR activity before being upregulated by LIN-12 activity. Also, regulatory sequence from the LIN-12 target *mir-61* can initiate expression of a fluorescent protein in the somatic gonad in α and β cells even if the LAG-1 binding sites in the regulatory region are deleted, indicating that the reporter is able to be activated independent of LIN-12 activity (Sallee, 2015). Also, an intronic region of *lag-1* paired with a minimal promoter region is upregulated in response to *lin-12* activity, but it was also expressed widely in tissues not known to express *lin-12* (Luo et al., 2020).

Synthesized regulatory regions containing multimerized CSL binding sites are commonly used in vertebrate models, cell lines, and *Drosophila* to generate Notch target transcriptional

reporters that are not subject to influence from other inputs (reviewed in Gridley and Groves, 2014; Zacharioudaki and Bray, 2014). A regulatory region containing 6 repeats of the EBV *TP1* gene promoter sequence, which has two CBF1/RBP-J consensus sequences, has been used to generate synthetic Notch transcriptional reporters in Zebrafish, mammalian cell lines, and the NAS (Notch Activity Sensor) transgenic mice (Kato et al., 1997; Kohyama et al., 2005; Parsons et al., 2009; Souilhol et al., 2006). Another regulatory region that contains 4 CSL binding sites and a minimal promoter is used in Transgenic Notch Reporter (TNR) mice (Duncan et al., 2005; Mizutani et al., 2007; Nowotschin et al., 2013). In *Drosophila*, the Notch Responsive Element (NRE) consists of 2 pairs of Su(H) binding sites from the *E(spl)-m8 gene* coupled with three repeats of the palindromic Grainyhead binding element (Gbe); the Su(H) binding sites provide sensitivity to Notch activity, while the Gbe repeats permit broad expression in the imaginal discs, epidermis, and trachea (Furriols and Bray, 2001). Synthetic Notch-responsive elements have generated neither strong nor Notch-sensitive expression in *C. elegans.* Although synthetic Notch responsive elements avoid some issues with inputs from other pathways, they may also be missing elements that are required to capture spatiotemporal nuance in Notch activity.

The final types of Notch target transcriptional reporter use heterologous transcription factor systems to indicate Notch activation. The heterologous factor is fused to or replaces the intracellular domain of Notch, with a separate transgene containing a reporter that is driven by the corresponding activation sequences (Fig. 7C). This type of Notch fusion reporter was first done in *Drosophila* to show that the intracellular domain of Notch required nuclear access; the transcription factor Gal4-VP16 was fused to the intracellular domain of a Notch transgene, and co-expressed with a UAS-lacZ reporter gene (Lecourtois and Schweisguth, 1998; Struhl and Adachi, 1998). Less ligand-independent Gal4 activity was observed when Gal4 was inserted just

inside the transmembrane domain as opposed to tagged to the C-terminus. Later versions in vertebrates and cell lines either replaced the RAM and Ank domains (Gordon et al., 2009b) or the entire intracellular domain with Gal4 (Smith et al., 2012; Sprinzak et al., 2010). Both of these reporters would allow for readout of Notch activation and cleavage, but are missing important components for negative regulation of the active Notch intracellular domain and accurate reporting of Notch activity over time. The former is missing domains that are required for inclusion in the Notch core nuclear complex, which is important for regulation (Deng and Greenwald, 2016); the latter is missing all degrons and ubiquitination sites that are present in the intracellular domain.

All Notch reporters that use transcription of a fluorescent protein as an output have similar limitations. There is a delay between the input and the output because the reporter protein has to be transcribed, translated, and mature; the maturation process is particularly lengthy compared to the rapidity of some of the molecular and subcellular processes that must be reported (Bothma et al., 2018). Fluorescent output from Notch target transcriptional reporters in *C. elegans* is not visible until after mutant analysis, temperature shift experiments, and cell ablation analysis suggest Notch activity is occurring. For example, transcriptional reporters like *mir-61p::gfp* are not well expressed in 2° VPC lineages until Pn.px, when the VPCs have already specified and divided (Yoo and Greenwald, 2005). Similar delays exist when the regulatory regions for *lst-5* and *dpy-23* are used to drive reporters in 2° fated cells (Yoo et al., 2004).

The MS2-GFP system may be used to speed up detection of a transcriptional target; stem loops are inserted into the untranslated regions of a target gene, allowing for visualization of the transcript when bound by MS2 coat protein-GFP fusions (Bertrand et al., 1998; Larson et al., 2009). GLP-1/Notch target transgenes with MS2 loops were used to confirm the spatial

distribution of GLP-1 activity in the *C. elegans* germline (Lee et al., 2019). However, the MS2-GFP system may be less amenable for use in other *C. elegans* tissues due to the lack of either Notch-specific target transgenes or endogenous Notch gene targets that will not affect development if gene expression is disrupted by the insertion of stem loops.

Another limitation is that fluorescent proteins lack native degrons or other regulatory sequences and may perdure after Notch signaling has ceased, reducing temporal sensitivity. Histone-tagged fluorescent proteins are commonly used as bright reporters, but they are also highly stable and greatly increase reporter perdurance. Attaching a degron or otherwise destabilizing the reporter protein may avoid issues with perdurance. For example, a Notch reporter in chick embryos was developed using the regulatory sequences for *Hes5-1* to drive expression of the fast-maturing, bright fluorescent protein Venus that was tagged with a PEST domain for destabilization (Vilas-Boas et al., 2011). The sequence also used the 3' UTR of *Hes5-1* to achieve a more accurate mimic of HES5-1 regulation and Notch activity. While the *Hes5-1* reporter accurately recapitulated HES5-1 expression during neural progenitor progression in chick embryos, the destabilized fluorescent protein reduced the intensity of the readout, which could lead to loss of information in cells with low but significant levels of Notch activity.

1.3.2 Direct visualization of the Notch intracellular domain

Notch activation can sometimes also be detected by the translocation of the intracellular domain from the membrane to the nucleus after cleavage. The simplest method to visualize nuclear Notch is by fusing a fluorescent protein to the intracellular domain (Fig. 7D). In *Drosophila*, transgenes expressing Notch::GFP constructs were shown to rescue Notch function, and to have GFP fluorescence on the membrane of the cells in which the construct was expressed

(Couturier et al., 2012; Kawahashi and Hayashi, 2010). However, GFP was not visible in the nucleus of cells with Notch activity under normal conditions with one transgene (Kawahashi and Hayashi, 2010), and was very dim with the other transgene (Couturier et al., 2012), although the latter was still used to quantify *in vivo* Notch activity over time during sensory organ precursor cell divisions. Notch::GFP fusions have also been made in *C. elegans*, as a *lin-12::gfp* transgene (Levitan and Greenwald, 1998) and as knock-ins at the endogenous locus for *lin-12* (Attner et al., 2019; Chan, 2020) and *glp-1* (Gutnik et al., 2018; Sorensen et al., 2020). Fluorescence at the cell membrane is observable with all of the Notch::GFP fusions, but the transgene has very little to no nuclear GFP fluorescence where there is known activity (Shaye and Greenwald, 2002), and the endogenous GLP-1::GFP fusion does not have nuclear GFP fluorescence in adult germline stem cells where GLP-1 is known to be active (Gutnik et al., 2018; Sorensen et al., 2020). The endogenous LIN-12::GFP knock-in does have some nuclear GFP fluorescence in cells with known Notch activity (Attner et al., 2019; Chan, 2020), but it is too dim to be imaged over time.

1.3.3 Other Notch sensors

Other Notch activity sensors have been created to try to overcome the limitations of fluorescent protein fusion tags and target gene transcriptional reporters. One such Notch activity sensor, Notch-LCI, used bioluminescence from luciferase complementation imaging to report formation of the Notch transcriptional complex (Ilagan et al., 2011; Fig. 7E). The Notch intracellular domain is fused with an N-terminal fragment of the luciferase protein (NLuc), and the CSL protein RBPjκ is fused with the complementary C-terminal fragment (CLuc). When active Notch::NLuc interacts with RBPjκ::CLuc in the nucleus, the luciferase protein is reconstituted, and bioluminescence activity is restored in the presence of the luciferin substrate.

Notch-LCI allowed for the visualization and quantitation of Notch activity dynamics, but is limited in practice to *in vitro* or *ex vivo* studies due to difficulty in delivering the substrate *in vivo* and the long exposure time required to capture bioluminescence.

Another alternative Notch activity sensor used the Cre/lox system to permanently activate reporter expression in mouse cells with Notch activity (Liu et al., 2015; Vooijs et al., 2007; Fig. 7F). Cre/lox is a site-specific recombinase system that uses the DNA recombinase Cre to either excise or invert DNA between two 34 bp *lox* sites depending on their relative orientation (Sauer, 1987; see chapter 1.5.2 for more details). In the N1IP-CRE system, the intracellular domain of the endogenous *Notch1* locus is replaced with Cre recombinase; the R26R reporter, which contains a floxed transcriptional stop sequence upstream of the *lacZ* coding region inserted into the permissive *ROSA26* locus, is the substrate for Cre activity. The transcriptional stop cassette prevents expression of *lacZ* except in cells in which *Notch1-Cre* activation allows for nuclear access of the Cre and excision of the cassette. Cells with *Notch1-Cre* activity are permanently marked by strong *lacZ* expression, as well as all descendants of that cell. N1IP-Cre is limited to detecting historical Notch1 activity, since permanent reporter activation after an initial Notch signaling event obscures any later Notch signaling events within the same lineage.

There are three versions of the N1IP-Cre system. N1IP-Cre^{LO} replaces the intracellular domain with a Cre that has a *6xmyc* tag at the C-terminus, and was able to report Notch activity in cells and tissues with high or repeated Notch signaling events (Vooijs et al., 2007). *Notch1-Cre6xmycErt2* reporters were later established to conditionally control Cre entry into the nucleus after Notch activation, so later Notch signaling events could be detected in cells or lineages with earlier events (Pellegrinet et al., 2011). However, N1IP-CreErt2 also only marked cells with relatively high levels of Notch1 activity. In N1IP-Cre^{HI}, the *6xmyc* tags were removed and

replaced with an extra polyadenylation sequence; these alterations increased Cre efficiency, thus increasing the sensitivity of the system to low levels of Notch activity (Liu et al., 2015). The three different versions can be used in parallel to determine the relative strength and timing of Notch signaling events.

1.3.4 Reporters and genetic tools that mimic Notch mechanism

Many sensors and genetic tools with robust outcomes are designed with inspiration from the Notch mechanism, despite the difficulty in detecting native Notch activity. SynNotch is a modular, genetically-encoded tool that uses the Notch regulatory region to control a transcriptional output with an external signal (Morsut et al., 2016; Fig. 8A). The signal that synNotch responds to is customized by replacing the Notch ligand-binding with a heterologous ligand-binding domain, and the output can be customized by replacing the intracellular domain with a heterologous transcription factor such as Gal4, tetR, or ZFHD1. SynNotch systems have been used to induce cell fate transitions and transdifferentiation (Morsut, 2016), induce cell-cell signaling cascades (Morsut 2016), engineer and customize CAR-T cells (Roybal et al., 2016; Srivastava et al., 2019), and control cell patterning (Toda et al., 2020). Recently, improvements to synNotches have been made that reduce ligand-independent activation (Yang et al., 2020). SynNQ is a similarly designed system used to detect cell-cell contact; the ligand binding domain is replaced with a GFP-binding nanobody that can interact with a synthetic, membrane-bound ligand on an adjacent cell (He et al., 2017). The intracellular domain is replaced with the QF transcription factor, so that when there is cell contact between a synNQ expressing cell and a ligand expressing cell, the QF is released from the membrane and transcribes a fluorescent reporter.

Other systems borrow from Notch the idea of proteolytic cleavage to release a transcription factor from a membrane tether, but use different mechanisms of activation. The GPCR sensor Tango tethers a transcription factor to a GPCR using a linker with the cleavage site for Tobacco Etch Virus protease, or TEVp (Barnea et al., 2008; Fig. 8B). An arrestin-TEVp fusion is recruited to the GPCR fusion when the latter is activated by ligand, bringing TEVp close enough to cleave the target site in the linker and release the transcription factor from the membrane. Tango assays were also established for detecting tyrosine kinase and steroid hormone activities. For the former, insulin-like growth factor 1 receptor was tagged via a TEVp cut site with a transcription factor; activation of the IGFR1 recruited an Shc1-TEVp fusion, which cleaves the target site and releases the transcription factor from the membrane. For the latter, transgenes were introduced in which Estrogen Receptor α was tethered to the membrane at one end and tagged with a transcription factor via a TEVp cut site, and then either another copy of Estrogen Receptor α or β was tagged with TEVp; ligand-induced dimerization between the ERα-transcription factor fusion and a free cytoplasmic ERα-TEVp or Erβ-TEVp fusion induced cleavage of the cut site and released the transcription factor from the membrane. Systems adapted from Tango have been used to detect dopamine receptor activity during neuromodulation in the *Drosophila* brain (Inagaki et al., 2012), discover new ligands for orphan human GPCRs (Kroeze et al., 2015), and interrogate endogenous GPCR activity (Katow et al., 2019).

The Modular Extracellular Sensor Architecture (MESA) system uses ligand-induced dimerization of synthetic transmembrane receptors to release a transcription factor from a membrane tether (Daringer et al., 2014; Fig. 8C). The intracellular end of the transmembrane domain from CD28 was either fused with TEVp or separated from a transcription factor by the

TEVp cleavage site. The extracellular portion of each CD28 fusion was then fused with peptide chains that dimerize in the presence of rapamycin, allowing for drug-induced interaction between TEVp and its cleavage site to release the transcription factor from the membrane.

1.4 Genetically-encoded biosensors

Genetically encoded biosensors, when applied to signaling pathways, are chimeric proteins engineered to translate the state of signal transduction into a measurable readout (reviewed in E.C. Greenwald et al., 2018). Biosensors generally have a sensing unit that identifies a signal or state of being, and a reporting unit that generates some type of detectable change in response to the recognized signal or state. The Notch activity reporters discussed in the previous section are biosensors, including the transcriptional reporters and translational fusions; the sensing unit is Notch itself, and the reporting unit is either the transgenic Notch target that is transcribed to generate fluorescent signal, or the fluorescent protein tag that reports changes in the subcellular localization of the active Notch intracellular domain. These simple biosensors have limitations in the speed and sensitivity of the reporting unit. Here, I introduce several other types of biosensors that attempt to increase the speed or intensity of the readout from the reporting unit as compared to transcriptional or protein fusion-based reporters.

1.4.1 Antibody-based biosensors

Antibodies can be used to increase the intensity of a detectable response by locally concentrating multiple antibodies onto a multimerized epitope. The SunTag system uses single chain fragment variable (scFv) antibodies, fused with superfolderGFP and a solubility tag to allow for intracellular expression (Tanenbaum et al., 2014; Fig. 9A). The SunTag scFv::GFP

proteins bind sequences from the yeast protein GCN4. Peptides consisting of up to 24x repeats of the GCN4 epitope, are tagged to proteins of interest, so that multiple scFv::GFP molecules can interact with the peptide repeat and concentrate a fluorescent signal into a bright dot around the protein of interest. SunTag has been used for single molecule imaging of cytoskeletal motors along microtubules.

I attempted to make a SunTag based LIN-12 activity sensor, in which the intracellular domain was tagged with the multimerized epitope peptide and scFv::GFP were expressed ubiquitously and constitutively in the nucleus; theoretically, GFP fluorescence would concentrate onto the epitope tags of active nuclear LIN-12 intracellular domains, allowing for sensitive detection of low levels of signal. While a low level of nuclear GFP expression was observed in the nucleus, there was no change in intensity or subnuclear localization in cells with LIN-12::epitope activity. The LIN-12 SunTag reporter could have failed for multiple reasons. The relative expression of the SunTag components may not have been optimized to ensure that the background signal from the free intrabodies did not drown out the concentrated signal of bound antibodies. Also, the protein components may not have folded properly in *C. elegans* cellular environment. Lastly, the size or structure of the epitope-tagged intracellular domain may have impaired nuclear entry; this would not have affected LIN-12-mediated cell fate decisions because LIN-12::epitope was expressed from a transgene in a LIN-12(+) background.

The LlamaTag sensor can rapidly detect changes in the subcellular localization of a protein (Bothma et al., 2018; Fig. 9B). It was designed to detect the expression and activity of transcription factors with shorter half-lives than the time to maturation of many FPs *in vivo*; detecting the dynamics of these proteins are difficult with FP fusions because they are already being degraded before the FP is mature and active. Llamatag uses nanobodies, which are

antibodies from llamas that naturally lack a light chain. In one application, anti-GFP nanobodies were fused to transcription factors in *Drosophila* embryos with maternally-produced cytoplasmic GFP; since the Llamatagged transcription factors are translated in the cytoplasm, they can bind fully mature and active GFP in transit to the nucleus, resulting in a rapid increase of nuclear GFP fluorescence during periods of transcription factor activity. The Llamatag system is able to detect rapidly changing molecular dynamics, but because each nanobody can only bind one GFP molecule, low levels of activity may still be beyond detection.

1.4.2 Split fluorescent protein biosensors

Some fluorescent proteins are able to be divided between the 10^{th} and 11^{th} β strand to create two separate molecules, FP_{1-10} and FP_{11}, that are not fluorescent on their own but can interact to restore fluorescent activity. Soluble, split versions of GFP, mNeongreen, and sfCherry have been shown to have fluorescent activity (Cabantous et al., 2005; Feng et al., 2017; Kamiyama et al., 2016), but split-FP systems are generally dimmer than their full FP counterparts so they are not ideal for detecting low levels of signal. The SpyTag/SpyCatcher system contains two peptide tags that form a spontaneous amine bond to irreversibly tether two proteins tagged with either peptide together (Zakeri et al., 2012); tagging the fragments of a split-FP with SpyTag/SpyCatcher peptides increases binding affinity of the fragments, thereby increasing brightness (Feng et al., 2019). Split-FPs can be used as biosensors by fusing the FP_{11} peptide to a protein of interest and expressing the FP_{1-10} in a specific subcellular compartment or tagged onto a different protein; co-localization of the protein-FP_{11} fusion with the FP_{10} fragment allows for reconstitution of the FP and fluorescent activity. Tagging a protein of interest with a multimerized array of FP_{11} molecules can concentrate multiple reconstituted FP molecules and

amplify the fluorescent signal into a bright dot, allowing for single molecule imaging (Kamiyama et al., 2016; Fig. 9C). However, as with SunTag, attaching a large peptide array to a protein of interest could inhibit its localization or function.

1.4.3 Biosensors based on changes in intramolecular fluorescent intensity

Fluorescence Resonance Energy Transfer, or FRET, is the transmission of an excited energy state from a donor fluorophore to a nearby acceptor fluorophore (reviewed in Cardullo, 2013). The donation process increases emission intensity from of the acceptor fluorophore at the cost of emission from the donor fluorophore. The two fluorophores need to be in very close proximity and with the appropriate orientation for FRET to occur, so the relative fluorescent intensities of a FRET pair can be used as a readout for protein interaction (reviewed in Newman et al., 2011). For example, an increase in FRET between fluorophores fused to different proteins can indicate when those the proteins are close and possibly interacting.

Dual-color reporters with FRET pairs can be used to indicate pathway activity using a linking peptide that alters the relative positioning of the fluorescent proteins in response to pathway activity. Kinase Activity Reporters use a linker that changes conformation in response to phosphorylation to alter the FRET efficiency between two fluorescent proteins (reviewed in E.C. Greenwald et al., 2018; Fig. 10A). The linker consists of a consensus sequence for a kinase with a phosphorylatable residue and a phosphoamino acid binding domain. Kinase activity results in phosphorylation of the consensus sequence; the binding domain then binds the phosphorylated residue intramolecularly, bending the linker and bringing the fluorescent proteins closer and causing an increase in FRET efficiency. Kinase Activity Reporters have been widely

adapted and designed to measure activity for a multitude of kinases, including PKA and multiple MAPKs (reviewed in E.C. Greenwald et al., 2018).

Protease reporters have also taken advantage of FRET activity by linking two fluorescent proteins via the consensus sequence for a protease; FRET is high in the absence of proteolytic activity, but FRET ceases when the reporter is cleaved and the fluorescent proteins are separated (Fig. 10B). FRET-based protease reporters have been used to study activity of caspases, membrane type 1 matric metalloproteases, and the autophagy-associated protease Atg4 (reviewed in E.C. Greenwald et al., 2018).

The advantage of FRET reporters is that they respond rapidly to signal or physical alteration, since both fluorescent proteins are already mature, and small changes to the relative positions and orientations of the proteins have large effects on FRET efficiency. However, the sensitivity of FRET reporters is also a disadvantage (reviewed in E.C. Greenwald et al., 2018). The signal to noise ratio is not great even in the most robust systems, and reporters need to be extensively tested and tuned for each context to maximize the ratio. The dynamic range of FRET intensity changes can also be fairly small, which makes it difficult to detect subtle changes. FRET reporters are also fickle *in vivo* due to more dynamic environmental conditions and lower reporter concentrations than standard *in vitro* solutions.

One alternative to FRET may be to use quenching peptides to regulate fluorescent intensity of a single fluorescent protein. The caspase reporter CA-GFP consists of a GFP molecule tethered to a quenching peptide by a linker containing the consensus sequence for a caspase (Nicholls et al., 2011; Fig. 10C). Cleavage of the consensus sequence frees the GFP from the quenching peptide, so caspase activity can be detected by re-activation of GFP

fluorescence. CA-GFP has been used in *C. elegans* to study the role of CED-3/CED-4 in axonal regeneration (Wang et al., 2019).

1.4.4 Translocation based reporters

Changes in subcellular localization of a visible reporter can also be used as readout for signaling activity. Several kinase activity sensors have sensing units that shuttle into or out of the nucleus in response to phosphorylation of a kinase-specific sequence. The first of such sensors was a reporter of CDK2 activity, which fused YFP to an element of human DNA helicase B, a target of CDK2 that is imported into the nucleus upon phosphorylation (Spencer et al., 2013; van Rijnberk et al., 2017). Similarly, Akt sensors were designed by fusing all or portions of FoxO proteins to the fluorescent protein Clover; the FoxO sequences contain nuclear localization and export sequences that have differing relative strengths depending on phosphorylation by AKT (Gross and Rotwein, 2015).

Kinase Translocation Reporters (KTRs) generalized the concept, fusing kinase-specific binding sites for JNK, p38, ERK, or PKA to a synthetic sequence with phospho-regulatable NLS and NES sequences and a fluorescent protein; phosphorylated reporter is exported from the nucleus, un-phosphorylated reporter is imported (Regot et al., 2014; Fig. 11A). A variation on the ERK-KTR, called the ERK-nKTR, was used in *C. elegans* to quantify EGFR-MAPK pathway activity over time (de la Cova et al., 2017). In the ERK-nKTR, the ERK-KTR is co-expressed with a red histone marker in a biscistronic construct using a viral 2A peptide to cause ribosomal skipping between the two parts of a single mRNA, generating an equimolar ratio of the sensor and the nuclear marker (Fig. 11B). The red histone marker was used to segment the

nuclei in cells expressing the ERK-nKTR, and the relative level of pathway activity was quantified by measuring the ratio of Red:Green fluorescence in the nucleus (Fig. 11C).

1.5 Systems for tissue-specific gene expression in *C. elegans*

The biosensors described in the previous sections, and many others not listed, have been shown to be able to translate changes in signaling activity into visual outputs. Unlike *in vitro* systems, biosensor proteins cannot be directly introduced into *C. elegans* or other *in vivo* or *ex vivo* models without damaging or fixing the sample, which defeats the advantages that biosensors have for imaging dynamic signaling. Therefore, it is necessary to express the biosensor components genetically. In order to be effective, genetically-encoded biosensors need to be expressed in the time and place in which signaling activity is occurring.

The spatiotemporal pattern of gene expression is regulated by 5', 3', and intronic non-coding DNA sequences. The sequences 5' to the coding region generally control when and where the transgene is transcribed while the intronic and 3' sequences regulate processing of the RNA transcript and translation; intronic regions and 3' UTR sequences can also regulate transcription, and the 5' UTR also regulates RNA processing and translation. Regulatory sequences from different genes can be cloned into transgenes in combinations that permit expression in a specific spatiotemporal pattern; in many cases, the chosen 5' regulatory sequence have an active role in controlling expression level and pattern, while the introns and 3'UTR are selected to be broadly permissive to high levels of expression with minimal effects on pattern. Characterized 5' regulatory regions often have trade-offs between strength and specificity; regulatory regions that drive high levels of expression may be ubiquitously expressed, while

regulatory regions that are highly spatially specific may drive low levels of expression. In this section, I will introduce some genetic tools for conditional transgene expression.

1.5.1 Multiunit, heterologous transcription systems

Tissue-specific expression can be achieved by expressing two parts of a transcriptional system in distinct but overlapping patterns, so only cells with both components have transcriptional activity. For example, split GAL4 is a system in which the yeast transcription factor is divided into complimentary DNA-binding and transcription-activation domains; either domain on its own does not drive expression from a transgene under control of upstream activating sequences, but when co-expressed together they heterodimerize and drive transgene expression (Luan et al., 2006). Intersectional strategies, in which the split GAL4 fragments are expressed separately using different regulatory regions with distinct patterns that overlap in a small subset of cells, have been used to generate spatial-specificity in the nervous system of *Drosophila* (Luan et al., 2006) and *C. elegans* (Wang et al., 2018).

Some systems use separate factors to regulate transcriptional function of a heterologous transcription factor. For example, GAL80 binds GAL4 to block transcriptional activity (Fig. 12A). Temperature sensitive alleles of GAL80 were developed to add a layer of temporal control to GAL4/GAL80 (McGuire et al., 2003). Although GAL4 has been adapted for *C. elegans* (Wang et al., 2017a; Wang et al., 2018), GAL80 has not. Additionally, the Q system also consists of a transcription factor, QF, that binds specific upstream activating sequences and can be repressed by QS; additional temporal control can be achieved by inhibiting the function of QS with quinic acid (Potter et al., 2010; Fig. 12B). Q has been shown to work in *C. elegans* (Wei et al., 2012). Either system can be used to generate spatial specificity can be achieved by driving

expression of transcriptional activator and repressor in distinct but overlapping expression patterns so that transcriptional activity is repressed in cells at the intersection of expression (Lee and Luo, 1999; Fig. 12C). The Q and GAL4 systems can be used combinatorially with each other, or with other heterologous transcription factor systems like LexA, to generate further spatial and temporal specificity (Lai and Lee, 2006).

The most significant issue with using heterologous transcriptional systems to generate spatiotemporal specificity is that the expression patterns of the transcription factors are still limited by the characterized promoters. The systems which rely on the intersectional expression of two components to generate specificity are prone to shortcomings since reduced expression of either component would impair the output. Systems that can irreversibly alter DNA to activate strong, permanent expression may be desirable in certain instances in which dynamic expression from characterized promoters precludes investigation of certain timepoints.

1.5.2 Site-specific recombinases

Site-specific recombinases (SSR) are enzymes that reversibly rearrange DNA between short target sequences. The two most common SSR systems are CRE/*lox* (Sauer, 1987; Sauer and Henderson, 1988) and FLP/*frt* (Golic and Lindquist, 1989), each consisting of an SSR enzyme (Cre or Flp) and 34 bp target sequences (*lox* or *frt*). The type of recombination event depends on the relative orientation of the two target sites; DNA sequences flanked by sites with opposite orientations are inverted, while DNA sequences flanked by sites in the same orientation are excised (Fig. 13A). Inversion events are usually reversible because both target sites remain intact and in *cis*. Excision events *in vivo* tend to be permanent because one of the target sites is incorporated into the excised DNA, which is circularized and degraded, while the other site remains in the DNA at the excision site. In the CRE/*lox* system, multiple recombination events

can occur simultaneously without promoting genome-wide instability by using pairs of mutually exclusive *lox* site variants, such as *loxP, lox2272, loxN,* and *lox551* (Hoess et al., 1986; Lee and Saito, 1998; Livet et al., 2007). Variants for *frt* sites exist as well, but require specific mutant FLP recombinase variants for each site (Shah et al., 2015; Voziyanov et al., 2002). SSRs are commonly used to generate conditional knockout alleles by flanking important coding sequence with SSR target sites in the same orientation. Expressing the SSR with a tissue-specific promoter excises the DNA between the target sites only in cells in which the SSR was expressed, creating a spatially restricted DNA deletion. Since excision is permanent, all descendants of the cells in which the event occurred also have the mutant allele.

1.5.3 Stop cassettes

SSRs can also be used to activate gene expression through removal of a DNA cassette that inhibits transcription. Stop cassettes are generally inserted into the 5' UTR of a gene locus, and contain sequences that prevent transcription of the downstream coding region that are flanked by SSR target sites. The cassette is excised by SSR-mediated recombination, leaving behind a target site scar in the 5' UTR that theoretically does not affect transcription. Thus, transcription of the gene is restored only in cells with SSR-mediated recombination events; spatiotemporal specificity can be introduced by using different 5' regulatory regions to control expression of the gene of interest after an excision event. The first stop cassettes were used in mammalian cells and mice, and consisted of a stop codon and polyA sequence repeated three times in tandem all flanked by *loxP* sites (Lakso et al., 1992; Maxwell et al., 1989). The first FLP/*frt*-based stop cassette, or '*flp*-out', was in *Drosophila*, and contained a transcriptional stop using sequence from the *Draf* gene flanked by minimal *frt* sites (Struhl and Basler, 1993). Full

coding regions that include transcriptional stops for phenotypic markers or fluorescent proteins are also used as the sequence within the stop cassette; the marker is expressed instead of the downstream gene until the sequence excision simultaneously removes the marker and activates transcription of the downstream gene (Basler and Struhl, 1994; Davis et al., 2008; Madisen et al., 2010; Voutev and Hubbard, 2008).

Stop cassettes have some limitations in flexibility and efficiency, mostly due to the relative inflexibility of the system in placement within a gene locus. Stop cassettes cannot be inserted into coding sequence because the target site scar after excision would cause a frameshift. Therefore, the stop cassette must be inserted into the 5' UTR to block expression, which may lead to several potential issues. First, a target site scar may interrupt uncharacterized but vital regulatory sequences even after excision of the cassette. Second, there can be some level of expression of the downstream gene even without excision of the stop cassette because the native start codon remains intact after the transcriptional stop in the cassette. Third, endogenous gene loci may have multiple isoforms with different start sites and 5' UTRs, and inserting a stop cassette upstream of the most 5' start may not block transcription from other isoforms with 5' variations. Fourth, inserting a stop cassette into regulatory regions of an operon may repress transcription from all of the genes in the locus because the same regulatory sequences are used for multiple genes. Finally, there may be some tradeoff between the efficiency of excision and the efficiency of halting transcription: larger stop cassettes that include full marker ORFs and other sequences may be recombined out less efficiently, but smaller cassettes may not put enough distance between the 5' regulatory region and the beginning of the downstream gene to fully prevent expression.

Some stop cassettes use the sequence inversion capability of SSR systems to prevent ectopic transcription from non-recombined loci. In these inversion-based systems, the reverse complement of the gene sequence of interest is flanked by two target sites in the opposite orientation and placed downstream of a 5' regulatory region; expression of the gene cannot occur until an SSR reverses the sequence between the target sites, restoring the proper orientation of the gene relative to the 5' regulatory region (Vázquez-Manrique et al., 2010). However, due to reversibility of SSR-mediateed inversion, the original orientation could be restored and prevent expression again.

Multiple strategies have been used to engineer irreversible flipping stop cassettes (Fig. 13B). The simplest strategy involves using a pair of *lox* variants, *lox66* and *lox71*, that are compatible for recombination but generate two incompatible sites, *loxP* and *lox72*, upon resolution of the event (Albert et al., 1995; Oberdoerffer et al., 2003; Zhang and Lutz, 2002). However, the recombination efficiency of the *lox66/lox71* pair is not as high as it is between homotypic variants, and higher for *loxP/lox72* than other incompatible sites (Araki et al., 2010; Chen et al., 2020b). Flip Excision (FLEx) cassettes, also known as Double-floxed inverse orientation (DiO) cassettes, flank the reversed sequence with two pairs of *lox* sites that are compatible with their homotypic partner and incompatible with the other pair (Fig. 13B), such as *loxP* and *lox2272* (Hoess et al., 1986; Langer et al., 2002; Lee and Saito, 1998; Siegel et al., 2001). Two sequential recombination events are required to excise the cassette. For example, DNA is inverted between the *lox2272* sites, which brings the *loxP* sites into the same orientation on one side of the gene sequence with one *lox2272* site between them. Second, an excision event between the *loxP* sites removes the flanked *lox2272* site, leaving the DNA sequence in an orientation in which it is able to be expressed with a *loxP* scar on one side and a *lox2272* site on

the other. The same result will be achieved if *loxP* is used for the inversion and *lox2272* is used for the excision. FLEx cassettes can be designed to indicate which cells have had recombination events by driving a marker from the promoter region prior to the event – inversion flips out the marker and flips in the gene of interest, and then excision makes the change permanent (Schnütgen et al., 2003). FLEx cassettes have been used in several organisms, including *C. elegans*, for successful gene activation (Atasoy et al., 2008; Flavell et al., 2013; Sohal et al., 2009). However, because two events are required, the chances of getting correct events are reduced if the efficiency of recombination is lower than optimal.

1.5.4 Stop cassettes in *C. elegans*

The first use of an SSR in *C. elegans* was using CRE/*lox* to selectively inactivate an *apr-1* rescuing transgene in vulval precursor cells after hatching, since *apr-1(0)* is embryonic lethal (Hoier et al., 2000). The first uses of FLP/*frt* were also the first uses of a '*flp*-out' cassette in *C. elegans*. In one system, the coding region and transcriptional terminator for GFP was flanked by *frt* sites and placed between a 5' regulatory region and a downstream coding region (Voutev and Hubbard, 2008). FLP-out was used to induce expression of markers for lineage tracing and disrupt gonad arm migration by conditionally activating expression of either a dominant negative allele of *hlh-12* or RNAi for *hlh-12*; however, the excision efficiency was very low. In the other FLP inducible system, the inclusion of the stop cassette resulted in mCherry expression, but when the stop cassette was excised the downstream GFP::protein fusion could be expressed; the system was used to activate transcription of GFP::tetanus toxin in GABA-specific neurons during adulthood without affecting development (Davis et al., 2008). CRE/*lox*-based stop cassettes have since been designed for use in *C. elegans*, both with markers in the cassette

sequence (Kage-Nakadai et al., 2014; Ruijtenberg and van den Heuvel, 2015) and without (Macosko et al., 2009; van der Vaart et al., 2020).

1.6 Summary

In Chapter 2, I describe a method for conditional gene activation using a modified stop cassette called Flexon that efficiently and permanently activates lineage-specific gene expression while avoiding some of the limitations of traditional stop cassettes. In chapter 3, I describe SALSA, a genetically-encoded biosensor for Notch activity, that I test in the *C. elegans* Notch signaling paradigms introduced above. Using Flexon and SALSA, I investigate how upstream stochastic events correlate with LIN-12/Notch activity to affect cell fate patterns during the AC/VU decision, a lateral specification event *C. elegans* gonadogenesis. Finally, in Chapter 4, I discuss how the findings in Chapter 3 fit into our model of the role of Notch during lateral specification and outline future directions for exploring the model as well as adapting and improving SALSA and Flexon.

Chapter 1: Figures

Figure 1

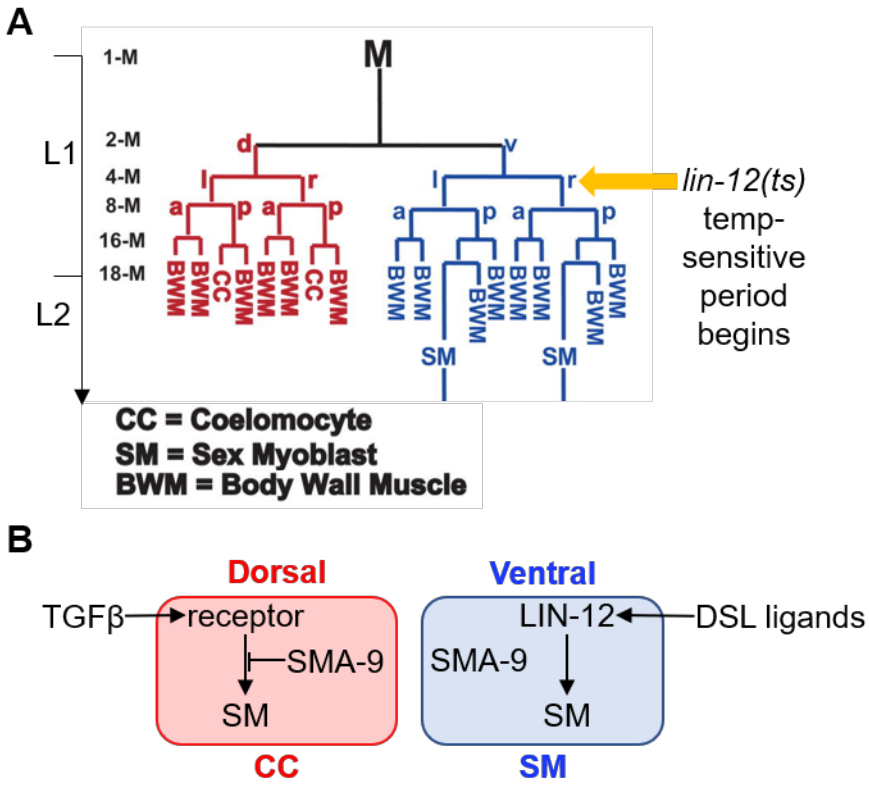

Figure 1. The mesodermal M cell lineage and development of SM/CC fates. Figure adapted from (Foehr and Liu, 2008). (A) *C. elegans* larva hatches with a single mesodermal M cell in the tail of the animal. The M cell divides first along the dorsal-ventral axis to create the precursors for dorsal (red) and ventral (blue) subgroups with distinct lineages and cell fate patterns. In the lineage diagram, vertical lines indicate the passage of time, and horizontal lines indicate cell divisions. The axis of division is indicated by the letters at the junctions indicating cell divisions; d=dorsal, v=ventral, a=anterior, p=posterior, l=left, r=right. The larval stages and lineal stages are labeled on the left. (B) The TGFβ pathway promotes SM fate in the M lineage descendants, but SMA-9 antagonizes the pathway to promote CC fate. In the ventral M descendants, LIN-12 activity bypasses the TGFβ pathway and promotes SM fate, while LIN-12 inactivity in the dorsal descendants fails to bypass the SMA-9 block and CC fate.

Figure 2

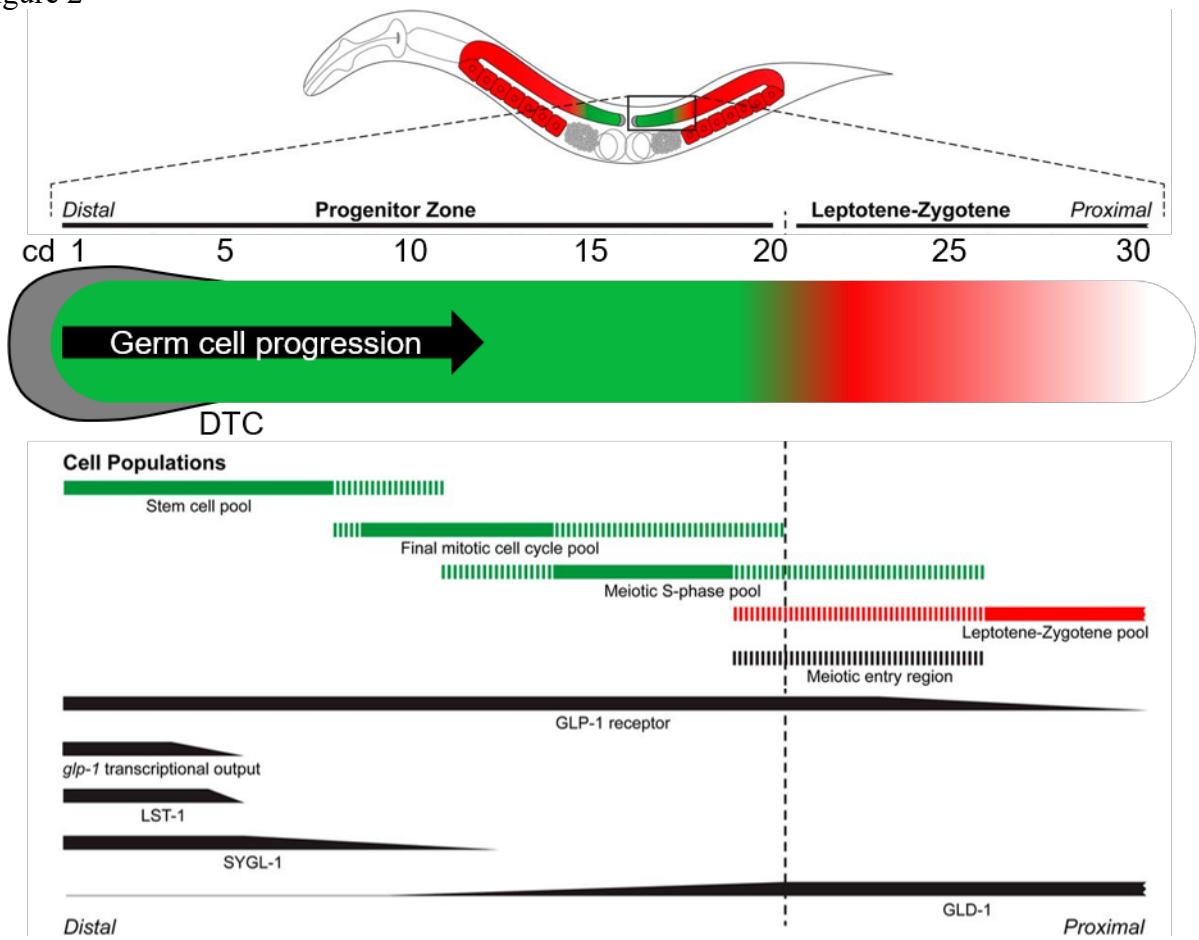

Figure 2. The adult germline in C. elegans. The adult gonad consists of two reflexed, U-shaped arms that contain the germline. At the distal end of each arm is the germline stem cell niche that is formed by the somatic Distal Tip Cell (DTC), which expresses ligands that activate GLP-1/Notch in the germ cells to maintain a mitotically proliferating stem cell pool. Constant division pushes germline stem cells proximally until they lose contact with signals from the niche, at which point they exit mitosis and enter meiotic S phase. Cells in mitosis and meiotic S phase are considered to be in the progenitor zone, which extends approximately 20 cell diameters (cd) from the distal end of the germline. Although GLP-1 is expressed in germ cells throughout and beyond the progenitor zone, protein and transcript from the GLP-1 targets LST-1 and SYGL-1 are detected within about 5 and 10 cell diameters, respectively. Figure adapted from (Hubbard and Schedl, 2019)

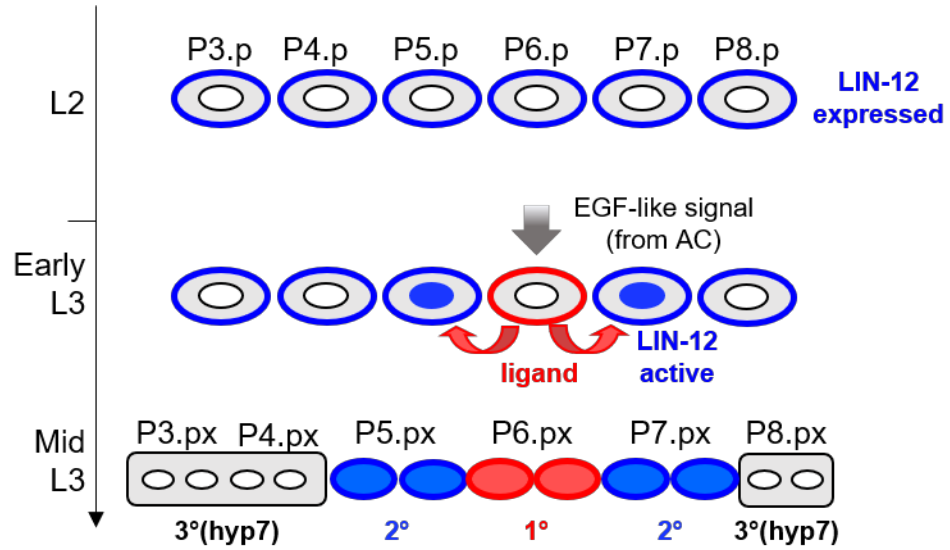

Figure 3. Vulval Precursor Cell (VPC) specification and development. The VPCs P3.p-P8.p express LIN-12/Notch and are competent for 1° or 2° fate, which generate distinct lineages that participate in vulval morphogenesis, or 3° fate, which does not. An inductive signal from the AC in the somatic gonad and interacts with LET-23/EGFR in P6.p, which activates a MAPK signaling cascade that induces 1° fate and upregulates transcription of Notch ligands to signal laterally to P5.p and P7.p and induces 2° fate. VPCs that do not receive the inductive or lateral signals assume 3° fate, divide once and fuse with the hypodermal syncytium, hyp7; the 1° and 2° VPCs divide multiple times through the rest of larval development and their descendants compose all cells of the vulva. Figure adapted from (Chan, 2020)

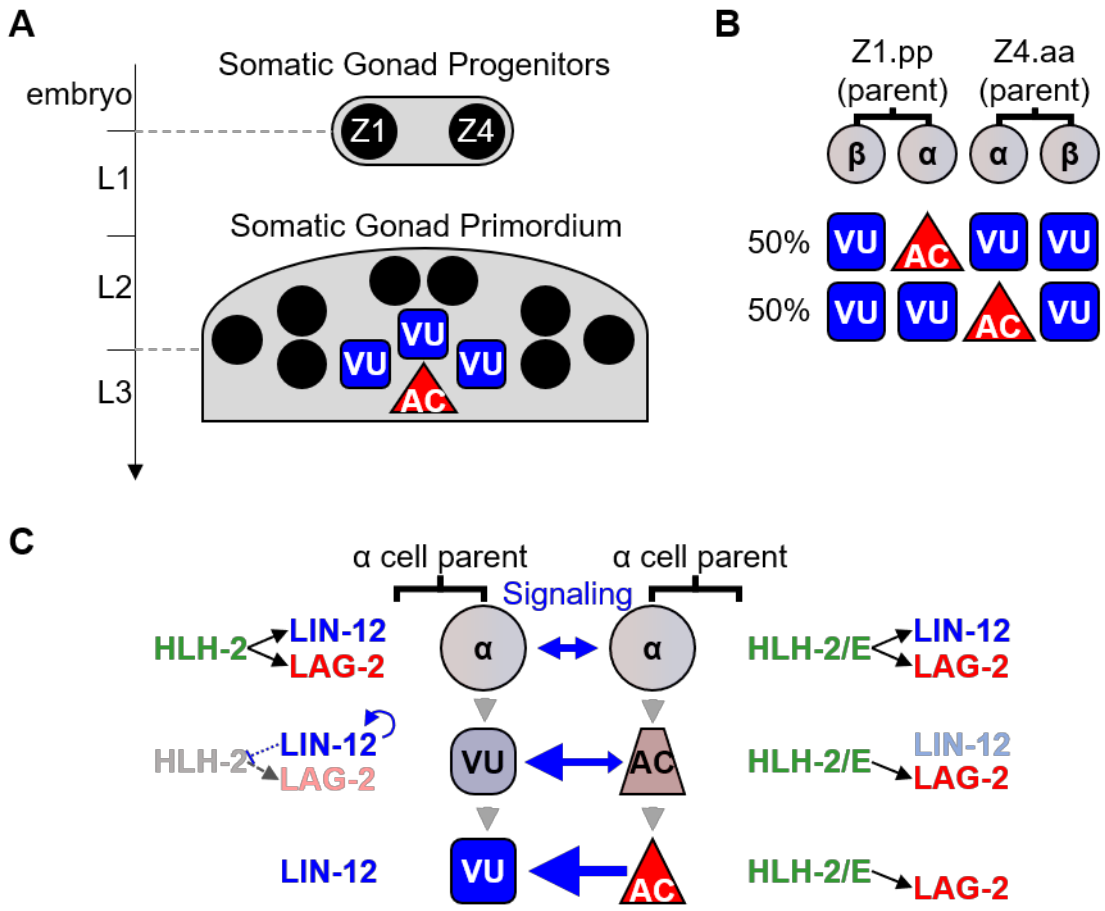

Figure 4. Formation of the somatic gonad primordium. (A)*C. elegans* L1 larvae hatch with two somatic gonad precursor cells, Z1 and Z4, which give rise to 12 cells that form the somatic gonad primordium by the L2/L3 molt. The primordium includes the Anchor Cell (AC) and three Ventral Uterine precursor cells (VU). (B) The α and β cells have AC fate competence. The β cells quickly lose AC competence and always become VUs. The proximal daughters, the α cells, retain AC competence and undergo a stochastic cell fate decision in which one of the cells assumes AC fate and the other cell assumes VU fate. (C) HLH-2/E activates initial expression of LIN-12/Notch and LAG-2/ligand in the α cells. LIN-12 activity triggers a positive autoregulatory feedback loop, while downregulating HLH-2 and LAG-2 expression. The α cell with an advantage in LIN-12 activity maintains LIN-12 expression, loses HLH-2 and LAG-2 expression, and assumes VU fate; the other α cell loses LIN-12 expression, maintains HLH-2 and LAG-2 expression, and becomes the AC. Figures adapted from (Attner et al., 2019).

Figure 5

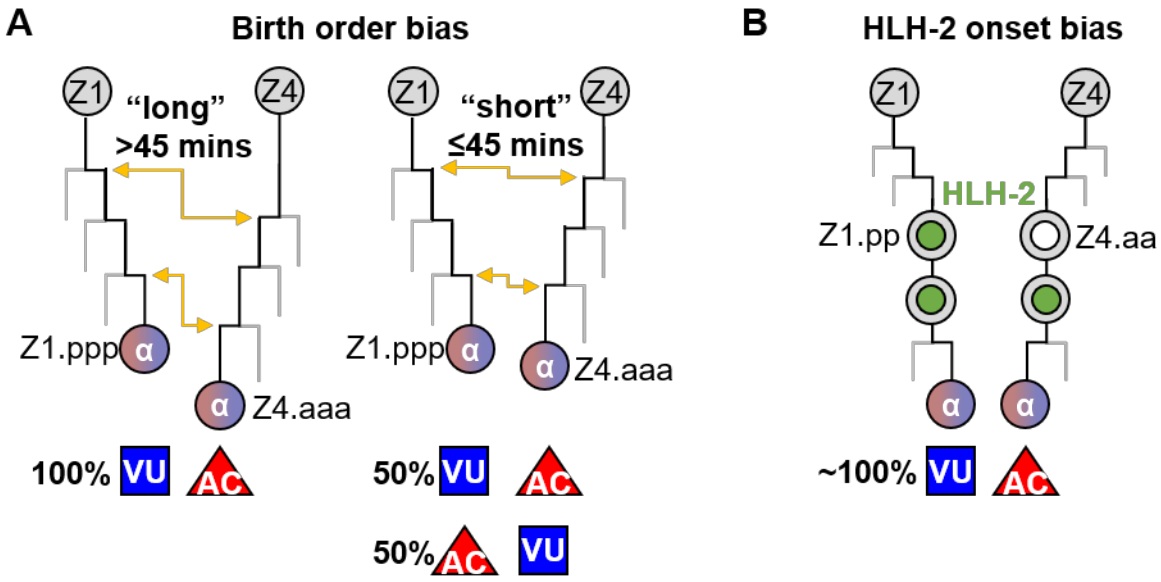

Figure 5. Two stochastic events bias the AC/VU fate pattern. (A) The division order between the somatic gonad precursors Z1 and Z4 is generally carried down the lineage so one α cell is born before the other. When the time interval between the α cell births is long, the first-born α cell always becomes the VU, but when time interval is short, the fate pattern is random with respect to birth order. (B) At all birth time intervals, the first parent to express HLH-2 gives rise to the α cell that becomes the VU. HLH-2 expression turns on within a specific window of time after the birth of the parent cells. Figure adapted from (Attner et al., 2019).

Figure 6

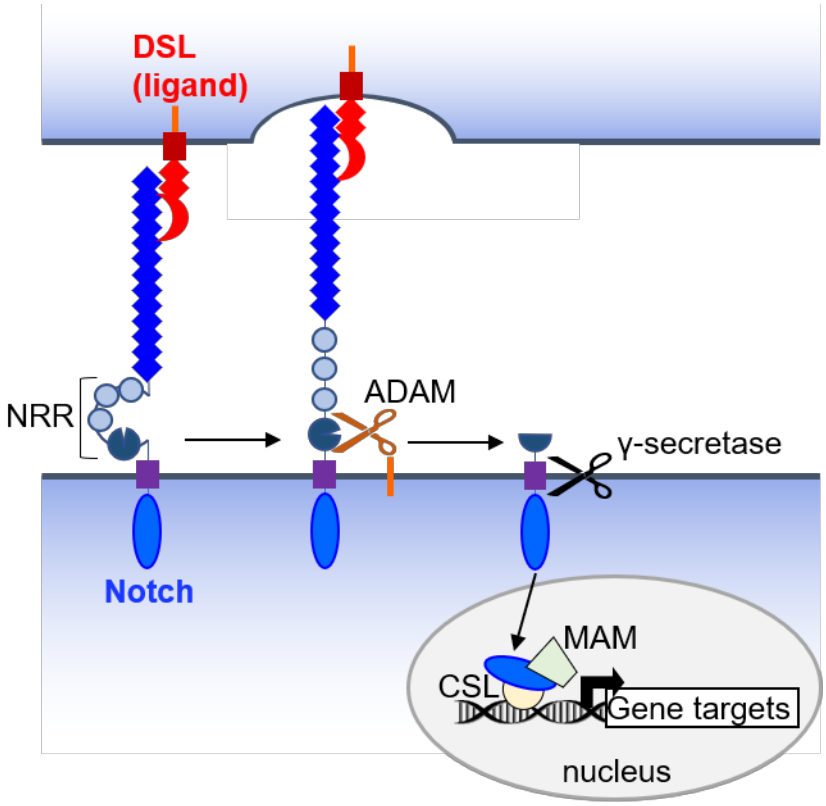

Figure 6. Canonical Notch activation and signal transduction. Notch is a single pass transmembrane receptor protein that is trans-activated by ligands of the DSL (Delta, Serrate, LAG-2) family of proteins, which are generally also transmembrane proteins. Interaction with a ligand creates a force that causes a conformational change in the Notch Regulatory Region (NRR) and exposes a cleavage site for an ADAM metalloprotease. The Notch transmembrane domain is then cleaved by the Presenilin subunit of γ-secretase, releasing the Notch intracellular domain from the membrane. The intracellular domain translocates to the nucleus, where it forms a transcriptional activation complex with a CSL (CBF1/RBP-J, Su(H), LAG-1) DNA binding protein and a Mastermind (MAM)-family transcriptional co-activator. Figure adapted from (Bray, 2016) and (Langridge et al., 2021).

Figure 7

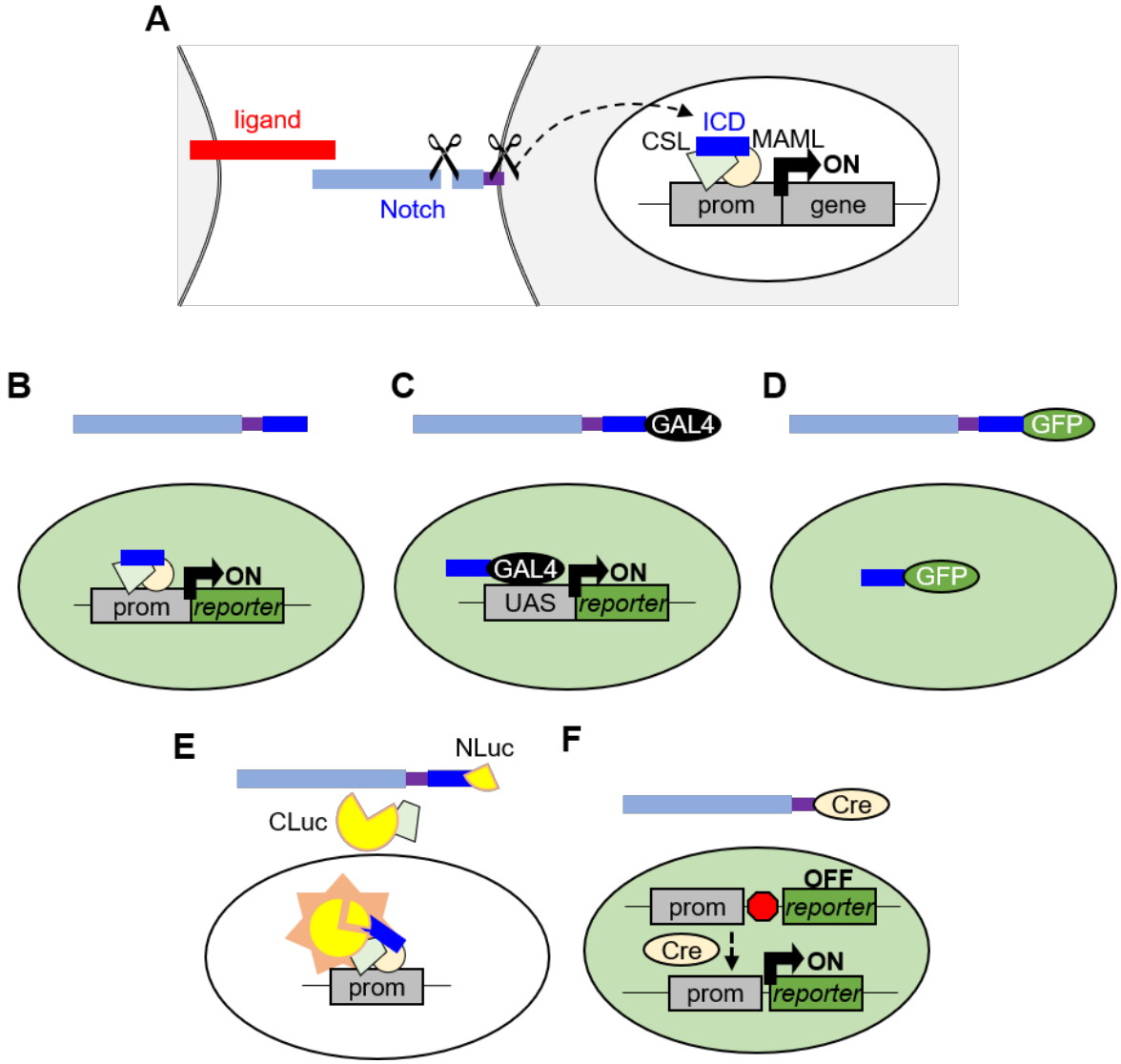

Figure 7. Notch reporters. (A) When Notch interacts with a ligand, cleavage events in the ectodomain and transmembrane domain release the intracellular domain (ICD) from the membrane so that it may translocate to the nucleus and form a transcriptional activation complex with a CSL DNA binding protein and a MAM transcriptional activator. See also Figure 6. (B-F) Examples of Notch reporters. The Notch construct is shown above, and a representation of a nucleus with Notch activity is shown below. (B) A Notch target transcriptional reporter in which a reporter protein is driven by either a native promoter from a Notch target or a synthetic promoter with CSL binding site repeats. (C) Notch target transcriptional reporter in which Notch is tagged with a heterologous transcription factor, such as GAL4, and a reporter gene is driven by activating sequences for the heterologous factor. The heterologous transcription factor can also totally replace the intracellular domain. (D) Fusions of a fluorescent protein to the C-terminus of Notch, such as Notch::GFP, allow visualization of the active ICD in the nucleus. (E) Figure adapted from (Ilagan et al., 2011). The Notch-LCI system, in which the Notch is tagged at the C-terminus with one fragment of split luciferase (NLuc) and the CSL protein is tagged at the N-

terminus with the other fragment of split luciferase (CLuc). Bioluminescent activity of the split luciferase is only rescued when the ICD::NLuc and CLuc::CSL interact, such as in the active transcriptional complex. (F) The NIP-CRE system, in which the Notch intracellular domain is replaced by Cre recombinase. Expression from a reporter is blocked by a floxed transcriptional stop sequence in the absence of Notch signaling, but Notch activation releases Cre, which excises the stop sequence, allowing permanent transcription of the reporter only in cells that had a Notch signaling event.

Figure 8

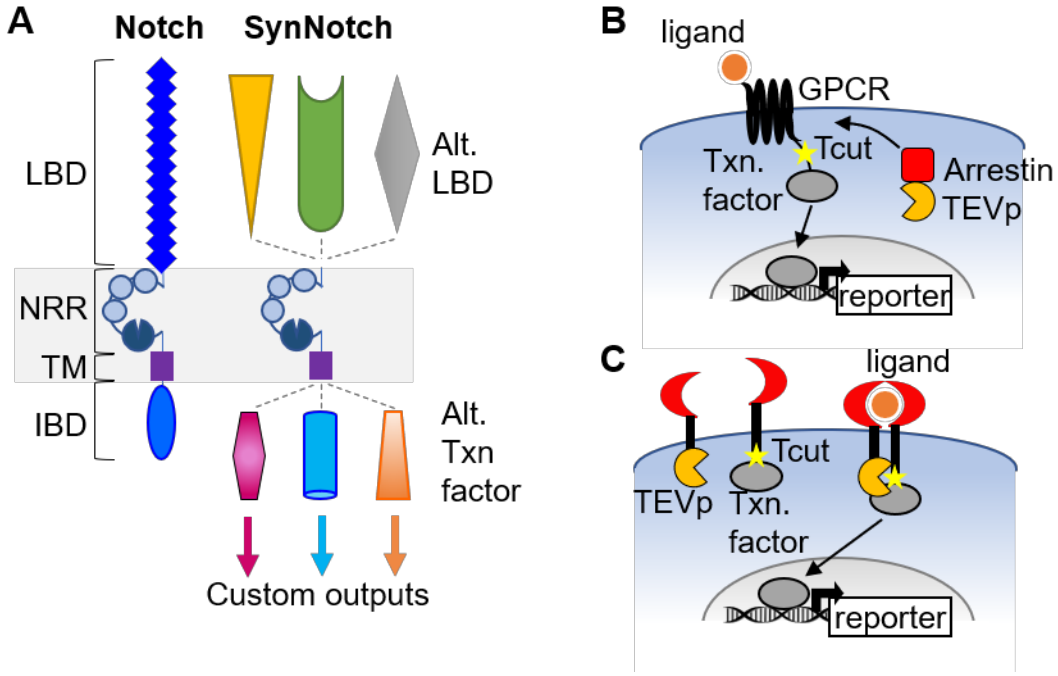

Figure 8. Reporters based on Notch mechanism. (A) SynNotch systems use synthetic Notch proteins to customize an output based on a membrane-bound signal. SynNotch proteins replace the native Notch ligand-binding domain and intracellular domain with alternate heterologous domains, but keep the Notch regulatory region and transmembrane domain. Release of the heterologous intracellular transcriptional activator from the membrane requires processing of the NRR and transmembrane domains after activation by the specified signal. Adapted from (Morsut et al., 2016). (B) Tango is a GPCR activity reporter in which a GPCR protein is tagged with a transcription factor via a TEV protease cleavage site (Tcut). Activation by the ligand recruits an arrestin::TEV protease (TEVp) fusion protein to the GPCR fusion; TEVp cleaves Tcut, releasing the transcription factor to translocate to the nucleus and activate transcription of a reporter gene. Adapted from (Barnea et al., 2008). (C) MESA uses synthetic, heterotypic transmembrane receptors to activate signal transduction in the presence of a specific ligand. Both chains of the receptor contain ligand-binding sequences that induce dimerization upon activation by the ligand. One chain has a transcription factor tethered via Tcut in the intracellular domain, and the other chain is tagged at the C-terminus with TEVp. When the receptor dimerizes, TEVp cleaves Tcut on the opposite chain, releasing the transcription factor to translocate to the nucleus and activate transcription of an output. Adapted from (Daringer et al., 2014).

Figure 9

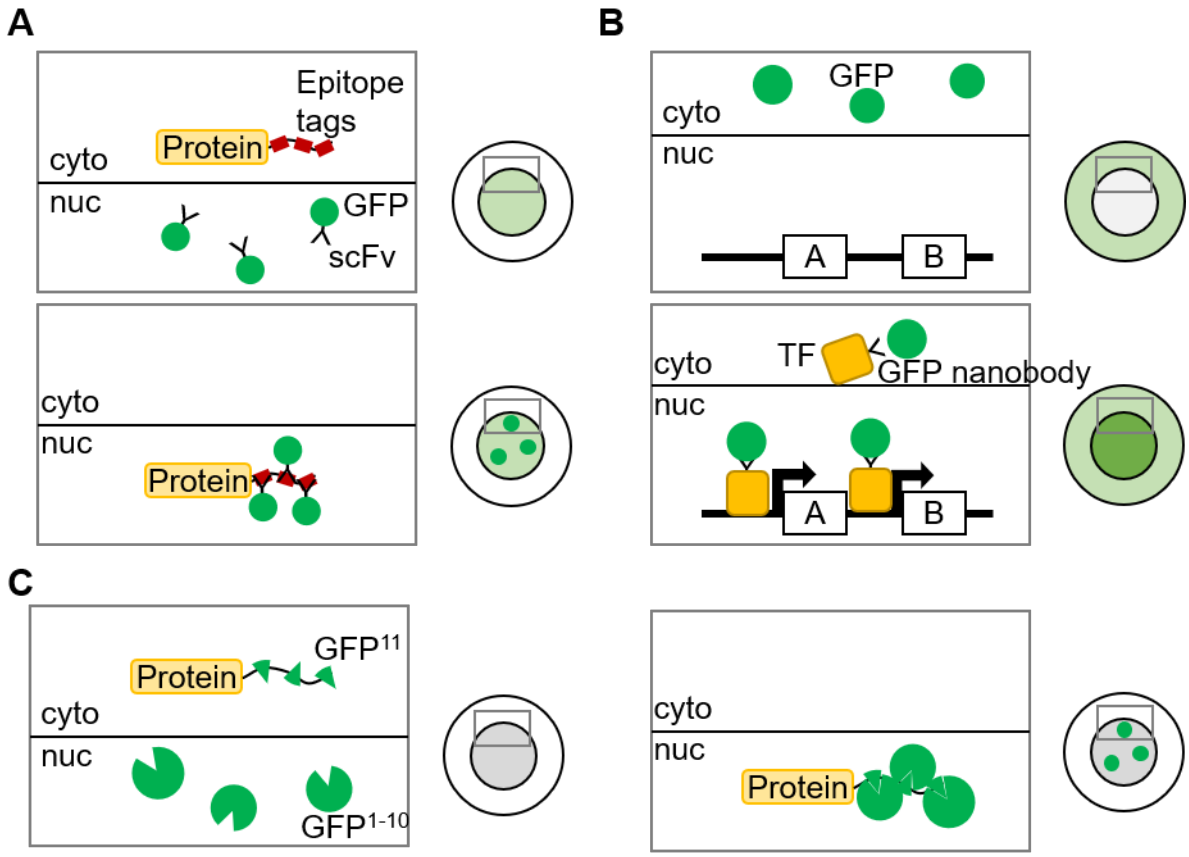

Figure 9. Reporters based on concentrating a fluorescent signal. (A) In the SunTag system, GFP-tagged single-chain, fragment variable (scFv) intrabodies are expressed in cells containing a protein tagged with multiple repeats of the scFv epitope. Multiple GFP::intrabodies can bind to the peptide at one time, concentrating a diffuse fluorescent signal to individual proteins. Adapted from (Tanenbaum et al., 2014). (B) In the LlamaTag system, cytoplasmic GFP is constantly expressed, but concentrated into the nucleus upon expression and activity of a transcription factor fused to a GFP-specific nanobody. Adapted from (Bothma et al., 2018). (C) The small fragment of split fluorescent proteins may be tagged in multiples to a protein of interest, so that many large fragments of the split fluorescent protein can interact simultaneously with the protein fusion and amplify local signal output. Adapted from (Kamiyama et al., 2016).

Figure 10

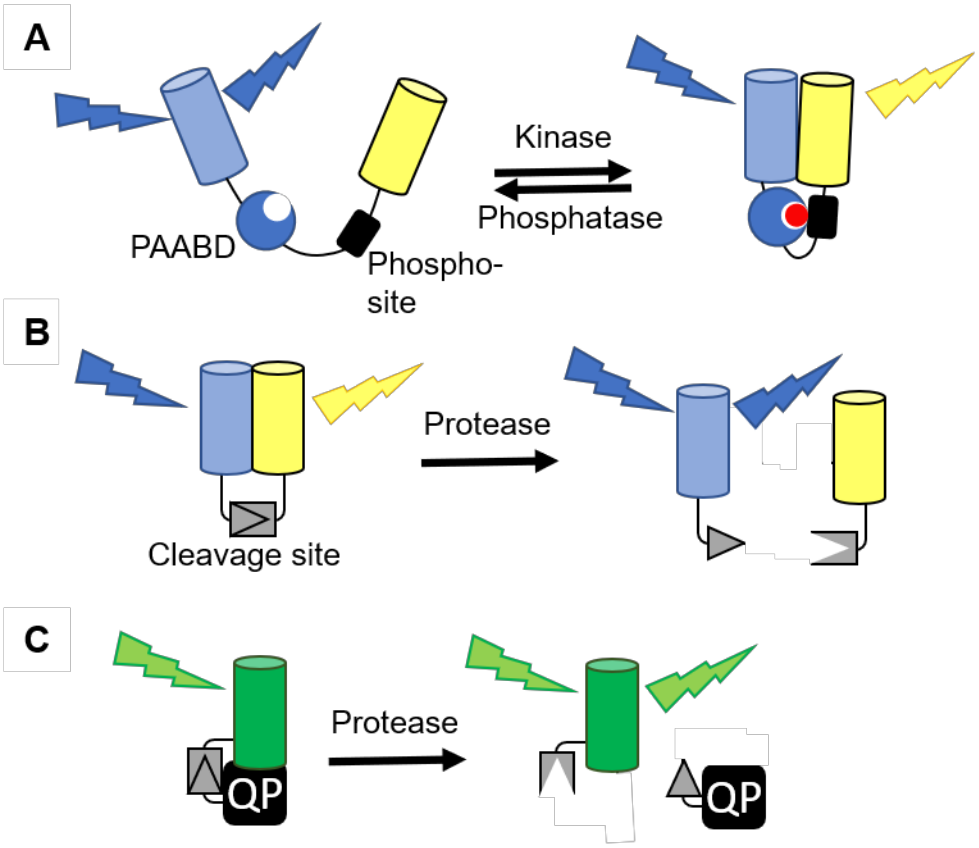

Figure 10. Reporters based on changes in intramolecular fluorescent intensity. (A) Kinase activity reporters consist of a FRET pair of fluorescent proteins tethered by a linker containing a kinase consensus sequence with a phosphosite and a phosphoamino acid binding domain (PAABD). When kinase activity phosphorylates the consensus sequence, the PAABD binds the phosphorylated residue and causes a conformational shift in the linker sequence that brings the fluorescent proteins into an orientation that increases FRET activity. Adapted from (E.C. Greenwald et al., 2018). (B) Reporters for proteolytic activity insert a cleavage site for a protease into the linker between a FRET pair of fluorescent proteins. The conformation of the intact reporter allows for high FRET activity, but proteolytic activity separates the FRET pair through cleavage of the linker and decreases FRET efficiency. Adapted from (Takemoto et al., 2003). (C) CA-GFP consists of GFP tethered to a fluorescence-quenching peptide (QP) via a cleavage site for a specific protease. The quenching peptide dampens GFP fluorescent signal in the intact reporter, but cleavage of the linker releases the peptide from GFP, restoring fluorescent signal from GFP. Adapted from (Wang et al., 2019).

Figure 11

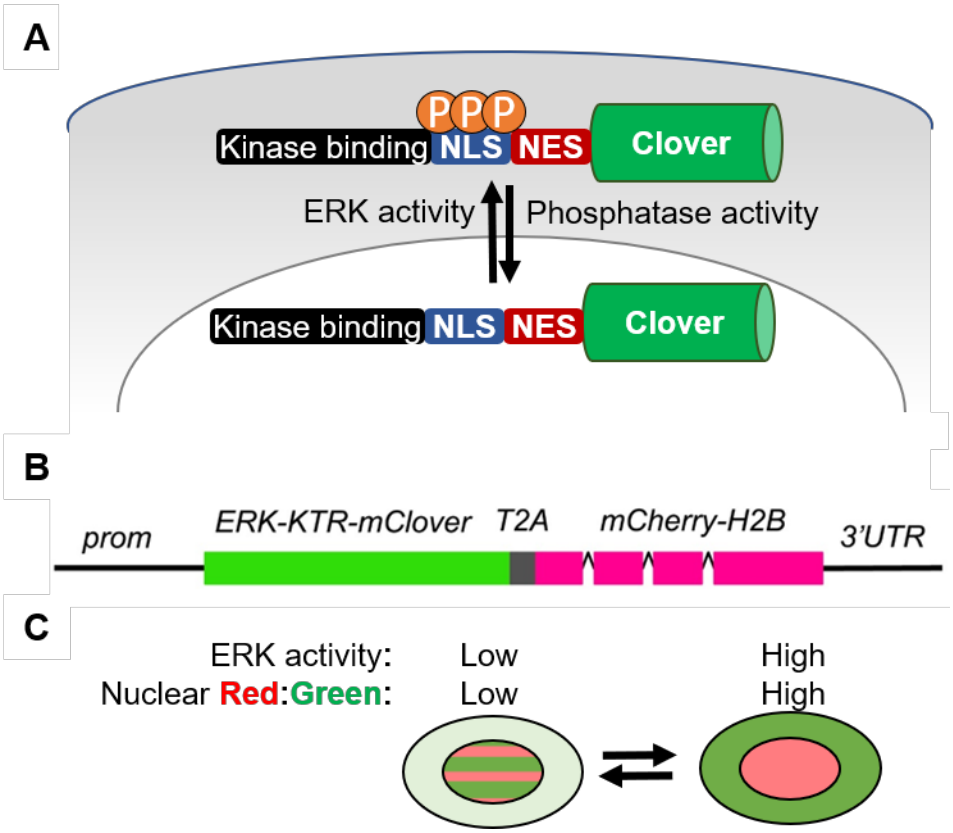

Figure 11. Kinase Translocation Reporters (KTRs) and the ERK-nKTR. (A) KTRs consist of a fluorescent protein tagged with a binding site for a kinase and phosphoregulatable nuclear localization and nuclear export sequences (NLS and NES). The KTR NLS is stronger than the NES when unphosphorylated, but the NES is stronger in when phosphorylated. (B) In the ERK-nuclear KTR (ERK-nKTR), an ERK-KTR is co-expressed with a nuclear fluorescent marker from a bicistronic transcript that uses a viral 2A peptide to induce ribosomal skipping between the reporter and marker sequences; the reporter and marker are expressed in equimolar amounts, (C) Relative levels of ERK activity between cells can be quantified using the nuclear Red:Green ratio of the ERK-nKTR. In cells with low kinase activity, the KTR is enriched in the nucleus and the nuclear Red:Green ratio is low, but in cells with high ERK activity, the KTR is exported from the nucleus and the nuclear Red:Green ratio is high. Adapted from (de la Cova et al., 2017).

Figure 12.

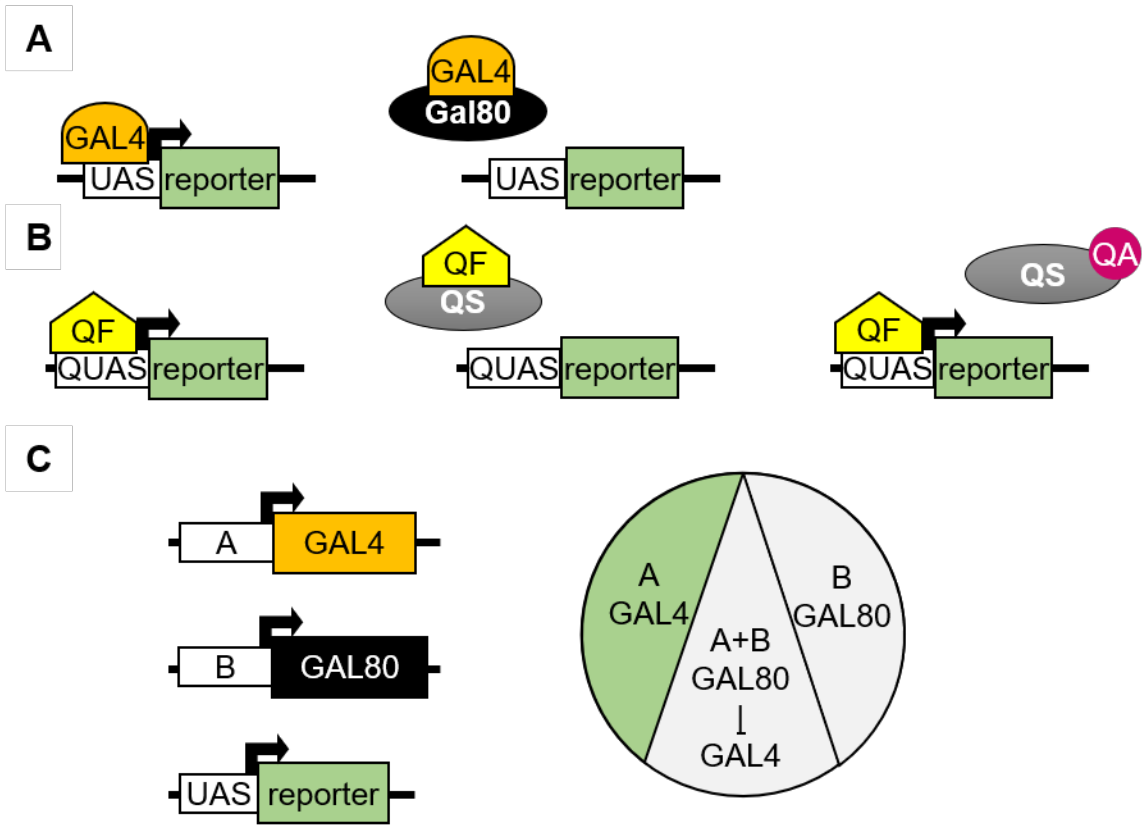

Figure 12. Systems for conditional control of transcription. (A) The GAL4/GAL80 system consists of the transcriptional activator GAL4 and the repressor GAL80. GAL4 binds to specific upstream activating sequences (UAS) that may be placed upstream of a gene of interest to be expressed in the presence of GAL4. GAL80 binds to GAL4 to prevent transcription. (B) The Q system consists of the transcriptional activator QF and the repressor QS. QF binds to Q upstream activating sequences (QUAS) to activate target gene transcription, but QS represses QF-dependent transcription. Additionally, transcription can be restored by introducing quinic acid (QA), which relieves the repression by QS. (C) Using GAL4/GAL80 to generate tissues specific expression. When GAL4 and GAL80 expression is driven using different promoters with overlapping expression patterns, expression from UAS-driven genes will only occur in tissues that have GAL4 without GAL80.

Figure 13

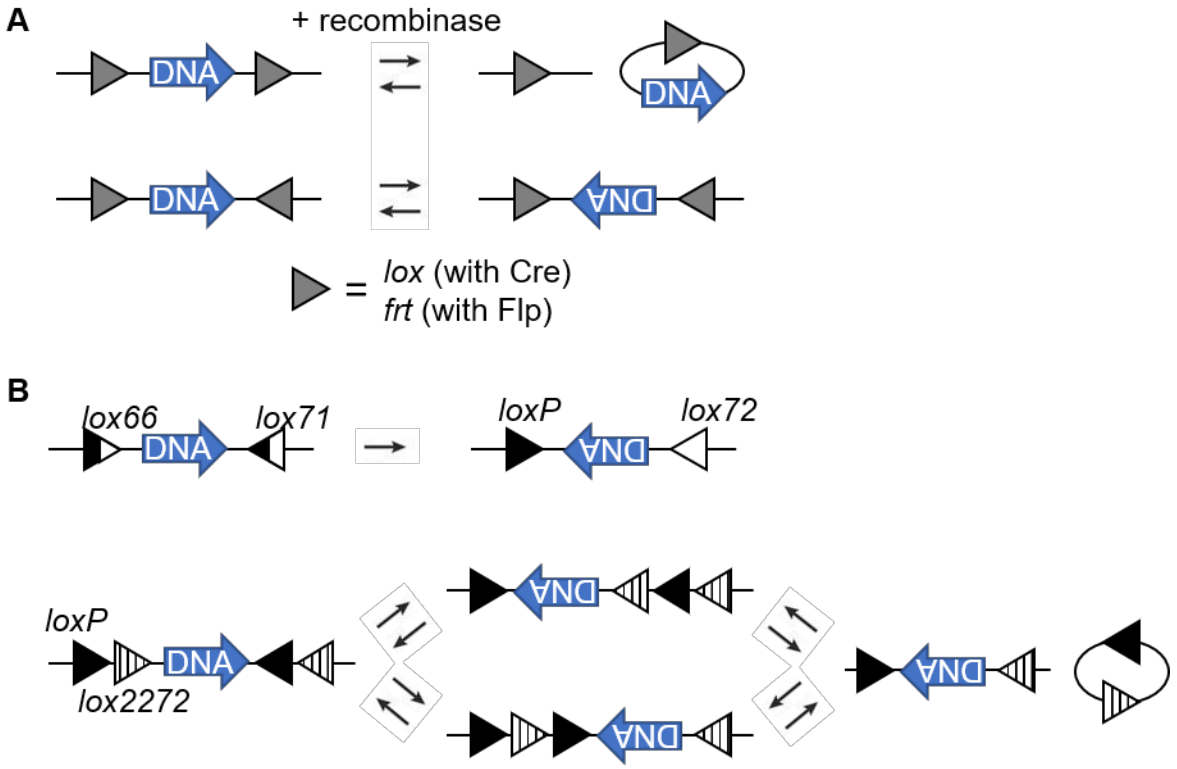

Figure 13. Conditional DNA editing using site-specific DNA recombinases. (A) Site-specific recombinases, such as Cre or FRT, induce recombination of DNA between short, specific sites called lox or frt, respectively. Recombination between sites in the same orientation results in the intervening sequence being excised and circularized; while this process is reversible, the circular DNA is generally lost in vivo or ex vivo. Recombination between sites in the opposite direction induces a reversible inversion of the intervening sequence. (B) Two common strategies exist to induce irreversible sequence inversion during site-specific recombination. Top, the sequence may be flanked by compatible, heterotypic lox variants that recombine to form new, incompatible variants during the inversion event. Bottom, two pairs of lox sites with inter-variant incompatibility may be used to generate a two-step process; in the first step, a reversible recombination event inverts the DNA between one pair of the lox variants, and in the second step, and excision event between the other pair of lox variants excises one of each variant lox site. The DNA sequence remains inverted between two incompatible lox variant sites.

Chapter 2: Floxed exon (Flexon): a flexibly-positioned stop cassette for recombinase-mediated conditional gene expression

The following chapter contains a paper published in *PNAS* (Shaffer and Greenwald, 2022).

I am responsible for all of the experiments and data presented in this chapter.

2.1 Summary

Conditional gene expression is a powerful tool for genetic analysis of biological phenomena. In the widely-used "lox-stop-lox" approach, insertion of a stop cassette consisting of a series of stop codons and poly-adenylation signals flanked by *lox* sites into the 5' untranslated region of a gene prevents expression until the cassette is excised by tissue-specific expression of Cre recombinase. Although lox-stop-lox and similar approaches using other site-specific recombinases have been successfully used in many experimental systems, this design has certain limitations. Here, we describe the Floxed exon (Flexon) approach, which uses a stop cassette composed of an artificial exon flanked by artificial introns, designed to cause premature termination of translation and nonsense-mediated decay of the mRNA, and allowing for flexible placement into a gene. We demonstrate its efficacy in *C. elegans* by showing that, when promoters that cause weak and/or transient cell-specific expression are used to drive Cre in combination with a *gfp(flexon)* transgene, strong and sustained expression is obtained in specific lineages. We also demonstrate its efficacy in an endogenous gene context: we inserted a *flexon* into the Argonaute gene *rde-1* to abrogate RNAi, and restored RNAi tissue-specifically by expression of Cre. Finally, we describe several potential additional applications of the Flexon approach, including more precise control of gene expression using intersectional methods, tissue-specific protein degradation, and generation of genetic mosaics. The Flexon approach should be feasible in any system where a site-specific recombination-based method may be applied.

Significance Statement

Tools that afford spatiotemporal control of gene expression are crucial for studying genes and processes in multicellular organisms. Stop cassettes consist of exogenous sequences that interrupt gene expression, and flanking site-specific recombinase sites to allow for tissue-specific excision and restoration of function by expression of the cognate recombinase. We describe a stop cassette called a *flexon,* composed of an artificial exon flanked by artificial introns that can be flexibly positioned in a gene. We demonstrate its efficacy in *C. elegans* for lineage-specific control of gene expression and for tissue-specific RNAi, and discuss other potential uses. The Flexon approach should be feasible in any system amenable to site-specific recombination-based methods and applicable to diverse areas including development, neuroscience, and metabolism.

2.2 Introduction

Conditional gene expression is an important tool for understanding how genes and proteins function in different tissues, lineages, and stages of development in complex organisms. Traditionally, control of gene expression is achieved by using regulatory regions derived from genes that are expressed in specific spatial and temporal patterns. However, the characterized regulatory regions do not always have the ideal expression pattern, and often trade-offs must be made between expression level and spatiotemporal specificity.

To address some of these limitations, we devised a variation on the stop cassette, a sequence that inhibits expression that can be removed by tissue-specific drivers of site-specific recombinase systems. In the widely-used lox-stop-lox system, the stop cassette generally consists of tandemly repeated poly-adenylation signals flanked by *lox* target sequences of Cre

recombinase, that is inserted into the 5' UTR of a gene of interest; tissue-specific expression of Cre leads to excision of the cassette to restore gene expression (Jackson et al., 2001; Lakso et al., 1992; Madisen et al., 2010; Maxwell et al., 1989; van der Vaart et al., 2020). Similar stop cassettes have also been used with the Flp/*frt* system (Potter et al., 2010; Struhl and Basler, 1993), and variations include the coding region for a selectable or visible marker within the cassette for easy identification of recombination events (Basler and Struhl, 1994; Cardot-Ruffino et al., 2020; Davis et al., 2008; Lyznik et al., 1993; Macosko et al., 2009; Madisen et al., 2010; Muñoz-Jiménez et al., 2017; O'Gorman et al., 1991; Voutev and Hubbard, 2008). In all of these cases, the stop cassette causes a transcriptional stop prior to the first exon, blocking expression of the gene, but when the recombinase is provided through a separate driver, the cassette is excised and the gene of interest is expressed. Stop cassettes are also used in transgenes to generate spatiotemporal specificity via tissue-specific recombinase drivers, and high expression levels by placing the cassette between the coding region and a strong promoter. For example, conditional control of transgene expression has been accomplished in mice by inserting transgenes with stop cassettes into the ROSA26 locus, a neutral locus with the potential for mid-level expression in multiple tissues after Cre-mediated excision of the stop cassette (Chu et al., 2016; Friedrich and Soriano, 1991; Hitoshi et al., 1991; Soriano, 1999; Xiao et al., 2007).

Stop cassettes that rely on transcription termination share certain limitations. Unwanted expression of the gene can occur from incomplete abrogation of transcription and translational initiation downstream of the stop cassette. Leaky expression has also been observed from read-through transcription that results from incomplete recombination between sequence repeats within the stop cassette (Bapst et al., 2020). While leaky expression is the chief concern for stop cassette usage in transgenes, further limitations apply when using a stop cassette in an

endogenous context. Different isoforms of a gene may have varying start sites, potentially complicating the application of lox-stop-lox to create likely null alleles. In addition, the 5' UTR may also contain uncharacterized but important regulatory sequences; in *C. elegans*, these could include trans-splicing signals upstream of conventional genes and internal to operons (reviewed in Arribere et al., 2020). Placing a stop cassette into these sequences could alter expression of the downstream gene; even after the cassette is excised, the *lox* scar could disrupt important regulatory sequences.

Here, we outline a strategy for a stop cassette that increases insertion site flexibility for both transgenes and endogenous genes, while retaining spatiotemporal control of expression. We call this strategy "Flexon," for "Floxed exon," in which we engineer a stop cassette that includes an artificial exon designed to prevent protein translation by causing premature termination in all three reading frames and to trigger nonsense-mediated decay of the mRNA that contains it. A *flexon* can be inserted into an intron or exon of a gene, providing different options for its placement within a transgene or endogenous locus. We demonstrate the efficacy of the Flexon approach for creating bright lineage markers and for abrogating function of an endogenous Argonaute gene to allow restoration of function for tissue-specific RNAi, and describe other potential applications of Flexon for genetic analysis.

2.3 Results

General design considerations

As with other stop cassettes, the principle behind the *flexon* is that it should prevent target gene expression in the absence of tissue-specific recombinase-mediated excision. In addition, the *flexon* is designed to be versatile regarding where it can be inserted in an open reading frame,

and prevent ectopic gene expression due to spurious initiation downstream of the cassette. Furthermore, although we have used *Cre-lox* in this study, the Flexon approach is compatible with any site-specific recombination system. We note that with regard to nomenclature, we use "Flexon" to describe the approach and "*flexon"* for the cassette used to create a new genotype.

Any *flexon* contains an artificial exon containing one or more stop codons flanked by artificial introns (Fig. 1A). Each flanking intron of the cassette contains a single *lox* site, and both *lox* sites are oriented in the same direction to allow for excision of the stop sequence in the exon (Dickinson et al., 2015). Due to the flanking introns, the stop sequence is spliced into the transcript if the cassette is inserted into an exon or an intron, allowing for flexible placement within the gene of interest (Fig. 1A).

A *flexon* is designed to block gene expression at the level of translation instead of transcription. The artificial exon contains redundant mechanisms designed to halt translation of the protein: it contains stop codons both in-frame and out-of-frame relative to the gene of interest, and creates a frameshift that introduces additional stop codons downstream (Fig. 1B). Since the *flexon* exon is a single, short, non-repetitive sequence, it is relatively easy to clone and adjust (see SI Appendix), and presumably would not be subject to incomplete recombination of repetitive stop sequences (Bapst et al., 2020). If the initial premature stop is read through, the subsequent frameshift mutations would be expected to create a non-functional protein. Furthermore, it would be expected to trigger nonsense-mediated decay (NMD) of the mRNA as a further guarantee against producing a protein. We note that in order to trigger NMD, premature stop codons need to be at least 50 nucleotides upstream of the final exon junction (Thermann et al., 1998; Zhang et al., 1998). When Cre-mediated recombination occurs, the exon with the stop

sequence is removed from the DNA sequence, leaving a single artificial intron with a *lox* scar in the middle and restoring the reading frame to encode for a functional protein (Fig. 1A).

Design of the *flexon* cassette used in this study

In the test cases here, we used a *flexon* with the following sequence elements (Figs. 1B). Design considerations that may apply to other *flexon* cassettes are addressed in the Discussion and in SI Appendix.

(1) In-frame exon sequence: the exon contains a three-codon leader to a stop codon that is in frame with the coding region the gene in which it was inserted (Fig. 1B).

(2) Frameshift-generating exon sequence: we used 62 bp of sequence from the neutral 3' UTR from *tbb*-2 (Merritt et al., 2008) to cause a frameshift of the downstream coding region (Fig. 1B). The total length of the exon sequence is the same as the 2nd exon in a widely-used, artificial intron-containing form of *gfp* (Dickinson et al., 2015) to ensure it is of sufficient length to be spliced into the mRNA. The length of the exon was kept as small as possible to ensure efficient Cre-mediated excision, facilitate cloning, and promote homologous repair for endogenous gene insertion.

(3) Intron sequences: the artificial introns were derived from a self-excising drug selection cassette (Dickinson et al., 2015). Artificial introns of similar sequences (Fire Vector Kit, 1995) are commonly used for transgenes in *C. elegans* because they demonstrate efficient splicing, due to the short sequence length and canonical splice acceptor and donor sequences.

(4) *lox* site selection: we used the *lox* variant *lox2272* to avoid recombination with *loxP* sites in existing transgenes or engineered loci we routinely use in our work.

Using the Flexon approach in a *gfp(flexon)* transgene for strong, Cre-mediated, tissue-specific expression of GFP

We replaced the first or second intron in codon-optimized GFP sequences typically used in *C. elegans* transgenes (see Materials and Methods) to create "*gfp(flexon)*" sequences (shown schematically in SI Appendix, Fig. S1) and used the strong ubiquitous promoter *rps-27p* (Giordano-Santini et al., 2010) to drive expression in all somatic cells. The resulting *rps-27p*::*gfp(flexon)* transgenes produce no or minimal visible GFP fluorescence on their own (SI Appendix, Fig. S2), indicating little to no ectopic expression in the absence of Cre. We then combined *rps-27p::gfp(flexon)* with two different Cre drivers that were made using tissue-specific promoters that drive weak and/or transient expression, as described below. The results were remarkable: the expected lineages were brightly marked throughout larval development (Figs. 2, 3 and SI Appendix, Fig. S3).

The first driver we used would be predicted to result in tissue-specific excision of *gfp(flexon)* in all somatic gonadal cells. A *C. elegans* L1 larvae hatches with two somatic gonad precursor cells, Z1 and Z4, which generate all of the structures of the somatic gonad during postembryonic development (Fig. 2A). During the first phase of gonadogenesis, Z1 and Z4 give rise to twelve cells that form the somatic gonad primordium in the L2 stage, and the somatic gonad blast cells divide in the L3 stage and give rise to many additional cells (Kimble and Hirsh, 1979).

The 5' regulatory region for the *ckb-3* gene, denoted *ckb-3p*, drives expression in the somatic gonad precursor cells Z1 and Z4 in embryos and L1 larvae, but expression rapidly diminishes as the lineage progresses (Kroetz and Zarkower, 2015). When *ckb-3p* is used to drive 2xNLS::GFP, nuclear GFP is readily visualized in Z1 and Z4 in the L1 stage, but progressively

dims and is essentially undetectable by the time the somatic gonad primordium has formed in the L2 stage (Fig. 2A, B). The combination of a *ckb-3p::Cre* driver that expresses a form of Cre recombinase optimized for *C. elegans* (Ruijtenberg and van den Heuvel, 2015; see Materials and Methods) with *rps-27p::2xnls::gfp(flexon)* produces sustained, strong, and specific expression of 2xNLS::GFP in the somatic gonad throughout development (Fig. 2B, SI Appendix, Fig. S3). Furthermore, when we used a histone tag to stabilize GFP as well as for nuclear localization [*rps-27p::gfp(flexon)::h2b*], fluorescence intensity was sufficient for visualization at lower exposure, and even using a dissecting microscope (Fig. 2B, C). Excision frequency approached 100% for both *gfp(flexon)* transgenes; animals without excision in both the Z1 and Z4 lineages were too rare to accurately measure excision rate.

The second driver we used would be expected to result in tissue-specific excision of *gfp(flexon)* in all vulval precursor cells (VPCs). The VPCs are six polarized epithelial cells, named P3.p-P8.p, that are born in the L1 stage and remain quiescent until the L3 stage. At that time, P5.p, P6.p, and P7.p are induced by EGFR and LIN-12/Notch signaling to adopt vulval fates; the descendants of these cells form the vulval primordium in the L4 stage (Gauthier and Rocheleau, 2017; Shin and Reiner, 2018; Sternberg, 2005). The other VPCs, P3.p, P4.p and P8.p, do not receive spatial patterning signals and divide once to generate daughter cells that fuse with the major hypodermal syncytium (P3.p sometimes fuses directly, without dividing). A composite regulatory region made from the 5' flanking region and introns of the *lin-31* gene, called *lin-31p* (de la Cova and Greenwald, 2012; Luo et al., 2020; Fig. 3A; Tan et al., 1998), displays a dynamic pattern of expression. GFP fluorescence is visible after the cells are born in the late L1 stage and appears uniform in all VPCs during the L2 stage; at the time VPCs commit to their fates in the L3 stage, fluorescence begins to decrease visibly in P5.p, P6.p, and P7.p, and

progressively dims and becomes undetectable as their lineages progress (Luo et al., 2020; Fig. 3B). Fluorescence in P3.p, P4.p and P8.p remains stronger than in the other VPCs at the beginning of the L3 stage but becomes undetectable after they divide in the L3 stage. By contrast, when *rps-27p*::*2xnls::gfp(flexon)* was combined with a *lin-31p::Cre* driver, GFP was strongly, uniformly, and continuously expressed in the VPCs and their descendants (Fig. 3B, C). As in the somatic gonad, the use of a histone tag to stabilize GFP results in fluorescence visible using a dissecting microscope.

Using the Flexon approach in an endogenous gene: an *rde-1(flexon)* allele enables tissue-specific RNAi

In *C. elegans,* RNAi is usually performed by feeding worms with bacteria that express double-stranded RNA for a gene of interest (Timmons et al., 2001). Tissue-specific RNAi has been accomplished by selectively expressing RDE-1/Argonaute in an *rde-1* hypomorphic or null mutant background (Qadota et al., 2007; Watts et al., 2020b). As with any other transgenic method, rescue experiments are affected by the strength and specificity of available regulatory regions; for example, our lab has had difficulty achieving effective tissue-specific RNAi using *ckb-3p* or *lin-31p* to drive RDE-1 expression in an *rde-1* null mutant background. The transgene-based Flexon approach described above would be one way to circumvent this problem, but for proof-of-concept to show that a *flexon* works in an endogenous gene context, we created an *rde-1(flexon)* allele that would allow for a physiological level of RDE-1 protein to be restored after tissue-specific, Cre-mediated recombination.

Design of the endogenous* rde-1(flexon) *allele. We used CRISPR/Cas9 to replace the small ninth intron of the endogenous locus of *rde-1* with the same *flexon* cassette used in the

gfp(flexon) transgenes (Fig. 4A). The resulting allele, *rde-1(ar660)*, is hereafter referred to as *rde-1(flexon)*. The position was chosen to disrupt the catalytic PIWI domain, as the goal was to create a sufficiently strong loss-of-function allele that would greatly reduce or eliminate gene activity even if there was a low level of leakiness in this gene context (see also "Limitations" below).

Design of the test of* rde-1(flexon) *for somatic gonad-specific RNAi. To create a strain suitable for somatic gonad-specific RNAi, we combined the endogenous *rde-1(flexon)* allele with the *ckb-3p::Cre* driver described above. The transcription factor HLH-2/E2A, an essential gene for early embryonic development and for gonadogenesis (Krause et al., 1997), offered an incisive test case. When L4 larvae are fed bacteria expressing double-stranded RNA ["*hlh-2(L4-RNAi)*"], all offspring arrest during embryogenesis (Kamath et al., 2000; Fig. 4B). When embryonic lethality is bypassed by feeding L1 larvae with bacteria expressing double-stranded RNA for *hlh-2* [*"hlh-2(L1-RNAi)"*], the treated larvae become sterile adults that lack or have compromised Distal Tip Cells (DTCs), which serve as the germline stem cell niche (Karp and Greenwald, 2004; Fig. 4B); sterility can be readily assessed at the dissecting microscope level. *hlh-2* is also required in the DTCs to lead gonad arm outgrowth in the L3 and L4 stages, so partial loss-of-function may also be readily assessed by examining the extent of gonad arm outgrowth in adults in the compound microscope. We therefore tested whether *rde-1(flexon)* on its own prevents these deleterious effects of *hlh-2(RNAi)* and if early lethality is prevented but highly penetrant defects in gonad development result when *rde-1(flexon)* is combined with *ckb-3p::Cre.* We also performed additional supplemental assessments as described below.

***rde-1(flexon)* strongly reduces *rde-1* activity.** We tested whether inserting a *flexon* into the endogenous *rde-1* gene causes a strong loss-of-function phenotype, a necessary prerequisite

for creating a system for tissue-specific RNAi. When we performed *hlh-2(L4-RNAi)* by treating N2 L4 larvae, all of their progeny arrested during embryogenesis (Fig. 4C). By contrast, when we treated *rde-1(flexon)* L4 larvae, all of their progeny hatched (Fig. 4C).

Similarly, when we performed *hlh-2(L1-RNAi)* on N2 wild-type larvae, we observed highly penetrant sterility which was not observed when *hlh-2(L1-RNAi)* was performed on *rde-1(flexon)* hermaphrodites (Fig. 4C). Treated N2 larvae also displayed a highly penetrant lack of gonad arm extension (Fig. 4C), whereas the treated *rde-1(flexon)* larvae had normal gonad arms, with a single exception of an individual that had one normal and one abnormal gonad arm that extended but did not turn, consistent with reduced *hlh-2* activity after the DTC had formed (Karp and Greenwald, 2004). Similarly, RNAi directed against *hlh-12*, which encodes the dimerization partner for HLH-2 for gonad arm extension (Tamai and Nishiwaki, 2007), had a low proportion of "escapers": 1/104 (1%) gonad arms of treated *rde-1(flexon)* L1 larvae had a DTC with abnormal extension. Because most animals are unaffected, we infer that the *rde-1(flexon)* allele strongly abrogates *rde-1* activity, but the low proportion of escapers suggests that it may not be a true null allele. While there may be some situations in which a low background of residual *rde-1* activity may be problematic (Watts et al., 2020a), we demonstrate below that it is eminently feasible to use *rde-1(flexon)* for tissue-specific RNAi.

We also tested two additional genes that have a cellular focus in tissues other than the somatic gonad: *dpy-10*, a cuticle collagen (Levy et al., 1993), and *pos-1*, an RNA-binding protein required for lineage specification in the early embryo (Tabara et al., 1999). All progeny of treated N2 hermaphrodites displayed the expected phenotype: a Dumpy body shape for *dpy-10(RNAi)* (84/84), and embryonic lethal progeny for *pos-1(RNAi)* (716/716 arrested embryos). By contrast, the progeny of treated *rde-1(flexon)* hermaphrodites were generally unaffected: for

dpy-10(RNAi), 0/462 progeny were Dpy, and for *pos-1(RNAi)*, 4/604 (0.7%) arrested embryos were observed (we did not examine these arrested embryos for specific *pos-1*-associated defects). These results support the inference from *hlh-2(RNAi)* that insertion of the *flexon* into *rde-1* severely compromises its activity.

Test of endogenous* rde-1(flexon) *for tissue-specific RNAi in the somatic gonad. We tested whether restoring *rde-1* function specifically to the somatic gonad via excision of the *flexon* using the *ckb-3p::Cre* driver would result in highly penetrant, gonad abnormalities. As Cre is expressed in Z1 and Z4, we would expect that RNAi would be restored prior to the birth and specification of the DTCs. Indeed, *hlh-2(L1-RNAi)* of *rde-1(flexon); ckb-3p::Cre* resulted in sterility and lack of gonad arms, indicating that RNAi was efficiently restored by excision of the *flexon* (Fig. 4C). Moreover, all progeny of *hlh-2(L4-RNAi)* of *rde-1(flexon); ckb-3p::Cre* hermaphrodites survived (Fig. 4C), indicating that restoration of RNAi was specific to the gonad.

The observed bypass of embryonic lethality by *hlh-2(RNAi)* is strong evidence that restoration of RNAi by the *ckb-3p::Cre* driver is limited to the gonad. We corroborated this inference by performing *dpy-10* and *pos-1* RNAi on the *rde-1(flexon); ckb-3p::Cre* strain: 555/556 *dpy-10(RNAi)* individuals were non-Dpy and 424/433 progeny of *pos-1(RNAi)* hermaphrodites were viable, indicating that RNAi had not been restored to the hypodermis and germ line.

Tissue-specific restoration of* rde-1 *activity to body wall muscle. We performed an additional test of tissue-specific RNAi by restoring *rde-1* activity to the body wall muscles using *hlh-1p::Cre*, which drives excision in the MS muscle founder cell lineage (Krause et al., 1994; Murray et al., 2008; Tenen and Greenwald, 2019), and performing RNAi against *unc-22*, which encodes the body wall muscle structural protein Twitchin/Titin (Moerman et al., 1988). *unc-*

22(RNAi) causes a fully penetrant Twitcher phenotype when N2 (15/15) or *rde-1(ar660); hlh-1p::Cre* hermaphrodites (16/16) are treated, but does not cause a phenotype when *rde-1(ar660)* (0/16) or *rde-1(ar660); ckb-3p::Cre* (0/13) hermaphrodites are treated. Thus, tissue-specific RNAi was achieved in this additional cell context.

Conclusions: We have provided proof-of-concept that the Flexon approach is applicable to endogenous genes, the main goal of this experiment, by showing that insertion strongly reduces *rde-1* gene activity and that expression of tissue-specific Cre drivers restore gene activity. Our analysis suggests that *rde-1(ar660[flexon])* is a strong loss-of-function allele that should facilitate many tissue-specific RNAi applications and be a valuable addition to the tissue-specific RNAi toolkit for *C. elegans*. It should be straightforward to assess the feasibility of using *rde-1(ar660[flexon])* for any specific purpose by performing RNAi in the absence of a Cre driver at the outset of a study to confirm that the associated phenotype is not observed from potential low-level leaky expression at significant penetrance (as indeed would also be necessary for transgene rescue-based approaches).

2.4 Discussion

Stop cassettes are a versatile method for achieving conditional gene expression, a powerful approach for genetic analysis of any biological process. Here, we developed and tested a stop cassette we call a *flexon*, composed of an artificial exon flanked by artificial introns and site-specific recombinase sequences. A *flexon* can be flexibly positioned in a gene to prevent translation of its protein product until excised by tissue-specific expression of the cognate recombinase. We have provided a prototype for strong, tissue-specific expression of a desired protein by achieving strong tissue- or lineage-specific expression of GFP using weaker, more

transiently expressed Cre drivers. We also inserted a *flexon* into the endogenous locus for *rde-1*, a gene required for RNAi, and showed that gene function was abrogated in the absence of Cre, but restored in specific tissues in the presence of a Cre driver. While it was used here as proof-of-concept for *flexon* function in an endogenous gene context, the *rde-1(flexon)* allele will be useful for tissue-specific RNAi in *C. elegans*. In this Discussion, we first generalize the design consideration for other *flexon* cassettes and then provide further examples of how the Flexon approach could be adapted to improve the efficiency of commonly used genetic tools and for additional genetic approaches in *C. elegans* and other experimental systems. Finally, we describe some potential limitations that should be borne in mind when applying the Flexon approach.

Design considerations for other *flexon* cassettes

In principle, a *flexon* may be used with any protein-coding gene. In Fig. 5A, we show several adjustments that may be made to the *flexon* cassette we used here, and highlight here and in the SI Appendix considerations that should be borne in mind when designing a *flexon*. In addition to cassette adjustments, when used in a transgene, different ubiquitous or more restricted promoters may be used to tune the level or tissue in which the *flexon*-containing construct is expressed after excision of the cassette (Fig. 5B; see also SI Appendix, Fig. S3).

(1) The artificial exon sequence design should be tested *in silico* by conceptual translation to ensure that it (a) causes a frameshift downstream and (b) introduces stop codons in all three reading frames. The exon design used in this study contains stop codons in two reading frames within the exon; stop codons in the third reading frame were generated in downstream

exons by the frameshift. The exon sequence may be modified to include additional out-of-frame stop codons within the exon if necessary.

(2) The specific pair of *lox* sequences selected to flank the exon can be chosen to allow for the possibility to excise multiple *flexon* cassettes simultaneously, or to guard against causing intergenic DNA recombination in the presence of other genes that have *loxP, loxN, or lox551* sequences (such as the loxP scar left from the self-excising cassette method of genome engineering in C. elegans; Dickinson et al., 2015). Alternatively, *frt* or other site-specific recombinase sequences can be used in place of *lox* sequences for spatiotemporal control of recombination and/or for differential control when combining different *flexon*-containing transgenes.

(3) Insertion of a *flexon* into an exon can be achieved by appending a splice donor site upstream of the first *lox* sequence and a splice acceptor sequence downstream of the second *lox* site. The introns here may be optimized in length or content for high splicing efficiency in alternate applications within *C. elegans* or for other organisms (see SI Appendix).

(4) When information about protein functional domains is available, it is preferable to insert the *flexon* such that expression from potential cryptic, downstream start sites would not result in an active protein.

Once a *flexon* has been designed and the desired insertion obtained, it is important to assess how well gene expression or activity has been abrogated by insertion of the *flexon* as an important control for tissue-specific excision experiments (see "Limitations" below).

Potential applications facilitated by incorporating a *flexon* into endogenous genes or transgenes

The Flexon approach may be incorporated into many different established strategies for manipulating gene activity or expression. We give some examples here, emphasizing *C. elegans* but applicable to other experimental systems.

Increasing the level of limiting effectors for tissue-specific protein degradation: Targeted protein degradation using natural degron/ubiquitin ligase pairs is a powerful method for studying gene function. Several degron/ubiquitin ligase pairs have been successfully used in *C. elegans*: the TIR1/AID system [applied to *C. elegans* by (Zhang et al., 2015)], the ZIF-1/ZF1 system (Armenti et al., 2014), and converting GFP itself into a degron by replacing the interaction domain of an E3 ubiquitin ligase with an anti-GFP nanobody (Wang et al., 2017b). However, the amount of the ubiquitin ligase expressed has been reported to be limiting for degradation (Aghayeva et al., 2021; Ashley et al., 2021; Dos Santos Maraschin et al., 2009), so we anticipate that the Flexon approach will facilitate such manipulations by enabling stronger tissue-specific expression of the ubiquitin ligase. Furthermore, by using different *lox* variants, Cre can be used to delete a floxed, degron-tagged gene while simultaneously using a *ubiquitin ligase(flexon)* to quickly eliminate perduring protein, a strategy that has been demonstrated to be effective when low residual protein levels obscure the null phenotype (van der Vaart et al., 2020).

Intersectional approaches to conditional gene expression: One way to achieve specific gene expression is to use two different tissue-specific promoters that have overlapping sites of expression to drive different recombinases, e.g. combining the Cre and Flp recombinases (Anastassiadis et al., 2010; Fig. 5C; Awatramani et al., 2003; Liu et al., 2020). The flexible placement of the *flexon* (Fig. 5D) may facilitate the use of such intersectional strategies. Combinatorial recombinase approaches have been used for marking specific cell types and

lineages in mice (reviewed in Dymecki et al., 2010); in *C. elegans*, these approaches may be used to generate GFP lineage markers that require lower intensity and exposure to visualize, avoiding damage from blue-light overexposure (Edwards et al., 2008; Ward et al., 2008).

Engineering genomic loci: For engineering genomic loci, the flexibility in placement of a *flexon* offers several potential advantages over stop cassettes that are placed in a 5' UTR. First, the Flexon approach facilitates engineering of conditional alleles for single or multiple isoforms (Fig. 5D). Second, the flexible placement reduces the chance of disrupting uncharacterized but important regulatory sequences in the 5' UTR by the single recombination site "scar" left after excision of the cassette. Third, in many cases introns are better defined than 5' UTRs, especially in *C. elegans* where about 84% of genes are trans-spliced by the addition of a splice-leader sequence to the 5' end of pre-mRNAs (Tourasse et al., 2017), and about 15% of genes are expressed from operons, in which a polycistronic pre-mRNA is processed into separate transcripts by trans-splicing of the downstream gene (Allen et al., 2011), with the trans-splice acceptor for the downstream gene embedded in a relatively short sequence that also contains a 3' UTR for the upstream gene. Thus, a *flexon* can be inserted into a trans-spliced gene, or into either gene of an operon, without potentially compromising regulatory sequences (Fig. 5D).

Finally, we note that manipulating endogenous gene expression using the Flexon approach offers an alternative to transgene-based methods for assessing tissue-specific rescue and creating genetic mosaics that may be advantageous in certain situations. For example, transgenes used for conventional tissue-specific rescue may not be expressed at endogenous levels, and when genes have multiple isoforms, the isoform selected may influence the results. By contrast, insertion of a *flexon* into an intron of an endogenous gene will allow for all isoforms

that share that intron to be expressed under control of its natural regulatory elements after excision using a tissue-specific Cre driver (Fig. 5D).

Potential Limitations

Although the Flexon approach addresses some of the issues that have been observed with traditional lox-stop-lox, it shares other limitations inherent to any stop cassette method. One is that site-specific recombination is irreversible and therefore cannot be used for dynamic control of gene expression by itself, although it may facilitate the implementation of dynamic methods such as AID, as described above. Another limitation is that transient or variable low-level expression that is not normally evident when the promoters are identified using fluorescent reporter genes may be more apparent when they are used to drive Cre (Tenen and Greenwald, 2019), so tissue-specific promoters used to drive site-specific recombinases may not be as specific as desired. A third limitation is that expression in different cells of a tissue may be uneven shortly after recombination events due to asynchronous cassette excision or when occasionally excision does not occur on both chromosomes in a cell. However, recombination tends to be very efficient given the small size of the *flexon*, so for many applications, this limitation may not be an issue.

A final limitation shared with other stop cassette approaches is potential "leakiness." Although we have attempted to address the causes of leakiness in traditional lox-stop-lox while also implementing the advantages of the flexible insertion of the stop cassette that a *flexon* offers, there is still the potential for leaky expression from a fortuitous downstream translational start site or alternative splicing/exon-skipping that excludes the *flexon* from the final mRNA transcript. Such exon-skipping may account for the rare "escapers" we observed when

evaluating *rde-1(flexon)* for abrogating RNAi, and may depend on the specific gene, the specific tissue, or the specific *flexon* design itself. For practical purposes, whether leakiness is a problem may be easily addressed by examining the phenotype of novel endogenous *flexon* alleles. If incomplete penetrance is an issue, repositioning the *flexon*, adding an additional *flexon,* or combining the Flexon approach with another conditional method such as AID (van der Vaart et al., 2020) are possible approaches to reducing such background activity.

One other consideration must be borne in mind when manipulating endogenous genes: insertion of a *flexon* will abrogate gene function, so if a lethal or sterile phenotype is anticipated, marked balancer chromosomes (Dejima et al., 2018; Iwata et al., 2016) or rescuing transgenes (such as extrachromosomal arrays that can be readily eliminated) should be included to circumvent this complication.

2.5 Materials and Methods

C. elegans strains

C. elegans was grown on 6 cm NGM plates seeded with *E. coli* OP50 and maintained at 20°C. Strain N2 (wild-type; Brenner, 1974), and two of the Cre drivers used in this study, were previously described: *arTi237 [ckb-3p::Cre(opti)::tbb-2 3' UTR] X* is a single-copy insertion transgene made as described in (Tenen and Greenwald, 2019), and mapped as part of this study, and *arTi235 [hlh-1::Cre(opti)::tbb-2 3' UTR]* was described in (Tenen and Greenwald, 2019). Cre(opti) refers to the codon-optimized Cre recombinase described previously (Ruijtenberg and van den Heuvel, 2015). The generation of other single-copy insertion transgenes and the allele

rde-1(ar660[flexon]) is described below. The full genotypes of strains used in this study are listed in SI Appendix, Table S1.

Generation of single-copy insertion transgenes

The plasmids pHK001 [*rps-27p::gfp(flexon)::his-58::unc-54 3' UTR*], pJS110 [*ckb-3p::2xnls::gfp::unc-54 3' UTR*], pJS145 [*rps-27p::2xnls::gfp(flexon)::unc-54 3' UTR*] (Addgene #179159), and pJS146 [*lin-31p::2xnls::gfp::unc-54 3' UTR*] were made in a miniMos vector backbone [pCFJ910] (Frøkjær-Jensen et al., 2014) using Gibson Assembly (NEB Inc., MA) and confirmed by sequencing. pJS110, pJS145, pJS146 contain a *C. elegans* codon-optimized GFP sequence tagged with an N-terminal SV40 and C-terminal *egl-13* nuclear localization sequences (*nls*), regulated by the neutral 3' UTR from *unc-54* (Hunt-Newbury et al., 2007). pHK001 uses a *C. elegans* GFP sequence with slightly different codon-optimization (Dickinson et al., 2015). Plasmids were injected into N2 hermaphrodites. Random, single-copy insertions were obtained and mapped using the standard protocol (Frøkjær-Jensen et al., 2014).

Generation of *rde-1(ar660)*, the endogenous *rde-1(flexon)* allele

The repair template plasmid pJS155 was made using Gibson cloning to insert the following sequences into a pBluescript vector: the final 500 bp of *rde-1* exon 9, a *flexon* cassette, and the first 500 bp of *rde-1* exon 10. The arrangement of the sequences in pJS155 will effectively replace the native intron 9 of *rde-1* with the *flexon* cassette when the plasmid is used as a repair template. Intron 9 lies between two exons that together encode the catalytic PIWI domain of RDE-1.

To generate *rde-1(ar660)*, an injection mix containing pJS155 (50 ng/µl) as the repair template and a crRNA (IDT, Inc.; tgagtatttaaaagatctctgttttagagctatgct) was prepared according to an established protocol (Ghanta and Mello, 2020) and injected into the gonads of young adult N2 hermaphrodites. Animals with potential gene editing events were isolated according to the protocol, and animals homozygous for a correct *rde-1(ar660)* allele were confirmed through PCR genotyping and sequencing.

We note that we made another allele by replacing the 2nd intron of the endogenous *rde-1* locus with a *flexon* cassette. In contrast to *rde-1(ar660)*, the allele resulting from this replacement had only a weak effect on *rde-1* function. Because the 2nd intron is upstream of the exons for all the known functional domains of RDE-1, we interpret the weak phenotype as an indication that cryptic, in-frame ATG start sites downstream of the *flexon* allowed for the transcription of a mutant RDE-1 protein that retained significant activity. This concern was incorporated into Design Considerations, point (5), and reiterated in the SI Appendix.

Microscopy

C. elegans larvae were imaged for fluorescence on a Zeiss AxioObserver Z1 inverted microscope with a 63x, 1.4NA oil immersion objective equipped with a spinning disk, CSU-X1A, a laser bench rack, and a Photometrics Evolve EMCCD camera. For GFP fluorescent imaging, a 488nm, 100mW laser was used for excitation. Larvae were mounted onto 3% agar pads, and immobilized with 10 mM levamisole.

Z stacks were collected from GS9684, GS9686, GS9691, and GS9692, and GS9401 larvae (Figs. 2 and 3) with slices at 500 nm intervals and were imaged for GFP fluorescence with the following parameters: 10% laser power, 200 ms exposure (or 50 ms exposure for GS9401),

and 400 EM gain. For SI Appendix, Fig. S3, the same parameters were used, but the animal was imaged with a 40x, 1.4 NA oil immersion objective, and with 1000 nm intervals between slices. For strains GS9684, GS9692, and GS9401, the number of slices used per larva varied with the size of the gonad to fully capture the nuclei of every somatic gonad cell present. The stage of the animal was determined by the number of somatic gonad cells and somatic gonad morphology. For GS9686 and GS9691, each stack contained 26 slices, which was sufficient to image the full volume of the nuclei of every VPC or VPC descendent. The stage of the animal was determined by the number of VPCs and somatic gonad morphology.

Z stacks were collected from GS9401 and GS9407 (SI Appendix, Fig. S1) with slices at 500 nm intervals and imaged for GFP fluorescence with the following parameters: 25% laser power, 500 EM gain, and the exposure time denoted in the figure. The number of slices used per larva varied with the size of the gonad to fully capture the nuclei of every somatic gonad cell present. The stage of the animal was determined by the number of somatic gonad cells and somatic gonad morphology.

Images in Figure 2C were taken on a phone camera through the eyepiece of a Zeiss Discovery V.12 SteREO dissecting microscope, GFP470 filter, Schott ACE 1 fiber optic light source, and X-cite series 120Q fluorescent lamp illuminator. Animals to be imaged were placed on a 60mm plates filled with 1.75% agarose, and then immobilized using 10 mM levamisole.

Image Quantification

Fluorescence intensity was quantified using FIJI (Linkert et al., 2010; Schindelin et al., 2012). Z stacks were sum projected for all slices containing cells of interest. Nuclei were manually

segmented, and the mean green fluorescent background from a random region outside of the animal was subtracted from the mean green fluorescent intensity of each nucleus.

RNA interference

The following RNAi clones were used: pKMS1196, which contains the full length *hlh*-2 cDNA (Karp and Greenwald, 2003), and commercially available library clones for *unc-22, pos-1, dpy-10, and hlh-12* (Kamath et al., 2003). For feeding RNAi (Timmons et al., 2001), plates were made using NGM with 6 mM IPTG and 100 μM carbenicillin, and seeded with 70μl of overnight culture of bacteria expressing a single RNAi clone. Experiments were performed at 25°C.

To test for embryonic lethality of *hlh-2(RNAi)*, N2, GS9801 and GS9802 individual L4 larvae were placed onto RNAi plates, and then removed after one day. The number of eggs and surviving larvae on each plate were counted immediately upon removal, and then the number of surviving larvae were counted one day later. To test for sterility of *hlh-2(RNAi)*, N2, GS9801 and GS9802 embryos were isolated using a standard bleaching protocol (Stiernagle, 2006) and plated onto unseeded NGM plates. Larvae were allowed to hatch for 1 hour, isolated onto RNAi plates, and were then assessed for fertility by checking for the presence of progeny 4 days after plating (Fig 4D, E). To assess gonad arm morphology in *hlh-2(RNAi)* and *hlh-12(RNAi),* N2, GS9801, and GS9802 embryos were isolated by bleaching, plated directly onto RNAi plates, and assessed for gonad arm phenotypes 2 days after plating. Assessed phenotypes included gonad arm absence, failure to extend, failure to turn, failure to extend back to the midpoint, and the presence of abnormal bulges. The gonad arms of N2 animals on *hlh-12(RNAi)* had a very high penetrance of morphological defects (47/48).

For *unc-22(RNAi)*, individual N2, GS9801 and GS9802, and GS9831 embryos or L1 larvae were placed onto RNAi plates and assessed for twitching at the L4 stage. To determine the effect of RNAi against *dpy-10* and *pos-1*, individual N2, GS9801 and GS9802 L1 larvae were placed onto RNAi plates and removed two days later after laying eggs. The progeny were then assessed for phenotypes; dumpy for *dpy-10* RNAi and lethality for *pos-1* RNAi.

2.6 Acknowledgments

We thank Katherine Luo for generating *arTi381* and Jee Hun (Henry) Kim for help in generating *arTi361*. We also thank Michael Shen, Michelle Attner, and Catherine O'Keeffe for valuable comments on the manuscript prior to submission, Gary Struhl for valuable comments after revision, and Barth Grant, John Kim, and Ann Rougvie for critical feedback and helpful suggestions that greatly improved this work. This work was supported by R35GM131746 from the National Institute of General Medical Sciences (to I.G.), F31EY030331 from the National Eye Institute (to J.M.S.). J.M.S. was also supported by training grant T32GM008798. Some strains were provided by the CGC, which is funded by NIH Office of Research Infrastructure Programs (P40 OD010440).

Chapter 2. Figures

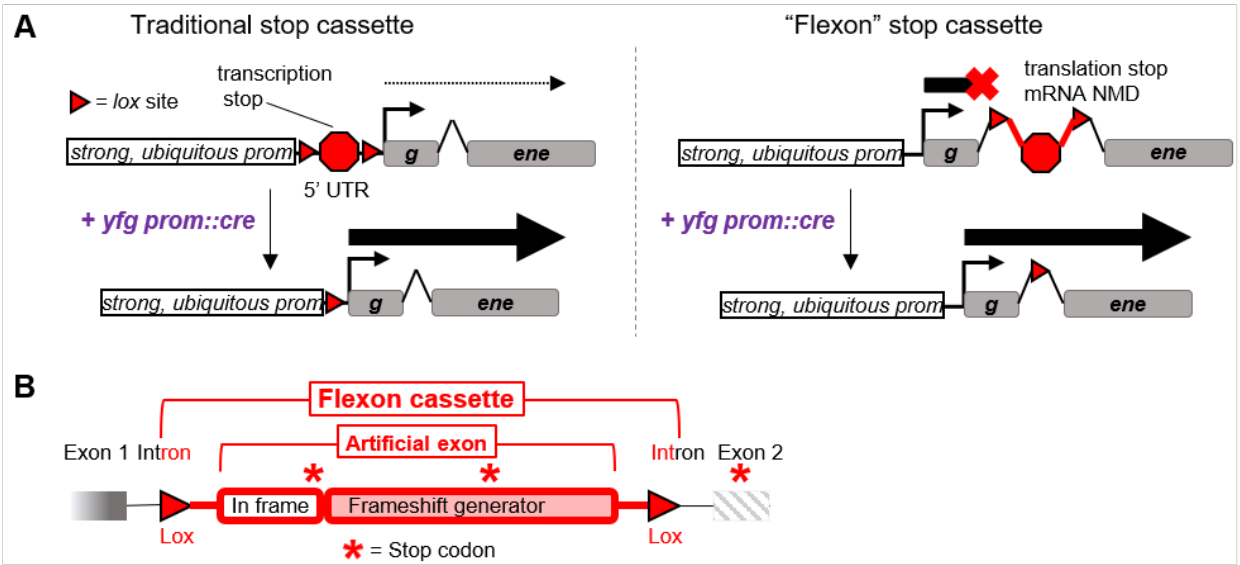

Figure 1. Design and use of a Floxed exon cassette (flexon).
(A) A traditional stop cassette (left) is placed in the 5' UTR of the gene of interest, and is designed to block gene expression through a transcriptional stop. A *flexon* stop cassette (right) is designed to abrogate gene expression by a translational stop and frameshift mutations leading to stop codons in other frames, and is also expected to result in nonsense-mediated decay (NMD) of the mRNA. Further differences are discussed in the text. Both traditional and *flexon* stop cassettes may use strong, ubiquitous promoters to drive expression in specific lineages or tissues after cassette excision by Cre recombinase driven by the promoter of "*your favorite gene*" (*yfg*). (B) In this study, the artificial exon of the *flexon* has an in-frame, three-codon leader sequence that ends with an in-frame stop codon followed by a frameshift-generating sequence that creates additional premature stop codons in all frames. The *flexon* used in this study is bounded by *lox2272* sites. Specific parameters may be varied as described in the text and SI Appendix.

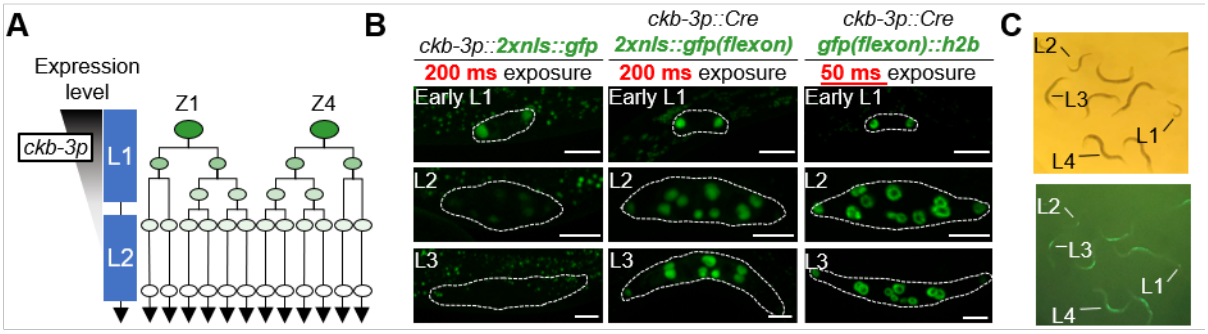

Figure 2. The Flexon approach enables strong, persistent expression of GFP in all cells of the somatic gonad lineage.
(A) *ckb-3p* drives expression of a high level of GFP specifically in the somatic gonad precursor cells Z1 and Z4 (Kroetz and Zarkower, 2015), but the level of GFP diminishes rapidly as the lineage progresses (see B, left column).
(B) GFP fluorescence from the transgene *arTi433[ckb-3p::2xnls::gfp]* (left column) is dimmer and does not persist as long as GFP fluorescence from *arTi435[rps-27p::2xnls::gfp(flexon)]* when the *flexon* excision is mediated by a *ckb-3p::Cre* driver (*arTi237*; middle column; see Materials and Methods), as seen in photomicrographs taken at the same exposure time and imaging parameters. Stabilization of GFP using a histone tag (*arTi361[rps-27p::gfp(flexon)::h2b];* right column) results in bright expression visible at a lower exposure time than *2xnls::gfp*. All scale bars are 10 μm.
(C) GFP(*flexon)*::histone in the presence of *ckb-3p::Cre* is visible on the dissecting scope at all larval stages. Magnification is 50x.

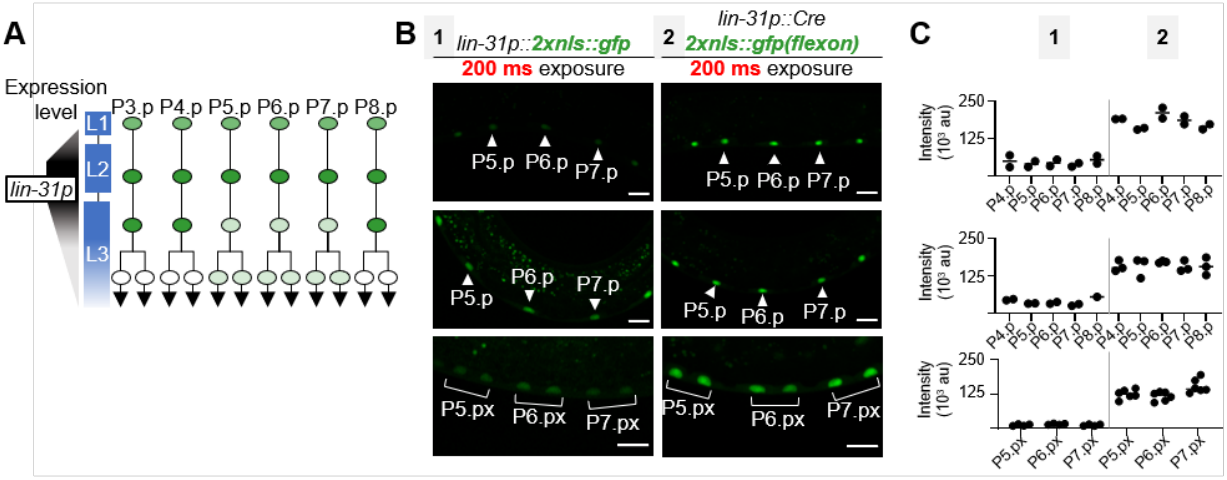

Figure 3. The Flexon approach enables strong, persistent expression of GFP in the vulval precursor cell (VPC) lineages.
(A) The *lin-31p* regulatory sequence drives expression of GFP in all VPCs in late L1 and L2, but GFP level becomes visibly non-uniform during vulval fate patterning in L3 and wanes as the lineages progress (de la Cova and Greenwald, 2012; Luo et al., 2020; Tan et al., 1998) (see B, left column).
(B) Photomicrographs of *arTi434[lin-31p::2xnls::gfp]* (left column, genotype 1), showing dynamic expression pattern of *lin-31p* schematized in A. By contrast, GFP fluorescence intensity from *arTi435[rps-27p::2xnls::gfp(flexon)]* (right column, genotype 2) is higher starting early in development, and persists strongly throughout the VPC lineages. These *flexon* excisions were mediated by the VPC Cre driver *arTi381[lin-31p::cre]*. All scale bars are 10 μm.
(C) Quantitation of several individuals of genotypes 1 and 2 shown in (B). Each dot represents one cell of one animal.

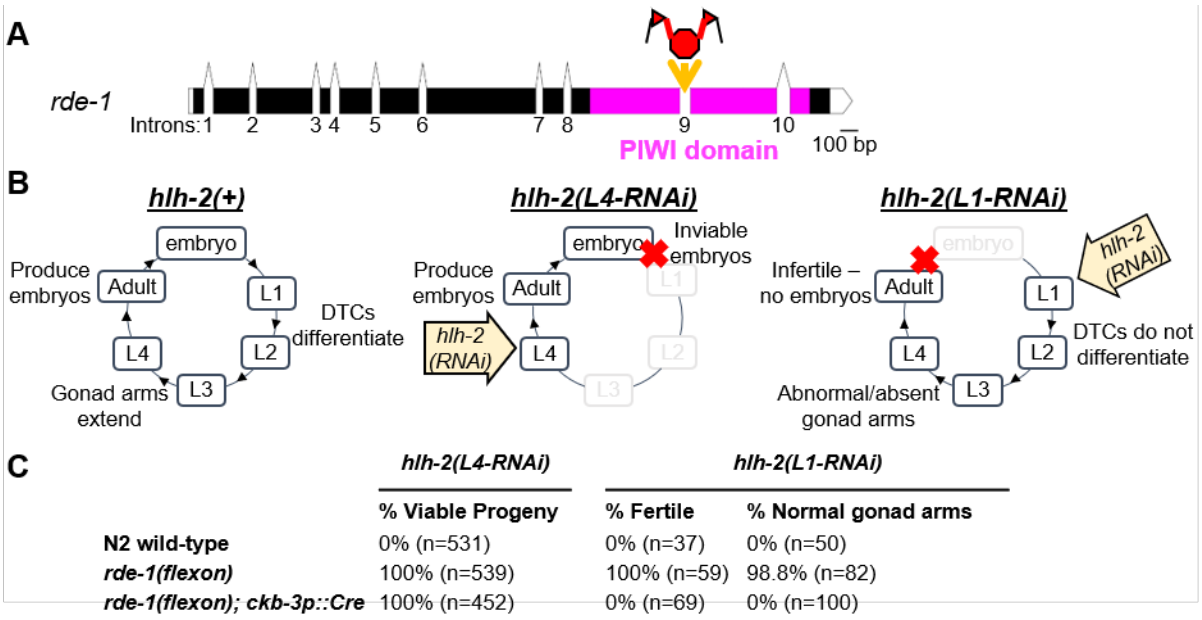

Figure 4. Tissue-specific RNAi using the endogenous rde-1(flexon) allele.
(A) The ninth intron of the endogenous *rde-1* locus was replaced with a *flexon* to generate *rde-1(ar660)*. Scale bar is 100 bp. White boxes in sequence indicate UTRs. The gene graphic was made using http://wormweb.org/exonintron.
(B) *hlh*-2 is required for viable embryogenesis and for the specification and function of the Distal Tip cells (DTCs) of the gonad, which lead proper gonad arm extension and maintain germline proliferation (left). When N2 wild-type hermaphrodites are exposed to *hlh-2* RNAi beginning in the L4 larval stage *[hlh-2(L4-RNAi)]*, their progeny arrest during embryogenesis (middle). When they are exposed to *hlh-2* RNAi beginning in the L1 stage *[hlh-2(L1-RNAi)]* (right), the treated hermaphrodites are sterile and have improper gonad morphology due to failures in Distal Tip Cell (DTC) differentiation and function.
(C) Phenotypes caused by targeting *hlh-2* by RNAi. For *hlh-2(L4-RNAi)*, the % viable progeny was assessed by counting the number dead eggs and moving larval progeny produced by treated hermaphrodites. For *hlh-2(L1-RNAi)*, fertility was assessed by the presence of eggs on the plate or in the gonad, and each gonad arm was assessed in adults for presence, shape, and length. See Materials and Methods for further details.

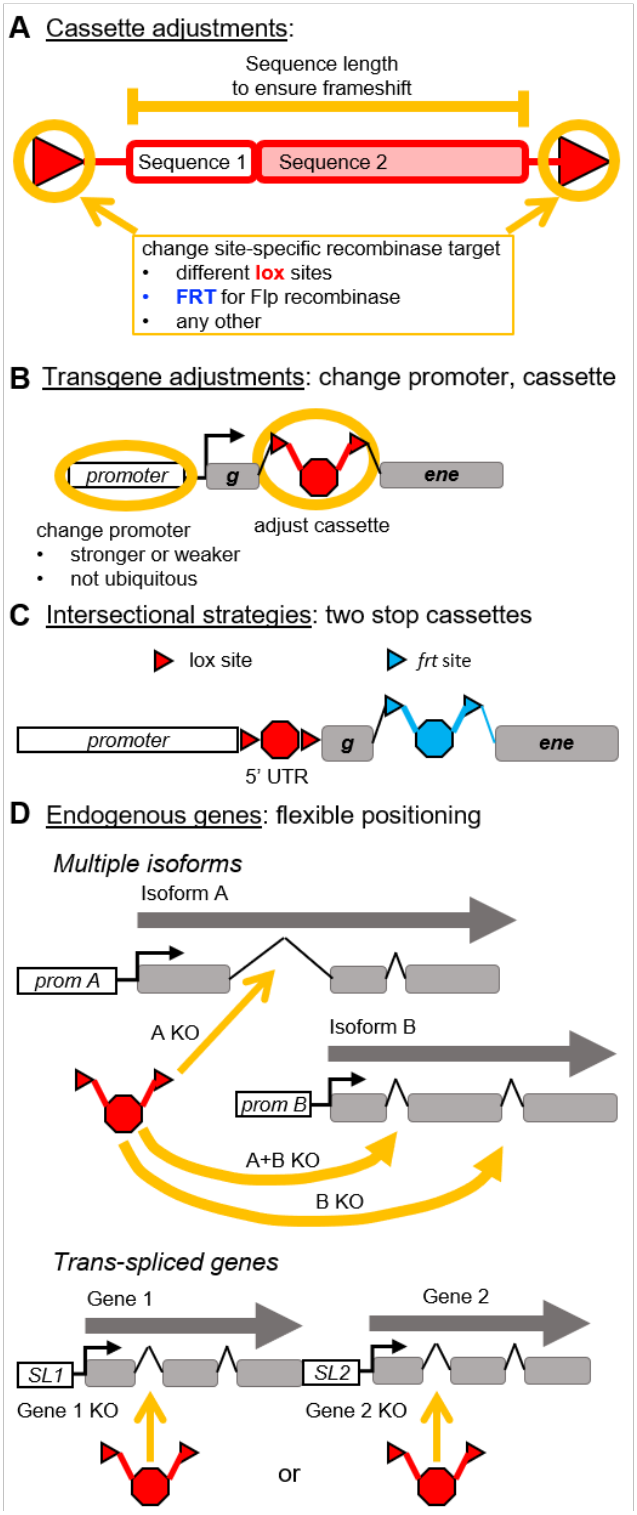

Figure 5. Potential adjustments to the flexon design and additional applications.
The Flexon system is tunable and may be incorporated into transgenes or endogenous loci to enable or improve genetic tools and approaches for manipulating gene activity as well as to mark lineages. Adjustments to the design for specific purposes (A, B) and some potential applications (C, D) are diagrammed here and described in the text.

Chapter 2. SI Appendix

Supplementary Information

Flexon plasmid construction

Flexon plasmids were engineered using Gibson cloning (NEB Inc., #E2621) to ligate dsDNA fragments, derived either from in-house PCR or external synthesis (GENEWIZ FragmentGENE), to create a seamless, *flexon*-containing gene construct. The *flexon* cassette design is shown in Figure 1A of the main paper and described in detail in the paper. In brief, the exon sequence should be designed to cause in-frame termination as well as to create frameshifts resulting in additional termination codons.

The specific *flexon* used in the paper was derived from pJS145; the plasmid and sequence file are available via Addgene [#179159]. The sequence file is also available on our lab website [http://greenwaldlab.org/links.html]. Annotations for the primer and fragment sequences used to construct pJS145 are included in the sequence file on the lab website. Other plasmids and sequence files are available upon request.

Modifications to the *flexon* sequence should also be made to fit your gene of interest; some of the modifications to consider are outlined in the Discussion and diagrammed in Figure 5.

The most important considerations when applying *flexon* to new applications will be whether incorporation of the exon into the transcript produces a frameshift downstream of insertion; if the artificial exon sequence and frameshift introduce stop codons in all reading frames, and if the length of the exon is appropriate for efficient incorporation into the transcript. In all cases, the sequence design should be checked by conceptual translation to ensure that these criteria are met.

Another common modification to consider is the site-specific recombinase (Cre, Flp, etc.) and/or specific sites (*loxP*, *lox2272, etc.)* that will be compatible with other genome engineering events.

As described in the text, we chose to use *lox2272* so as not to create rearrangements with engineered genes that already contain *loxP* sites left from a popular method used in *C. elegans.*

Recommended cloning strategies

The *flexon* cassette contains identical sequences for the *lox*-containing introns that flank the artificial exon, makes it challenging to design primers to amplify the *flexon* cassette as well as to synthesize a linear dsDNA fragment that contains both introns. We found that the easiest way to clone a sequence like this was to order two dsDNA fragments that contained either intron and overlapped in the middle of the *flexon* exon at one end, and had overlaps with the gene of interest at the other end (Figure A). The synthesized gene fragments were then incorporated into standard Gibson cloning reactions with PCR fragments containing sequence from the desired gene and a restriction digested vector to create a seamless, *flexon*-containing gene construct. With this strategy, primers do not need to be used with homology to the introns or lox sites. This strategy may be of interest to those making modifications to the Flexon sequence – like changing the length of the sequence or making additional stop codons – because the sequence within the ordered, synthesized DNA fragments is entirely customizable.

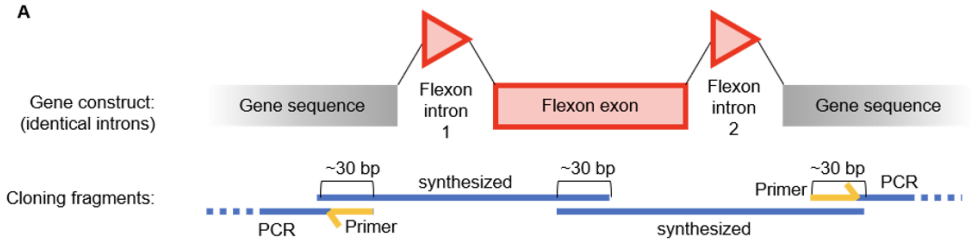

Minor adjustments to the *flexon* cassette sequence may facilitate future cloning. For example, the sequences for each intron outside of the lox sites may be varied to create unique sequences for priming so that the entire cassette may be amplified from a plasmid in one piece using PCR

(Figure B). To create the unique priming sequences, DNA may be added to either or both introns to avoid disrupting the splice donor and acceptor sequences. Adding intronic sequence may also be an important consideration when designing a *flexon* for models other than *C. elegans* (see below).

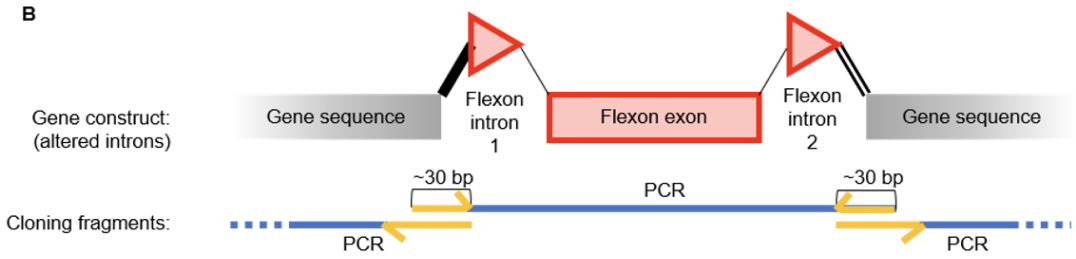

Designing *flexon* alleles of endogenous loci

When designing a strategy for inserting *flexon* into an endogenous gene, it is important to consider the location of the Flexon within the locus. The insertion site for the *flexon* cassette should be chosen to avoid the production of transcripts from cryptic start sites downstream of a *flexon* insertion that encode intact domains with functional capability.

In this paper, we replaced an endogenous intron with the *flexon* cassette (see Fig. 4A), but the cassette may also be inserted into an endogenous intron without deleting any of the natural sequence. The latter design permits the ability to retain known regulatory information contained within the endogenous intron, but may affect splicing efficiency. If inserting *flexon* into an exon, placement should be considered so that the exonic residues surrounding the insertion site are permissive to efficient splicing, for example, into a MAG/R sequence (Dibb and Newman, 1989).

To generate *rde-1(ar660[flexon])*, we used an established protocol (Ghanta and Mello, 2020) to replace the 9th intron of the endogenous *rde-1* gene with a *flexon* cassette, as described in

Materials and Methods. We note that we used a plasmid repair template instead of the suggested linear dsDNA repair template because the identical flanking introns made it difficult to design PCR primers for amplifying a dsDNA fragment with homology arms to the region of interest. As described above, altering the artificial intron sequences to create unique sequences to use for priming would also facilitate generation of a linear dsDNA PCR product from a base *flexon* plasmid to use as a repair template. In that case, all that would be required would be oligos with priming sequences that match the unique intron sequences on either side of the cassette, with and without 35 bp sequences homologous to the regions flanking the desired insertion site.

Adapting the Flexon approach for other organisms

The length and content of the introns may need to be altered from the sequence presented here in view of what is known about splicing in other systems. For example, mean intron length in *D. melanogaster* and *H. sapiens* differs greatly depending on the relative intron position within the gene, and mean intron length varies greatly between species (Bradnam and Korf, 2008). Additionally, the artificial introns in the *flexon* design in this paper do not contain a branch point, consistent with the lack of a conserved branch sequence in *C. elegans* introns (Blumenthal and Thomas, 1988).

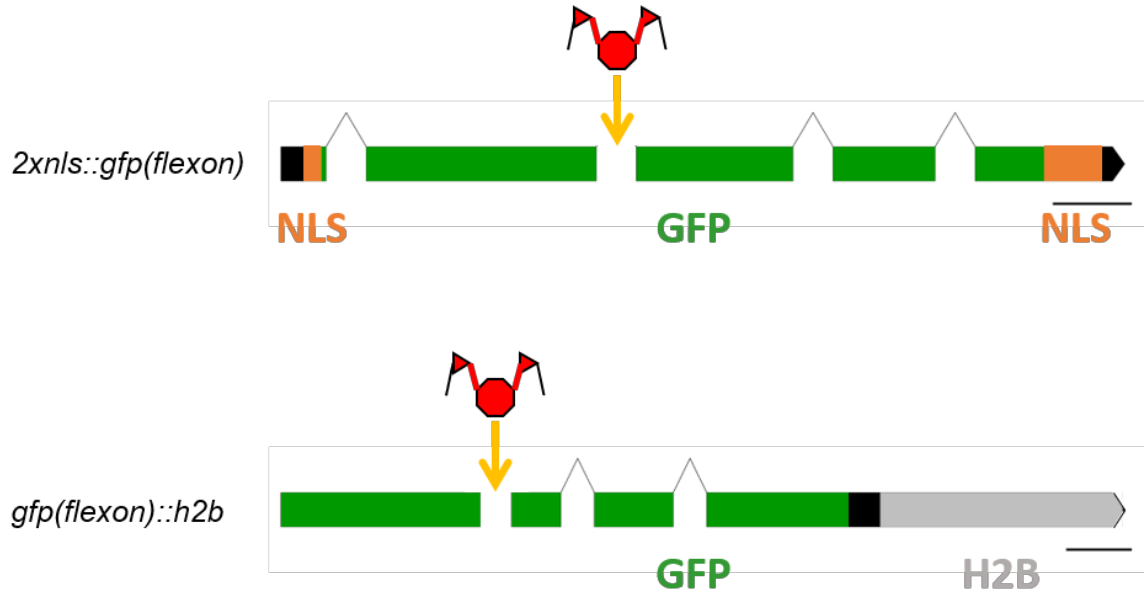

Figure S1. Design of transgenes for 2xnls::gfp(flexon) and gfp(flexon)::h2b, in which the flexon cassette replaced the 2nd and 1st introns, respectively. Scale bars are 100 bp relative to the gfp sequences; the flexon cartoons are not to scale. Gene graphics were made using http://wormweb.org/exonintron.

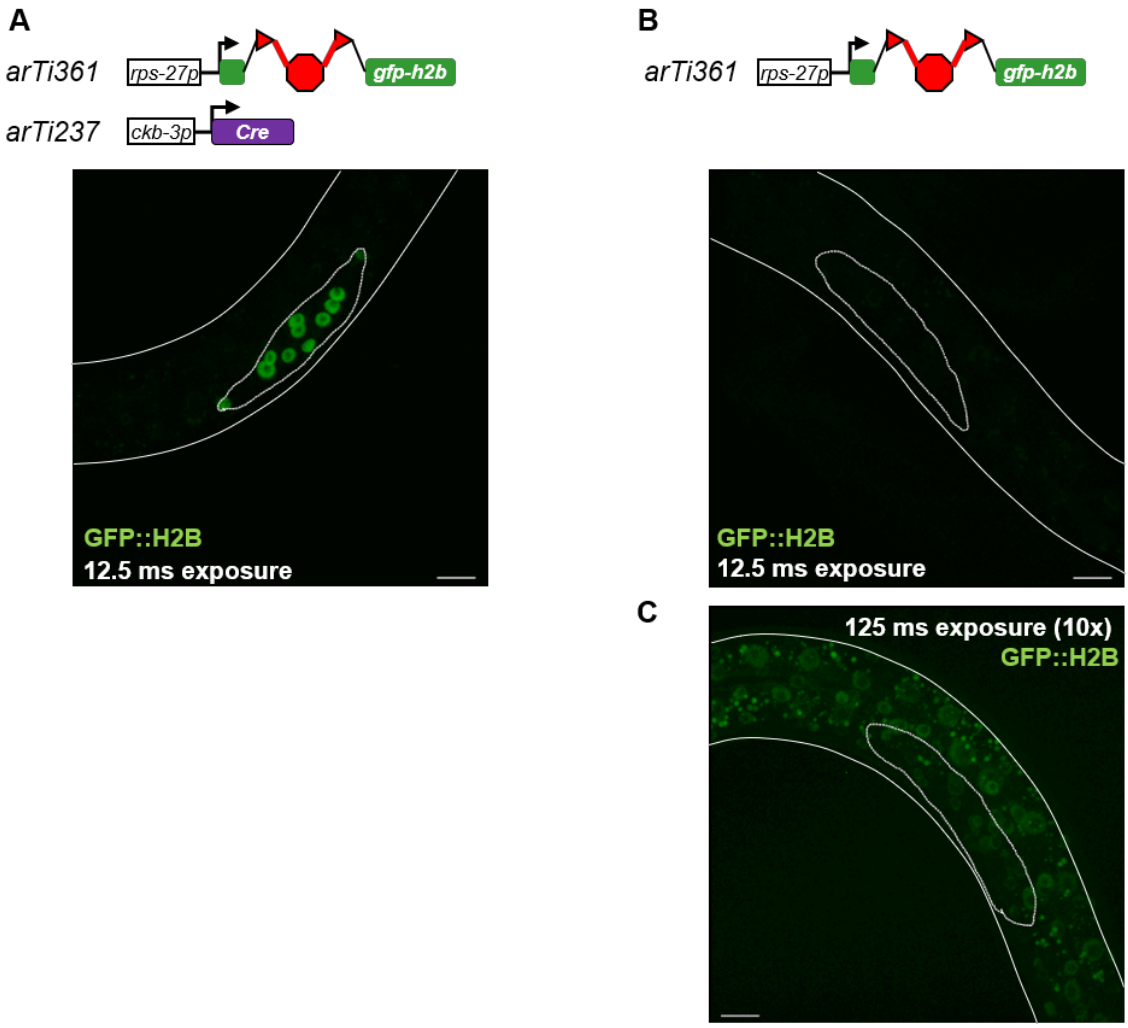

Figure. S2. Limited ectopic fluorescent expression of GFP::H2B protein from a flexon transgene in the absence of a Cre driver. Note that H2B strongly stabilizes GFP (*cf.* Figure 2) so the very dim signal at the 10-fold higher exposure time suggests that the level of ectopic expression is very low. Accordingly, this ectopic expression is not seen with 2xNLS::GFP. Lineage marking experiments and many functional studies are not likely to be affected at this low level of ectopic expression; adjustments to the *flexon* sequence may be tried to reduce background if necessary.
A, B: In photomicrographs taken at an exposure time that limits photo-saturation (12.5 ms under the laser power and gain setting here; see Materials and Methods), there is no visible ectopic fluorescent expression from *arTi361[rps-27p::gfp(flexon)::h2b]* transgene in the presence or absence of a somatic gonad Cre driver *(arTi237[ckb-3p::Cre]).*
C: Upon increasing the exposure time tenfold (125 ms), some dim ectopic expression from *arTi361* is apparent (compare with B).
Each photomicrograph is a maximum intensity projection of an entire Z stack image of late L2/early L3 animals. Solid lines denote the worm, dotted lines denote the gonad. Scale bars are 10 μm.

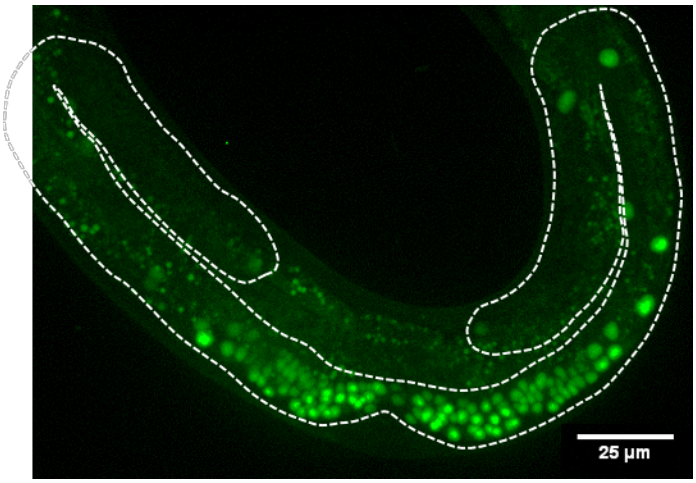

Fig. S3. GFP(flexon) expression is sustained throughout larval development in GS9692 *arTi435[rps-27p::2xnls::gfp(flexon)]; arTi237[ckb-3p::Cre]*. The photomicrograph is a maximum projection of a late L4 stage larva. Bright GFP fluorescence is visible in all somatic gonad cells, whereas it is absent in *arTi433[ckb-3p::2xnls::gfp]* at this stage. Differences in brightness between the distal cells in the anterior and posterior gonad arms is due to imaging depth within the animal; the anterior side is further from the objective than the posterior. The white dashed line outlines the gonad.

We note that for multiple transgenes including *arTi435*, GFP fluorescence expressed using *rps-27p* becomes dimmer in some terminally differentiated cells during larval development and in adults. We have not assessed other canonical ubiquitous promoters in *flexon* transgenes but suggest that other regulatory regions be considered when strong conditional expression is desirable in adults.

Table S1. Strains used in this text

Name	Genotype	Contents	Figure or text	Reference
N2	*wild-type*	wild-type	4C	(Brenner, 1974)
GS8795	*arTi237 [ckb-3p::Cre(opti)::tbb-2 3' UTR]* X	*ckb-3p::Cre*	text	(Tenen and Greenwald, 2019)
GS8793	*arTi235 (hlh-1p::Cre(opti)::tbb-2 3' UTR] (not mapped)*	*hlh-1p::Cre*	text	(Tenen and Greenwald, 2019)
GS9443	*arTi381 [lin-31p::Cre(opti)::tbb-2 3' UTR]* V	*lin-31p::Cre*	text	this paper
GS9407	*arTi361 [pHK001(rps-27p::gfp(flexon)::his-58::unc-54 3' UTR)]* I	*gfp(flexon)::h2b*	S2	this paper
GS9684	*arTi433 [pJS110(ckb-3p::2xnls::gfp::unc-54 3' UTR)]* V	*ckb-3p:2xnls::GFP*	2B	this paper
GS9690	*arTi435 [pJS145(rps-27p::2xnls::gfp(flexon)::unc-54 3' UTR)]* I	*2xnls::gfp(flexon)*	text	this paper
GS9686	*arTi434 [pJS146(lin-31p::2xnls::gfp::unc-54 3' UTR)]* IV	*lin-31p::2xnls::GFP*	2B	this paper
GS9401	*arTi361* I*; arTi237* X	*gfp(flexon)::h2b; ckb-3p::Cre*	S2, 2B	this paper
GS9692	*arTi435* I*; arTi237* X	*2xnls::gfp(flexon); ckb-3p::Cre*	S3, 2B	this paper
GS9532	*arTi361* I*; arTi381* X	*gfp(flexon)::h2b; lin-31p::Cre*	text	this paper
GS9691	*arTi435* I*; arTi381* V	*2xnls::gfp(flexon); lin-31p::Cre*	3B	this paper
GS9801	*rde-1(ar660[flexon])* V	*rde-1(flexon)*	4C	this paper
GS9802	*rde-1(ar660)* V*; arTi237* X	*rde-1(flexon); ckb-3p::Cre*	4C	this paper
GS9831	*rde-1(ar660)* V*; arTi235*	*rde-1(flexon); hlh-1p::Cre*	text	this paper

Chapter 3: SALSA: a genetically-encoded biosensor for spatiotemporal quantification of Notch signal transduction in vivo

The following chapter contains a paper in press at *Developmental Cell*.

I am responsible for all of the experiments and data presented in this chapter.

3.1 Summary

Notch-mediated lateral specification is a fundamental mechanism to resolve stochastic cell fate choices by amplifying initial differences between equivalent cells. To study how stochastic events impact Notch activity, we developed a biosensor, SALSA (Sensor Able to detect Lateral Signaling Activity), consisting of an amplifying "switch" — Notch tagged with TEV protease — and a "reporter" — GFP fused to a nuclearly-localized red fluorescent protein, separated by a TEV cut site. When ligand activates Notch, TEVp enters the nucleus and releases GFP from its nuclear tether, allowing Notch activation to be quantified based on changes in GFP subcellular localization. We show that SALSA accurately reports Notch activity in different signaling paradigms in *Caenorhabditis elegans*, and use time-lapse imaging to test hypotheses about how stochastic elements ensure a reproducible and robust outcome in a canonical *lin-12/Notch*-mediated lateral signaling paradigm. SALSA should be generalizable to other experimental systems, and adaptable to increase options for bespoke "SynNotch" applications.

3.2 Introduction

Notch signaling plays profound and pervasive roles in development and disease. Notch is one of the major receptors for cell-cell interactions, and uniquely mediates lateral specification (also called lateral inhibition), a process by which initially equivalent cells interact with each other and then adopt different alternative fates. Lateral specification allows for stochastic cell fate

decisions to be resolved into reproducible and robust final outcomes. To further our studies of a canonical example of Notch-mediated lateral specification, the Anchor Cell (AC)/Ventral Uterine precursor cell (VU) decision (reviewed in Greenwald, 2012), and test a new model for the relationship between stochastic events and the outcome of the AC/VU decision (Attner et al., 2019), we needed a way to visualize the onset of LIN-12 signaling and track the relative levels of signaling activity in individual cells over time. However, conventional methods including transcriptional reporters (described herein) are not sensitive enough and lack the temporal resolution required for this purpose,

To accomplish these goals, we developed Sensor Able to detect Lateral Signaling Activity (SALSA), a genetically-encoded biosensor that allows for ratiometric quantitation of nuclear Red:Green fluorescence as a measure of Notch signaling activity. We demonstrate the efficacy and fidelity of SALSA in four different cell fate paradigms using both *C. elegans* Notch proteins, LIN-12 and GLP-1. By combining SALSA with time-lapse imaging to quantify LIN-12 signaling during the AC/VU decision, we provide evidence in strong support of the new model for how stochastic events become determinative to ensure a reproducible and robust outcome. Our success in multiple *C. elegans* paradigms suggests that this approach will be generally useful for studies of Notch signaling in other systems. We also discuss potential adaptations based on SALSA to increase the options for customized "SynNotch" applications.

3.3 Results

Design

The intracellular domain of Notch is essentially a membrane-tethered transcriptional coactivator. Ligand-binding leads to sequential proteolytic cleavages; the first, mediated by an ADAM

protease, leads to ectodomain shedding, and the second, mediated by γ-secretase, occurs within the transmembrane domain and releases the intracellular domain from its tether. The intracellular domain then translocates to the nucleus and becomes part of a transcriptional activation complex (reviewed in Falo-Sanjuan and Bray, 2020; Greenwald and Kovall, 2013; Henrique and Schweisguth, 2019; Figure 1A). This simple, direct mechanism was the starting point for the development of SALSA (Figure 1B).

Established assays for quantifying* Notch *activity. Most measurements of Notch activity have relied on transcriptional outputs. For native Notch, these outputs may be natural target gene products or transcriptional reporters incorporating single or multimerized consensus binding sites for the Notch nuclear complex (Hansson et al., 2006; Souilhol et al., 2006; reviewed in Zacharioudaki and Bray, 2014). If the intracellular domain of Notch is instead tagged with, or replaced by, a heterologous transcription factor such as yeast Gal4, nuclear access is revealed by a transcriptional reporter for the heterologous factor (reviewed in Housden et al., 2014; Lecourtois and Schweisguth, 1998; Struhl and Adachi, 1998). However, transcription-based reporters have limitations for the temporal resolution of signaling onset and cessation. Limitations to the on-rate include a lag for visualizing the onset and changes in signal transduction due to the time it takes for sufficient protein encoded by the reporter gene to be transcribed and translated, and in the case of fluorescent proteins used for live imaging, to mature (Bothma et al., 2018); a potential limitation to the off-rate is perdurance of the reporter proteins. In addition, the expression of natural target genes or transgene reporters may be influenced by other inputs from their cellular and/or genomic context.

Available assays based on cleavage and release of the intracellular domain per se do not have these limitations, but have others. In cell culture, luciferase complementation imaging

measures Notch nuclear complex formation by fusing the amino terminal fragment of luciferase to the intracellular domain of Notch and the carboxy terminal fragment of luciferase to the CSL protein of the Notch nuclear complex, reconstituting luciferase activity when the complex forms (Ilagan et al., 2011). However, this method is limited by the amount and stability of the nuclear complex, and in *C. elegans*, the ability for the substrate to penetrate the cuticle of intact worms (Sfarcic et al., 2019). These limitations may be considerable for live imaging in vivo over time because developmentally meaningful signaling is effective at low levels and the Notch intracellular domain is rapidly degraded in the nucleus. Similar limitations also apply to measurements of the nuclear level of the intracellular domain directly tagged with fluorescent proteins. The low native level of cleavage product is particularly problematic for time-lapse imaging in *C. elegans*, as the level of blue-light illumination required for imaging weak signals from GFP-tagged proteins is damaging to animal development (Edwards et al., 2008; Ward et al., 2008).

The low level and instability of the natural cleavage product has been circumvented by replacing the intracellular domain with Cre recombinase and looking for excision of a lox-stop-lox cassette from a target, which permanently marks lineages in which Notch signaling has occurred, and has therefore been valuable for identifying lineages in which Notch has been active (Liu et al., 2015; Vooijs et al., 2007). However, this method is not suitable for quantifying signal transduction in a cell over time, and an earlier event in a lineage would mask a later, independent one.

GPCR and ERK biosensor antecedents. In designing our ideal Notch biosensor, which would include an amplification step while eschewing a transcriptional readout, we were inspired by features of two other biosensors. One is the “Tango” assay (Barnea et al., 2008; Inagaki et al.,

2012; Katow et al., 2019), in which ligand-dependent recruitment of an arrestin::Tobacco Etch Virus protease (TEVp; Kapust et al., 2002) fusion protein releases a transcription factor fused to a second receptor through cleavage of an intervening TEV recognition site (Tcut); the released transcription factor activates expression of a target gene reporter. The other is the ERK-KTR (kinase translocation reporter), which converts ERK activity into a change in nucleocytoplasmic localization of KTR::Clover (Regot et al., 2014); when expressed as a bicistronic transcript with a nuclear-tethered red fluorescent protein, ERK activity may be quantified as a Red:Green ratio of nuclear fluorescence, an advantage when cells are small, closely packed together, and change in size, shape, or form syncytia during development, as in *C. elegans* (de la Cova et al., 2017).

Design of SALSA. SALSA is a bipartite system, consisting of a "switch" and a "reporter" (Figure 1B). For the switch, we used CRISPR/Cas9 to create endogenously-tagged alleles for both *C. elegans* Notch homologs, LIN-12 and GLP-1, that encode TEVp fused to the carboxy terminus of the intracellular domain (STAR Methods). Homozygotes for the switch alleles for *lin-12(ar640)* [LIN-12::TEVp] and *glp-1(ar648)* [GLP-1::TEVp] are viable, fertile, and phenotypically indistinguishable from wild type, indicating that the tagged proteins are fully functional (STAR Methods). When GFP is added to endogenous LIN-12 at the same position, the animals also appear phenotypically wild-type, and LIN-12::GFP is observed primarily at the cell surface as expected, indicating that trafficking is not compromised (Attner et al., 2019; Chan, PhD thesis); GFP and other tags placed at or near the carboxy terminus of GLP-1 also appear functional and permit proper trafficking (Sorensen et al., 2020). The use of endogenous *lin-12* and *glp-1* allowed us to measure the level of signaling during cell fate decisions with potential regulatory mechanisms intact, including rapid turnover of the untethered intracellular domain::TEVp fusion by regulators such as the E3 ubiquitin ligase SEL-10/Fbxw7 (de la Cova

and Greenwald, 2012; Deng and Greenwald, 2016; Hubbard et al., 1997), which should also lead to degradation of the TEVp moiety. Alternate transgenic switch designs and applications are described in the Discussion.

The reporter is a substrate for TEVp: GFP coupled to an RFP::H2B (here, usually mScarlet), separated by a linker containing the recognition site for TEVp (GFP::Tcut::RFP::H2B) (STAR Methods). The cleavage state of the reporter will reflect the subcellular localization of TEVp: when Notch is inactive, TEVp is tethered to the membrane and GFP remains attached to RFP::H2B in the nucleus; when Notch is activated, TEVp enters the nucleus and cleaves the reporter, allowing GFP to diffuse out of the nucleus. Thus, Notch signaling activity can be quantified as a "Red:Green" ratio of RFP ("Red"):GFP ("Green") fluorescence in the nucleus, (using RFP as the nuclear segmentation marker, Figure 1B; for other ratios that can be used, see Figure S3). This cleavable reporter was able to distinguish cells with active Notch signal transduction from cells with inactive Notch signal transduction in live worms, and allowed for the cumulative increase in signal transduction to be observed over time during the AC/VU decision.

We note that we did not observe fluorescence resonance energy transfer (FRET) or photoconversion of mScarlet using this reporter design, and that addition of nuclear export signal (NES) sequences to the GFP proved to be problematic (see STAR Methods). We also note that we expressed the cleavable reporter tissue-specifically to simplify image collection and cell identification (de la Cova et al., 2017), although tissue-specific expression is not required to implement SALSA.

Testing SALSA in signaling paradigms with stereotyped patterns of Notch activity: Vulval Precursor Cells, the M lineage, and the germ line

We tested the fidelity of SALSA as a readout for Notch signaling activity in different signaling paradigms for which extensive prior genetic studies coupled with target gene transcriptional outputs give confidence about the expected patterns of Notch activity and inactivity at the level of individual cells. In all cases, SALSA faithfully reported activity based on the expectations. Each paradigm offered the opportunity to gain additional insights into the performance of SALSA.

VPCs: measurements with signaling manipulation. Three VPCs, named P5.p, P6.p, and P7.p, give rise to the vulva (Sulston and Horvitz, 1977). They are initially multipotent, and are patterned in the L3 stage: in wild-type hermaphrodites, the central VPC, P6.p, always adopts the "1º" vulval fate, and the flanking VPCs, P5.p and P7.p, always adopt the "2º" fate (Gauthier and Rocheleau, 2017; Shin and Reiner, 2018; Sternberg, 2005). This fate pattern results when an EGF-like signal from the AC activates EGFR and a canonical Ras cascade in P6.p, inducing it to adopt the 1º fate, downregulate LIN-12 protein levels, and produce the "lateral signal" composed of ligands for LIN-12/Notch (Figure 2A). These ligands activate LIN-12/Notch in P5.p and P7.p, causing them to adopt the 2º vulval fate. In the L3 stage, several LIN-12 target transcriptional reporters are expressed specifically in, or upregulated in, P5.p and P7.p and their descendants, with expression depending on cis-acting binding sites for the LIN-12 nuclear complex (Berset et al., 2001; Luo et al., 2020; Yoo et al., 2004; Yoo and Greenwald, 2005).

We drove expression of the GFP::Tcut::mScarlet::H2B cleavable reporter in VPCs and their descendants (STAR Methods). If SALSA faithfully reports LIN-12 signaling activity, we would expect a high nuclear Red:Green fluorescence ratio in P5.p and P7.p compared to P6.p in

the presence of the LIN-12::TEVp switch, and a uniformly low nuclear Red:Green ratio in P5.p, P6.p and P7.p in the absence of the LIN-12::TEVp switch (reporter-only control). These expectations were met (Figure 2B). As a further test of SALSA fidelity, we removed the lateral signal. To do so, we genetically blocked the AC from forming [using *hlh-2(ar614)*; see STAR Methods], thereby removing the source of the EGF-like signal that causes P6.p to express the ligands that normally activate LIN-12 in P5.p and P7.p. If SALSA faithfully reports LIN-12 signaling activity, we would expect that, in the absence of an AC, these three VPCs would have uniformly low nuclear Red:Green ratios even in the presence of the LIN-12::TEVp switch, similar to when the switch is absent. Indeed, we found this to be the case (Figure 2B). Finally, we found that removing the SEL-10 E3 ubiquitin ligase that targets the intracellular domain of LIN-12 for degradation in VPCs increases the nuclear Red:Green ratio, in accordance with expectations (Figure S1).

M lineage: different ratiometric measurements of signal transduction. The postembryonic mesoblast M generates dorsally-located and ventrally-located descendants that adopt distinct fates based on signals they receive. LIN-12/Notch is necessary to specify ventral cell fates; the relevant signaling begins at the 4-M stage (granddaughters of M), when ligand begins to be expressed by cells adjacent to only the ventral M lineage cells (Foehr and Liu, 2008) (Figure 3A). LIN-12::GFP is expressed at similar levels in the dorsal and ventral cells of the M lineage at the 4-M to 8-M stages (Foehr and Liu, 2008). We evaluated the performance of SALSA in individual worms carrying the LIN-12::TEVp switch and a transgene that expresses the GFP::Tcut::mScarlet::H2B cleavable reporter in M and all of its descendants (STAR Methods). If SALSA faithfully reports LIN-12 signaling activity, we would expect a higher nuclear Red:Green fluorescence ratio in ventral descendants, where M lineage cells are

juxtaposed to ligand, than in dorsal descendants, where cells are not exposed to ligand. These expectations were met, as shown in quantification of nuclear Red:Green at the 8-M stage (Figure 3B-D) and in time-lapse movies that show the onset of signaling in ventral cells in the 4-M stage (Figure S2).

The relatively wide spacing between cells at the 8-M stage also allowed us to compare alternate methods for quantifying signal transduction. Of particular note, we were able to use a "cytoring" (Regot et al., 2014) to determine that similar results are obtained using the Cytoplasmic:Nuclear (C:N) fluorescence ratio, which may be advantageous in certain contexts, particularly in other systems where cells are larger or spaced further apart than is generally true in *C. elegans* (see Discussion and Figure S3 legend).

Germ line: GLP-1/Notch SALSA. The *C. elegans* gonad has two arms that extend outwards from the centrally-located uterus. Ligands produced by the somatic distal tip cell (DTC) at the end of each gonad arm activate GLP-1/Notch in nearby Germline Stem Cells (GSCs) to inhibit entry into meiosis (reviewed in Hubbard and Schedl, 2019). As the proliferating GSCs are displaced proximally out of the GSC niche, they undergo a transition to meiosis. Genetic analysis established that *glp-1* activity is necessary and sufficient to sustain the GSC fate (Austin and Kimble, 1987; Berry et al., 1997; Priess et al., 1987). In L4 hermaphrodites (Figure 4A), activation of GLP-1 peaks in a zone that extends approximately 5 cell diameters from the DTCs, where there is maximal contact with DTC processes, based on the visualization of the nuclearly-localized intracellular domain of GLP-1 (Gutnik et al., 2018) and *in situ* hybridization or antibody staining for targets of GLP-1 in the germ line (Chen et al., 2020a; Kershner et al., 2014; Lee et al., 2016). Transcripts for a direct target of GLP-1 are detected up to ~8-10 cell diameters from the distal end (Chen et al., 2020a; Kershner et al., 2014; Lee et al.,

2019; Lee et al., 2016), and GLP-1 is expressed throughout (and beyond) the progenitor zone (Crittenden et al., 1994), which ends ~21 cell diameters from the distal end.

We expressed the GFP::Tcut::mCherry::H2B cleavable reporter in all germline cells (STAR Methods), and visualized and quantified fluorescence in L4 hermaphrodites. If SALSA accurately reports GLP-1 activity, we would expect to see visibly reddened germline nuclei at least 5 cell diameters from the distal end of the gonad arm and a low nuclear Red:Green ratio from uncleaved reporter more proximally in the presence of the GLP-1::TEVp switch, and a uniformly low nuclear Red:Green ratio in the absence of the GLP-1::TEVp switch. The appearance of the germ line (Figure 4B) and our quantitative analysis (Figure 4C) conformed to this expectation. In particular, when we quantified the nuclear Red:Green ratio at 0, 5, 10, and 15 cell diameters from the distal end, we found that in the presence of the GLP-1::TEVp switch, the nuclear Red:Green ratio was high at 0 and 5 diameters and low at 10 and 15 cell diameters (Figure 4C), approaching the level of the no-switch control. These results are consistent with expectations based on the evidence for maximal activity extending five cell diameters and the absence of activity beyond the GSC zone.

Because the distance from the DTC in cell diameters represents a temporal progression in which GLP-1 signaling activity decreases as cells are displaced from contact with the DTC, the germ line data also suggest that the "off-rate" of SALSA is relatively responsive to the cessation of GLP-1 activation: there is a low nuclear Red:Green ratio past the GSC region, where GLP-1 target genes appear not to be actively transcribed (Lee et al., 2016; Lee et al., 2019).

Testing SALSA in the AC/VU decision

The LIN-12/Notch-mediated AC/VU decision is a canonical example of lateral specification (reviewed in Greenwald, 2012). The α cells descend from the two somatic gonad precursor cells present at hatching, Z1 and Z4 (Figure 5A). Each α cell is born with the potential to be the sole Anchor Cell (AC), a terminally differentiated cell that organizes development of the uterus and vulva, or a Ventral Uterine precursor cell (αVU), which generates uterine structural cells. In any individual, one α cell becomes the AC and the other becomes the αVU. However, the outcome is stochastic: 50% of the time the α cell descended from Z1 becomes the AC, and the other 50% of the time the α cell descended from Z4 becomes the AC. This decision is precise and robust because the two α cells interact with each other via LIN-12 and its ligand LAG-2 to resolve which will be the AC and which will be the αVU.

lin-12 acts as a classic "switch gene" in mediating the AC/VU decision (Greenwald et al., 1983). Both α cells initially express LIN-12 and LAG-2; genetic and expression studies suggested that a stochastic initial difference in *lin-12* activity between the two uncommitted α cells becomes amplified by feedback mechanisms, ensuring that the α cell with higher *lin-12* activity continues to express *lin-12*, ceases to express *lag-2*, and becomes the αVU while the other α cell ceases to express *lin-12*, continues to express *lag-2*, and becomes the AC (reviewed in Greenwald, 2012; Figure 5B). When the cells have committed to their fates, the AC expresses only LAG-2 and the αVU expresses only LIN-12. Several readouts of LIN-12 activity are seen in the committed αVU and not in the AC in the early L3 stage: (i) nuclear GFP produced after cleavage of endogenous LIN-12::GFP (Attner et al., 2019), (ii) the transcriptional reporter *arIs107[mir-61p::2xnls::yfp]* (Yoo and Greenwald, 2005), and (iii) positive autoregulation of endogenous *lag-1::gfp*, the CSL protein in *C. elegans* (Luo et al., 2020). Transcriptional

reporters containing multimerized CSL binding sites are not expressed in the somatic gonad (or VPCs) (e.g. Li, 2011) so cannot be used to follow LIN-12 activation.

We tested whether the readout of SALSA conforms to expectations by examining the specified AC and αVU in the L3 stage (Figure 5B). To implement SALSA in the somatic gonad, we used a variation on "*lox-stop-lox*" called Flexon (Shaffer and Greenwald, 2022) to express GFP::Tcut::mScarlet::H2B strongly, specifically, and constitutively in all somatic gonadal cells (Figure 5C) under the control of a ribosomal protein gene promoter (*rps-27p*), thereby avoiding transcriptional regulatory mechanisms that operate in the AC/VU decision (Wilkinson et al., 1994). One transgene, *arTi237,* drives expression of Cre recombinase specifically in the somatic gonad precursor cells Z1 and Z4; the other, *arTi355*, contains a *flexon* stop cassette that prevents expression of the GFP::Tcut::mScarlet::H2B cleavable reporter from *rps-27p* unless Cre-mediated excision of the *flexon* occurs (Figure 5C; STAR Methods). Excision is very efficient in Z1 and Z4, the great-grandparents of the α cells, (Shaffer and Greenwald, 2022), so the cleavable reporter is strongly and uniformly expressed in both α cells in all animals. Hereafter, we refer to the combination of these two transgenes as the “somatic gonad cleavable reporter."

When we quantified the somatic gonad cleavable reporter in the AC and αVU, we observed a significantly higher nuclear Red:Green ratio in the αVU than in the AC in the presence of the LIN-12::TEVp switch (Figure 5D), and a similar, low nuclear Red:Green ratio in both the AC and αVU in the cleavable reporter-only control (Figure 5E), indicating that SALSA is an accurate reporter of *lin-12* activity in this context.

SALSA illuminates the relationship between birth-time interval and relative birth order at the outset of the AC/VU decision

High-throughput lineage analysis identified two inter-related stochastic events that *precede* the AC/VU decision and predict its outcome (Attner et al., 2019). The first stochastic element is the relative birth order of the α cells: one of the α cells is usually born before the other, so there is a "first-born" α cell and a "second-born" α cell. When the birth-time interval between the α cells is "long", there is a birth-order bias such that the first-born α cell always becomes the VU. When the birth-time interval between the α cells is "short," the decision is random with respect to relative birth order; instead, the first *parent* of an α cell (Z1.pp or Z4.aa) that expresses the transcription factor HLH-2 gives rise to the α cell that becomes the VU. These two elements are inter-related because the relative order and timing of the first division of the precursors Z1 and Z4 are largely maintained throughout their lineages, so one parent is often born before the other; and the onset of HLH-2 expression begins within a narrow window after the birth of a parent cell, so if the birth-time interval is long, the first parent born will also express HLH-2 before the other parent does. However, when birth-time intervals are short, which parent expresses HLH-2 first is stochastic. A potential deterministic mechanism for the HLH-2 expression bias was suggested by the finding that HLH-2 is required for LIN-12 expression in the α cells. Thus, the new model proposed that earlier expression of HLH-2 in a parent cell might give its α daughter an "edge" in LIN-12 activation, by promoting earlier *lin-12* transcription directly or indirectly, and therefore biases it to be the αVU (Attner et al., 2019).

This model makes several predictions for the relationship between birth-time interval, relative birth-order, and LIN-12 activity (Figure 6A). These predictions could not be tested using the readouts of LIN-12 activity described above because none of them can be visualized early in the AC/VU decision, when the α cells are being influenced by stochastic events. The evidence described above suggests that SALSA is a faithful reporter of LIN-12 activity; in testing the

predictions of the model, we would also be testing whether SALSA can perform as a rapid-response biosensor and reveal differences in signaling over time. We collected time-lapse spinning disk confocal videos of 58 worms with both the somatic gonad cleavable reporter and LIN-12::TEVp switch corresponding to 33 long and 25 short birth-time intervals (Figure S4 shows ten representative videos), and 16 individuals with only the somatic gonad cleavable reporter as a negative control. Under the imaging conditions used here and in Attner et al. (2019), a long birth-time interval corresponds to >45 minutes and a short birth-time interval, to ≤45 minutes (STAR Methods). By analyzing the level of LIN-12 activity in the α cells as a function of birth-time interval, and changes over time, we found evidence consistent with the new model.

α cells do not differ in their initial level of LIN-12 activity. Although endogenous LIN-12::GFP expression has not been detected in the parents of the α cells, endogenous GFP::HLH-2 and LAG-2::GFP have been observed (Attner et al., 2019). If there is a low level of LIN-12 activity in the parent cells, the first-born α cell may be born with an already-apparent advantage in LIN-12 activity. However, by quantifying the nuclear Red:Green between the first- and second-born α cells immediately after the birth of each cell, we ascertained that there is no significant difference in initial *lin-12* activity between the α cells regardless of birth-time interval, indicating that the birth-order bias for long birth-time intervals is not due to an inherent LIN-12 activity advantage in the first-born α cell at birth (Figure 6B). In addition, the parent cells do not appear to experience significant LIN-12 signaling (Figure S5), suggesting that differences in LIN-12 activity arise following the birth of the α cells.

When the birth-time interval is long, the first-born α cell gains a relative advantage in LIN-12 activity. A fundamental prediction of the model is that for long birth-time intervals, the

first-born α cell would experience significant LIN-12 signaling before the second-born α cell, and sustain an advantage over time, accounting for the "edge." LAG-2 is detectable in the parents as well as in the α cells and their sisters, the β cells, when they are born (Attner et al., 2019). It is therefore conceivable that LIN-12 may be activated in the first-born α cell by ligand from its sister β cell and/or the undivided parent of the other α cell; alternatively, productive signaling may only occur between the two α cells and hence begins only after both have been born. In the former case, a long birth-time interval would give the first-born α cell a head-start in accumulating active LIN-12, a potential explanation for its bias towards VU fate. We quantified the level of LIN-12 activity in the first- and second-born α cells at the timepoint immediately following the birth of the second α cell (Figure 6C). This analysis revealed that the first-born α cell already has developed a significantly greater level of LIN-12 activity than the second-born α cell has at its birth when the birth-time interval is long, but not when the birth-time interval is short (Figure 6D).

When the birth-time interval is short, the relative birth order does not predict which α cell will gain a relative advantage in lin-12 activity. At short birth-time intervals, the α cell that adopts the VU fate is random with respect to birth order (Attner et al., 2019); we therefore tested whether the LIN-12 activity advantage is random as well (Figure 6E). We identified twelve animals with “short” birth-time intervals for which we could determine the relative birth order and observe the development of a clear difference in nuclear Red:Green ratio during the time period covered by the video (see STAR Methods for full details). The first-born α cell had a clear activity advantage in 6/12 cases and the second-born α cell had the advantage in the remaining 6/12 cases, demonstrating that when the birth-time interval is short, which α cell gains a LIN-12

activity advantage over the other is random with respect to birth order, as predicted by the new model.

3.4 Discussion

SALSA as a tool for studying Notch signaling in vivo

We developed SALSA as a novel Notch biosensor for live readouts of Notch activity and tested its efficacy in *C. elegans* for two different Notch proteins and in four different cell fate specification paradigms. In all cases, SALSA gave the anticipated readouts for Notch activity based on extensive prior genetic analysis and reporter gene studies. Our validation of SALSA in multiple paradigms provides optimism that it may be applied more generally to other systems.

We also successfully used SALSA for quantitative longitudinal imaging to test a recent model (Attner et al., 2019) for a simple lateral specification paradigm, the decision of two bipotential α cells between Anchor Cell (AC) and Ventral Uterine precursor cell (VU) fates. In each individual worm, one α cell becomes the AC and the other becomes the αVU; however, each α cell has a 50% chance of being the AC. During the AC/VU decision, two stochastic elements, (i) the relative birth order, which begins with the division of the precursor three cell generations earlier, and (ii) the onset of expression of the transcription factor HLH-2 in the parent of the α cells, resolve into a deterministic mechanism. The model proposes that earlier HLH-2 expression in the parent cell gives its α daughter a head start towards the onset of LIN-12 activation by ligand from neighboring cells so that it is biased to be the αVU (Attner et al., 2019). Using SALSA, we corroborated three key predictions of the model. First, LIN-12 activity was not detected in the parent cells, and the first-born and second-born α cells had comparable levels of LIN-12 activity at their births, affirming that relevant LIN-12 activity occurs from

signal transduction within the bipotential α cells themselves. Second, when the interval between the birth of the α cells was long, the first-born α cell gained a distinct advantage in LIN-12 activity before the second-born α cell was born, and sustained that advantage over time. Third, when the interval between the birth of the α cells was short, the α cell that developed the LIN-12 activity advantage was random with respect to birth order. The success of SALSA in the AC/VU decision paradigm suggests that it will allow Notch responses to be studied as cell fate decisions progress in other lateral signaling paradigms.

Other potential applications of SALSA for studies of Notch signaling in vivo or ex vivo, and for further customizing SynNotch responses

We suggest here other potential applications, and the modularity of switch and reporter design (Figure 7) should allow others to be devised.

(i) SALSA may be incorporated into cell-based assays or organoids ex vivo in situations where its design features may offer advantages over other methods.

(ii) For noncanonical Notch signaling mechanisms, transcription of targets of the canonical pathway are not useful reporters of signaling (Hunter and Giniger, 2020). Thus, SALSA offers an approach to assessing noncanonical Notch signaling mechanisms that involve cleavage, such as regulation of the cytoskeleton by suppression of Abl activity in the growth cone that occurs during axon guidance in Drosophila (Kannan et al., 2018). The switch or the reporter design may be varied (Figure 7) to facilitate detection of activity if the intracellular domain does not gain sufficient access to the nucleus during these noncanonical signaling events.

(iii) SALSA may help identify as-yet unknown cell contexts where Notch is active, independent of potential context-dependent effects on transcriptional reporters of signaling activity. This

potential application may be particularly valuable for reporting activation of individual Notch paralogs when there is functional redundancy, as has been seen in *C. elegans* and mammals (Krebs et al., 2000; Lambie and Kimble, 1991; Pompa de la et al., 1997). It may also be valuable when pleiotropic effects from Notch pathway mutants such as embryonic lethality precludes easy assessment of the contribution of Notch signaling to later developmental events or by lineage-marking strategies.

(iv) "SynNotch" proteins incorporate the force-sensing negative regulatory region of Notch into chimeric receptors that contain a heterologous recognition domain in the ectodomain and a heterologous transcription factor as the intracellular domain. This arrangement allows for a novel signal that binds to the recognition domain to cause cleavage and release of the tethered transcription factor, producing a novel transcriptional output (Ho and Morsut, 2021; Morsut et al., 2016), and its practical applications include anti-cancer therapy by engineered chimeric antigen receptor T cells (Cho et al., 2018; Choe et al., 2021; Hyrenius-Wittsten et al., 2021; Roybal et al., 2016; Srivastava et al., 2019).

We envisage that a SynNotch modeled on our Notch::TEVp switch, combined with novel reporters modeled on our nuclear-tethered GFP (Figure 7), could be used to expand the range of "SynNotch"-type applications in artificial circuits to processes other than transcription. For example, ligand-mediated release and translocation of TEVp to the nucleus could release a nuclear-tethered protein to function in the cytosol, or convert a nuclear-tethered pro-protein into an active protein via cleavage of a Tcut site. This type of activation would allow for immediate, amplified production of active protein without the caveats of a transcriptional activation step.

Limitations of SALSA

Our analysis suggests that SALSA is sensitive to the onset of signal transduction, and the increase in the nuclear Red:Green ratio over time as the α cells interact via LIN-12/Notch suggests that it is a good proxy for the cumulative level of signaling they experience, fulfilling our aims for studying how stochastic differences affect signaling in the initial stages of the AC/VU decision. However, for some quantitative applications, it may be valuable to characterize a dose-response relationship by systematically varying the ligand concentration; it may also be valuable to characterize how rapidly the nuclear Red:Green ratio (or Cytoplasmic:Nuclear Green ratio) returns to baseline after ligand is initially present but then withdrawn. These tests were not feasible in our analysis, as we relied on natural ligand expression, and could only perform a simple presence-or-absence ligand comparison (as we did in the M lineage and VPCs). The correlation of activity based on GLP-1/Notch SALSA in the germ line with known target gene expression patterns suggests that SALSA will perform well in such tests, since the distance from the DTC represents a temporal progression from a region of high signaling to a region of low signaling, a gradient which has been proposed to be determined in part by decreasing levels of interaction with ligand expressed by the DTC as cells moves proximally (Lee et al., 2016).

The question about the "off rate" is pertinent to the potential suitability of SALSA for studying modulation of properties such as frequency, amplitude and duration of signal transduction, which have been demonstrated to cause different outcomes for some signaling pathways (Albeck et al., 2013; Atay and Skotheim, 2017; Johnson and Toettcher, 2019; Purvis and Lahav, 2013; Ryu et al., 2015). For Notch, little is known about whether such properties are modulated during signaling. The main evidence to date for such modulation comes from a study of responses to different mouse ligands ex vivo (Nandagopal et al., 2018). This study reported that a ligand with low affinity for Notch causes pulsatile cleavage and a ligand with high affinity

causes more sustained cleavage, correlated with expression of different Notch target genes. However, the study did not exclude the possibility that the relevant parameter is the absolute level of signaling and not the dynamics; indeed, it has been proposed that the different transcriptional profiles may instead be explained by feedback circuits elicited by different levels of signal transduction (Henrique and Schweisguth, 2019). Such robust feedback mechanisms are characteristic of diverse Notch-mediated cell fate decisions in vivo, such as the generation of spaced bristle patterns in Drosophila (Corson et al., 2017; Couturier et al., 2019; Heitzler et al., 1996), reiterated somite formation in vertebrates (Diaz-Cuadros et al., 2021; Hubaud and Pourquié, 2014; Hubaud et al., 2017), and the AC/VU decision (Greenwald, 2012). Furthermore, there is also evidence in Drosophila that in individual cells, the cumulative amount of Notch activation is what governs expression of a key target gene during development (Falo-Sanjuan et al., 2019; Viswanathan et al., 2019), consistent with the view of LIN-12/Notch activity as a binary switch driven by feedback amplification of stochastic initial differences during the AC/VU decision and the measurements of signal transduction described here.

As with any biosensor system, an intrinsic limitation of SALSA is the requirement to optimize the levels of expression as well as other properties of the interacting components to detect biologically meaningful responses *in vivo*. We used Notch::TEVp knock-in alleles to achieve physiological levels of expression and activity of the switch, and single-copy insertion transgenes driving uniform expression of cleavable reporters at levels we could easily visualize and quantify. Our characterization indicated that these conditions were appropriate for our experimental goals. However, for implementing SALSA in other experimental systems, some of these details may need to be varied, and for some applications, it may also be necessary to assess the performance of SALSA further; for example, if genetic backgrounds that are known to

sensitize for perturbations in Notch activity are going to be used for the study, then it may be necessary to test if the tagged alleles behave like wild-type alleles in the relevant backgrounds.

For analysis, we used the nuclear Red:Green ratio to quantify activity, and as described herein, our analysis suggests it was accurate for our applications. However, a ratiometric measurement using a "cytoring" to calculate a Green Cytoplasmic:Nuclear (C:N) fluorescence ratio (Regot et al., 2014) of free GFP after reporter cleavage may be more accurate or more sensitive if the two fluorescent proteins have different half-lives or photobleaching rates, although the cells must be large and spaced enough to allow for good segmentation. Both the nuclear Red:Green and Green C:N ratiometric measurements have the virtue that they internally control for differences in expression level of the reporter in different cells.

Finally, we note that modifications to the cleavable reporter, such as adding a degron to one of the fluorescent proteins or changing the nuclear localization signal in the cleavable reporter from a histone to an NLS, may alter the sensitivity or resolution of the system. Moreover, a cleavable reporter may be engineered to make measurements based on relieving FRET instead of a change in nucleocytoplasmic localization. The modular nature of SALSA and the large number of modifiable parameters offer many potential ways to optimize it for other systems and purposes.

3.5 Acknowledgements

We gratefully acknowledge Michelle Attner for suggesting the use of TEVp and additional discussion throughout this project. We also thank Claire de la Cova for much helpful advice on statistical analysis, Tim Schedl for discussion about the germ line, Ruben Gonzalez and Colin Kinz-Thompson for advice on testing for FRET, and Michelle Attner, Catherine O'Keeffe, Gary

Struhl and Sergi Regot for insightful comments on the manuscript. This work was supported by R35GM131746 from the National Institute of General Medical Sciences (to I.G.), and F31EY030331 from the National Eye Institute (to J.M.S.). J.M.S. was also supported by training grant T32GM008798. Some strains used during the course of genetic manipulations were provided by the CGC, which is funded by NIH Office of Research Infrastructure Programs (P40 OD010440).

Author Contributions

J.M.S. and I.G. designed the experiments. J.M.S. conducted the experiments and performed all statistical analysis. J.M.S. and I.G. interpreted the data. J.M.S. and I.G. wrote the paper.

Declaration of Interests

The authors declare no competing interests.

3.6 STAR Methods

RESOURCE AVAILABILITY

Lead contact

Further information and requests for resources and reagents should be directed to and will be fulfilled by the Lead Contact, Iva Greenwald (isg4@columbia.edu).

Materials Availability

All materials are available upon request.

Data and code availability

This paper does not report original code.

Any additional information required to reanalyze the data reported in this paper is available from the lead contact upon request.

EXPERIMENTAL MODEL AND SUBJECT DETAILS

C. elegans alleles and transgenes

C. elegans strains were maintained at 20°C on 6 cm NGM plates seeded with *E. coli* OP-50. See the Key Resources Table for full list of strains. All experiments were performed at 25°C to maximize fluorescent reporter intensity.

Details on the generation of all novel alleles are outlined in the Method Details section. The alleles *lin-12(ar640)* and *glp-1(ar648)*, which encode for the LIN-12::TEVp and GLP-1::TEVp switches, respectively, were generated using CRISPR/Cas9 to tag the endogenous loci at the C-terminus with TEV protease.

The transgenes *arTi355, arTi351*, *arTi359*, and *arTi356* were made using miniMos transposons (Frøkjær-Jensen et al., 2014) to generate single copy genomic insertions, described in Method details.

arTi237[ckb-3p::Cre(opti)] is a miniMos-based transgene, made as described in (Tenen and Greenwald, 2019) and found in strain GS8795, that expresses Cre recombinase optimized for use in *C. elegans* (Ruijtenberg and van den Heuvel, 2015) in the developing somatic gonad. The *ckb-3p* sequence drives expression in Z1 and Z4 beginning in the embryo (Kroetz and Zarkower, 2015) and results in highly efficient excision of the *flexon* cassette of the SALSA reporter *arTi355[rps-27p::gfp(flexon)::tcut::mScarlet::h2b]*, resulting in strong, tissue-specific expression of the cleavable reporter in all somatic gonad cells. The Flexon approach is described in Shaffer and Greenwald (2022).

hlh-2(ar614), described in (Attner et al., 2019) contains a deletion of a regulatory element that eliminates HLH-2 expression only in Z1.pp, Z4.aa, and their daughter cells. Because *hlh-2* activity in these cells is necessary for an AC to be specified (Karp and Greenwald, 2003; 2004; Sallee and Greenwald, 2015), this mutant lacks an AC. Thus, P6.p is not induced to express the lateral signal that activates LIN-12/Notch in P5.p and P7.p. Because both the EGF-like and lateral signals are missing, the daughters of the VPCs fuse to the major hypodermal syncytium.

The strains GS9324, GS9399, and GS9317 were generated directly through injection and transgenesis, as described in Method Details. The strains GS9215, GS9338, GS9854, GS9339, GS9452, GS9447, GS9322, and GS9314 were generated through crosses and checked for homozygosity by genotyping PCR.

METHOD DETAILS

Generating *lin-12(ar640)*

We used the self-excising cassette (SEC) method to generate *lin-12(ar640)[lin-12::tevp]* (Dickinson et al., 2015). The repair template pJS106 was made in a two-step Gibson cloning process (Gibson et al., 2009; NEB Inc. E2621) in which (1) an intermediate plasmid pJS87 was generated by replacing the GFP and tev cut site sequences of a pBluescript based SEC vector pJC41 with a 2.1 kb 5' homology arm for the *lin-12* locus, and (2) the coding sequence for TEV protease (Barnea et al., 2008) and a 1.6 kb 3' homology arm for the *lin-12* locus were added.

To generate the *lin-12(ar640)* allele, we injected the repair template pJS106 (50 ng/µl), two *lin-12* directed sgRNA and Cas9 expressing plasmids pJC54 and pJC55 (25ng/µl each), and the co-injection markers pCFJ90 (7.5 ng/µl) and pGH8 (10 ng/µl) into the germline of GS8949 *hlh-2(ar623)[gfp::tcut::hlh-2]* hermaphrodites. The injected hermaphrodites were placed at 25°C, and treated with hygromycin after 3 days to select for integrants. Progeny with a roller

(Rol) phenotype were picked 7 days post-injection, and checked for homozygosity. The SEC was then excised by heat shocking at 32° for 4 hours and picking non-Rol progeny. The *lin-12(ar640)* allele was then isolated by standard crossing to generate the strain GS9215.

To generate *glp-1(ar648)[glp-1::tevp]*, we used a *dpy-5* co-CRISPR strategy (Kim et al., 2014). The repair template pJS135 was made using Gibson cloning to insert fragments containing a 676 bp 5' homology arm for the *glp-1* locus, the coding sequence for TEVp, and a 661 bp 3' homology arm for the *glp-1* locus into a pBlueScript (KS)+ vector backbone. The sgRNA and Cas9 expressing plasmids pJS131 and pJS132 were generated using Gibson cloning to replace the *pha-1* targeting sequence in pJW1285 (Ward, 2015) with sequences targeting the *glp-1* locus.

To generate the *glp-1(ar648[glp-1::tevp])* allele, we injected the repair template plasmid pJS135 (50 ng/µl), the *glp-1* directed sgRNA and Cas9 expressing plasmids pJS131 and pJS135 (25 ng/µl each), and a *dpy-5* directed sgRNA and Cas9 expressing plasmid pDR91 (gift from Abhishek Bhattacharya) into N2 hermaphrodites. Injected animals were placed at 25°C. Dpy progeny were isolated 4 days post-injection and allowed to lay eggs for 1 day prior to lysis and PCR to check that the sequence was inserted.

Phenotypic analysis of *Notch::tevp alleles*

lin-12(ar640) and *glp-1(ar648)* hermaphrodites appear indistinguishable from wild-type hermaphrodites, in that we observed no apparent defects in egg-laying or fecundity that might indicate compromised Notch activity during the course of maintaining and working with strains containing these alleles. Nevertheless, to support this inference, we examined GS9314 *lin-*

12(ar640)[lin-12::tevp]; somatic gonad cleavable reporter and GS9447 *arSi85[mex-5p::reporter]; glp-1(ar648)[glp-1::tevp]* hermaphrodites more closely.

To verify that GS9314 does not have defects associated with compromised *lin-12* function, we examined hallmark cell fate decisions in gonadal and vulval development analyzed in Figures 2, 5, and 6. We allowed 13 adult GS9314 hermaphrodites to lay eggs for 2 hours on one plate and then examined the progeny in mid-L4 for the number of ACs and vulval morphology; all (100%) had 1 AC and wild-type vulval morphology (n=41). We also examined late L4 for uterine-seam (utse) cell formation, which requires *lin-12*-mediated cell fate decisions in VU descendants (Newman et al., 1995); all (100%) had proper utse formation (n=25). Furthermore, we examined GS9314 hermaphrodites for egg-laying defects, which, in addition to normal vulval and uterine development, requires proper *lin-12* function during sex muscle differentiation (Foehr and Liu, 2008; Hale et al., 2014; Li et al., 2013): we picked 50 GS9314 L4 larvae to individual plates and verified that all were able to lay eggs normally.

To verify that *glp-1(ar648)* does not cause defects associated with compromised *glp-1* activity, we performed two assessments. Maternal *glp-1* is required early in embryogenesis; *glp-1(-)* mutations cause embryonic lethality in the progeny (Austin and Kimble, 1987; Priess et al., 1987). To test for embryonic viability, we examined progeny of ten GS9447 *arSi85[mex-5p::reporter]; glp-1(ar648)[glp-1::tevp]* and nine N2 wild-type hermaphrodites: we placed individual L4 larvae on separate plates, removed the hermaphrodites the next day, and scored for dead eggs after allowing the progeny to hatch overnight. There were five total dead eggs on ten plates total for GS9447 and four dead eggs on nine total plates for N2, suggesting that *glp-1(ar648)* function is wild-type during embryogenesis. In addition, as hypomorphic mutations in *glp-1* can reduce brood size due to the combination of embryonic lethality and reduced germline

stem cell maintenance (Austin and Kimble, 1987), we counted total broods for three L4 larvae of GS9447 and N2, passing them every day onto new plates, and counting the number of progeny on each plate about 24 hours after passage. We found that GS9447 (n=244, 223, 195; average=220.7) and N2 (n=242, 236, 179; average=219.0) animals produced similar levels of progeny, and the number expected for wild-type worms raised at 25° (Byerly et al., 1976), indicating that *glp-1(648)* functioned indistinguishably from *glp-1(+)*.

Reporters

The cleavable reporters presented in this study use diffusion of GFP out of nucleus after cleavage from a nuclear RFP::H2B tether by TEV protease as a readout for LIN-12 activity. The GFP sequence is from pDD282 (Dickinson et al., 2015) and is codon-optimized for *C. elegans*. The mScarlet sequence is also codon optimized for *C. elegans* (wrmScarlet; El Mouridi et al., 2017) with a synthetic intron added for efficient expression; the H2B sequence is from *his-58*. The reporters used in Figure S1 and 4 use mCherry::H2B instead of mScarlet::H2B, but all other components are identical. A 51 bp linker sequence between the GFP and RFP sequences (GAGAATCTGTACTTTCAATCCGGAAAGGGAGGTGGATCCGGAGCCGGATCT) encodes the 7 amino acid residue long TEV recognition site (ENLYFQS) and a 10 residue long flexible linker sequence (GKGGGSGAGS). Under our imaging conditions, we did not detect any FRET between the two fluorescent proteins in the cleavable reporter, or photoconversion of mScarlet, as described below in Still imaging in the M lineage, VPCs, germline, and somatic gonad.

We also tested cleavable reporters that added a nuclear export signal (NES) tag onto GFP: NES sequences from HIV-1 Rev, human MAP2K2, *C. elegans* MEK-2, and human

RANBP1 (Xu et al., 2012). All of the NES sequences facilitated the nuclear export of free GFP in cells with reporter cleavage, but they all also caused uncleaved reporter to localize to the cytoplasm, thus obscuring segmentation and reducing the overall dynamic range of the system. The extent of ectopic cytoplasmic localization varied by cell type, so it remains possible that an NES sequence may improve reporter performance in other tissues and systems, but is not ideal for a universal reporter.

VPC cleavable reporters: The 5' regulatory region for the VPC cleavable reporters consist of the 5' and intronic sequences from *lin-31*, called *lin-31p* (Tan et al., 1998). *arTi351[lin-31p::gfp::tcut::mScarlet::h2b]* was made using plasmid pJS119, and *arTi356 [lin-31p::gfp::tcut::mCherry::h2b]* was made using plasmid pJ128. Both plasmids were cloned using Gibson assembly to insert the respective coding regions into pCC249, a miniMos vector with the *lin-31p* regulatory sequence.

M lineage cleavable reporter: The 5' regulatory region of the M lineage cleavable reporter consists of sequences from the 5' region of *hlh-8*, called *hlh-8p* (Harfe et al., 1998). *arTi359[hlh-8p::gfp::tcut::mScarlet::h2b]* was made using pJS136, which was made by restriction cloning with *Age*I-HF and *Bgl*II to insert *gfp::tcut::mScarlet* from pJS119 into the miniMos vector pJS107 that contained *hlh-8p* and *h2b*. The transgene was generated in the *lin-12(ar640)* background and fortuitously inserted at a site tightly linked to *lin-12*, and was not separated for analysis on its own.

Somatic gonad cleavable reporter: *arTi355[rps-27p::gfp(flexon)::tcut::mScarlet::h2b*] was made using plasmid pJS126, which was cloned using Gibson assembly to insert the gene region into the blank miniMos vector pCFJ910. The *flexon* is flanked by *lox2272* sites so as not

to recombine with the *loxP* site present in the *lin-12(ar640)* switch which was generated during the course of engineering that allele using the method (Dickinson et al., 2015).

Standard protocols for isolating and mapping single copy insertions from miniMos vectors were used to generate each of the above transgenes from their respective plasmids (Frøkjær-Jensen et al., 2014; wormbuilder.org). Young adult hermaphrodites were injected with a solution containing the vector plasmid (10 ng/µl), the Mos transposase-containing plasmid pCFJ601 (50 ng/µl), the heat shock-induced negative selection plasmid pMA122 (10ng/µl), and the co-injection markers pGH8 (10 ng/µl) and pCFJ90 (2.5 ng/µl). After injection, plates were placed at 25°. 250 µl of 25 mg/ml G418 was added to the plates 2-3 days after injection, and then the plates were left to starve. About 7-10 days after injection, plates that starved out and had lost co-injection marker expression were subjected to a 2 hour heat shock at 34°, and then plates were chunked the next day onto plates containing G418. After another day, individuals that appeared healthy were isolated; the transgene was mapped in their progeny by inverse PCR and then homozygosed by genotyping PCR.

Germline cleavable reporter: The 5' regulatory region for the germline cleavable reporter contains 5' sequences from *mex-5*, called *mex-5p*; the 3' UTR from *tbb-2* was used for germline permissibility (Merritt et al., 2008). *arSi85[mex-5p::gfp::tcut::mCherry::h2b:tbb-2 3' UTR]* was generated using the SEC method to insert a single-copy transgene into a locus (*ttTi4348*) that is permissive to germline and early embryonic expression (Frøkjær-Jensen et al., 2012). The repair template pJS134 was made using Gibson cloning to insert *gfp::tcut::mCherry::h2b* into the SEC vector pCC357 (de la Cova et al., 2017), which contains homology arms for the *ttTi4348* locus and the sequences for *mex-5p* and *tbb-2 3' UTR*. To generate *arSi85*, adult N2 hermaphrodites were injected with the repair template pJS134 (50ng/µl), the Cas9 and *ttTi4348* targeting sgRNA

expressing plasmid pAP582 (50 ng/µl; Pani and Goldstein, 2018), and the coinjection markers pGH8 (10 ng/µl) and pCFJ90 (2.5 ng/µl). The allele was isolated following the protocol outlined above in the generation of *lin-12(ar640)*.

Still imaging

Animals were imaged using a Zeiss AxioObserver Z1 inverted microscope with a 63X, 1.4NA oil immersion objective and a spinning disk. A 488 nm, 100mW laser was used to excite GFP and a 561 nm, 75 mW laser was used to excite the RFPs. Z-stacks of GFP and RFP fluorescence were simultaneously captured with a dual-camera system.

When indicated, timed egg-lays were performed for developmental synchronization. Gravid hermaphrodites were placed on a seeded plate and allowed to lay eggs for 1 hour before removal, and progeny were allowed to grow until the desired developmental stage was reached.

VPCs (Figure 2B, S1): For GS9338 *lin-12(ar640)[lin-12::tevp]; arTi351[lin-31::reporter]* and GS9324 *arTi351*, larvae were incubated for approximately 30 hours after egglay prior to imaging. Since GS9854 *hlh-2(ar614); lin-12(ar640); arTi351* do not have vulvae and do not lay eggs, animals were synchronized using a standard bleaching protocol (Stiernagle, 2006) to isolate embryos; hatched larvae were collected three hours after bleaching and incubated prior to imaging for about 22 hours. For imaging, larvae for each genotype were mounted onto a 3% agarose pad and immobilized with 10 mM levamisole. The following parameters were used for imaging: 250 ms exposure in both channels, 400 EM gain, 3% GFP 488 nm laser power, 25% 561 nm laser power, and 600 nm slice intervals. The same egglay conditions, preparations, and imaging parameters were used for GS9339 *arTi356[lin-31::reporter]; lin-12(ar640)* and GS9452 *arTi356; lin-12(ar640); sel-10(ar41).* GS9452 also

contains transgenes for fluorescent somatic gonad markers that do not interfere with segmentation or quantitation of the VPCs (Key Resource Table).

M lineage (Figure 3,S3): Approximately 17 hours after egg lay, GS9399 *arTi359[hlh-8p::reporter] lin-12(ar640)[lin-12::tevp]* larvae were mounted onto a 3% agarose pad and immobilized with 10 mM levamisole. The following parameters were used for imaging: 250 ms exposure in both channels, 400 EM gain, 15% GFP 488 nm laser power, 30% 561 nm laser power, and 600 nm slice intervals.

Germ line (Figure 4): L4 larvae from unsynchronized plates of either GS9447 *arSi85[mex-5p::reporter]; glp-1(ar648)[glp-1::tevp]* or GS9317 *arSi85* were mounted onto a 3% agarose pad and immobilized with 10 mM levamisole. The following parameters were used for imaging: 250 ms exposure in both channels, 400 EM gain, 4% GFP 488 nm laser power, 25% 561 nm laser power, and 1 μm slice intervals.

Specified AC and VU (Figure 5): GS9314 *lin-12(ar640)[lin-12::tevp]; somatic gonad cleavable reporter* or control GS9322 *somatic gonad cleavable reporter* larvae were picked from unsynchronized plates, mounted onto a 3% agarose pad and immobilized with 10 mM levamisole. Late L2/early L3 larvae were selected for imaging based on gonad size and morphology. The following imaging parameters were used: 150 ms exposure in both channels, 400 EM gain, 4% GFP 488 nm laser power, 25% 561 nm laser power, and 600 nm slice intervals.

To test for FRET activity, GS9322 *somatic gonad cleavable reporter* animals were imaged using identical conditions to those outlined above, but with 0% 561 nm laser power; the photomicrographs were then inspected for red fluorescence. The somatic gonad cleavable reporter was used for assessing FRET because the Flexon system produces the brightest reporter

expression of all strains used; if there was FRET activity, it would be the most evident with this reporter. However, there was no observable red fluorescent emission under these imaging conditions.

To test for mScarlet photoconversion from red to green emission under simulated time-lapse imaging conditions, GS9770 *arTi430[rps-27p::mScarlet(flexon)::h2b::unc-54 3'UTR]; arTi237[ckb-3p::cre(opti)]* [gift of Jee Hun (Henry) Kim] were prepared for imaging as described above and then illuminated with the 561 nm laser at 25% power for 10 minutes prior to imaging with identical parameters to the what was used for time-lapse imaging. No green spectrum fluorescence was observed after the extended illumination.

Time-Lapse Imaging

We note that the use of confocal imaging required keeping worms anesthetized, limiting the length of the videos we could take of young larvae without introducing complications from starvation or the inability to molt. The microfluidic device used previously for high-throughput lineage analysis of the AC/VU decision is not compatible with confocal microscopy (Keil et al., 2017; Attner et al., 2019). The possibility of microfluidic devices compatible with confocal microscopy may allow for longer-term imaging of SALSA in *C. elegans* (Berger et al., 2021). These constraints would not necessarily apply to other ex vivo (e.g. Hung et al., 2017; Regot et al., 2014; Ryu et al., 2015) or in vivo (Johnson and Toettcher, 2019; Pokrass et al., 2020; Simon et al., 2020) systems.

M lineage (Figure S3): GS9399 L1 larvae were picked from an asynchronous plate into 48 ul of 0.1% tricaine/0.01% tetramisole in M9 and incubated at room temperature for 30 minutes. Anesthetized larvae were then mounted into 0.01% tricaine/0.001% tetramisole in M9

on a 4% agarose pad. Animals in the 2-M stage were selected for movies. Imaging was performed using spinning disk microscopy, with the following parameters: 250 ms exposure for both channels, 800 EM gain, 3% 488 nm laser power, 25% 561 nm laser power, and 600nm slice intervals. Z stacks for up to 6 larvae per pad were taken at 15 minute intervals for 25 timepoints, which does not compromise larval development.

Somatic Gonad (Figure 6, S4): GS9314 and GS9322 animals were synchronized with egg lays in which 15 gravid hermaphrodites were allowed to lay eggs on a plate for 1 hour followed by removal of the adults. The plate was then incubated at 25°C for 21-21.5 hours to begin imaging in mid L1. Larvae were mounted and anesthetized using the same protocol as outlined for the M lineage movies. Larvae were selected for imaging by the extent of gonad progression (undivided Z1.pp and/or Z4.aa).

Imaging was performed using spinning disk confocal microscope setup described above, to produce images allowing for accurate ratiometric quantification. The larvae are viable for approximately 6 hours under these conditions, allowing for capture of the birth-time interval and birth order, but not the final cell fate, which was inferred based on earlier studies (Attner et al., 2019). Imaging parameters were the same as for the M lineage movies, except with 150 ms exposure for both fluorescent channels.

Image quantification

Images for the M lineage (Figure 3C,D), and the somatic gonad (Figures 5,6,S5), were processed and quantified using published protocol, workflow, and code (de la Cova et al., 2017; Luo et al., 2020). In summary, after illumination correction, the red fluorescence intensity value was divided by the green fluorescence intensity value for each pixel of every slice, and then

normalized between 0.1 and 99.9% to avoid pixel artifacts. Segmentation by red fluorescence and quantitation was performed with Cellprofiler (Kamentsky et al., 2011). Tracking the nuclei was done using Matlab scripts from de la Cova et al. (2017) with the leniency parameter increased from 5 to 10 to accommodate for increased worm movement during time-lapse imaging, and extraction of the average upper quartile intensity of the three most equatorial slices for each nuclei of interest was performed using Matlab scripts adapted from Luo et al. (2020). For the time-lapse imaging in the somatic gonad, the "method to draw dividing lines between clumped objects" parameter in the CellProfiler pipeline module "IdentifyPrimaryObjects" was changed to *shape* to draw borders between close nuclei based on shape instead of intensity.

For quantifying the VPCs (Figure 2B,S1), prior to entering the pipeline the GFP and red channels were aligned using auto channel alignment in Zen for translational and rotational alignment, with the red channel as reference and using the highest quality setting. This prevented us from using the Red:Green pixel values, so Matlab scripts adapted from Luo et al. (2020) were used extract the average nuclear red and green fluorescence intensities for the three equatorial slices and divide the average red by the average green values to create a nuclear Red:Green ratio.

For testing different quantitation methods using the M lineage (Figure S2), the channels were aligned as described above. The original pipeline was altered to define the cytoring in the following way. After primary object identification and segmentation of a "prenucleus," the edges of each object were expanded by 1 pixel to form a "postnucleus," and then a secondary object was identified by expanding the postnucleus by 5 pixels; the area between the outer ring and the postnucleus was called the cytoring. The cytoring was used as the cytoplasmic measurement because it was difficult to distinguish cell borders *in vivo* in multilayered, complex tissues without an additional membrane marker which would affect segmentation. Using this pipeline,

we extracted the values for average nuclear Red:Green, nuclear 1/Green, and Cytoring:Nuclear Green fluorescence for the three equatorial slices of each cell as described above, and compared them to each other and to the original nuclear pixel Red:Green values used in Figure 3C.

For quantifying the germ line (Figure 4), images of the germ line of L4 larvae were first aligned using Zen's channel alignment tool as described above. There were too many nuclei in too many planes in each image for effective segmentation using our pipeline, so nuclei were manually segmented using ImageJ to draw circles around the nuclei of interest. Nuclei were selected for quantification according to distance in microns from the distal end using the conversion of 3.5 microns per cell diameter, which is approximately the average of previously used conversion metrics (Chen et al., 2020a; Lee et al., 2019). Three nuclei per position (0, 5, 10, 15 cd) were quantified for each germline arm. The equatorial three slices of each nuclei were found based on the integrated density of red fluorescence, and the average nuclear Red:Green integrated density per slice was averaged across the three equatorial slices for each nuclei. .

The slightly different methods to generate the nuclear Red:Green ratios, as well as differences in imaging parameters in different contexts, are what creates discrepancies in the scaling of measurements between tissues. However, we present internal controls for each tissue context for which all parameters and measurements methods were identical.

QUANTIFICATION AND STATISTICAL ANALYSIS

All statistical analysis was performed in GraphPad Prism. The minimum level of significance for all analysis was set at 0.05 prior to corrections for multiple testing. Every data set was subjected to D'Agostino & Pearson tests of normality before proceeding with the appropriate statistical tests. To compare nuclear Red:Green ratios of VPCs within genotypes (Figure 2), we performed

a repeated measures ANOVA with Greenhouse-Geisser correction, and post hoc comparisons using the Tukey HSD test for every possible pairwise comparison for each genotype. To compare nuclear Red:Green ratios between genotypes in the VPCs (Figure 2) and in the germline (Figure 4), we performed ordinary one-way ANOVA tests and post hoc comparisons using Tukey HSD tests for every possible pairwise comparison. For comparing nuclear Red:Green fluorescence in *sel-10(+)* and *sel-10(-)* animals (Figure S1), we performed an ordinary one-way ANOVA, and post hoc comparisons with Bonferroni corrections to compare each VPC between the two genotypes. When comparing SALSA activity in dorsal and ventral cells in the M lineage, we performed an unpaired t-test (Figures 3C,S1), and a one sample t-test was used to compare the difference in nuclear Red:Green between the dorsal and ventral cells within every worm to the expected mean of zero (Figure 3D). To compare nuclear Red:Green between the αVU and the AC in L3 (Figure 5), we performed paired t-tests. To compare the differences in nuclear Red:Green between alpha cells (Figure 6) and parent cells (Figure S5) for different birth-time intervals, we used a Kruskal-Wallis H test with post hoc comparisons using Dunn's correction for every possible pairwise comparison within each test.

The imaging conditions we used here, with fluorescence images captured every 15 minutes, were comparable to those used in Attner et al. (2019), where the cut-off between "long" and "short" birth orders were established according to cell fate outcome. Assessing outcome in that study was possible because it utilized a microfluidic device. In this study, we could not observe the final fate outcomes of the cells imaged in the short-term imaging conditions we had to use to allow for confocal microscopy, so in addition to using the bins established previously, we performed an independent statistical analysis of our data to determine the cutoff between short and long birth-time intervals under these conditions. We binned animals into "short" or

"long" birth-time intervals based on whether the α cells were born less than or greater than a specific time interval apart. We used Mann-Whitney tests to compare the nuclear Red:Green differences between alpha cells within every worm for "short" vs. "long" birth-time intervals, beginning with a 30 minute birth-time interval cutoff and increasing the time interval stepwise. The most statistical significance was generated when the "short" bin included birth-time intervals ≤45 minutes, and the "long" bin included birth-time intervals >45 minutes; therefore, we considered α cell pairs with ≤45 minute birth-time intervals to be "short", and α cell pairs with >45 minute birth-time intervals to be "long". These bins are consistent with those used in (Attner et al., 2019).

For short birth-time intervals, we considered an α cell to have developed an advantage in LIN-12 activity if it had a higher nuclear Red:Green ratio than the other α cell for at least three successive timepoints, or a difference in nuclear Red:Green ratio of >0.1 units, at the end of the video or last comparable time point.

Chapter 3 Figures

Figure 1

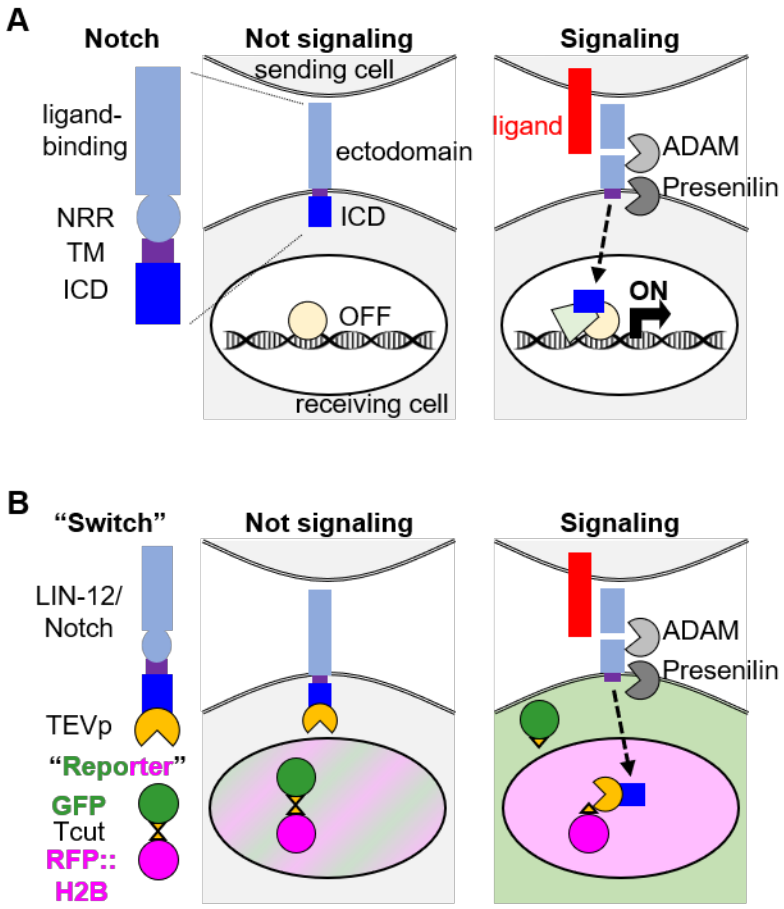

Figure 1. SALSA design

(A) Notch is a membrane tethered transcriptional activator. When Notch is inactive, the intracellular domain (ICD) remains at the cell membrane and target gene transcription is repressed by a sequence-specific DNA binding protein of the CSL family, which in the absence of Notch activation is associated with co-repressors. When Notch interacts with ligand, cleavage in the ectodomain by an ADAM protease followed by cleavage in the transmembrane domain by Presenilin, the catalytic component of the □-secretase complex, releases the ICD from the membrane. ICD enters the nucleus and forms the Notch nuclear complex with CSL and other coactivators to promote transcription of target genes (reviewed in Falo-Sanjuan and Bray, 2020; Greenwald and Kovall, 2013; Henrique and Schweisguth, 2019).

(B) SALSA is a bipartite Notch activity sensor, consisting of a "switch" and cleavable "reporter." The "switch" is Notch fused to TEV protease (TEVp). The cleavable "reporter" is a fusion protein::GFP tethered to the nucleus by an RFP::H2B, with an intervening TEV protease recognition site (Tcut). When Notch is inactive, TEVp does not gain access to the nucleus, so the reporter is uncleaved and the nuclear Red:Green ratio is low; when Notch is activated, TEVp-tagged ICD enters the nucleus and cleaves the reporter, releasing GFP from the RFP::H2B tether to diffuse out of the nucleus, resulting in a high nuclear Red:Green ratio.

Figure 2

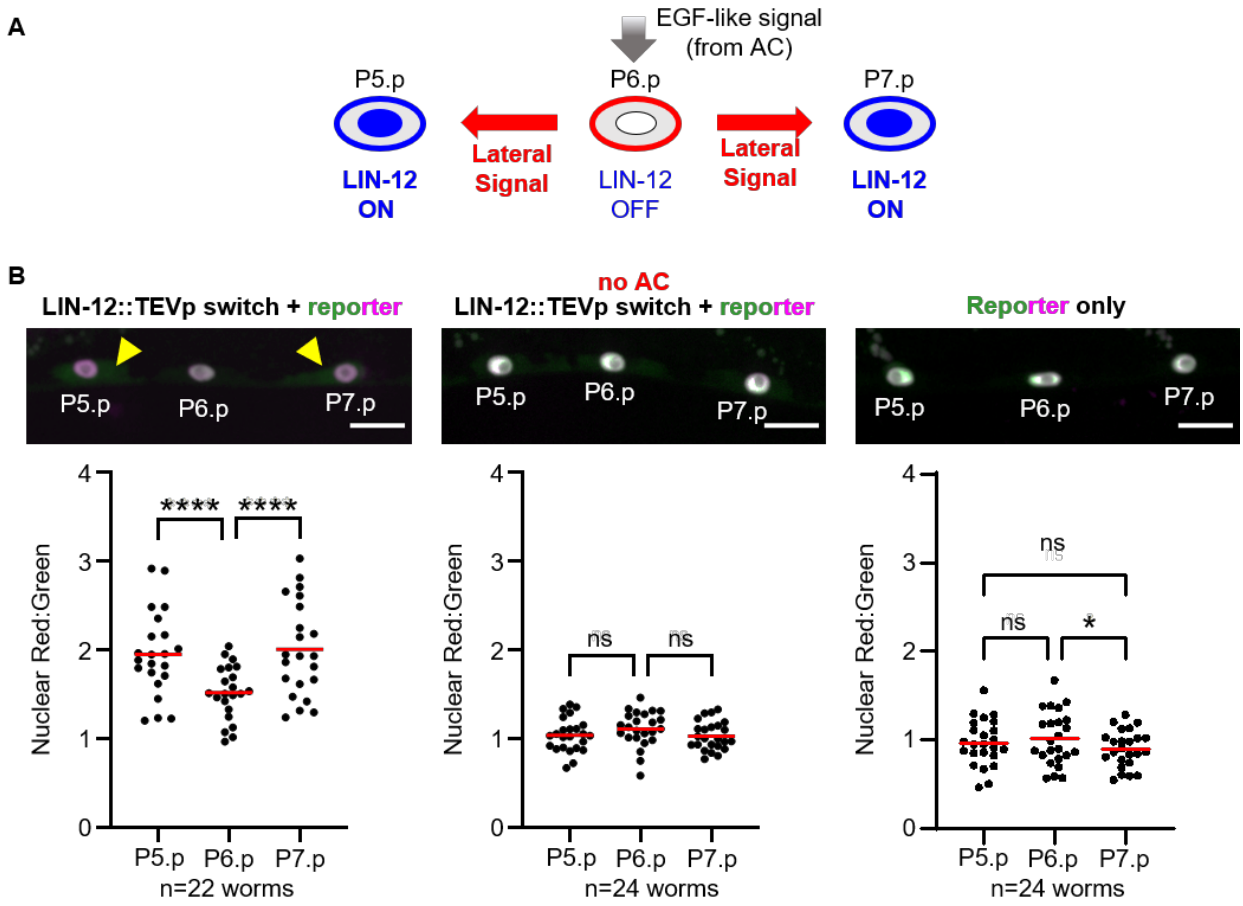

Figure 2. SALSA agrees with expectations for LIN-12/Notch activity in in the Vulval Precursor Cells (VPCs).

(A) Schematic representation of LIN-12/Notch activity in VPCs and descendants. Three VPCs, named P5.p, P6.p, and P7.p, are patterned during the L3 stage by a combination of LET-23/EGF Receptor and LIN-12/Notch activity (Gauthier and Rocheleau, 2017; Shin and Reiner, 2018; Sternberg, 2005). An EGF-like inductive signal from the Anchor Cell (AC) of the gonad induces P6.p to express the lateral signal, consisting of ligands for LIN-12. These ligands activate LIN-12 in P5.p and P7.p. There are multiple regulatory mechanisms that ensure that LIN-12 is maximally activated in P5.p and P7.p, and LET-23/EGFR is maximally activated in P6.p (Sundaram, 2005). These mechanisms include multiple direct transcriptional targets of LIN-12 that antagonize EGFR activity in P5.p and P7.p (Berset et al., 2001; Yoo et al., 2004), and of LET-23/EGFR that lead to loss of LIN-12 protein in P6.p (Levitan and Greenwald, 1998; Shaye and Greenwald, 2002).

(B) SALSA agrees with expectations based on genetic analysis and LIN-12/Notch transcriptional target reporters in VPCs. Photomicrographs are maximum orthogonal projections for all Z planes with visible fluorescence. Scale bars are 10 μm. Yellow arrowhead, cytoplasmic GFP.

For each genotype, we performed an RM one-way ANOVA to compare the nuclear Red:Green ratios in the VPCs. There was a statistically significant difference in nuclear Red:Green ratios between the VPCs in the presence of the LIN-12::TEVp switch (left,

$F(2,21)=18.24$, $p<0.0001$). Post hoc comparisons (STAR Methods) indicate that there is a significantly higher nuclear Red:Green fluorescence in P5.p and P7.p compared to P6.p (****$p<0.0001$). Center, when the AC is eliminated, LIN-12/Notch is not activated in P5.p and P7.p, and there was no statistically significant difference in nuclear Red:Green ratio between the VPCs ($F(2,23)=2.143$, $p=0.1337$). In the reporter only genotype, a low statistically significant difference was seen ($F(2,23)=4.661$, $p<0.05$); post hoc comparisons (STAR Methods) indicated a slight difference between P6.p and P7.p in the reporter only control (*$p<0.05$), but not between P5.p and either other VPC ($p>0.05$), suggesting that the slight difference is not biologically meaningful. See also Figure S1 for analysis of a sel-10/FBXW7 E3 ubiquitin ligase mutant. We also performed ordinary one-way ANOVAs to compare P5.p and P7.p between genotypes, and found significant differences (P5.p, $F(2,67)=63.37$, $p<0.0001$; P7.p, $F(2,67)=72.84$, $p<0.0001$). Post hoc comparisons (STAR methods) revealed that in the presence of the LIN-12:TEVp switch and an AC, P5.p and P7.p had significantly higher nuclear Red:Green ratios than in the absence of the switch or the absence of the AC (****$p<0.0001$), but there was no difference in nuclear Red:Green ratios between the no AC and the reporter only genotypes for both P5.p and P7.p ($p>0.05$).

Figure 3

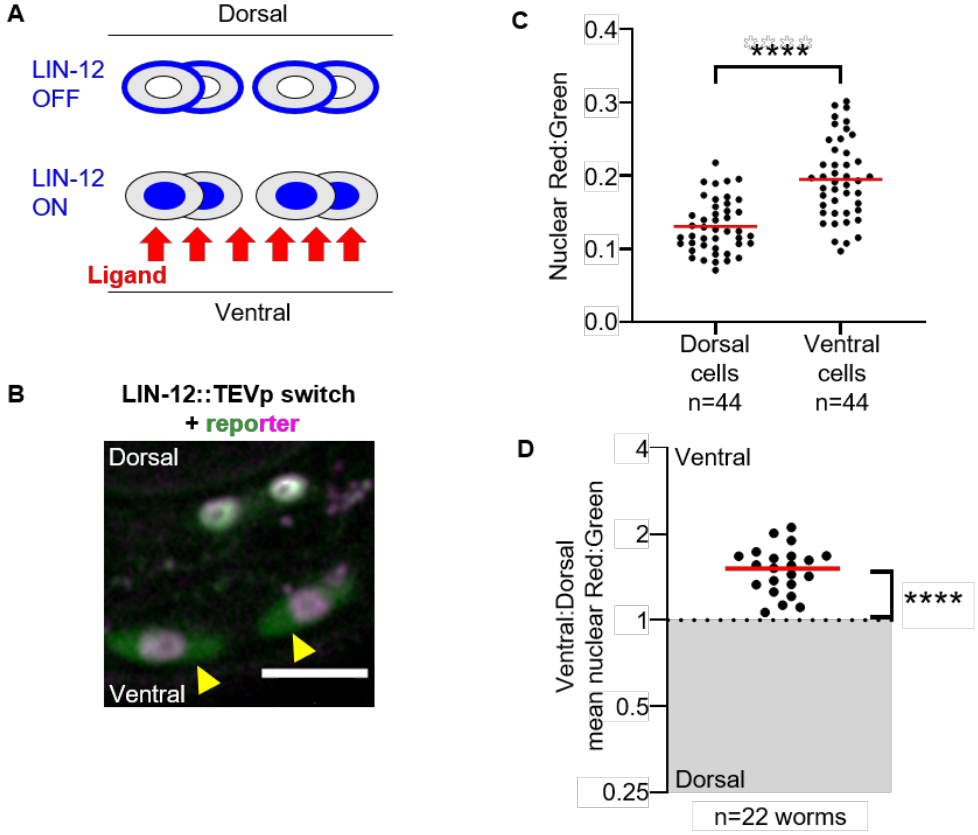

Figure 3. SALSA agrees with expectations for LIN-12/Notch activity in the M lineage of C. elegans.

(A) Schematic representation of LIN-12/Notch activity in the M lineage. Both dorsal and ventral descendants of the M mesoblast express LIN-12, but LIN-12 is activated only in the ventral descendants by ligand from the ventral hypodermis (Foehr and Liu, 2008).

(B) Visual evidence that LIN-12 is active in ventral but not dorsal M descendants. Photomicrograph is one Z slice taken at the 8-M stage of a hermaphrodite carrying the LIN-12::TEVp switch and the cleavable reporter expressed in the M lineage (strain GS9399). At this stage, four of the eight cells are on the right, and the other four are on the left; this slice captures one side. Yellow arrowhead, cytoplasmic GFP is readily apparent. Scale bar is 10 μm. See Figure S3 for time-lapse videos of three worms.

(C) Nuclear Red:Green quantification at the 8-M stage. Red lines indicate the mean. The nuclear Red:Green ratio was significantly higher in ventral cells than in dorsal cells (Unpaired t-test, $t(168)=8.699$, ****$p<0.0001$). See Figure S2 for alternative quantification strategies.

(D) On a per-animal basis, the nuclear Red:Green ratio is greater in ventral cells compared to dorsal cells. Each point represents the ratio of the average nuclear Red:Green between the ventral cells and dorsal cells within each animal from (C). When compared to a null hypothesis of the dorsal and ventral cells having equivalent LIN-12 activity (a ratio of 1), the mean was significantly greater than 1, indicating that the average nuclear Red:Green ratio is greater in ventral cells than dorsal cells (One sample t-test, $t(21)=27.95$, ****$p<0.0001$).

Figure 4

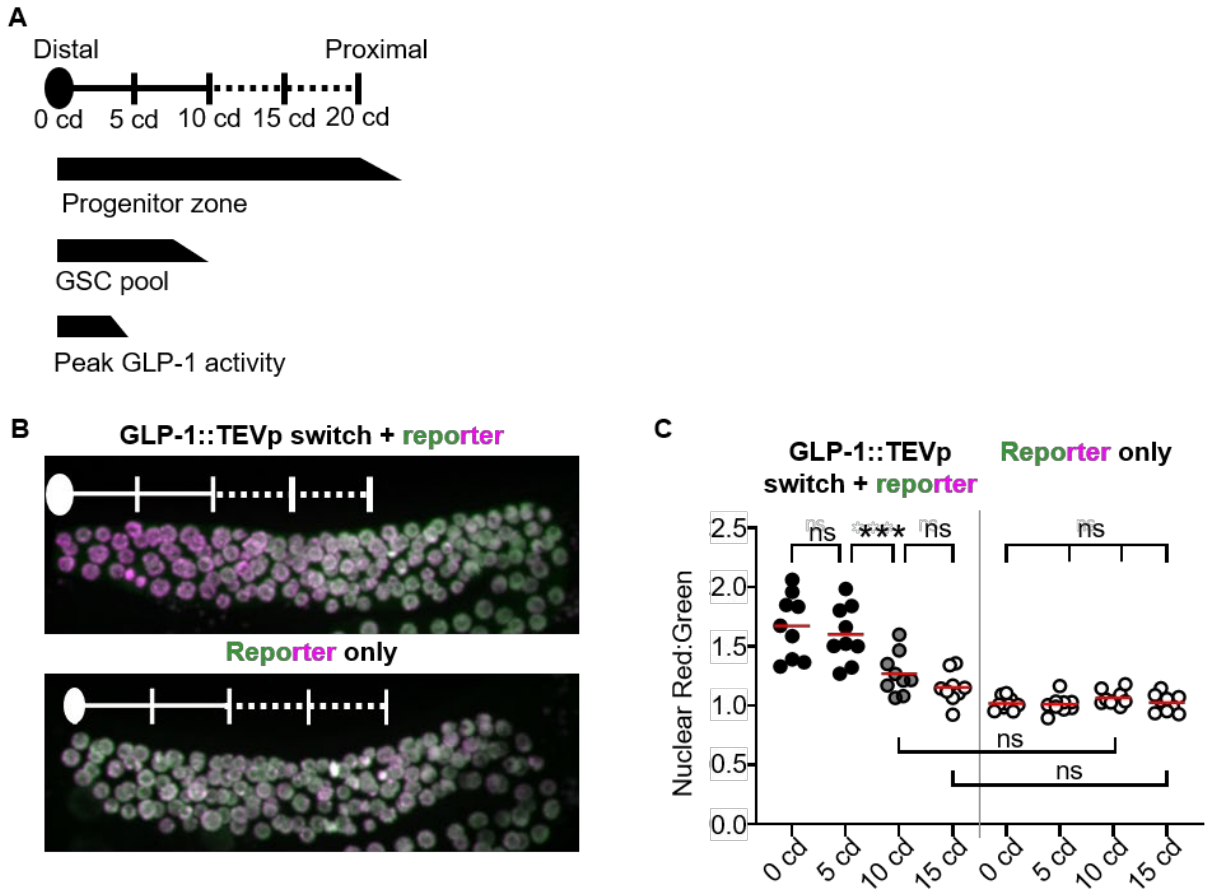

Figure 4. SALSA agrees with expectations for GLP-1/Notch activity in the germ line of C. elegans.

(A) Schematic representation of GLP-1 activity and expression of transcriptional targets in the germ line. GLP-1 activity peaks in Germline Stem Cells (GSCs) within 5 cell diameters (cd) of the distal end of the gonad arm; GLP-1 activity is detectable throughout the GSC pool ~8-10 cd from the distal end (see text).

(B) SALSA detects GLP-1 activity in GSCs at the distal end of the gonad arm. Each photomicrograph shows a single gonad arm from an L4 larva. See STAR Methods for measurement details. The reddened distal end of the germ line from the larvae expressing the GLP-1::TEVp switch correlates with the known pattern of GLP-1 activity.

(C) GLP-1 activity peaks from 0-5 cd, ceases by ~10 cd. Each dot represents one germ nucleus; red lines indicate the mean. A one-way ANOVA found a significant effect of the position of the cells in the presence of the switch on nuclear Red:Green ratio in GSCs ($F(7, 64) = 26.16$, $p<0.0001$). Post hoc pairwise comparisons showed that in the presence of the GLP-1::TEVp switch, nuclear Red:Green significantly decreased between 5 and 10 cd (***$p<0.001$). The nuclear Red:Green ratio for 10 cd was not significantly different from 15 cd, and neither were significantly different from the same relative position in the reporter only control ($p>0.05$). In the absence of the GLP-1::TEVp switch, all regions had similar nuclear Red:Green ratios ($p>0.05$).

Figure 5

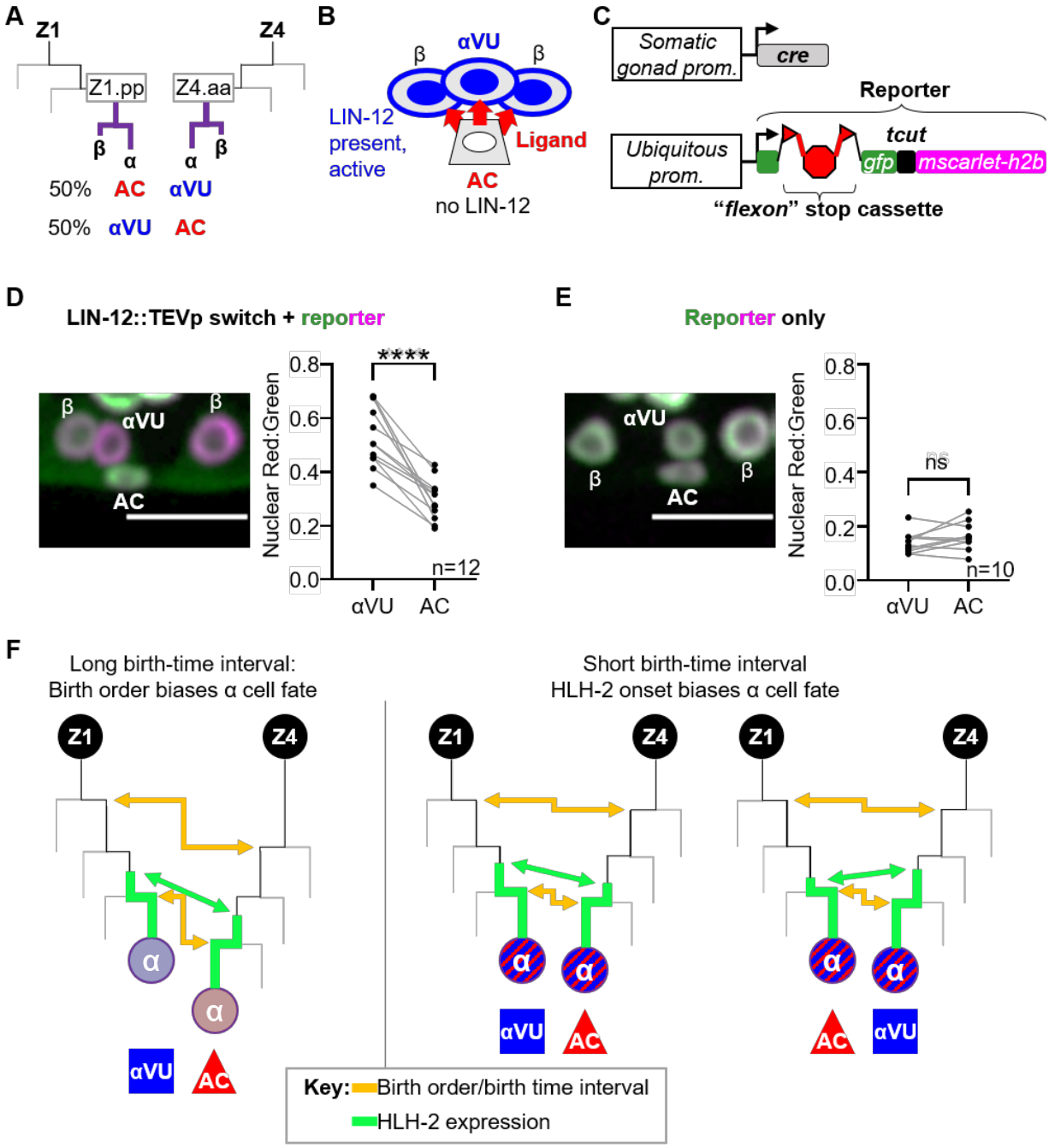

Figure 5. SALSA agrees with expectations for LIN-12 activity in the committed AC and VU.

(A) Lineal origin of the α cells. The somatic gonad precursor cells Z1 and Z4 give rise to the α cells, Z1.ppp and Z4.aaa, which undergo a stochastic, binary cell fate decision to ensure one becomes the AC and the other the αVU. The sisters of the α cells, called the β cells, always become VUs; they do not strictly require *lin-12* activity for VU fate (Sallee et al., 2015) and are not considered further here. The parents of the α cells are Z1.pp and Z4.aa.

(B) Schematic representation of LIN-12 activity in the proximal somatic gonad in the early L3 stage. LAG-2 and LIN-12 are initially expressed in both α cells, but during the AC/VU

decision, feedback loops lead to reciprocal expression patterns that are sustained in the committed progeny. The differentiated AC expresses the ligand LAG-2, and the αVU expresses LIN-12 as well as reporters for transcriptional targets of LIN-12 (Luo et al., 2020; Yoo and Greenwald, 2005).
(C) Diagram of the "somatic gonad cleavable reporter" transgenes. One transgene (*arTi237*) drives expression of Cre recombinase in Z1 and Z4, leading to excision of a *flexon* stop cassette from transgene *arTi355*, allowing for strong, specific expression of GFP::Tcut::mScarlet::H2B from a pan-somatic ribosomal protein gene promoter (STAR Methods; Shaffer and Greenwald, 2022).
(D) SALSA agrees with expectations that LIN-12 is active in the αVU and not in the AC. The photomicrograph is a maximum orthogonal projection of an individual expressing the LIN-12::TEVp switch and the somatic gonad cleavable reporter in early L3. Scale bar is 10 μm. The early L3 hermaphrodite displays visibly reddened VU nuclei. The nuclear Red:Green ratio for the αVU is statistically higher than the AC (paired t-test, t=7.932, df=11, ****p<0.0001). Regardless of the absolute value, the nuclear Red:Green ratio in the αVU is always higher than the AC in any given animal in the presence of the LIN-12::TEVp switch.
(E) Reporter only control for D. The photomicrograph is a maximum orthogonal projection of all Z planes with visible fluorescence of an individual expressing only the reporter. Scale bar is 10 μm. No significant difference between the AC and αVU was seen was seen in nuclear Red:Green quantitation (paired t-test, t=1.514, df=9, p=0.1644).
(F) Two stochastic elements prior to the birth of the α cells bias the outcome of the AC/VU decision. The birth-time interval is indicated by yellow double-headed arrows, and HLH-2 expression is indicated in green. See text for details.

Figure 6

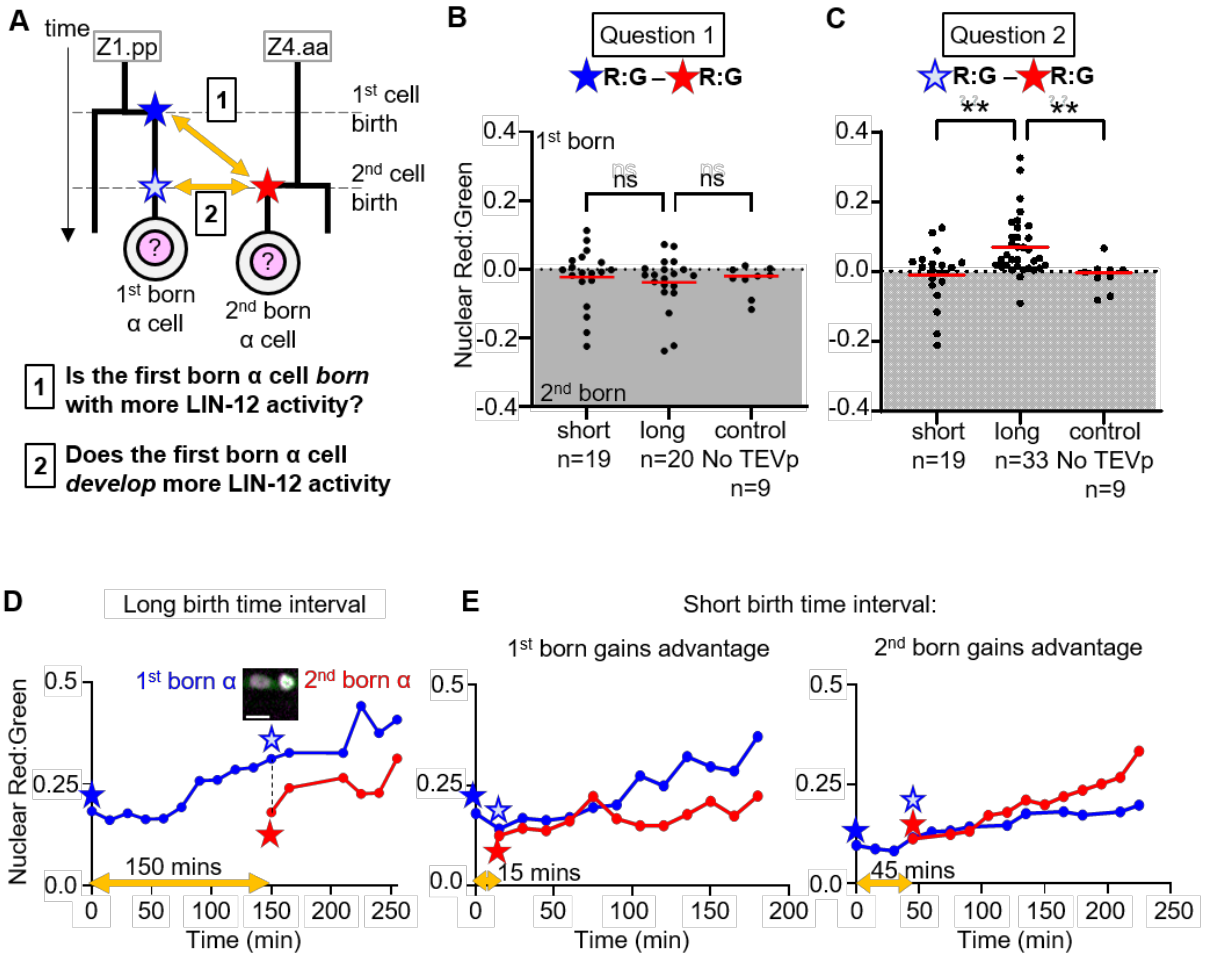

Figure 6. SALSA provides evidence for the proposed activity of LIN-12 with respect to stochastic events that influence the AC/VU decision.

(A) Schematic diagram of critical timepoints. The solid blue star represents the first-born α cell immediately after its birth, and the blue outlined star represents the first-born α cell at the time that the second-born cell is born (solid red star). The yellow double-arrowed lines indicate the comparisons made in (B) and (C) to answer the questions posed below the diagram. See Figure S4 for ten time-lapse videos of SALSA across the timepoints represented here.

(B) Each α cell is born with a similar level of LIN-12 activity, regardless of birth-time interval or relative birth-order. We determined the difference in nuclear Red:Green ratio between the first-born and second-born α cells at the timepoint after each of their birth. Each α cell pair was binned into short and long birth-time intervals for animals expressing the LIN-12::TEVp switch and somatic gonad cleavable reporter (STAR Methods) and the bins were compared to each other and to a cleavable reporter only control. Each dot represents one cell α pair, and the red lines indicate the mean. No significant difference was seen after statistical analysis (Kruskal-Wallis, H = 1.196, df = 3, p = 0.55). See Figure S5 for quantitation of SALSA in the parents of the α cells, and STAR methods for details of quantitation and statistical tests. For both strains, only animals in which both α cell births were captured and able to be quantified were included in this analysis.

(C) When the birth-time interval is long, the first-born α cell gains a relative advantage in LIN-12 activity. We determined the difference in nuclear Red:Green ratio between the first-born and second-born α cells at the timepoint after the birth of the second-born cell. Animals were binned and the difference in nuclear Red:Green ratio compared as in (B). Kruskal-Wallis tests indicated significant differences between the groups ($H = 16.26$, $df = 3$, $p=0.0003$). Post hoc pairwise comparisons (STAR Methods) find the long birth-time interval bin had significantly greater differences in nuclear Red:Green ratio between α cells than in the short birth-time interval bin or cleavable reporter only control (**$p<0.01$). Animals were included in this analysis only if both α cells were able to be quantified at the timepoint following the birth of the second-born α cell.
(D) Example of a long birth-time interval. Quantitation of the nuclear Red:Green ratios over time for an individual with a long birth-time interval. The trajectory of the first-born α cell is indicated by a blue line and the second-born α cell by a red line; the birth-time interval in this case is 150 minutes (yellow double-arrowed line). The α cells are born with similar nuclear Red:Green ratios (solid blue and red stars), but by time the second-born α cell is born, the first-born α cell has a higher nuclear Red:Green ratio (blue outlined star), and the difference is sustained over time. The inset shows the α cells at the timepoint immediately following the birth of the second-born α cell. Scale bar is 4 μm.
(E) Examples of short birth-time intervals. Cells are represented as in D. The first- and second-born α cells have similar nuclear Red:Green ratios when they are born (solid stars). Left, the first-born α cell gains a LIN-12 advantage; right, the second-born α cell does (STAR Methods).

Figure 7

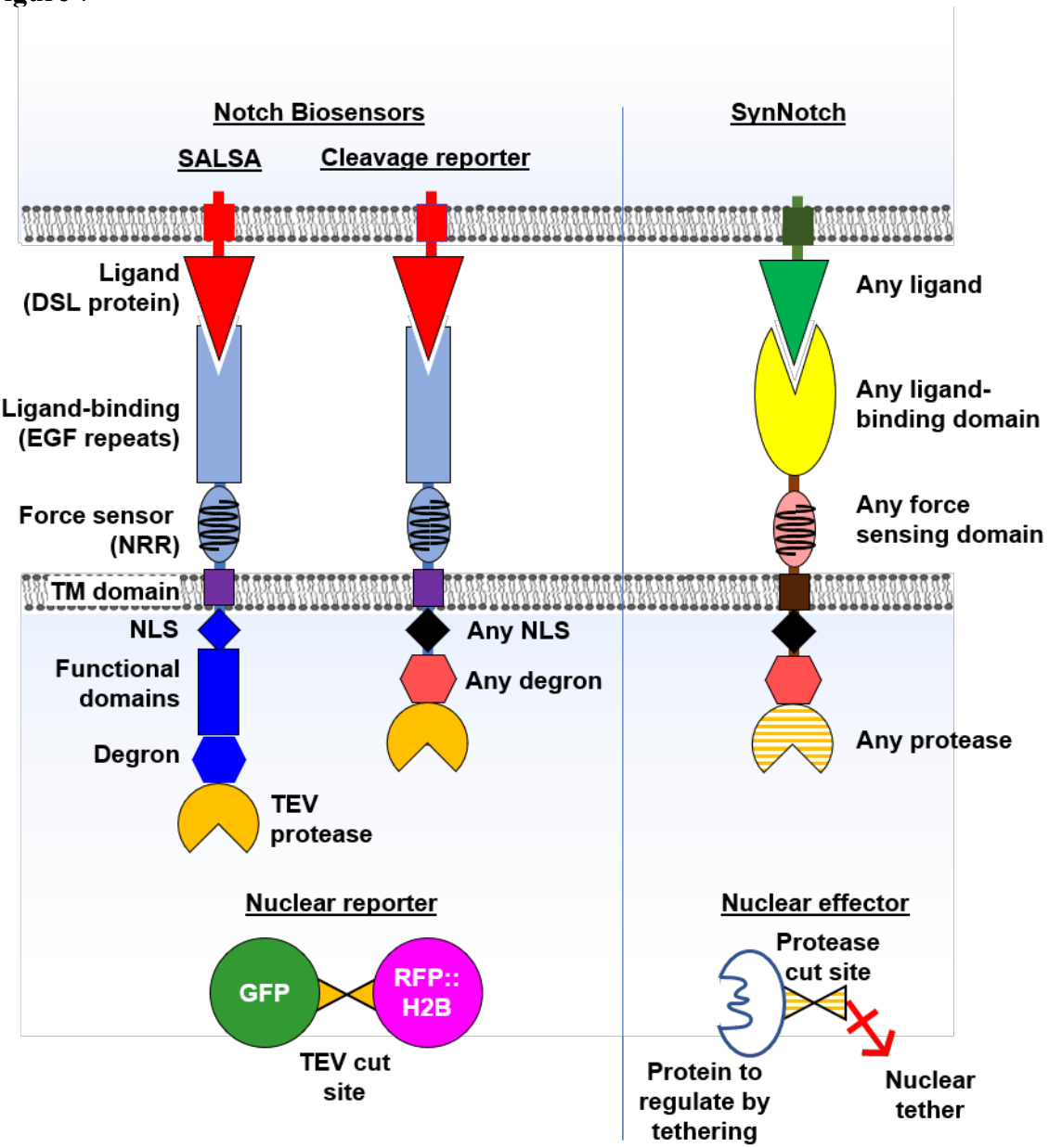

Figure 7. The modular design of the SALSA switch and reporter may be adapted for other potential applications.

Switch design: For this study, we used TEVp fused to the C-terminus of endogenous LIN-12/Notch, as our primary goal was to measure LIN-12 signaling activity during cell fate decisions. However, each component of the switch may be altered depending on the application, and any switch may be introduced as a transgene. For example, replacement of the ICD with an exogenous NLS, with or without an alternative degron, would remove native regulation of the active Notch intracellular domain for focusing on ligand, ADAM protease, or Presenilin/γ-secretase activity. "SynNotch" proteins that have outputs other than transcriptional activation may be modeled on SALSA by using alternatives for any of the Notch domains, and TEVp or other protease moieties with an NLS, further tuned by presence or absence of a degron.

Reporter design: Modifications can change the purpose from reporting switch activity to regulating the activity of a nuclear-tethered protein. For example, tethering a cytosolic ubiquitin ligase or kinase using a histone or other nuclear anchor via the Tcut site would allow for conditional degradation or phosphorylation of specific cytosolic targets that is dependent upon switch activity, or tethering a pro-protein that is matured by cleavage at the protease cut site would allow for ligand-controlled regulation of its activity.

Chapter 3 Supplement

Figure S1

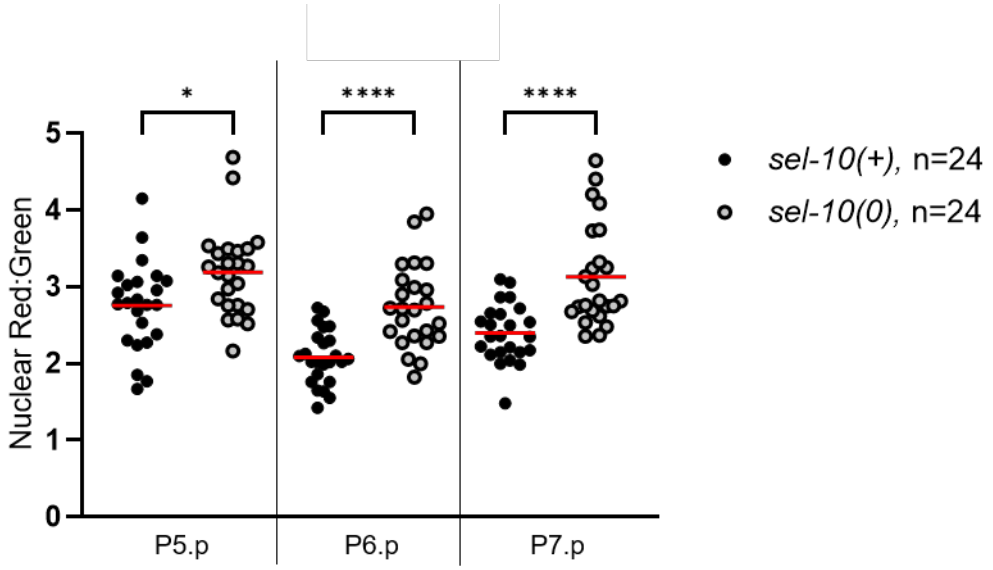

Figure S1. The nuclear Red:Green ratio is increased by removing the E3 ubiquitin ligase that targets the intracellular domain of LIN-12. Related to Figure 2.
The ubiquitin ligase SEL-10/Fbxw7 is the substrate-recognition subunit of Cullin-based E3 ubiquitin ligase that recognizes a phopho-degron sequence in the intracellular domain of LIN-12/Notch proteins (reviewed in Welcker and Clurman, 2008). VPC fates are normal in a *sel-10* null mutant, but mutation of the CPD stabilizes the intracellular domain of LIN-12 (Hubbard et al., 1997; de la Cova and Greenwald, 2012; Deng and Greenwald, 2016).
Here, we show that in a *sel-10* null background, the inferred stabilization of the LIN-12::TEVp switch leads to an elevated Red:Green ratio in VPCs (one-way ANOVA, $F(5,138)=15.65$, $p<0.0001$; pairwise comparisons with Bonferroni corrections, *$p<0.05$, ****$p<0.0001$). These results indicate that the limit of detection of SALSA in an otherwise wild-type background was not reached, and together with the data for signaling in the absence of lateral signal (Figure 2), supports the inference that SALSA has adequate dynamic range for quantifying LIN-12/Notch activity *in vivo*.

Figure S2

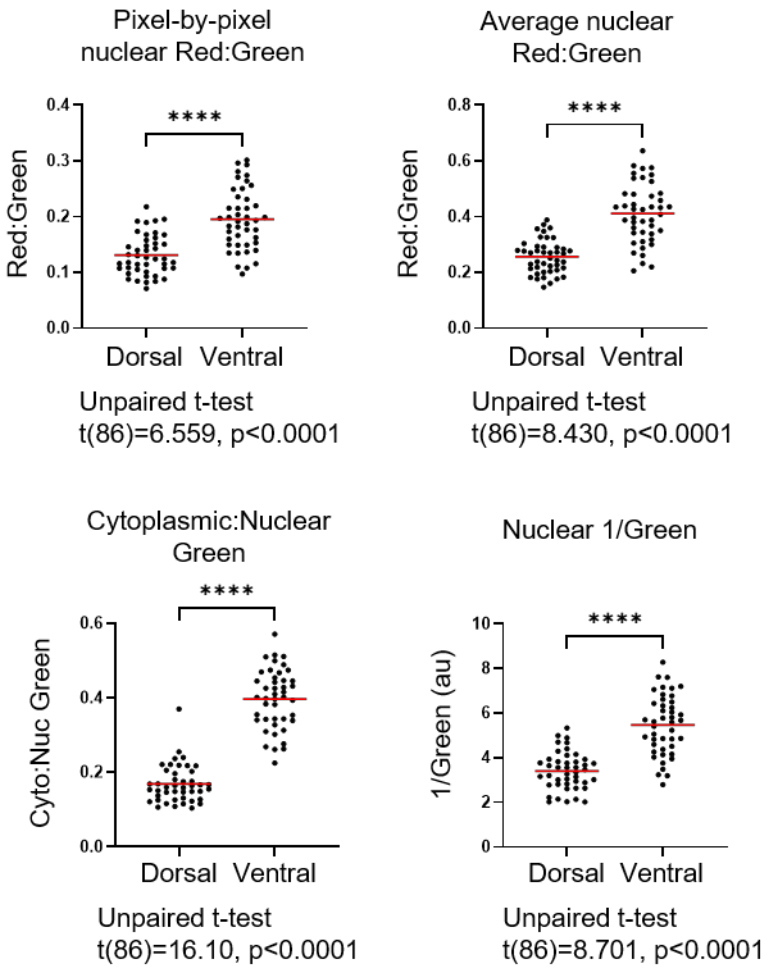

Figure S2. Different methods of quantifying using SALSA give similar results. Related to Figure 1 and Figure 3.

We quantified LIN-12 activity four different ways (numbered 1-4) in the strain GS9399, which contains the M lineage cleavable reporter and the LIN-12:TEVp switch. At the 8-M stage, the M cell descendants are permissive to multiple quantification methods because they are large and far apart, facilitating the use of a cytoring as a component of the measurement. We compared the reporter in the dorsal and ventral descendants for each method, and found similar results and statistical significance for each (unpaired t-test).

Pixel-by-pixel nuclear Red:Green was used in all figures and supplemental figures except for Figures 2, 4 and S1. Average nuclear Red:Green is an equivalent way to achieve the same goal and was used in Figures 2, 4, and S1, where we had to do manual channel alignment to adjust for issues with our setup.

Cytoplasmic:Nuclear (C:N) Green and Nuclear 1/Green may be useful if there is concern about different stabilities or photobleaching properties of different fluorescent proteins. However, only the C:N ratio is ratiometric and controls for different expression levels between cells.

Figure S3

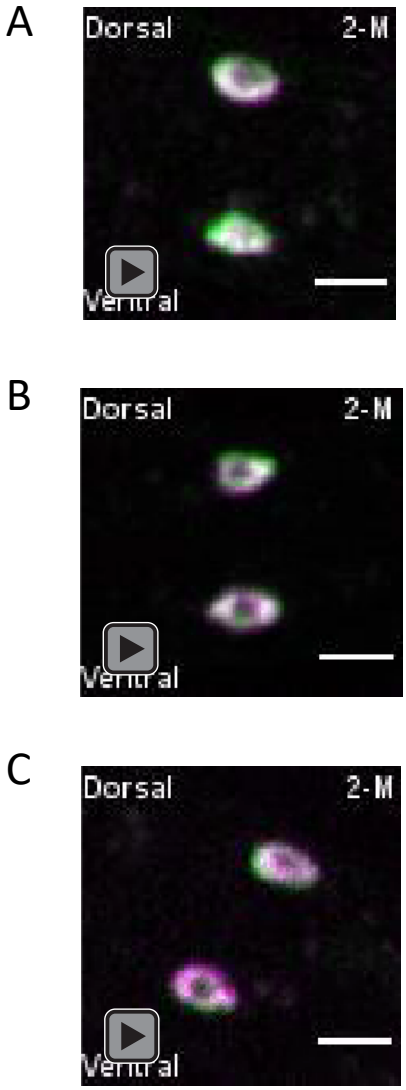

Figure S3: Time-lapse videos of SALSA in the M lineage. Related to Figure 3.

Time-lapse videos of strains carrying the LIN-12::TEVp switch and M lineage cleavable reporter were taken beginning at the 2-M stage (see STAR Methods). The videos for the three individuals shown were compiled wherein each frame contains one slice of the Z stack taken at each time-point that captures as close to the center of as many cells as possible. Stage transitions from 2-M to 4-M and 4-M to 8-M are noted. Scale bars are 5 μm.

A −division plane from 2-M to 4-M was anterior-posterior
B −division plane from 2-M to 4-M was left-right so only the left cells are shown (closest to the light source)
C −division plane from 2-M to 4-M was anterior-posterior

Figure S4

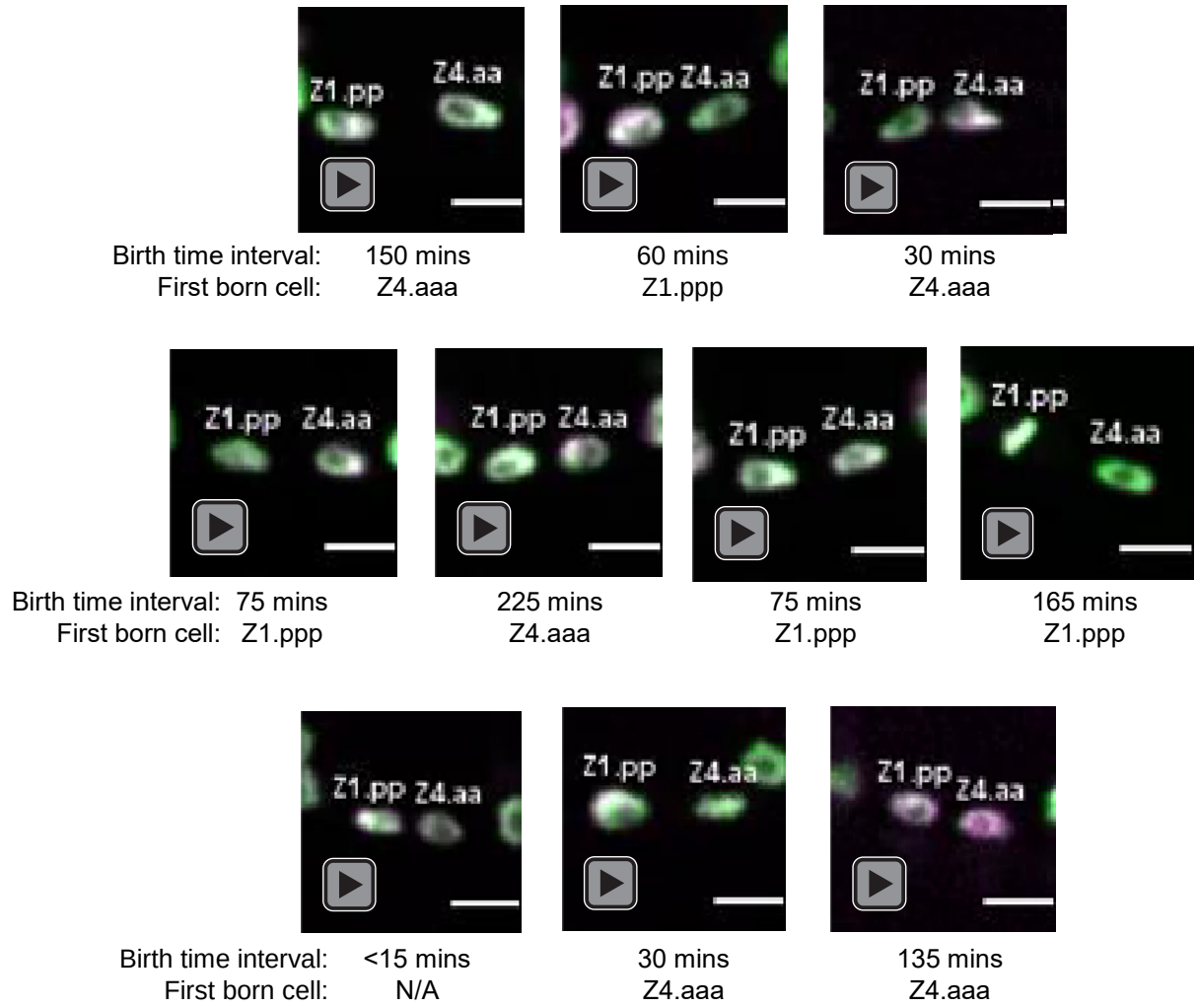

Figure S4: Time-lapse videos of SALSA during the early stages of the AC/VU decision. Related to Figure 6.

Time-lapse videos begin with Z1.pp and Z4.aa, the parents of the α cells, Z1.ppp and Z4.aaa. See STAR Methods for details. Larvae were viable for up to 6 hours under the anesthesia conditions necessary to immobilize them for videos, allowing for capture of the birth-time interval and birth order but not final cell fate, which could be inferred based on the data of Attner et al. (2019). Each video was compiled wherein each frame contains one slice of the Z stack taken at each time-point that captures both cells in the frame. The birth time interval and first-born cell is noted under each movie. A ”long” birth-time interval is ≥45 minutes. Scale bars are 5 μm.

Figure S5

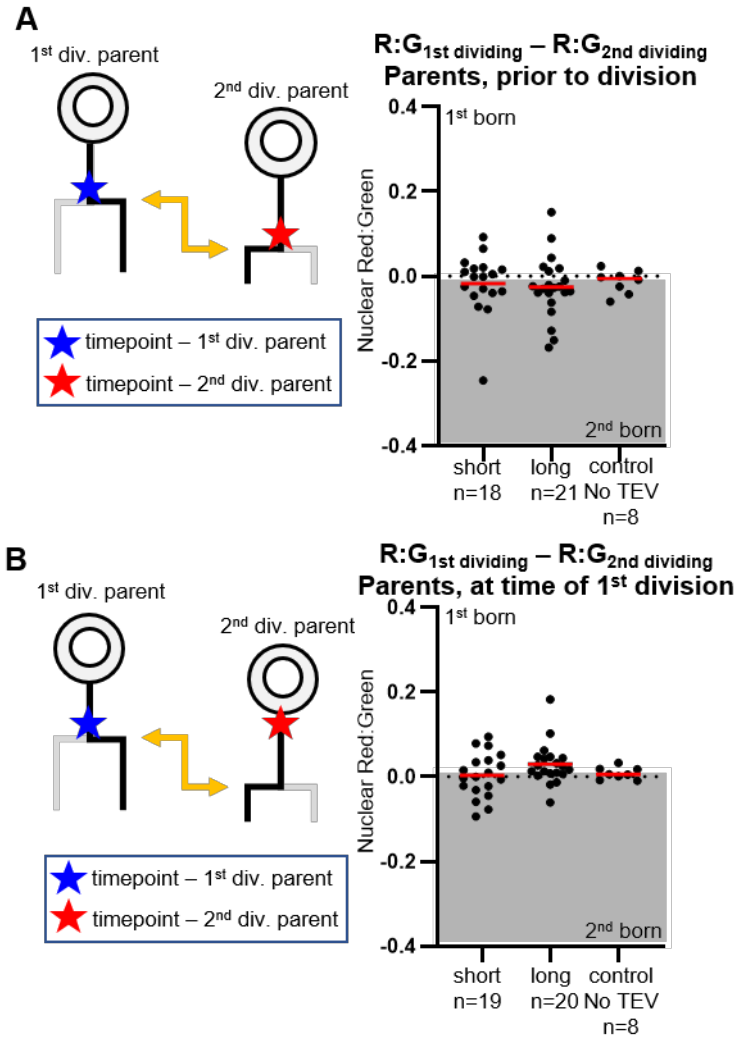

Figure S5. SALSA does not detect LIN-12 activity in Z1.pp and Z4.aa, the parents of the a cells. Related to Figure 6.

The nuclear Red:Green ratio was quantified in the parent cells (A) at the timepoint before each cell divided and (B) at the timepoint immediately before the division of the first parent. The difference was taken between the first-dividing parent and second-dividing parent in each worm and binned according to the length of the time interval for GS9314 *lin-12(ar640)[lin-12::tevp]; somatic gonad reporter*. Statistical analysis between these bins and the control GS9322 *somatic gonad reporter* was performed, with no significant difference between any categories for either analysis (STAR Methods; for A, H = 0.7701, df = 3, p = 0.6804; for B, H = 3.113, df = 3, p = 0.2108). This analysis includes all animals for which both parent cells were able to be quantified at the appropriate timepoints.

Chapter 4: General Discussion

4.1 Summary

In this thesis, I have described two independent but co-developed, genetically-encoded tools that were used to investigate Notch signaling activity in *C. elegans*.

In chapter 2, I presented Flexon, a small, CRE/*lox*-based stop cassette that is encoded into a synthetic exon and synthetic introns. A f*lexon* can be inserted into the coding region of a transgene or endogenous gene to block expression in the absence of Cre, and restore expression conditionally in the presence of tissue-specific Cre drivers. Reporter transgenes with a *gfp(flexon)* sequence driven by the ubiquitous promoter *rps-27p* had no or minimal fluorescence in the absence of a Cre driver. Fluorescence was restored to the somatic gonad or vulval lineages in the presence of the respective tissue-specific Cre drivers, and was maintained for longer in the lineage and at a higher intensity than transgenes with *gfp* sequences driven by the same tissue-specific promoters. A *flexon* was also inserted into the endogenous *rde-1/Argonaute* locus to create a tissue-specific RNAi strain. The *rde-1(flexon)* allele was shown to be highly defective for RNAi in multiple tissues and in all developmental stages in the absence of a Cre driver. However, RNAi activity could be restored to specific tissues in the presence of a tissue-specific Cre driver.

In chapter 3, I presented SALSA, a biosensor for the visualization and quantification of Notch signaling *in vivo*. SALSA consists of a "switch", an endogenous Notch protein tagged with the Tobacco Etch Virus protease (TEVp) at the C-terminus of the intracellular domain, and "reporter" with a GFP and RFP::H2B tethered together by the TEVp consensus sequence (Tcut). Notch activity is indicated by changes to the nuclear Red:Green ratio when Tcut cleavage by active nuclear Notch::TEVp frees the GFP from the nuclear RFP, allowing GFP to diffuse out of

the nucleus. I showed that patterns of the nuclear Red:Green ratio reflected expected LIN-12/Notch activity patterns in inductive signaling (M lineage) and lateral signaling (VPCs and somatic gonad primordium) events, and GLP-1/Notch signaling events (germline) in *C. elegans*. I also took time-lapse videos of SALSA and quantified nuclear Red:Green across the births of the α cells. I found that the α cells are born with relatively similar levels of LIN-12 activity regardless of birth time interval or birth order, but when the birth time interval between the α cells is long the first-born α cell accumulates an edge in LIN-12 activity over the second-born α cell; short birth time intervals do not give the first-born α cell time to accumulate an edge, and a LIN-12 activity difference develops randomly with respect to birth order. These results are consistent with data in which the first-born α cell has a VU fate bias when there is a long birth time interval between α cells (Attner et al., 2019).

4.2 Further investigations of the AC/VU decision

Attner et al. (2019) showed that the outcome of the AC/VU decision could be predicted by two stochastic, interrelated events upstream of the α cells. The first stochastic event is the relative birth order of the α cells. At birth time intervals >40-45 minutes between the α cells, the first-born α cell always becomes the VU, but the AC/VU fate decision is random with respect to birth order at birth time intervals <40-45 minutes. Stochastic differences in the birth order and birth time interval of the α cells are considered upstream of the AC/VU decision because the birth order and birth time interval is generally consistent throughout the lineage, beginning with the somatic gonad precursors Z1 and Z4. The SALSA data from the time-lapse videos of the somatic gonad agree: a LIN-12 activity advantage is present in the first-born α cell over the second-born α cell at the time of birth of the second-born α cell when the birth time interval is

>45 minutes, but the LIN-12 activity advantage is random with respect to birth order at birth time intervals ≤45 minutes.

The second stochastic event is the relative timing of onset of HLH-2 expression in the parents of the α cells. The parent cell in which fluorescence from an endogenous HLH-2::GFP protein fusion begins first almost always gives rise to the α cell that assumes VU fate, even at short birth time intervals. HLH-2::GFP expression and birth order are related because HLH-2::GFP expression begins within an approximately 30-minute window about 100 minutes after the birth of the parents; the window of HLH-2::GFP expression always occurs earlier in the first-born parent when birth time intervals are long, but the windows overlap when birth time intervals are short so that the order of onset of HLH-2::GFP expression is random with respect to birth time order.

It remains unknown how the relative order and timing of HLH-2::GFP expression in the parents correlates with LIN-12 activity dynamics. Since HLH-2::GFP and the SALSA reporter both use nuclear GFP fluorescence as readout, they were unable to be imaged simultaneously. Therefore, we were unable to determine whether the order of HLH-2 onset in the parent cells correlated with the development of a LIN-12 activity advantage in the α cells. We would expect that the first parent cell with HLH-2::GFP fluorescence would always give rise to the α cell that accumulates the LIN-12 activity advantage. It is unclear if there will be any relation between the time of HLH-2 onset in the parent and the onset of LIN-12 activity in the α cells, such as LIN-12 activity always beginning a certain amount of time after HLH-2 expression begins.

It is possible that a LIN-12 advantage could begin to develop in the parents of the α cells if there is significant time between HLH-2 onset and parent cell division. HLH-2 expression begins in the parent cells, and is required for initial LIN-12 expression in the α cells, but there is

no evidence for LIN-12 expression in the parents using an endogenous LIN-12::GFP fusion (Attner et al., 2019) nor for LIN-12 activity in the parents using SALSA. The delay between HLH-2::GFP fluorescence and LIN-12 reporter activity could be for several reasons: LIN-12 levels in the parents may be so low that expression and activity are undetectable, there may be a molecular block to LIN-12 in the parent cells, or there is insufficient time between the onset of HLH-2::GFP expression and the birth of the α cell for LIN-12 to be made prior to division of the parent cells. Since HLH-2 drives LAG-2 expression in the parent cells to detectable levels, it is possible that LIN-12 activity could begin prior to the birth of the α cells if it was expressed in the parents, even at levels too low to detect with traditional reporters or with SALSA under normal conditions. Technical limitations, such as a lack of strong of specific promoters, prevent precise manipulation of *lin-12* in the parent cells to further test whether *lin-12* is expressed or active, and if it is, whether it is biologically relevant. However, closer examination of SALSA in parent cells with long intervals of time between cell divisions may indicate whether there is LIN-12 activity in the second-dividing parent. Furthermore, using *flexon* to drive a LIN-12::TEVp switch transgene along with the *flexon* reporter in the parents could indicate whether or not there is a block to LIN-12 signal transduction in the parent cells.

Regulatory feedback loops ensure that upstream stochastic events, like the relative time differences in α cell births and of HLH-2 onset in the parent cells, are turned into a deterministic and robust cell fate outcome for the AC/VU decision. LIN-12 activity positively regulates LIN-12 (Wilkinson et al., 1994) and LAG-1 (Luo et al., 2020) expression while leading to proteosome-dependent degradation of HLH-2 protein dimers, *lag*-2 downregulation, and possibly downregulation of HLH-2 activity through pathways independent of HLH-2 degradation (Benavidez et al., 2022; Karp and Greenwald, 2003; Sallee and Greenwald, 2015).

The mechanism by which LIN-12 activity leads to HLH-2 degradation remains unknown. In Benavidez *et al.* (2022), an RNAi screen of conserved ubiquitin-related genes found four E3 ubiquitin ligases for which knock-down strongly stabilizes HLH-2::GFP; the authors pointed out that the hits are implicated in processes that regulate AC/VU fate in the α and β cells such as *lin-12* signaling, Wnt/β-catenin signaling, and the cell cycle. Further testing is required to determine if any of these factors act directly on HLH-2, and if they act combinatorially or independently for robust HLH-2 degradation.

The mechanism that controls the timing of HLH-2 onset in the parents is also unknown. HLH-2 expression begins in a specific window after the birth of the parent cells (Attner et al., 2019), suggesting that onset of expression may be tied to the cell cycle. An enhancer sequence approximately five kb 5' of the HLH-2 start site, called *hlh-2prox*, is required for HLH-2 expression in the proximal somatic gonad (Attner et al., 2019; Sallee and Greenwald, 2015). While *hlh-2prox* is a relatively short sequence, a scan for potential transcription factor binding sites using CIS-BP (Weirauch et al., 2014) reveals an extensive number of *trans*-activators that potentially interact with the enhancer; this analysis is to be approached cautiously, as the consensus sequences for many of these *trans*-factors are poorly characterized and may be falsely attributed. A systematic mutational "bash" of *hlh-2prox* could pare down the list of predicted consensus sequences to a manageable number for analysis, which may include analysis of conditional knock outs of the *trans*-factor and directed mutation of the consensus in *cis*. Nonetheless, a gene ontology search of the entire list of factors indicated that seven of the *trans*-factors have been implicated in gonad development: *blmp-1, ceh-22, cog-1, elf-1, fkh-6, lim-7,* and *pop-1*. Gene ontology searches are limited in both scope and specificity, and may miss essential and pleiotropic genes or return genes that do not act in the desired context. However,

POP-1/TCF is a promising candidate because it has both a well-defined consensus sequence and is implicated in regulating VU fate and *hlh-2* expression in the α and β cells. To determine whether POP-1 directly regulates *hlh*-2 expression in the α and β parents through *hlh-2prox*, one could mutate the *hlh-2prox* POP-1 consensus in *hlh-2* reporters, as well as conditionally knock out *pop-1* in the somatic gonad in the presence of *hlh-2* reporters.

4.3 Adaptations of the SALSA biosensor

4.3.1 Adaptations for simultaneous quantitation of SALSA and nuclear protein expression

Improvements or adaptations would need to be made to SALSA in order to simultaneously quantify LIN-12 activity and HLH-2 expression, or expression of any other nuclear proteins. One adjustment would be to use three fluorescent proteins with non-overlapping emission spectra; since red and green fluorescence are being used in SALSA, HLH-2 would have to be tagged with a blue fluorescent protein or a near-infrared (NIR) fluorescent protein. However, both blue and NIR fluorescent proteins have significant limitations in *C. elegans*. Blue fluorescent protein tags are not amenable to long-term imaging because the wavelength of light required for excitation of blue fluorescent proteins is damaging to *C. elegans* over extended periods of time (Edwards et al., 2008; Ward et al., 2008). NIR fluorescent proteins require biliverdin, a product of heme breakdown, to use as a chromophore (reviewed in E.C. Greenwald et al., 2018). *C. elegans* do not synthesize heme, instead relying on ingested bacteria for the nutrient (Rao et al., 2005). NIR fluorescent proteins driven by the *myo-3* promoter are active in *C. elegans* in a background with transgenically supplied heme oxygenase for increased biliverdin production, but fluorescence is restricted to pharyngeal cells that experience the highest concentration of heme supplied by the bacteria (Ding et al., 2017), and supplying a

steady concentration of external heme or bilirubin may not be practical for imaging over time. Additionally, NIR fluorescent proteins tend to be dim relative to other fluorescent proteins.

Reducing the nuclear fluorescent proteins in the SALSA reporter from two to one could also allow for the simultaneous imaging of SALSA and HLH-2. For example, a GFP::tcut::H2B reporter would permit simultaneous imaging with an HLH-2::RFP fusion. However, nuclear segmentation for quantitation may be difficult in cells with LIN-12 activity due to the cytoplasmic fluorescence of the cleaved reporter and fluorescent-tagged HLH-2.

Alternatively, spatial separation within the nucleus between the fluorophores used for nuclear segmentation, Notch activity detection, and HLH-2 expression could provide a way to distinguish between all three; I discuss some designs for SALSA reporters that take this approach in Appendix A. The nucleus can be segmented using fluorescent tags of proteins that localize to the nuclear membrane, such the inner nuclear membrane marker LEM-2::mCherry (Morales-Martínez et al., 2015). HLH-2::RFP expression can then be distinguished from the segmentation marker as red fluorescence within the nucleus. Since both the nuclear marker and the HLH-2 tag use red fluorescent proteins, the Notch sensor is free to use GFP fluorescence. A GFP::tcut::H2B reporter could be used to find the nuclear 1/Green or Cytoplasmic:Nuclear fluorescent measurements to quantify Notch activity. Alternatively, FIB-1/fibrillarin could be used to localize a reporter strongly to the nucleolus (Lee et al., 2010); Notch activity could be quantified using a FIB-1::tcut::GFP::NLS reporter; if active Notch::TEVp has nuclear access, it would cleave the GFP-NLS from the nucleolar tether, allowing it to diffuse freely throughout the nucleoplasm.

4.3.2 Improving the "off-rate" of SALSA

SALSA was able to indicate Notch activity earlier than previously possible with Notch transcriptional reporters in the M lineage and the somatic gonad, and robustly recapitulated expected Notch activity patterns in the VPCs and germline. Also, quantitation of SALSA over time in the somatic gonad allowed us to determine small differences in LIN-12 activity in the α cells that, through feedback loops, could ultimately determine the pattern of the AC/VU outcome in each worm. Therefore, SALSA appears to be a valuable tool for detecting low levels of Notch activity at the onset of signaling events. The size of the region of GLP-1 activity in the germline as indicated by SALSA is comparable with GLP-1 target protein staining and transcript labeling, suggesting that SALSA may also be capable of detecting reduction or cessation of Notch activity on the time scale it takes for germ cells to transition out of the niche. However, the sensitivity of SALSA to detect more rapid drops in Notch activity remains in question.

Since cleavage of the SALSA reporter is irreversible, return of the nuclear Red:Green level to base level after Notch activity is dependent on replacement of the cleaved reporter with newly created and matured uncleaved reporter. Histone tagged fluorescent proteins are known to be highly stable and may not be turned over quickly even if new reporter is being rapidly generated, thereby delaying the return to the baseline fluorescent ratio after cessation of Notch activity. Destabilized fluorescent proteins, in which the fluorophore is tagged with a degradation sequence like PEST (Aulehla et al., 2008; Kitsera et al., 2007; Li et al., 1998; Vilas-Boas et al., 2011) could be used to facilitate turnover, but doing so could also destabilize uncleaved reporter and reduce the overall fluorescent intensity and dynamic range of the system.

Selective degradation of cleaved SALSA reporter components could be achieved by incorporating a TEV protease induced protein inactivation (TIPI)-degron into the SALSA

reporter. TIPI contains a unidirectional (Taxis et al., 2009) or bidirectional (Jungbluth et al., 2010) degron built around the consensus sequence for TEV protease; cleavage of the sequence results in activation of the degrons incorporated into the TIPI for degradation of either or both cleavage products. TIPI has been used to deplete target proteins in yeast (Jungbluth et al., 2012; Renicke et al., 2017), plants (Daum et al., 2014), and *E. coli* (Copeland et al., 2016; Fernandez-Rodriguez and Voigt, 2016; Henrichs et al., 2005; Martínez et al., 2017; Sekar et al., 2016), but has not been used in more complex eukaryotic model systems. Using TIPI to selectively degrade free GFP after cleavage of the reporter may increase the speed in which SALSA responds to Notch activity onset, but also may increase the length of time it takes to return to base nuclear Red:Green. Alternatively, using TIPI to selectively degrade the RFP::H2B after reporter cleavage could further sensitize the reporter to decreases in Notch activity, but may reduce the ability to detect small differences in nuclear Red:Green. Thus, the reporter would have to be finely tuned to ensure a good balance between sensitivity to changes in Notch activity and the robustness of readout if TIPI was incorporated into the SALSA reporter.

4.3.3 Improving the "on-rate" of SALSA

Although we were able to use SALSA to visualize and quantify Notch at earlier time points than we with other Notch reporters, there are technical reasons to believe that the response time of SALSA to Notch activity can be improved. SALSA relies on the diffusion of GFP out of the nucleus to report Notch activity, but GFP without a localization sequence spreads evenly between the nucleus and the cytoplasm. Some concentration of GFP remains in the nucleus after cleavage from the reporter, reducing the dynamic range of the system, particularly when there are low levels of Notch::TEVp activity such as at the onset of signaling. Additionally, the rate of

diffusion for GFP across the nuclear membrane can be 100x slower than diffusion within the cytoplasm or nucleus (Wei et al., 2003). Slow diffusion of cleaved GFP out of the nucleus could delay detection of changes to nuclear Red:Green or Cytoplasmic:Nuclear green fluorescence. We attempted to actively transport GFP that was cleaved from the reporter out of the nucleus by tagging it with a Nuclear Export Signal (NES); this is discussed in Appendix B. However, the NES tag appeared to compete with the histone tag on the RFP and caused some of the uncleaved reporter to localize to the cytoplasm, making it available for cleavage by inactive LIN-12::TEVp on the membrane.

One way to increase the speed of the readout from the Notch reporter is to increase the scale of the response; the greater the quantity of free GFP that is generated by each nuclear Notch::TEVp molecule, the higher the likelihood of sufficient changes to the nuclear Red:Green or Cytoplasmic:Nuclear ratio to detect low levels of signaling early in events. TEV protease variants have been made to increase efficiency and speed of cleavage *in vitro* over the native TEV protease that is used in the switch. Mutating serine 219 to valine or asparagine increases the rate of reaction by preventing autoproteolysis and autoinactivation; additional combinations of mutations have been shown to increase reaction rate and enzymatic activity by increasing the solubility of the protease (Fang et al., 2013; Kapust et al., 2001; Nam et al., 2020; van den Berg et al., 2006; Waugh, 2011; Zhu et al., 2017). Incorporating some or all of these mutations into the TEVp in the switch could increase cleavage efficiency and generate a greater response to lower levels of signal.

Another way to increase the efficiency of SALSA readout would be to use changes in fluorescence intensity as a reporter for Notch activity. Changes in FRET activity have been used to report the proteolytic activity of caspases, membrane type 1 metalloproteases, and proteases

associated with autophagy (reviewed in E.C. Greenwald et al., 2018). FRET-based protease biosensors place the target site for the protease in a linker between a FRET pair of fluorophores, such that catalytic cleavage of the target site separate the fluorophores and results in a decrease in FRET activity, visualized as an increase in fluorescence from the donor and a decrease from the acceptor. The change in FRET activity would be immediate because FRET efficiency decreases dramatically with miniscule changes to intramolecular distance and orientation. However, FRET sensors can have poor signal to noise ratios, which may limit the ability to detect subtle changes in Notch activity.

The CA-GFP system puts a caspase target site in a linker between GFP and a quenching peptide, so that catalytic cleavage of the target site relieves the suppression of GFP fluorescence; CA-GFP has been used in *C. elegans* to quantify caspase activity (Nicholls et al., 2011; Wang et al., 2019). CA-GFP could be used as the reporter for SALSA by replacing the caspase target site with a Tcut site and tagging the GFP with an NLS or histone, so that nuclear GFP fluorescence is quenched in the absence of active Notch::TEVp, but is restored in the presence of active Notch::TEVp after cleavage of the linker releases the quenching peptide from GFP.

4.4 Using SALSA to quantify Notch activity in other models

SALSA is amenable for use as a Notch activity sensor in other models outside of *C. elegans* because it uses components, such as TEVp and fluorescent proteins, and techniques, such as CRISPR/Cas9 and standard transgenesis, that have been established across model organisms. A transgenic Notch::TEVp switch could be used instead of an endogenous switch if tagging the endogenous Notch locus is not feasible or preferred. Fluorescent proteins in the reporter can be swapped to optimize the output signal for different biological contexts and

imaging setups. The speed and sensitivity of SALSA could be useful for investigating tissue-wide Notch activity dynamics in complex lateral signaling paradigms, or to discern the signaling contributions of different Notch homologs during development and in disease states; I discuss one example of each paradigm here.

4.4.1 Lateral signaling in the *Drosophila* notum

Two types of sensory bristles form on the notum during *Drosophila* development; macrochaetae arise at stereotyped positions, and microchaetae form in five regularly-distributed, dorso-central rows in each hemi-notum. Both bristles arise from sensory organ precursor cells (SOPs) which are specified from cells on the notum with potential for epidermal or neural cell fates. Notch-mediated lateral signaling generates cells with low Notch activity that become the SOPs, while the other cells with relatively greater levels of Notch activity assume epidermal cells fates (Heitzler and Simpson, 1991). Notch activity activates transcription of genes in the E(spl)-C locus, which are basic helix-loop-helix proteins that interact with *Hairy* and *Groucho* to downregulate the proneural transcription factors Achaete and Schute (Bailey and Posakony, 1995; Heitzler et al., 1996; Lecourtois and Schweisguth, 1995; Oellers et al., 1994; Paroush et al., 1994; Van Doren et al., 1994). Achaete and Schute are bHLH proteins that interact with the Daughterless (Kunisch et al., 1994), the *Drosophila* homolog of HLH-2, to activate transcription of the Notch ligand Delta; therefore, increased Notch activity results in a reduction of Delta expression (Parks et al., 1997).

Macrochaetae positions are determined by regions of enhancer sequences in the achaete-schute locus that restrict high levels of proneural expression to a few cells in precise positions (Gómez-Skarmeta et al., 1995); Notch-mediated lateral signaling then ensures the formation of

only one SOP per proneural cluster (Heitzler and Simpson, 1991; Simpson, 1997). Microchaetae instead arise from stripes of cells with increased proneural potential (Parks et al., 1997); Notch activity not only mediates microchaetae SOP specification from within the stripe, but also defines the stripes themselves through dynamic tissue patterning (Corson et al., 2017). The role change for Notch from stripe definition to SOP specification is thought to occur in cooperation with achate-schute activity to induce a shift in the relative expression levels of the genes within in the *E(spl)-C* locus (Couturier et al., 2019). However, it has been suggested that pulsatile or sustained Notch signaling can have different effects on transcriptional output in cell culture (Nandagopal et al., 2018); this may be because the different signaling dynamics result in different levels of active Notch available at one time for transcriptional activation (Henrique and Schweisguth, 2019). SALSA could be used investigate Notch activity during *Drosophila* notal development, including to determine how relative levels of Notch activity during the phases of proneural stripe and SOP specification could be affecting the expression patterns of different *E(spl)-C* genes in addition to *achaete-schute* activity. Although the *Drosophila* notum is traditionally fixed and stained, live imaging has been used to study changes in Notch expression and subcellular localization during fate specification of the SOP descendants using NiGFP, a transgenic Notch tagged at the intracellular domain with GFP (Couturier et al., 2012). SALSA may allow for more robust live imaging of Notch activity across more stages of sensory organ specification than NiGFP, which had relatively dim GFP fluorescence.

4.4.2 Investigating contributions from Notch homologs in immune cells

Notch has roles throughout the developmental pathways of T and B lymphocytes in the thymus (Brandstadter and Maillard, 2019; Radtke et al., 2010). Indeed, NOTCH1 activity blocks

the B cell and other dendritic cell potential of Bone Marrow (BM) progenitors in the thymus (Bell and Bhandoola, 2008; Feyerabend et al., 2009); inactivation of NOTCH1 or Notch pathway components blocks T cell fate and leads to ectopic B cell accumulation (Han et al., 2002; Radtke et al., 1999) while NOTCH1 intracellular domain overexpression leads to ectopic T cell development at the expense of B cells (Pui et al., 1999). Notch signaling also has diverse downstream roles in intracellular signaling, mature cell function, and cell differentiation in both T cells and B cells (Garis and Garrett-Sinha, 2021; Radtke et al., 2004). Activating NOTCH1 mutations are prevalent in T-cell acute lymphoblastic leukemia (Li and von Boehmer, 2011; Weng et al., 2004), and NOTCH1 and NOTCH2 mutations are found in B cell lymphomas (Brandstadter and Maillard, 2019).

NOTCH1, NOTCH2, and NOTCH3 have been shown to have numerous roles for T and B cell differentiation, maturation, and function; some of these roles are exclusive, while others are redundant (Brandstadter and Maillard, 2019; Garis and Garrett-Sinha, 2021; Radtke et al., 2010; Radtke et al., 2013; Radtke et al., 2004). However, the relative contributions of each homolog to each developmental event can be difficult to investigate because traditional Notch target gene transcriptional reporters respond indiscriminately to activity from all homologs. SALSA would allow for the activity of each Notch homolog to be quantified separate from the others. Thus, the relative contributions of each Notch homolog to immune cell development or disease could be directly quantified.

4.5 Potential adaptations and improvements of Flexon

Flexon was highly effective at blocking gene function in the absence of recombination, but the *flexon* alleles tested were not completely null prior to excision of the cassette. Animals

expressing *gfp(flexon)::h2b* had dim nuclear GFP fluorescence when imaged with long exposure times, indicating that some functional GFP::H2B was being made. Likewise, *hlh-2(RNAi)* had some gonad arm outgrowth defects in *rde-1(flexon)* animals, suggesting that RNAi activity was not completely defective. Exon skipping could be one explanation for the "leaky" gene function for both *gfp(flexon)* and *rde-1(flexon)*; if the splice donor of the upstream synthetic intron and the splice acceptor of the downstream synthetic intron are spliced together, all *flexon* sequences that could disrupt translation are excluded from the transcript.

It is not entirely clear why an exon such as the synthetic *flexon* exon may be skipped, although certain factors may contribute to an increased likelihood of skipping. It is unlikely that differences in splice signal strength of the flanking introns would contribute to *flexon* exon skipping because the splice signals are identical. Sequences within the *flexon* exon could be affecting the retention of the exon (Crotti and Horowitz, 2009). However, predicting the effect of sequence motifs in exons on splicing efficiency is difficult because it may also depend on a range of factors like the position of the motifs within the sequence, chromatin structure, and secondary structure of the transcript (Ke et al., 2018; Ke et al., 2011). Skipped exons tend to have a shorter median length than constitutively included exons in human and mouse (Galante et al., 2004; Stamm et al., 2000; Zheng et al., 2005). We intentionally designed the *flexon* exon to be the length of the shortest exon in GFP because Cre/lox excision rate may be inversely proportional to the distances between *lox* sites (Vooijs et al., 2001). However, it may be that replacing the current *flexon* sequence with a slightly longer sequence that includes motifs known to encourage constitutive splicing could improve the efficiency of *flexon* for blocking gene function without affecting the excision efficiency of the cassette.

References

Aghayeva, U., Bhattacharya, A., Sural, S., Jaeger, E., Churgin, M., Fang-Yen, C., and Hobert, O. (2021). DAF-16/FoxO and DAF-12/VDR control cellular plasticity both cell-autonomously and via interorgan signaling. PLOS Biology *19*, e3001204.

Albeck, John G., Mills, Gordon B., and Brugge, Joan S. (2013). Frequency-Modulated Pulses of ERK Activity Transmit Quantitative Proliferation Signals. Molecular Cell *49*, 249-261.

Albert, H., Dale, E.C., Lee, E., and Ow, D.W. (1995). Site-specific integration of DNA into wild-type and mutant lox sites placed in the plant genome. The Plant Journal *7*, 649-659.

Allen, B.L., and Taatjes, D.J. (2015). The Mediator complex: a central integrator of transcription. Nature Reviews Molecular Cell Biology *16*, 155-166.

Allen, M.A., Hillier, L.W., Waterston, R.H., and Blumenthal, T. (2011). A global analysis of C. elegans trans-splicing. Genome Research *21*, 255-264.

Anastassiadis, K., Glaser, S., Kranz, A., Bernhardt, K., and Stewart, A.F. (2010). Chapter Seven - A Practical Summary of Site-Specific Recombination, Conditional Mutagenesis, and Tamoxifen Induction of CreERT2. In Methods in Enzymology, P.M. Wassarman, and P.M. Soriano, eds. (Academic Press), pp. 109-123.

Araki, K., Okada, Y., Araki, M., and Yamamura, K.-i. (2010). Comparative analysis of right element mutant lox sites on recombination efficiency in embryonic stem cells. BMC Biotechnology *10*, 29.

Armenti, S.T., Lohmer, L.L., Sherwood, D.R., and Nance, J. (2014). Repurposing an endogenous degradation system for rapid and targeted depletion of *C. elegans* proteins. Development (Cambridge, England) *141*, 4640-4647.

Arribere, J.A., Kuroyanagi, H., and Hundley, H.A. (2020). mRNA Editing, Processing and Quality Control in *Caenorhabditis elegans*. Genetics *215*, 531-568.

Ashley, G.E., Duong, T., Levenson, M.T., Martinez, M.A.Q., Johnson, L.C., Hibshman, J.D., Saeger, H.N., Palmisano, N.J., Doonan, R., Martinez-Mendez, R.*, et al.* (2021). An expanded auxin-inducible degron toolkit for Caenorhabditis elegans. Genetics *217*.

Atasoy, D., Aponte, Y., Su, H.H., and Sternson, S.M. (2008). A FLEX Switch Targets Channelrhodopsin-2 to Multiple Cell Types for Imaging and Long-Range Circuit Mapping. The Journal of Neuroscience *28*, 7025.

Atay, O., and Skotheim, J.M. (2017). Spatial and temporal signal processing and decision making by MAPK pathways. Journal of Cell Biology *216*, 317-330.

Attner, M.A., Keil, W., Benavidez, J.M., and Greenwald, I. (2019). HLH-2/E2A Expression Links Stochastic and Deterministic Elements of a Cell Fate Decision during *C. elegans* Gonadogenesis. Current Biology *29*, 3094-3100.e3094.

Aulehla, A., Wiegraebe, W., Baubet, V., Wahl, M.B., Deng, C., Taketo, M., Lewandoski, M., and Pourquié, O. (2008). A β-catenin gradient links the clock and wavefront systems in mouse embryo segmentation. Nature cell biology *10*, 186-193.

Austin, J., and Kimble, J. (1987). *glp-1* is required in the germ line for regulation of the decision between mitosis and meiosis in C. elegans. Cell *51*, 589-599.

Awatramani, R., Soriano, P., Rodriguez, C., Mai, J.J., and Dymecki, S.M. (2003). Cryptic boundaries in roof plate and choroid plexus identified by intersectional gene activation. Nature Genetics *35*, 70-75.

Bailey, A.M., and Posakony, J.W. (1995). Suppressor of hairless directly activates transcription of enhancer of split complex genes in response to Notch receptor activity. Genes & development *9*, 2609-2622.

Bapst, A.M., Dahl, S.L., Knöpfel, T., and Wenger, R.H. (2020). Cre-mediated, loxP independent sequential recombination of a tripartite transcriptional stop cassette allows for partial read-through transcription. Biochimica et Biophysica Acta (BBA) - Gene Regulatory Mechanisms *1863*, 194568.

Barkan, R., Zahand, A.J., Sharabi, K., Lamm, A.T., Feinstein, N., Haithcock, E., Wilson, K.L., Liu, J., and Gruenbaum, Y. (2011). Ce-emerin and LEM-2: essential roles in Caenorhabditis elegans development, muscle function, and mitosis. Molecular biology of the cell *23*, 543-552.

Barnea, G., Strapps, W., Herrada, G., Berman, Y., Ong, J., Kloss, B., Axel, R., and Lee, K.J. (2008). The genetic design of signaling cascades to record receptor activation. Proceedings of the National Academy of Sciences of the United States of America *105*, 64-69.

Basler, K., and Struhl, G. (1994). Compartment boundaries and the control of Drosophila limb pattern by hedgehog protein. Nature *368*, 208-214.

Beitel, G.J., Tuck, S., Greenwald, I., and Horvitz, H.R. (1995). The Caenorhabditis elegans gene lin-1 encodes an ETS-domain protein and defines a branch of the vulval induction pathway. Genes & development *9*, 3149-3162.

Bell, J.J., and Bhandoola, A. (2008). The earliest thymic progenitors for T cells possess myeloid lineage potential. Nature *452*, 764-767.

Benavidez, J.M., Kim, J.H., and Greenwald, I. (2022). Influences of HLH-2 stability on anchor cell fate specification during Caenorhabditis elegans gonadogenesis. G3 Genes|Genomes|Genetics, jkac028.

Berger, S., Spiri, S., deMello, A., and Hajnal, A. (2021). Microfluidic-based imaging of complete C. elegans larval development. Development (Cambridge, England).

Berry, L.W., Westlund, B., and Schedl, T. (1997). Germ-line tumor formation caused by activation of glp-1, a Caenorhabditis elegans member of the Notch family of receptors. Development (Cambridge, England) *124*, 925-936.

Berset, T., Hoier, E.F., Battu, G., Canevascini, S., and Hajnal, A. (2001). Notch Inhibition of RAS Signaling Through MAP Kinase Phosphatase LIP-1 During *C. elegans* Vulval Development. Science (New York, NY) *291*, 1055-1058.

Bertrand, E., Chartrand, P., Schaefer, M., Shenoy, S.M., Singer, R.H., and Long, R.M. (1998). Localization of ASH1 mRNA Particles in Living Yeast. Molecular Cell *2*, 437-445.

Blumenthal, T., and Thomas, J. (1988). Cis and trans mRNA splicing in C. elegans. Trends in Genetics *4*, 305-308.

Bothma, J.P., Norstad, M.R., Alamos, S., and Garcia, H.G. (2018). LlamaTags: A Versatile Tool to Image Transcription Factor Dynamics in Live Embryos. Cell *173*, 1810-1822.e1816.

Brachner, A., and Foisner, R. (2011). Evolvement of LEM proteins as chromatin tethers at the nuclear periphery. Biochemical Society Transactions *39*, 1735-1741.

Brachner, A., Reipert, S., Foisner, R., and Gotzmann, J. (2005). LEM2 is a novel MAN1-related inner nuclear membrane protein associated with A-type lamins. Journal of cell science *118*, 5797-5810.

Bradnam, K.R., and Korf, I. (2008). Longer First Introns Are a General Property of Eukaryotic Gene Structure. PLOS ONE *3*, e3093.

Brandstadter, J.D., and Maillard, I. (2019). Notch signalling in T cell homeostasis and differentiation. Open Biology *9*, 190187.

Bray, S.J. (2016). Notch signalling in context. Nature Reviews Molecular Cell Biology *17*, 722-735.

Bray, S.J., and Gomez-Lamarca, M. (2018). Notch after cleavage. Current Opinion in Cell Biology *51*, 103-109.

Brenner, S. (1974). THE GENETICS OF *CAENORHABDITIS ELEGANS*. Genetics *77*, 71-94.

Brou, C., Logeat, F., Gupta, N., Bessia, C., LeBail, O., Doedens, J.R., Cumano, A., Roux, P., Black, R.A., and Israël, A. (2000). A Novel Proteolytic Cleavage Involved in Notch Signaling: The Role of the Disintegrin-Metalloprotease TACE. Molecular Cell *5*, 207-216.

Byerly, L., Cassada, R.C., and Russell, R.L. (1976). The life cycle of the nematode Caenorhabditis elegans: I. Wild-type growth and reproduction. Developmental biology *51*, 23-33.

Byrd, D.T., Knobel, K., Affeldt, K., Crittenden, S.L., and Kimble, J. (2014). A DTC Niche Plexus Surrounds the Germline Stem Cell Pool in Caenorhabditis elegans. PLOS ONE *9*, e88372.

Cabantous, S., Terwilliger, T.C., and Waldo, G.S. (2005). Protein tagging and detection with engineered self-assembling fragments of green fluorescent protein. Nature Biotechnology *23*, 102-107.

Cardot-Ruffino, V., Chauvet, V., Caligaris, C., Bertrand-Chapel, A., Chuvin, N., Pommier, R.M., Valcourt, U., Vincent, D.F., Martel, S., Aires, S.*, et al.* (2020). Generation of a conditional Flpo/FRT mouse model expressing constitutively active TGFβ in fibroblasts. Scientific Reports *10*, 3880.

Cardullo, R.A. (2013). Chapter 19 - Theoretical Principles and Practical Considerations for Fluorescence Resonance Energy Transfer Microscopy. In Methods in Cell Biology, G. Sluder, and D.E. Wolf, eds. (Academic Press), pp. 441-456.

Chan, J. (2020). Investigations into roles for endocytosis in LIN-12/Notch signaling and its regulation. In Biological Sciences (Columbia University).

Chen, H., Ko, G., Zatti, A., Di Giacomo, G., Liu, L., Raiteri, E., Perucco, E., Collesi, C., Min, W., Zeiss, C.*, et al.* (2009). Embryonic arrest at midgestation and disruption of Notch signaling produced by the absence of both epsin 1 and epsin 2 in mice. Proceedings of the National Academy of Sciences *106*, 13838.

Chen, J., Mohammad, A., Pazdernik, N., Huang, H., Bowman, B., Tycksen, E., and Schedl, T. (2020a). GLP-1 Notch—LAG-1 CSL control of the germline stem cell fate is mediated by transcriptional targets lst-1 and sygl-1. PLOS Genetics *16*, e1008650.

Chen, N., and Greenwald, I. (2004). The lateral signal for LIN-12/Notch in C. elegans vulval development comprises redundant secreted and transmembrane DSL proteins. Dev Cell *6*, 183-192.

Chen, Y., Mao, S., Liu, B., Jing, Z., Zang, Y., Xia, J., Sun, J., and Chi, T. (2020b). Novel mosaic mice with diverse applications. bioRxiv, 2020.2003.2021.001388.

Chesney, M.A., Lam, N., Morgan, D.E., Phillips, B.T., and Kimble, J. (2009). C. elegans HLH-2/E/Daughterless controls key regulatory cells during gonadogenesis. Developmental biology *331*, 14-25.

Cho, J.H., Collins, J.J., and Wong, W.W. (2018). Universal Chimeric Antigen Receptors for Multiplexed and Logical Control of T Cell Responses. Cell *173*, 1426-1438.e1411.

Choe, J.H., Watchmaker, P.B., Simic, M.S., Gilbert, R.D., Li, A.W., Krasnow, N.A., Downey, K.M., Yu, W., Carrera, D.A., Celli, A.*, et al.* (2021). SynNotch-CAR T cells overcome challenges of specificity, heterogeneity, and persistence in treating glioblastoma. Science Translational Medicine *13*, eabe7378.

Choi, M.S. (2009). Genes that act in specification of the vulval secondary fate in Caenorhabditis elegans. In Biological Sciences (Columbia University).

Christensen, S., Kodoyianni, V., Bosenberg, M., Friedman, L., and Kimble, J. (1996). lag-1, a gene required for lin-12 and glp-1 signaling in Caenorhabditis elegans, is homologous to human CBF1 and Drosophila Su(H). Development (Cambridge, England) *122*, 1373-1383.

Chu, V.T., Weber, T., Graf, R., Sommermann, T., Petsch, K., Sack, U., Volchkov, P., Rajewsky, K., and Kühn, R. (2016). Efficient generation of Rosa26 knock-in mice using CRISPR/Cas9 in C57BL/6 zygotes. BMC Biotechnology *16*, 4.

Copeland, M.F., Politz, M.C., Johnson, C.B., Markley, A.L., and Pfleger, B.F. (2016). A transcription activator–like effector (TALE) induction system mediated by proteolysis. Nature Chemical Biology *12*, 254-260.

Corson, F., Couturier, L., Rouault, H., Mazouni, K., and Schweisguth, F. (2017). Self-organized Notch dynamics generate stereotyped sensory organ patterns in *Drosophila*. Science (New York, NY) *356*, eaai7407.

Couturier, L., Mazouni, K., Corson, F., and Schweisguth, F. (2019). Regulation of Notch output dynamics via specific E(spl)-HLH factors during bristle patterning in Drosophila. Nature Communications *10*, 3486.

Couturier, L., Vodovar, N., and Schweisguth, F. (2012). Endocytosis by Numb breaks Notch symmetry at cytokinesis. Nature cell biology *14*, 131-139.

Crittenden, S.L., Leonhard, K.A., Byrd, D.T., and Kimble, J. (2006). Cellular Analyses of the Mitotic Region in the Caenorhabditis elegans Adult Germ Line. Molecular biology of the cell *17*, 3051-3061.

Crittenden, S.L., Troemel, E.R., Evans, T.C., and Kimble, J. (1994). GLP-1 is localized to the mitotic region of the C. elegans germ line. Development (Cambridge, England) *120*, 2901-2911.

Crotti, L.B., and Horowitz, D.S. (2009). Exon sequences at the splice junctions affect splicing fidelity and alternative splicing. Proceedings of the National Academy of Sciences *106*, 18954.

Daringer, N.M., Dudek, R.M., Schwarz, K.A., and Leonard, J.N. (2014). Modular Extracellular Sensor Architecture for Engineering Mammalian Cell-based Devices. ACS Synthetic Biology *3*, 892-902.

Daum, G., Medzihradszky, A., Suzaki, T., and Lohmann, J.U. (2014). A mechanistic framework for noncell autonomous stem cell induction in *Arabidopsis*. Proceedings of the National Academy of Sciences *111*, 14619.

Davis, M.W., Morton, J.J., Carroll, D., and Jorgensen, E.M. (2008). Gene Activation Using FLP Recombinase in C. elegans. PLOS Genetics *4*, e1000028.

de la Cova, C., and Greenwald, I. (2012). SEL-10/Fbw7-dependent negative feedback regulation of LIN-45/Braf signaling in C. elegans via a conserved phosphodegron. Genes & development *26*, 2524-2535.

de la Cova, C., Townley, R., Regot, S., and Greenwald, I. (2017). A Real-Time Biosensor for ERK Activity Reveals Signaling Dynamics during C elegans Cell Fate Specification. Developmental Cell *42*, 542-553.e544.

Dejima, K., Hori, S., Iwata, S., Suehiro, Y., Yoshina, S., Motohashi, T., and Mitani, S. (2018). An Aneuploidy-Free and Structurally Defined Balancer Chromosome Toolkit for *Caenorhabditis elegans*. Cell reports *22*, 232-241.

Deng, Y., and Greenwald, I. (2016). Determinants in the LIN-12/Notch Intracellular Domain That Govern Its Activity and Stability During Caenorhabditis elegans Vulval Development. G3 Genes|Genomes|Genetics *6*, 3663-3670.

Deng, Y., Luo, K.L., Shaye, D.D., and Greenwald, I. (2019). A Screen of the Conserved Kinome for Negative Regulators of LIN-12 Negative Regulatory Region ("NRR")-Missense Activity in *Caenorhabditis elegans*. G3: Genes|Genomes|Genetics *9*, 3567.

Diaz-Cuadros, M., Pourquié, O., and El-Sherif, E. (2021). Patterning with clocks and genetic cascades: Segmentation and regionalization of vertebrate versus insect body plans. PLOS Genetics *17*, e1009812.

Dibb, N.J., and Newman, A.J. (1989). Evidence that introns arose at proto-splice sites. The EMBO Journal *8*, 2015-2021.

Dickinson, D.J., Pani, A.M., Heppert, J.K., Higgins, C.D., and Goldstein, B. (2015). Streamlined Genome Engineering with a Self-Excising Drug Selection Cassette. Genetics *200*, 1035-1049.

Ding, W.-L., Miao, D., Hou, Y.-N., Jiang, S.-P., Zhao, B.-Q., Zhou, M., Scheer, H., and Zhao, K.-H. (2017). Small monomeric and highly stable near-infrared fluorescent markers derived from the thermophilic phycobiliprotein, ApcF2. Biochimica et Biophysica Acta (BBA) - Molecular Cell Research *1864*, 1877-1886.

Dos Santos Maraschin, F., Memelink, J., and Offringa, R. (2009). Auxin-induced, SCFTIR1-mediated poly-ubiquitination marks AUX/IAA proteins for degradation. The Plant Journal *59*, 100-109.

Doyle, T.G., Wen, C., and Greenwald, I. (2000). SEL-8, a nuclear protein required for LIN-12 and GLP-1 signaling in *Caenorhabditis elegans*. Proceedings of the National Academy of Sciences *97*, 7877.

Duncan, A.W., Rattis, F.M., DiMascio, L.N., Congdon, K.L., Pazianos, G., Zhao, C., Yoon, K., Cook, J.M., Willert, K., Gaiano, N.*, et al.* (2005). Integration of Notch and Wnt signaling in hematopoietic stem cell maintenance. Nature Immunology *6*, 314-322.

Dymecki, S.M., Ray, R.S., and Kim, J.C. (2010). Chapter Eleven - Mapping Cell Fate and Function Using Recombinase-Based Intersectional Strategies. In Methods in Enzymology, P.M. Wassarman, and P.M. Soriano, eds. (Academic Press), pp. 183-213.

Edwards, S.L., Charlie, N.K., Milfort, M.C., Brown, B.S., Gravlin, C.N., Knecht, J.E., and Miller, K.G. (2008). A Novel Molecular Solution for Ultraviolet Light Detection in Caenorhabditis elegans. PLOS Biology *6*, e198.

El Mouridi, S., Lecroisey, C., Tardy, P., Mercier, M., Leclercq-Blondel, A., Zariohi, N., and Boulin, T. (2017). Reliable CRISPR/Cas9 Genome Engineering in Caenorhabditis elegans Using a Single Efficient sgRNA and an Easily Recognizable Phenotype. G3 Genes|Genomes|Genetics *7*, 1429-1437.

Falo-Sanjuan, J., and Bray, S.J. (2020). Decoding the Notch signal. Development, Growth & Differentiation *62*, 4-14.

Falo-Sanjuan, J., Lammers, N.C., Garcia, H.G., and Bray, S.J. (2019). Enhancer Priming Enables Fast and Sustained Transcriptional Responses to Notch Signaling. Developmental Cell *50*, 411-425.e418.

Fang, J., Chen, L., Cheng, B., and Fan, J. (2013). Engineering soluble tobacco etch virus protease accompanies the loss of stability. Protein expression and purification *92*, 29-35.

Feng, S., Sekine, S., Pessino, V., Li, H., Leonetti, M.D., and Huang, B. (2017). Improved split fluorescent proteins for endogenous protein labeling. Nature Communications *8*, 370.

Feng, S., Varshney, A., Coto Villa, D., Modavi, C., Kohler, J., Farah, F., Zhou, S., Ali, N., Müller, J.D., Van Hoven, M.K.*, et al.* (2019). Bright split red fluorescent proteins for the visualization of endogenous proteins and synapses. Communications Biology *2*, 344.

Fernandez-Rodriguez, J., and Voigt, C.A. (2016). Post-translational control of genetic circuits using Potyvirus proteases. Nucleic Acids Research *44*, 6493-6502.

Feyerabend, T.B., Terszowski, G., Tietz, A., Blum, C., Luche, H., Gossler, A., Gale, N.W., Radtke, F., Fehling, H.J., and Rodewald, H.-R. (2009). Deletion of Notch1 Converts Pro-T Cells to Dendritic Cells and Promotes Thymic B Cells by Cell-Extrinsic and Cell-Intrinsic Mechanisms. Immunity *30*, 67-79.

Fitzgerald, K., and Greenwald, I. (1995). Interchangeability of Caenorhabditis elegans DSL proteins and intrinsic signalling activity of their extracellular domains in vivo. Development (Cambridge, England) *121*, 4275-4282.

Flavell, Steven W., Pokala, N., Macosko, Evan Z., Albrecht, Dirk R., Larsch, J., and Bargmann, Cornelia I. (2013). Serotonin and the Neuropeptide PDF Initiate and Extend Opposing Behavioral States in C. elegans. Cell *154*, 1023-1035.

Foehr, M.L., Lindy, A.S., Fairbank, R.C., Amin, N.M., Xu, M., Yanowitz, J., Fire, A.Z., and Liu, J. (2006). An antagonistic role for the C. elegans Schnurri homolog SMA-9 in modulating TGFβ signaling during mesodermal patterning. Development (Cambridge, England) *133*, 2887-2896.

Foehr, M.L., and Liu, J. (2008). Dorsoventral patterning of the C. elegans postembryonic mesoderm requires both LIN-12/Notch and TGFbeta signaling. Developmental biology *313*, 256-266.

Friedland, A.E., Tzur, Y.B., Esvelt, K.M., Colaiácovo, M.P., Church, G.M., and Calarco, J.A. (2013). Heritable genome editing in C. elegans via a CRISPR-Cas9 system. Nature Methods *10*, 741-743.

Friedrich, G., and Soriano, P. (1991). Promoter traps in embryonic stem cells: a genetic screen to identify and mutate developmental genes in mice. Genes & development *5*, 1513-1523.

Frøkjær-Jensen, C., Davis, M.W., Ailion, M., and Jorgensen, E.M. (2012). Improved Mos1-mediated transgenesis in C. elegans. Nature Methods *9*, 117-118.

Frøkjær-Jensen, C., Davis, M.W., Sarov, M., Taylor, J., Flibotte, S., LaBella, M., Pozniakovsky, A., Moerman, D.G., and Jorgensen, E.M. (2014). Random and targeted transgene insertion in Caenorhabditis elegans using a modified Mos1 transposon. Nature Methods *11*, 529-534.

Fryer, C.J., White, J.B., and Jones, K.A. (2004). Mastermind Recruits CycC:CDK8 to Phosphorylate the Notch ICD and Coordinate Activation with Turnover. Molecular Cell *16*, 509-520.

Furriols, M., and Bray, S. (2001). A model Notch response element detects Suppressor of Hairless–dependent molecular switch. Current Biology *11*, 60-64.

Fuxman Bass, J.I., Tamburino, A.M., Mori, A., Beittel, N., Weirauch, M.T., Reece-Hoyes, J.S., and Walhout, A.J.M. (2014). Transcription factor binding to Caenorhabditis elegans first introns reveals lack of redundancy with gene promoters. Nucleic Acids Research *42*, 153-162.

Galante, P.A.F., Sakabe, N.J., Kirschbaum-Slager, N., and De Souza, S.J. (2004). Detection and evaluation of intron retention events in the human transcriptome. RNA *10*, 757-765.

Garis, M., and Garrett-Sinha, L.A. (2021). Notch Signaling in B Cell Immune Responses. Frontiers in Immunology *11*.

Gauthier, K., and Rocheleau, C.E. (2017). C. elegans Vulva Induction: An In Vivo Model to Study Epidermal Growth Factor Receptor Signaling and Trafficking. In ErbB Receptor Signaling Methods in Molecular Biology, Z. Wang, ed. (New York, NY: Humana Press).

Ghanta, K.S., and Mello, C.C. (2020). Melting dsDNA Donor Molecules Greatly Improves Precision Genome Editing in *Caenorhabditis elegans*. Genetics *216*, 643-650.

Gibson, D.G., Young, L., Chuang, R.-Y., Venter, J.C., Hutchison, C.A., and Smith, H.O. (2009). Enzymatic assembly of DNA molecules up to several hundred kilobases. Nature Methods *6*, 343-345.

Giordano-Santini, R., Milstein, S., Svrzikapa, N., Tu, D., Johnsen, R., Baillie, D., Vidal, M., and Dupuy, D. (2010). An antibiotic selection marker for nematode transgenesis. Nature Methods *7*, 721-723.

Golic, K.G., and Lindquist, S. (1989). The FLP recombinase of yeast catalyzes site-specific recombination in the drosophila genome. Cell *59*, 499-509.

Gómez-Skarmeta, J.L., Rodríguez, I., Martínez, C., Culí, J., Ferrés-Marcó, D., Beamonte, D., and Modolell, J. (1995). Cis-regulation of achaete and scute: shared enhancer-like elements drive their coexpression in proneural clusters of the imaginal discs. Genes & development *9*, 1869-1882.

Gordon, W.R., Arnett, K.L., and Blacklow, S.C. (2008). The molecular logic of Notch signaling – a structural and biochemical perspective. Journal of cell science *121*, 3109-3119.

Gordon, W.R., Roy, M., Vardar-Ulu, D., Garfinkel, M., Mansour, M.R., Aster, J.C., and Blacklow, S.C. (2009a). Structure of the Notch1-negative regulatory region: implications for normal activation and pathogenic signaling in T-ALL. Blood *113*, 4381-4390.

Gordon, W.R., Vardar-Ulu, D., Histen, G., Sanchez-Irizarry, C., Aster, J.C., and Blacklow, S.C. (2007). Structural basis for autoinhibition of Notch. Nature Structural & Molecular Biology *14*, 295-300.

Gordon, W.R., Vardar-Ulu, D., L'Heureux, S., Ashworth, T., Malecki, M.J., Sanchez-Irizarry, C., McArthur, D.G., Histen, G., Mitchell, J.L., Aster, J.C.*, et al.* (2009b). Effects of S1 Cleavage on the Structure, Surface Export, and Signaling Activity of Human Notch1 and Notch2. PLOS ONE *4*, e6613.

Gordon, Wendy R., Zimmerman, B., He, L., Miles, Laura J., Huang, J., Tiyanont, K., McArthur, Debbie G., Aster, Jon C., Perrimon, N., Loparo, Joseph J.*, et al.* (2015). Mechanical Allostery: Evidence for a Force Requirement in the Proteolytic Activation of Notch. Developmental Cell *33*, 729-736.

Greenwald, E.C., Mehta, S., and Zhang, J. (2018). Genetically Encoded Fluorescent Biosensors Illuminate the Spatiotemporal Regulation of Signaling Networks. Chemical Reviews *118*, 11707-11794.

Greenwald, I. (2012). *Notch* and the Awesome Power of Genetics. Genetics *191*, 655.

Greenwald, I., and Kovall, R. (2013). Notch signaling: genetics and structure. WormBook : the online review of C elegans biology, 1-28.

Greenwald, I., and Seydoux, G. (1990). Analysis of gain-of-function mutations of the lin-12 gene of Caenorhabditis elegans. Nature *346*, 197-199.

Greenwald, I.S., Sternberg, P.W., and Horvitz, H.R. (1983). The lin-12 locus specifies cell fates in Caenorhabditis elegans. Cell *34*, 435-444.

Gridley, T., and Groves, A.K. (2014). Overview of Genetic Tools and Techniques to Study Notch Signaling in Mice. In Notch Signaling: Methods and Protocols, H.J. Bellen, and S. Yamamoto, eds. (New York, NY: Springer New York), pp. 47-61.

Gross, S.M., and Rotwein, P. (2015). Akt signaling dynamics in individual cells. Journal of cell science *128*, 2509-2519.

Grummt, I. (2013). The nucleolus—guardian of cellular homeostasis and genome integrity. Chromosoma *122*, 487-497.

Gutnik, S., Thomas, Y., Guo, Y., Stoecklin, J., Neagu, A., Pintard, L., Merlet, J., and Ciosk, R. (2018). PRP-19, a conserved pre-mRNA processing factor and E3 ubiquitin ligase, inhibits the nuclear accumulation of GLP-1/Notch intracellular domain. Biology Open *7*, bio034066.

Hale, J.J., Amin, N.M., George, C., Via, Z., Shi, H., and Liu, J. (2014). A role of the LIN-12/Notch signaling pathway in diversifying the non-striated egg-laying muscles in C. elegans. Developmental biology *389*, 137-148.

Han, H., Tanigaki, K., Yamamoto, N., Kuroda, K., Yoshimoto, M., Nakahata, T., Ikuta, K., and Honjo, T. (2002). Inducible gene knockout of transcription factor recombination signal binding protein-J reveals its essential role in T versus B lineage decision. International Immunology *14*, 637-645.

Hansen, D., Albert Hubbard, E.J., and Schedl, T. (2004). Multi-pathway control of the proliferation versus meiotic development decision in the Caenorhabditis elegans germline. Developmental biology *268*, 342-357.

Hansson, E.M., Teixeira, A.I., Gustafsson, M.V., Dohda, T., Chapman, G., Meletis, K., Muhr, J., and Lendahl, U. (2006). Recording Notch Signaling in Real Time. Developmental Neuroscience *28*, 118-127.

Harfe, B.D., Gomes, A.V., Kenyon, C., Liu, J., Krause, M., and Fire, A. (1998). Analysis of a Caenorhabditis elegans Twist homolog identifies conserved and divergent aspects of mesodermal patterning. Genes & development *12*, 2623-2635.

He, L., Huang, J., and Perrimon, N. (2017). Development of an optimized synthetic Notch receptor as an in vivo cell–cell contact sensor. Proceedings of the National Academy of Sciences *114*, 5467.

Heitzler, P., Bourouis, M., Ruel, L., Carteret, C., and Simpson, P. (1996). Genes of the Enhancer of split and achaete-scute complexes are required for a regulatory loop between Notch and Delta during lateral signalling in Drosophila. Development (Cambridge, England) *122*, 161-171.

Heitzler, P., and Simpson, P. (1991). The choice of cell fate in the epidermis of Drosophila. Cell *64*, 1083-1092.

Henderson, S.T., Gao, D., Lambie, E.J., and Kimble, J. (1994). lag-2 may encode a signaling ligand for the GLP-1 and LIN-12 receptors of C. elegans. Development (Cambridge, England) *120*, 2913-2924.

Henrichs, T., Mikhaleva, N., Conz, C., Deuerling, E., Boyd, D., Zelazny, A., Bibi, E., Ban, N., and Ehrmann, M. (2005). Target-directed proteolysis at the ribosome. Proceedings of the National Academy of Sciences of the United States of America *102*, 4246.

Henrique, D., and Schweisguth, F. (2019). Mechanisms of Notch signaling: a simple logic deployed in time and space. Development (Cambridge, England) *146*.

Hitoshi, N., Ken-ichi, Y., and Jun-ichi, M. (1991). Efficient selection for high-expression transfectants with a novel eukaryotic vector. Gene *108*, 193-199.

Ho, C., and Morsut, L. (2021). Novel synthetic biology approaches for developmental systems. Stem Cell Reports *16*, 1051-1064.

Hoess, R.H., Wierzbicki, A., and Abremski, K. (1986). The role of the loxP spacer region in PI site-specific recombination. Nucleic Acids Research *14*, 2287-2300.

Hoier, E.F., Mohler, W.A., Kim, S.K., and Hajnal, A. (2000). The Caenorhabditis elegans APC-related gene apr-1 is required for epithelial cell migration and Hox gene expression. Genes & development *14*, 874-886.

Holmer, L., and Worman, H.J. (2001). Inner nuclear membrane proteins: functions and targeting. Cellular and Molecular Life Sciences CMLS *58*, 1741-1747.

Horvitz, H.R., Sternberg, P.W., Greenwald, I.S., Fixsen, W., and Ellis, H.M. (1983). Mutations That Affect Neural Cell Lineages and Cell Fates during the Development of the Nematode Caenorhabditis elegans. Cold Spring Harbor Symposia on Quantitative Biology *48*, 453-463.

Housden, B.E., Li, J., Bray, S.J., Marathe, S., Alberi, L., Ilagan, M.X.G., Kopan, R., Shimojo, H., Harima, Y., and Kageyama, R. (2014). In Notch signaling Methods in Molecular Biology (Methods and Protocols), H.J. Bellen, and S. Yamamoto, eds. (New York, NY: Humana Press), pp. 101-180.

Hubaud, A., and Pourquié, O. (2014). Signalling dynamics in vertebrate segmentation. Nature Reviews Molecular Cell Biology *15*, 709-721.

Hubaud, A., Regev, I., Mahadevan, L., and Pourquié, O. (2017). Excitable Dynamics and Yap-Dependent Mechanical Cues Drive the Segmentation Clock. Cell *171*, 668-682.e611.

Hubbard, E.J.A., and Schedl, T. (2019). Biology of the Caenorhabditis elegans Germline Stem Cell System. Genetics *213*, 1145-1188.

Hubbard, E.J.A., Wu, G., Kitajewski, J., and Greenwald, I. (1997). sel-10, a negative regulator of lin-12 activity inCaenorhabditis elegans, encodes a member of the CDC4 family of proteins. Genes & development *11*, 3182-3193.

Hung, Y.P., Teragawa, C., Kosaisawe, N., Gillies, T.E., Pargett, M., Minguet, M., Distor, K., Rocha-Gregg, B.L., Coloff, J.L., Keibler, M.A.*, et al.* (2017). Akt regulation of glycolysis mediates bioenergetic stability in epithelial cells. eLife *6*, e27293.

Hunt-Newbury, R., Viveiros, R., Johnsen, R., Mah, A., Anastas, D., Fang, L., Halfnight, E., Lee, D., Lin, J., Lorch, A.*, et al.* (2007). High-Throughput In Vivo Analysis of Gene Expression in Caenorhabditis elegans. PLOS Biology *5*, e237.

Hunter, G.L., and Giniger, E. (2020). Phosphorylation and Proteolytic Cleavage of Notch in Canonical and Noncanonical Notch Signaling. In Notch signaling in Embryology and Cancer Advances in Experimental Medicine and Biology, J. Reichrath, and S. Reichrath, eds. (Cham: Springer).

Hyrenius-Wittsten, A., Su, Y., Park, M., Garcia Julie, M., Alavi, J., Perry, N., Montgomery, G., Liu, B., and Roybal Kole, T. (2021). SynNotch CAR circuits enhance solid tumor recognition and promote persistent antitumor activity in mouse models. Science Translational Medicine *13*, eabd8836.

Ilagan, M.X.G., Lim, S., Fulbright, M., Piwnica-Worms, D., and Kopan, R. (2011). Real-Time Imaging of Notch Activation with a Luciferase Complementation-Based Reporter. Science Signaling *4*, rs7-rs7.

Imayoshi, I., Shimojo, H., Sakamoto, M., Ohtsuka, T., and Kageyama, R. (2013). Genetic visualization of notch signaling in mammalian neurogenesis. Cellular and Molecular Life Sciences *70*, 2045-2057.

Inagaki, H.K., Ben-Tabou de-Leon, S., Wong, A.M., Jagadish, S., Ishimoto, H., Barnea, G., Kitamoto, T., Axel, R., and Anderson, D.J. (2012). Visualizing neuromodulation in vivo: TANGO-mapping of dopamine signaling reveals appetite control of sugar sensing. Cell *148*, 583-595.

Iwata, S., Yoshina, S., Suehiro, Y., Hori, S., and Mitani, S. (2016). Engineering new balancer chromosomes in C. elegans via CRISPR/Cas9. Scientific Reports *6*, 33840.

Jackson, E.L., Willis, N., Mercer, K., Bronson, R.T., Crowley, D., Montoya, R., Jacks, T., and Tuveson, D.A. (2001). Analysis of lung tumor initiation and progression using conditional expression of oncogenic K-ras. Genes & development *15*, 3243-3248.

Jacobs, D., Beitel, G.J., Clark, S.G., Horvitz, H.R., and Kornfeld, K. (1998). Gain-of-Function Mutations in the Caenorhabditis elegans lin-1 ETS Gene Identify a C-Terminal Regulatory Domain Phosphorylated by ERK MAP Kinase. Genetics *149*, 1809-1822.

Jarriault, S., and Greenwald, I. (2005). Evidence for functional redundancy between C. elegans ADAM proteins SUP-17/Kuzbanian and ADM-4/TACE. Developmental biology *287*, 1-10.

Johnson, H.E., and Toettcher, J.E. (2019). Signaling Dynamics Control Cell Fate in the Early Drosophila Embryo. Developmental Cell *48*, 361-370.e363.

Jungbluth, M., Mösch, H.-U., and Taxis, C. (2012). Acetate Regulation of Spore Formation Is under the Control of the Ras/Cyclic AMP/Protein Kinase A Pathway and Carbon Dioxide in Saccharomyces cerevisiae. Eukaryotic Cell *11*, 1021-1032.

Jungbluth, M., Renicke, C., and Taxis, C. (2010). Targeted protein depletion in Saccharomyces cerevisiae by activation of a bidirectional degron. BMC Systems Biology *4*, 176.

Kage-Nakadai, E., Imae, R., Suehiro, Y., Yoshina, S., Hori, S., and Mitani, S. (2014). A Conditional Knockout Toolkit for Caenorhabditis elegans Based on the Cre/loxP Recombination. PLOS ONE *9*, e114680.

Kamath, R.S., Fraser, A.G., Dong, Y., Poulin, G., Durbin, R., Gotta, M., Kanapin, A., Le Bot, N., Moreno, S., Sohrmann, M.*, et al.* (2003). Systematic functional analysis of the Caenorhabditis elegans genome using RNAi. Nature *421*, 231-237.

Kamath, R.S., Martinez-Campos, M., Zipperlen, P., Fraser, A.G., and Ahringer, J. (2000). Effectiveness of specific RNA-mediated interference through ingested double-stranded RNA in Caenorhabditis elegans. Genome Biology *2*, research0002.0001.

Kamentsky, L., Jones, T.R., Fraser, A., Bray, M.-A., Logan, D.J., Madden, K.L., Ljosa, V., Rueden, C., Eliceiri, K.W., and Carpenter, A.E. (2011). Improved structure, function and compatibility for CellProfiler: modular high-throughput image analysis software. Bioinformatics *27*, 1179-1180.

Kamiyama, D., Sekine, S., Barsi-Rhyne, B., Hu, J., Chen, B., Gilbert, L.A., Ishikawa, H., Leonetti, M.D., Marshall, W.F., Weissman, J.S.*, et al.* (2016). Versatile protein tagging in cells with split fluorescent protein. Nature Communications *7*, 11046.

Kannan, R., Cox, E., Wang, L., Kuzina, I., Gu, Q., and Giniger, E. (2018). Tyrosine phosphorylation and proteolytic cleavage of Notch are required for non-canonical Notch/Abl signaling in Drosophila axon guidance. Development (Cambridge, England) *145*, dev151548.

Kapust, R.B., Tözsér, J., Copeland, T.D., and Waugh, D.S. (2002). The P1′ specificity of tobacco etch virus protease. Biochemical and Biophysical Research Communications *294*, 949-955.

Kapust, R.B., Tözsér, J., Fox, J.D., Anderson, D.E., Cherry, S., Copeland, T.D., and Waugh, D.S. (2001). Tobacco etch virus protease: mechanism of autolysis and rational design of stable mutants with wild-type catalytic proficiency. Protein Engineering, Design and Selection *14*, 993-1000.

Karp, X., and Greenwald, I. (2003). Post-transcriptional regulation of the E/Daughterless ortholog HLH-2, negative feedback, and birth order bias during the AC/VU decision in C. elegans. Genes & development *17*, 3100-3111.

Karp, X., and Greenwald, I. (2004). Multiple roles for the E/Daughterless ortholog HLH-2 during C. elegans gonadogenesis. Developmental biology *272*, 460-469.

Karp, X., and Greenwald, I. (2013). Control of cell-fate plasticity and maintenance of multipotency by DAF-16/FoxO in quiescent *Caenorhabditis elegans*. Proceedings of the National Academy of Sciences *110*, 2181.

Kato, H., Taniguchi, Y., Kurooka, H., Minoguchi, S., Sakai, T., Nomura-Okazaki, S., Tamura, K., and Honjo, T. (1997). Involvement of RBP-J in biological functions of mouse Notch1 and its derivatives. Development (Cambridge, England) *124*, 4133-4141.

Katow, H., Takahashi, T., Saito, K., Tanimoto, H., and Kondo, S. (2019). Tango knock-ins visualize endogenous activity of G protein-coupled receptors in Drosophila. Journal of Neurogenetics *33*, 44-51.

Kawahashi, K., and Hayashi, S. (2010). Dynamic intracellular distribution of Notch during activation and asymmetric cell division revealed by functional fluorescent fusion proteins. Genes to Cells *15*, 749-759.

Ke, S., Anquetil, V., Zamalloa, J.R., Maity, A., Yang, A., Arias, M.A., Kalachikov, S., Russo, J.J., Ju, J., and Chasin, L.A. (2018). Saturation mutagenesis reveals manifold determinants of exon definition. Genome Research *28*, 11-24.

Ke, S., Shang, S., Kalachikov, S.M., Morozova, I., Yu, L., Russo, J.J., Ju, J., and Chasin, L.A. (2011). Quantitative evaluation of all hexamers as exonic splicing elements. Genome Research *21*, 1360-1374.

Keil, W., Kutscher, L.M., Shaham, S., and Siggia, E.D. (2017). Long-Term High-Resolution Imaging of Developing C. elegans Larvae with Microfluidics. Dev Cell *40*, 202-214.

Kershner, A.M., Shin, H., Hansen, T.J., and Kimble, J. (2014). Discovery of two GLP-1/Notch target genes that account for the role of GLP-1/Notch signaling in stem cell maintenance. Proceedings of the National Academy of Sciences *111*, 3739-3744.

Kidd, S., and Lieber, T. (2002). Furin cleavage is not a requirement for Drosophila Notch function. Mechanisms of Development *115*, 41-51.

Kim, H., Ishidate, T., Ghanta, K.S., Seth, M., Conte, D., Shirayama, M., and Mello, C.C. (2014). A Co-CRISPR Strategy for Efficient Genome Editing in *Caenorhabditis elegans*. Genetics *197*, 1069-1080.

Kimble, J. (1981). Alterations in cell lineage following laser ablation of cells in the somatic gonad of Caenorhabditis elegans. Developmental biology *87*, 286-300.

Kimble, J., and Hirsh, D. (1979). The postembryonic cell lineages of the hermaphrodite and male gonads in Caenorhabditis elegans. Developmental biology *70*, 396-417.

Kitsera, N., Khobta, A., and Epe, B. (2007). Destabilized green fluorescent protein detects rapid removal of transcription blocks after genotoxic exposure. BioTechniques *43*, 222-227.

Kohyama, J., Tokunaga, A., Fujita, Y., Miyoshi, H., Nagai, T., Miyawaki, A., Nakao, K., Matsuzaki, Y., and Okano, H. (2005). Visualization of spatiotemporal activation of Notch signaling: Live monitoring and significance in neural development. Developmental biology *286*, 311-325.

Kovall, R.A., and Blacklow, S.C. (2010). Chapter Two - Mechanistic Insights into Notch Receptor Signaling from Structural and Biochemical Studies. In Current Topics in Developmental Biology, R. Kopan, ed. (Academic Press), pp. 31-71.

Krause, M., Harrison, S.W., Xu, S.-Q., Chen, L., and Fire, A. (1994). Elements Regulating Cell- and Stage-Specific Expression of the C. elegans MyoD Family Homolog hlh-1. Developmental biology *166*, 133-148.

Krause, M., Park, M., Zhang, J.M., Yuan, J., Harfe, B., Xu, S.Q., Greenwald, I., Cole, M., Paterson, B., and Fire, A. (1997). A C. elegans E/Daughterless bHLH protein marks neuronal but not striated muscle development. Development (Cambridge, England) *124*, 2179-2189.

Krebs, L.T., Xue, Y., Norton, C.R., Shutter, J.R., Maguire, M., Sundberg, J.P., Gallahan, D., Closson, V., Kitajewski, J., Callahan, R*., et al.* (2000). Notch signaling is essential for vascular morphogenesis in mice. Genes & development *14*, 1343-1352.

Kroetz, M.B., and Zarkower, D. (2015). Cell-Specific mRNA Profiling of the Caenorhabditis elegans Somatic Gonadal Precursor Cells Identifies Suites of Sex-Biased and Gonad-Enriched Transcripts. G3: Genes|Genomes|Genetics *5*, 2831-2841.

Kroeze, W.K., Sassano, M.F., Huang, X.-P., Lansu, K., McCorvy, J.D., Giguère, P.M., Sciaky, N., and Roth, B.L. (2015). PRESTO-Tango as an open-source resource for interrogation of the druggable human GPCRome. Nature Structural & Molecular Biology *22*, 362-369.

Kunisch, M., Haenlin, M., and Campos-Ortega, J.A. (1994). Lateral inhibition mediated by the Drosophila neurogenic gene delta is enhanced by proneural proteins. Proceedings of the National Academy of Sciences *91*, 10139.

Lai, E.C. (2002). Keeping a good pathway down: transcriptional repression of Notch pathway target genes by CSL proteins. EMBO reports *3*, 840-845.

Lai, S.-L., and Lee, T. (2006). Genetic mosaic with dual binary transcriptional systems in Drosophila. Nature Neuroscience *9*, 703-709.

Lakso, M., Sauer, B., Mosinger, B., Lee, E.J., Manning, R.W., Yu, S.H., Mulder, K.L., and Westphal, H. (1992). Targeted oncogene activation by site-specific recombination in transgenic mice. Proceedings of the National Academy of Sciences *89*, 6232-6236.

Lambie, E.J., and Kimble, J. (1991). Two homologous regulatory genes, lin-12 and glp-1, have overlapping functions. Development (Cambridge, England) *112*, 231-240.

Langer, S.J., Ghafoori, A.P., Byrd, M., and Leinwand, L. (2002). A genetic screen identifies novel non-compatible loxP sites. Nucleic Acids Research *30*, 3067-3077.

Langridge, P.D., Chan, J.Y., Garcia-Diaz, A., Greenwald, I., and Struhl, G. (2021). The C. elegans Notch proteins LIN-12 and GLP-1 are tuned to lower force thresholds for activation than Drosophila Notch. bioRxiv, 2021.2002.2011.429991.

Langridge, P.D., and Struhl, G. (2017). Epsin-Dependent Ligand Endocytosis Activates Notch by Force. Cell *171*, 1383-1396.e1312.

Larson, D.R., Singer, R.H., and Zenklusen, D. (2009). A single molecule view of gene expression. Trends in Cell Biology *19*, 630-637.

Lecourtois, M., and Schweisguth, F. (1995). The neurogenic suppressor of hairless DNA-binding protein mediates the transcriptional activation of the enhancer of split complex genes triggered by Notch signaling. Genes & development *9*, 2598-2608.

Lecourtois, M., and Schweisguth, F. (1998). Indirect evidence for Delta-dependent intracellular processing of Notch in Drosophila embryos. Current Biology *8*, 771-775.

Lee, C., Shin, H., and Kimble, J. (2019). Dynamics of Notch-Dependent Transcriptional Bursting in Its Native Context. Developmental Cell *50*, 426-435.e424.

Lee, C., Sorensen, E.B., Lynch, T.R., and Kimble, J. (2016). C. elegans GLP-1/Notch activates transcription in a probability gradient across the germline stem cell pool. eLife *5*, e18370.

Lee, G., and Saito, I. (1998). Role of nucleotide sequences of loxP spacer region in Cre-mediated recombination. Gene *216*, 55-65.

Lee, L.-W., Lo, H.-W., and Lo, S.J. (2010). Vectors for co-expression of two genes in Caenorhabditis elegans. Gene *455*, 16-21.

Lee, T., and Luo, L. (1999). Mosaic Analysis with a Repressible Cell Marker for Studies of Gene Function in Neuronal Morphogenesis. Neuron *22*, 451-461.

Levitan, D., and Greenwald, I. (1995). Facilitation of lin-12-mediated signalling by sel-12, a Caenorhabditis elegans S182 Alzheimer's disease gene. Nature *377*, 351-354.

Levitan, D., and Greenwald, I. (1998). LIN-12 protein expression and localization during vulval development in C. elegans. Development (Cambridge, England) *125*, 3101-3109.

Levy, A.D., Yang, J., and Kramer, J.M. (1993). Molecular and genetic analyses of the Caenorhabditis elegans dpy-2 and dpy-10 collagen genes: a variety of molecular alterations affect organismal morphology. Molecular biology of the cell *4*, 803-817.

Li, J. (2011). Temporal control of Vulval Precursor Cell fate patterning in Caenorhabditis elegans (Columbia University).

Li, J., and Greenwald, I. (2010). LIN-14 inhibition of LIN-12 contributes to precision and timing of C. elegans vulval fate patterning. Current biology : CB *20*, 1875-1879.

Li, P., Collins, K.M., Koelle, M.R., and Shen, K. (2013). LIN-12/Notch signaling instructs postsynaptic muscle arm development by regulating UNC-40/DCC and MADD-2 in Caenorhabditis elegans. eLife *2*, e00378.

Li, X., and Greenwald, I. (1997). HOP-1, a Caenorhabditis elegans presenilin, appears to be functionally redundant with SEL-12 presenilin and to facilitate LIN-12 and GLP-1 signaling. Proceedings of the National Academy of Sciences of the United States of America *94*, 12204-12209.

Li, X., and von Boehmer, H. (2011). Notch Signaling in T-Cell Development and T-ALL. ISRN Hematology *2011*, 921706.

Li, X., Zhao, X., Fang, Y., Jiang, X., Duong, T., Fan, C., Huang, C.-C., and Kain, S.R. (1998). Generation of Destabilized Green Fluorescent Protein as a Transcription Reporter*. Journal of Biological Chemistry *273*, 34970-34975.

Lieber, T., Kidd, S., Alcamo, E., Corbin, V., and Young, M.W. (1993). Antineurogenic phenotypes induced by truncated Notch proteins indicate a role in signal transduction and may point to a novel function for Notch in nuclei. Genes & development *7*, 1949-1965.

Linkert, M., Rueden, C.T., Allan, C., Burel, J.-M., Moore, W., Patterson, A., Loranger, B., Moore, J., Neves, C., MacDonald, D.*, et al.* (2010). Metadata matters: access to image data in the real world. Journal of Cell Biology *189*, 777-782.

Liu, J., Lee Kenneth, K., Segura-Totten, M., Neufeld, E., Wilson Katherine, L., and Gruenbaum, Y. (2003). MAN1 and emerin have overlapping function(s) essential for chromosome segregation and cell division in Caenorhabditis elegans. Proceedings of the National Academy of Sciences *100*, 4598-4603.

Liu, K., Jin, H., and Zhou, B. (2020). Genetic lineage tracing with multiple DNA recombinases: A user's guide for conducting more precise cell fate mapping studies. Journal of Biological Chemistry *295*, 6413-6424.

Liu, Z., Brunskill, E., Boyle, S., Chen, S., Turkoz, M., Guo, Y., Grant, R., and Kopan, R. (2015). Second-generation Notch1 activity-trap mouse line (N1IP::CreHI) provides a more comprehensive map of cells experiencing Notch1 activity. Development (Cambridge, England) *142*, 1193-1202.

Livet, J., Weissman, T.A., Kang, H., Draft, R.W., Lu, J., Bennis, R.A., Sanes, J.R., and Lichtman, J.W. (2007). Transgenic strategies for combinatorial expression of fluorescent proteins in the nervous system. Nature *450*, 56-62.

Logeat, F., Bessia, C., Brou, C., LeBail, O., Jarriault, S., Seidah, N.G., and Israël, A. (1998). The Notch1 receptor is cleaved constitutively by a furin-like convertase. Proceedings of the National Academy of Sciences *95*, 8108.

Luan, H., Peabody, N.C., Vinson, Charles R., and White, B.H. (2006). Refined Spatial Manipulation of Neuronal Function by Combinatorial Restriction of Transgene Expression. Neuron *52*, 425-436.

Luca Vincent, C., Kim Byoung, C., Ge, C., Kakuda, S., Wu, D., Roein-Peikar, M., Haltiwanger Robert, S., Zhu, C., Ha, T., and Garcia, K.C. (2017). Notch-Jagged complex structure implicates a catch bond in tuning ligand sensitivity. Science (New York, NY) *355*, 1320-1324.

Luo, K.L., Underwood, R.S., and Greenwald, I. (2020). Positive autoregulation of *lag-1* in response to LIN-12 activation in cell fate decisions during *C. elegans* reproductive system development. Development (Cambridge, England) *147*, dev193482.

Lusk, C.P., Blobel, G., and King, M.C. (2007). Highway to the inner nuclear membrane: rules for the road. Nature Reviews Molecular Cell Biology *8*, 414-420.

Lyznik, L.A., Mitchell, J.C., Hirayama, L., and Hodges, T.K. (1993). Activity of yeast FLP recombinase in maize and rice protoplasts. Nucleic Acids Research *21*, 969-975.

Macosko, E.Z., Pokala, N., Feinberg, E.H., Chalasani, S.H., Butcher, R.A., Clardy, J., and Bargmann, C.I. (2009). A hub-and-spoke circuit drives pheromone attraction and social behaviour in C. elegans. Nature *458*, 1171-1175.

Madisen, L., Zwingman, T.A., Sunkin, S.M., Oh, S.W., Zariwala, H.A., Gu, H., Ng, L.L., Palmiter, R.D., Hawrylycz, M.J., Jones, A.R.*, et al.* (2010). A robust and high-throughput Cre reporting and characterization system for the whole mouse brain. Nature Neuroscience *13*, 133-140.

Martínez, V., Lauritsen, I., Hobel, T., Li, S., Nielsen, A.T., and Nørholm, Morten H.H. (2017). CRISPR/Cas9-based genome editing for simultaneous interference with gene expression and protein stability. Nucleic Acids Research *45*, e171-e171.

Masamizu, Y., Ohtsuka, T., Takashima, Y., Nagahara, H., Takenaka, Y., Yoshikawa, K., Okamura, H., and Kageyama, R. (2006). Real-time imaging of the somite segmentation clock: Revelation of unstable oscillators in the individual presomitic mesoderm cells. Proceedings of the National Academy of Sciences *103*, 1313.

Maxwell, I.H., Harrison, G.S., Wood, W.M., and Maxwell, F. (1989). A DNA cassette containing a trimerized SV40 polyadenylation signal which efficiently blocks spurious plasmid-initiated transcription. BioTechniques *7*, 276-280.

McGuire, S.E., Le Phuong, T., Osborn Alexander, J., Matsumoto, K., and Davis Ronald, L. (2003). Spatiotemporal Rescue of Memory Dysfunction in Drosophila. Science (New York, NY) *302*, 1765-1768.

Meloty-Kapella, L., Shergill, B., Kuon, J., Botvinick, E., and Weinmaster, G. (2012). Notch Ligand Endocytosis Generates Mechanical Pulling Force Dependent on Dynamin, Epsins, and Actin. Developmental Cell *22*, 1299-1312.

Merritt, C., Rasoloson, D., Ko, D., and Seydoux, G. (2008). 3′ UTRs Are the Primary Regulators of Gene Expression in the C. elegans Germline. Current Biology *18*, 1476-1482.

Mizutani, K.-i., Yoon, K., Dang, L., Tokunaga, A., and Gaiano, N. (2007). Differential Notch signalling distinguishes neural stem cells from intermediate progenitors. Nature *449*, 351-355.

Moerman, D.G., Benian, G.M., Barstead, R.J., Schriefer, L.A., and Waterston, R.H. (1988). Identification and intracellular localization of the unc-22 gene product of Caenorhabditis elegans. Genes & development *2*, 93-105.

Morales-Martínez, A., Dobrzynska, A., and Askjaer, P. (2015). Inner nuclear membrane protein LEM-2 is required for correct nuclear separation and morphology in C. elegans. Journal of cell science *128*, 1090-1096.

Morsut, L., Roybal, Kole T., Xiong, X., Gordley, Russell M., Coyle, Scott M., Thomson, M., and Lim, Wendell A. (2016). Engineering Customized Cell Sensing and Response Behaviors Using Synthetic Notch Receptors. Cell *164*, 780-791.

Mumm, J.S., Schroeter, E.H., Saxena, M.T., Griesemer, A., Tian, X., Pan, D.J., Ray, W.J., and Kopan, R. (2000). A Ligand-Induced Extracellular Cleavage Regulates γ-Secretase-like Proteolytic Activation of Notch1. Molecular Cell *5*, 197-206.

Muñoz-Jiménez, C., Ayuso, C., Dobrzynska, A., Torres-Mendéz, A., Ruiz, P.d.l.C., and Askjaer, P. (2017). An Efficient FLP-Based Toolkit for Spatiotemporal Control of Gene Expression in *Caenorhabditis elegans*. Genetics *206*, 1763-1778.

Murray, J.I., Bao, Z., Boyle, T.J., Boeck, M.E., Mericle, B.L., Nicholas, T.J., Zhao, Z., Sandel, M.J., and Waterston, R.H. (2008). Automated analysis of embryonic gene expression with cellular resolution in C. elegans. Nature Methods *5*, 703-709.

Nadarajan, S., Govindan, J.A., McGovern, M., Hubbard, E.J.A., and Greenstein, D. (2009). MSP and GLP-1/Notch signaling coordinately regulate actomyosin-dependent cytoplasmic streaming and oocyte growth in C. elegans. Development (Cambridge, England) *136*, 2223-2234.

Nam, H., Hwang, B.J., Choi, D.-Y., Shin, S., and Choi, M. (2020). Tobacco etch virus (TEV) protease with multiple mutations to improve solubility and reduce self-cleavage exhibits enhanced enzymatic activity. FEBS Open Bio *10*, 619-626.

Nandagopal, N., Santat, L.A., LeBon, L., Sprinzak, D., Bronner, M.E., and Elowitz, M.B. (2018). Dynamic Ligand Discrimination in the Notch Signaling Pathway. Cell *172*, 869-880.e819.

Newman, A.P., White, J.G., and Sternberg, P.W. (1995). The Caenorhabditis elegans lin-12 gene mediates induction of ventral uterine specialization by the anchor cell. Development (Cambridge, England) *121*, 263-271.

Newman, R.H., Fosbrink, M.D., and Zhang, J. (2011). Genetically Encodable Fluorescent Biosensors for Tracking Signaling Dynamics in Living Cells. Chemical Reviews *111*, 3614-3666.

Nicholls, S.B., Chu, J., Abbruzzese, G., Tremblay, K.D., and Hardy, J.A. (2011). Mechanism of a Genetically Encoded Dark-to-Bright Reporter for Caspase Activity. Journal of Biological Chemistry *286*, 24977-24986.

Nowotschin, S., Xenopoulos, P., Schrode, N., and Hadjantonakis, A.-K. (2013). A bright single-cell resolution live imaging reporter of Notch signaling in the mouse. BMC Developmental Biology *13*, 15.

O'Gorman, S., Fox, D.T., and Wahl, G.M. (1991). Recombinase-Mediated Gene Activation and Site-Specific Integration in Mammalian Cells. Science (New York, NY) *251*, 1351-1355.

Oberdoerffer, P., Otipoby, K.L., Maruyama, M., and Rajewsky, K. (2003). Unidirectional Cre-mediated genetic inversion in mice using the mutant loxP pair lox66 / lox71. Nucleic Acids Research *31*, e140-e140.

Öberg, C., Li, J., Pauley, A., Wolf, E., Gurney, M., and Lendahl, U. (2001). The Notch Intracellular Domain Is Ubiquitinated and Negatively Regulated by the Mammalian Sel-10 Homolog*. Journal of Biological Chemistry *276*, 35847-35853.

Oellers, N., Dehio, M., and Knust, E. (1994). bHLH proteins encoded by theEnhancer of split complex ofDrosophila negatively interfere with transcriptional activation mediated by proneural genes. Molecular and General Genetics MGG *244*, 465-473.

Ohtsuka, T., Imayoshi, I., Shimojo, H., Nishi, E., Kageyama, R., and McConnell, S.K. (2006). Visualization of embryonic neural stem cells using Hes promoters in transgenic mice. Molecular and Cellular Neuroscience *31*, 109-122.

Oswald, F., Täuber, B., Dobner, T., Bourteele, S., Kostezka, U., Adler, G., Liptay, S., and Schmid Roland, M. (2001). p300 Acts as a Transcriptional Coactivator for Mammalian Notch-1. Molecular and Cellular Biology *21*, 7761-7774.

Overstreet, E., Fitch, E., and Fischer, J.A. (2004). Fat facets and Liquid facets promote Delta endocytosis and Delta signaling in the signaling cells. Development (Cambridge, England) *131*, 5355-5366.

Pan, D., and Rubin, G.M. (1997). Kuzbanian Controls Proteolytic Processing of Notch and Mediates Lateral Inhibition during Drosophila and Vertebrate Neurogenesis. Cell *90*, 271-280.

Pani, A.M., and Goldstein, B. (2018). Direct visualization of a native Wnt in vivo reveals that a long-range Wnt gradient forms by extracellular dispersal. eLife *7*, e38325.

Parks, A.L., Huppert, S.S., and Muskavitch, M.A.T. (1997). The dynamics of neurogenic signalling underlying bristle development in Drosophila melanogaster. Mechanisms of Development *63*, 61-74.

Paroush, Z.e., Finley, R.L., Kidd, T., Wainwright, S.M., Ingham, P.W., Brent, R., and Ish-Horowicz, D. (1994). Groucho is required for Drosophila neurogenesis, segmentation, and sex determination and interacts directly with hairy-related bHLH proteins. Cell *79*, 805-815.

Parsons, M.J., Pisharath, H., Yusuff, S., Moore, J.C., Siekmann, A.F., Lawson, N., and Leach, S.D. (2009). Notch-responsive cells initiate the secondary transition in larval zebrafish pancreas. Mechanisms of Development *126*, 898-912.

Pellegrinet, L., Rodilla, V., Liu, Z., Chen, S., Koch, U., Espinosa, L., Kaestner, K.H., Kopan, R., Lewis, J., and Radtke, F. (2011). Dll1- and Dll4-Mediated Notch Signaling Are Required for Homeostasis of Intestinal Stem Cells. Gastroenterology *140*, 1230-1240.e1237.

Petcherski, A.G., and Kimble, J. (2000). LAG-3 is a putative transcriptional activator in the C. elegans Notch pathway. Nature *405*, 364-368.

Pokrass, M.J., Ryan, K.A., Xin, T., Pielstick, B., Timp, W., Greco, V., and Regot, S. (2020). Cell-Cycle-Dependent ERK Signaling Dynamics Direct Fate Specification in the Mammalian Preimplantation Embryo. Developmental Cell *55*, 328-340.e325.

Pompa de la, J.L., Wakeham, A., Correia, K.M., Samper, E., Brown, S., Aguilera, R.J., Nakano, T., Honjo, T., Mak, T.W., Rossant, J.*, et al.* (1997). Conservation of the Notch signalling pathway in mammalian neurogenesis. Development (Cambridge, England) *124*, 1139-1148.

Potter, C.J., Tasic, B., Russler, E.V., Liang, L., and Luo, L. (2010). The Q System: A Repressible Binary System for Transgene Expression, Lineage Tracing, and Mosaic Analysis. Cell *141*, 536-548.

Priess, J.R., Schnabel, H., and Schnabel, R. (1987). The glp-1 locus and cellular interactions in early C. elegans embryos. Cell *51*, 601-611.

Pui, J.C., Allman, D., Xu, L., DeRocco, S., Karnell, F.G., Bakkour, S., Lee, J.Y., Kadesch, T., Hardy, R.R., Aster, J.C.*, et al.* (1999). Notch1 Expression in Early Lymphopoiesis Influences B versus T Lineage Determination. Immunity *11*, 299-308.

Purvis, Jeremy E., and Lahav, G. (2013). Encoding and Decoding Cellular Information through Signaling Dynamics. Cell *152*, 945-956.

Qadota, H., Inoue, M., Hikita, T., Köppen, M., Hardin, J.D., Amano, M., Moerman, D.G., and Kaibuchi, K. (2007). Establishment of a tissue-specific RNAi system in C. elegans. Gene *400*, 166-173.

Radtke, F., Fasnacht, N., and MacDonald, H.R. (2010). Notch Signaling in the Immune System. Immunity *32*, 14-27.

Radtke, F., MacDonald, H.R., and Tacchini-Cottier, F. (2013). Regulation of innate and adaptive immunity by Notch. Nature Reviews Immunology *13*, 427-437.

Radtke, F., Wilson, A., and MacDonald, H.R. (2004). Notch signaling in T- and B-cell development. Current Opinion in Immunology *16*, 174-179.

Radtke, F., Wilson, A., Stark, G., Bauer, M., van Meerwijk, J., MacDonald, H.R., and Aguet, M. (1999). Deficient T Cell Fate Specification in Mice with an Induced Inactivation of Notch1. Immunity *10*, 547-558.

Rao, A.U., Carta, L.K., Lesuisse, E., and Hamza, I. (2005). Lack of heme synthesis in a free-living eukaryote. Proceedings of the National Academy of Sciences of the United States of America *102*, 4270.

Regot, S., Hughey, Jacob J., Bajar, Bryce T., Carrasco, S., and Covert, Markus W. (2014). High-Sensitivity Measurements of Multiple Kinase Activities in Live Single Cells. Cell *157*, 1724-1734.

Reinke, A.W., Mak, R., Troemel, E.R., and Bennett, E.J. (2017). In vivo mapping of tissue- and subcellular-specific proteomes in Caenorhabditis elegans. Science advances *3*, e1602426.

Renicke, C., Allmann, A.-K., Lutz, A.P., Heimerl, T., and Taxis, C. (2017). The Mitotic Exit Network Regulates Spindle Pole Body Selection During Sporulation of Saccharomyces cerevisiae. Genetics *206*, 919-937.

Rodriguez-Corona, U., Sobol, M., Rodriguez-Zapata, L.C., Hozak, P., and Castano, E. (2015). Fibrillarin from Archaea to human. Biology of the Cell *107*, 159-174.

Rooke, J., Pan, D., Xu, T., and Rubin Gerald, M. (1996). KUZ, a Conserved Metalloprotease-Disintegrin Protein with Two Roles in Drosophila Neurogenesis. Science (New York, NY) *273*, 1227-1231.

Roybal, K.T., Williams, J.Z., Morsut, L., Rupp, L.J., Kolinko, I., Choe, J.H., Walker, W.J., McNally, K.A., and Lim, W.A. (2016). Engineering T Cells with Customized Therapeutic Response Programs Using Synthetic Notch Receptors. Cell *167*, 419-432.e416.

Ruijtenberg, S., and van den Heuvel, S. (2015). G1/S Inhibitors and the SWI/SNF Complex Control Cell-Cycle Exit during Muscle Differentiation. Cell *162*, 300-313.

Ryu, H., Chung, M., Dobrzyński, M., Fey, D., Blum, Y., Lee, S.S., Peter, M., Kholodenko, B.N., Jeon, N.L., and Pertz, O. (2015). Frequency modulation of ERK activation dynamics rewires cell fate. Molecular systems biology *11*, 838.

Sallee, M.D. (2015). Function and regulation of the transcription factor HLH-2/E2A during gonadogenesis in Caenorhabditis elegans. In Biological Sciences (Columbia University).

Sallee, M.D., Aydin, T., and Greenwald, I. (2015). Influences of LIN-12/Notch and POP-1/TCF on the Robustness of Ventral Uterine Cell Fate Specification in Caenorhabditis elegans Gonadogenesis. G3 Genes|Genomes|Genetics *5*, 2775-2782.

Sallee, M.D., and Greenwald, I. (2015). Dimerization-driven degradation of C. elegans and human E proteins. Genes & development *29*, 1356-1361.

Sanchez-Irizarry, C., Carpenter Andrea, C., Weng Andrew, P., Pear Warren, S., Aster Jon, C., and Blacklow Stephen, C. (2004). Notch Subunit Heterodimerization and Prevention of Ligand-Independent Proteolytic Activation Depend, Respectively, on a Novel Domain and the LNR Repeats. Molecular and Cellular Biology *24*, 9265-9273.

Sauer, B. (1987). Functional expression of the cre-lox site-specific recombination system in the yeast Saccharomyces cerevisiae. Molecular and Cellular Biology *7*, 2087-2096.

Sauer, B., and Henderson, N. (1988). Site-specific DNA recombination in mammalian cells by the Cre recombinase of bacteriophage P1. Proceedings of the National Academy of Sciences *85*, 5166.

Schindelin, J., Arganda-Carreras, I., Frise, E., Kaynig, V., Longair, M., Pietzsch, T., Preibisch, S., Rueden, C., Saalfeld, S., Schmid, B.*, et al.* (2012). Fiji: an open-source platform for biological-image analysis. Nature Methods *9*, 676-682.

Schnütgen, F., Doerflinger, N., Calléja, C., Wendling, O., Chambon, P., and Ghyselinck, N.B. (2003). A directional strategy for monitoring Cre-mediated recombination at the cellular level in the mouse. Nature Biotechnology *21*, 562-565.

Schroeter, E.H., Kisslinger, J.A., and Kopan, R. (1998). Notch-1 signalling requires ligand-induced proteolytic release of intracellular domain. Nature *393*, 382-386.

Sekar, K., Gentile, A.M., Bostick, J.W., and Tyo, K.E.J. (2016). N-Terminal-Based Targeted, Inducible Protein Degradation in Escherichia coli. PLOS ONE *11*, e0149746.

Seo, D., Southard, K.M., Kim, J.-w., Lee, H.J., Farlow, J., Lee, J.-u., Litt, D.B., Haas, T., Alivisatos, A.P., Cheon, J.*, et al.* (2016). A Mechanogenetic Toolkit for Interrogating Cell Signaling in Space and Time. Cell *165*, 1507-1518.

Seydoux, G., and Greenwald, I. (1989). Cell autonomy of lin-12 function in a cell fate decision in C. elegans. Cell *57*, 1237-1245.

Seydoux, G., Schedl, T., and Greenwald, I. (1990). Cell-cell interactions prevent a potential inductive interaction between soma and germline in C. elegans. Cell *61*, 939-951.

Sfarcic, I., Bui, T., Daniels, E.C., and Troemel, E.R. (2019). Nanoluciferase-Based Method for Detecting Gene Expression in Caenorhabditis elegans. Genetics *213*, 1197-1207.

Shaffer, J.M., and Greenwald, I. (2022). Floxed exon (Flexon): A flexibly positioned stop cassette for recombinase-mediated conditional gene expression. Proceedings of the National Academy of Sciences *119*, e2117451119.

Shah, R., Li, F., Voziyanova, E., and Voziyanov, Y. (2015). Target-specific variants of Flp recombinase mediate genome engineering reactions in mammalian cells. The FEBS Journal *282*, 3323-3333.

Shaye, D.D., and Greenwald, I. (2002). Endocytosis-mediated downregulation of LIN-12/Notch upon Ras activation in Caenorhabditis elegans. Nature *420*, 686-690.

Shin, H., Haupt, K.A., Kershner, A.M., Kroll-Conner, P., Wickens, M., and Kimble, J. (2017). SYGL-1 and LST-1 link niche signaling to PUF RNA repression for stem cell maintenance in Caenorhabditis elegans. PLOS Genetics *13*, e1007121.

Shin, H., and Reiner, D.J. (2018). The Signaling Network Controlling C. elegans Vulval Cell Fate Patterning. Journal of Developmental Biology *6*, 30.

Siegel, R.W., Jain, R., and Bradbury, A. (2001). Using an in vivo phagemid system to identify non-compatible loxP sequences. FEBS Letters *505*, 467-473.

Simon, C.S., Rahman, S., Raina, D., Schröter, C., and Hadjantonakis, A.-K. (2020). Live Visualization of ERK Activity in the Mouse Blastocyst Reveals Lineage-Specific Signaling Dynamics. Developmental Cell *55*, 341-353.e345.

Simpson, P. (1997). Notch signalling in development: on equivalence groups and asymmetric developmental potential. Current Opinion in Genetics & Development *7*, 537-542.

Smith, E., Claudinot, S., Lehal, R., Pellegrinet, L., Barrandon, Y., and Radtke, F. (2012). Generation and characterization of a Notch1 signaling-specific reporter mouse line. genesis *50*, 700-710.

Sohal, V.S., Zhang, F., Yizhar, O., and Deisseroth, K. (2009). Parvalbumin neurons and gamma rhythms enhance cortical circuit performance. Nature *459*, 698-702.

Sorensen, E.B., Seidel, H.S., Crittenden, S.L., Ballard, J.H., and Kimble, J. (2020). Corrigendum: A toolkit of tagged glp-1 alleles reveals strong glp-1 expression in the germline, embryo, and spermatheca.

Soriano, P. (1999). Generalized lacZ expression with the ROSA26 Cre reporter strain. Nature Genetics *21*, 70-71.

Sotillos, S., Roch, F., and Campuzano, S. (1997). The metalloprotease-disintegrin Kuzbanian participates in Notch activation during growth and patterning of Drosophila imaginal discs. Development (Cambridge, England) *124*, 4769-4779.

Souilhol, C., Cormier, S., Monet, M., Vandormael-Pournin, S., Joutel, A., Babinet, C., and Cohen-Tannoudji, M. (2006). Nas transgenic mouse line allows visualization of Notch pathway activity in vivo. genesis *44*, 277-286.

Spencer, Sabrina L., Cappell, Steven D., Tsai, F.-C., Overton, K.W., Wang, Clifford L., and Meyer, T. (2013). The Proliferation-Quiescence Decision Is Controlled by a Bifurcation in CDK2 Activity at Mitotic Exit. Cell *155*, 369-383.

Spieth, J., Brooke, G., Kuersten, S., Lea, K., and Blumenthal, T. (1993). Operons in C. elegans: Polycistronic mRNA precursors are processed by trans-splicing of SL2 to downstream coding regions. Cell *73*, 521-532.

Sprinzak, D., Lakhanpal, A., LeBon, L., Santat, L.A., Fontes, M.E., Anderson, G.A., Garcia-Ojalvo, J., and Elowitz, M.B. (2010). Cis-interactions between Notch and Delta generate mutually exclusive signalling states. Nature *465*, 86-90.

Srivastava, S., Salter, A.I., Liggitt, D., Yechan-Gunja, S., Sarvothama, M., Cooper, K., Smythe, K.S., Dudakov, J.A., Pierce, R.H., Rader, C.*, et al.* (2019). Logic-Gated ROR1 Chimeric Antigen Receptor Expression Rescues T Cell-Mediated Toxicity to Normal Tissues and Enables Selective Tumor Targeting. Cancer Cell *35*, 489-503.e488.

Stamm, S., Zhu, J., Nakai, K., Stoilov, P., Stoss, O., and Zhang, M.Q. (2000). An Alternative-Exon Database and Its Statistical Analysis. DNA and Cell Biology *19*, 739-756.

Stephenson, N.L., and Avis, J.M. (2012). Direct observation of proteolytic cleavage at the S2 site upon forced unfolding of the Notch negative regulatory region. Proceedings of the National Academy of Sciences *109*, E2757.

Sternberg, P.W. (1988). Lateral inhibition during vulval induction in Caenorhabditis elegans. Nature *335*, 551-554.

Sternberg, P.W. (2005). Vulval development. In WormBook : the online review of C elegans biology, T.*C.e.*R. Community, ed., pp. 1-28.

Sternberg, P.W., and Horvitz, H.R. (1986). Pattern formation during vulval development in C. elegans. Cell *44*, 761-772.

Stiernagle, T. (2006). Maintenance of C. elegans. WormBook : the online review of C elegans biology, 1-11.

Struhl, G., and Adachi, A. (1998). Nuclear Access and Action of Notch In Vivo. Cell *93*, 649-660.

Struhl, G., and Adachi, A. (2000). Requirements for Presenilin-Dependent Cleavage of Notch and Other Transmembrane Proteins. Molecular Cell *6*, 625-636.

Struhl, G., and Basler, K. (1993). Organizing activity of wingless protein in Drosophila. Cell *72*, 527-540.

Struhl, G., Fitzgerald, K., and Greenwald, I. (1993). Intrinsic activity of the lin-12 and Notch intracellular domains in vivo. Cell *74*, 331-345.

Struhl, G., and Greenwald, I. (1999). Presenilin is required for activity and nuclear access of Notch in Drosophila. Nature *398*, 522-525.

Struhl, G., and Greenwald, I. (2001). Presenilin-mediated transmembrane cleavage is required for Notch signal transduction in *Drosophila*. Proceedings of the National Academy of Sciences *98*, 229.

Sulston, J.E., and Horvitz, H.R. (1977). Post-embryonic cell lineages of the nematode, Caenorhabditis elegans. Developmental biology *56*, 110-156.

Sulston, J.E., and White, J.G. (1980). Regulation and cell autonomy during postembryonic development of Caenorhabditis elegans. Developmental biology *78*, 577-597.

Sundaram, M., and Greenwald, I. (1993). Suppressors of a lin-12 hypomorph define genes that interact with both lin-12 and glp-1 in Caenorhabditis elegans. Genetics *135*, 765-783.

Sundaram, M.V. (2005). The love–hate relationship between Ras and Notch. Genes & development *19*, 1825-1839.

Sundaram, M.V. (2006). RTK/Ras/MAPK signaling. In WormBook : the online review of C elegans biology, T.C.e.R. Community, ed. (WormBook).

Tabara, H., Hill, R.J., Mello, C.C., Priess, J.R., and Kohara, Y. (1999). pos-1 encodes a cytoplasmic zinc-finger protein essential for germline specification in C. elegans. Development (Cambridge, England) *126*, 1-11.

Takács-Vellai, K., Vellai, T., Chen, E.B., Zhang, Y., Guerry, F., Stern, M.J., and Müller, F. (2007). Transcriptional control of Notch signaling by a HOX and a PBX/EXD protein during vulval development in C. elegans. Developmental biology *302*, 661-669.

Takemoto, K., Nagai, T., Miyawaki, A., and Miura, M. (2003). Spatio-temporal activation of caspase revealed by indicator that is insensitive to environmental effects. Journal of Cell Biology *160*, 235-243.

Tamai, K.K., and Nishiwaki, K. (2007). bHLH Transcription factors regulate organ morphogenesis via activation of an ADAMTS protease in C. elegans. Developmental biology *308*, 562-571.

Tan, P.B., Lackner, M.R., and Kim, S.K. (1998). MAP kinase signaling specificity mediated by the LIN-1 Ets/LIN-31 WH transcription factor complex during C. elegans vulval induction. Cell *93*, 569-580.

Tanenbaum, Marvin E., Gilbert, Luke A., Qi, Lei S., Weissman, Jonathan S., and Vale, Ronald D. (2014). A Protein-Tagging System for Signal Amplification in Gene Expression and Fluorescence Imaging. Cell *159*, 635-646.

Tax, F.E., Thomas, J.H., Ferguson, E.L., and Horvitzt, H.R. (1997). Identification and Characterization of Genes That Interact With lin-12 in Caenorhabditis elegans. Genetics *147*, 1675-1695.

Taxis, C., Stier, G., Spadaccini, R., and Knop, M. (2009). Efficient protein depletion by genetically controlled deprotection of a dormant N-degron. Molecular systems biology *5*, 267.

Tenen, C.C., and Greenwald, I. (2019). Cell Non-autonomous Function of daf-18/PTEN in the Somatic Gonad Coordinates Somatic Gonad and Germline Development in C. elegans Dauer Larvae. Current biology : CB *29*, 1064-1072.e1068.

Tessarz, P., Santos-Rosa, H., Robson, S.C., Sylvestersen, K.B., Nelson, C.J., Nielsen, M.L., and Kouzarides, T. (2014). Glutamine methylation in histone H2A is an RNA-polymerase-I-dedicated modification. Nature *505*, 564-568.

Thermann, R., Neu-Yilik, G., Deters, A., Frede, U., Wehr, K., Hagemeier, C., Hentze, M.W., and Kulozik, A.E. (1998). Binary specification of nonsense codons by splicing and cytoplasmic translation. The EMBO Journal *17*, 3484-3494.

Timmons, L., Court, D.L., and Fire, A. (2001). Ingestion of bacterially expressed dsRNAs can produce specific and potent genetic interference in Caenorhabditis elegans. Gene *263*, 103-112.

Toda, S., McKeithan Wesley, L., Hakkinen Teemu, J., Lopez, P., Klein Ophir, D., and Lim Wendell, A. (2020). Engineering synthetic morphogen systems that can program multicellular patterning. Science (New York, NY) *370*, 327-331.

Tourasse, N.J., Millet, J.R.M., and Dupuy, D. (2017). Quantitative RNA-seq meta-analysis of alternative exon usage in C. elegans. Genome Research *27*, 2120-2128.

Underwood, R.S., Deng, Y., and Greenwald, I. (2017). Integration of EGFR and LIN-12/Notch Signaling by LIN-1/Elk1, the Cdk8 Kinase Module, and SUR-2/Med23 in Vulval Precursor Cell Fate Patterning in *Caenorhabditis elegans*. Genetics *207*, 1473-1488.

van den Berg, S., Löfdahl, P.-Å., Härd, T., and Berglund, H. (2006). Improved solubility of TEV protease by directed evolution. Journal of Biotechnology *121*, 291-298.

van der Vaart, A., Godfrey, M., Portegijs, V., and van den Heuvel, S. (2020). Dose-dependent functions of SWI/SNF BAF in permitting and inhibiting cell proliferation in vivo. Science advances *6*, eaay3823.

Van Doren, M., Bailey, A.M., Esnayra, J., Ede, K., and Posakony, J.W. (1994). Negative regulation of proneural gene activity: hairy is a direct transcriptional repressor of achaete. Genes & development *8*, 2729-2742.

van Rijnberk, L.M., van der Horst, S.E.M., van den Heuvel, S., and Ruijtenberg, S. (2017). A dual transcriptional reporter and CDK-activity sensor marks cell cycle entry and progression in C. elegans. PLOS ONE *12*, e0171600.

Vázquez-Manrique, R.P., Legg, J.C., Olofsson, B., Ly, S., and Baylis, H.A. (2010). Improved gene targeting in C. elegans using counter-selection and Flp-mediated marker excision. Genomics *95*, 37-46.

Vilas-Boas, F., Fior, R., Swedlow, J.R., Storey, K.G., and Henrique, D. (2011). A novel reporter of notch signalling indicates regulated and random notch activation during vertebrate neurogenesis. BMC Biology *9*, 58.

Viswanathan, R., Necakov, A., Trylinski, M., Harish, R.K., Krueger, D., Esposito, E., Schweisguth, F., Neveu, P., and De Renzis, S. (2019). Optogenetic inhibition of Delta reveals digital Notch signalling output during tissue differentiation. EMBO reports *20*, e47999.

Vooijs, M., Jonkers, J., and Berns, A. (2001). A highly efficient ligand-regulated Cre recombinase mouse line shows that LoxP recombination is position dependent. EMBO reports *2*, 292-297.

Vooijs, M., Ong, C.-T., Hadland, B., Huppert, S., Liu, Z., Korving, J., van den Born, M., Stappenbeck, T., Wu, Y., Clevers, H.*, et al.* (2007). Mapping the consequence of Notch1 proteolysis in vivo with NIP-CRE. Development (Cambridge, England) *134*, 535-544.

Voutev, R., and Hubbard, E.J.A. (2008). A "FLP-Out" System for Controlled Gene Expression in *Caenorhabditis elegans*. Genetics *180*, 103-119.

Voziyanov, Y., Stewart, A.F., and Jayaram, M. (2002). A dual reporter screening system identifies the amino acid at position 82 in Flp site-specific recombinase as a determinant for target specificity. Nucleic Acids Research *30*, 1656-1663.

Wallberg, A.E., Pedersen, K., Lendahl, U., and Roeder, R.G. (2002). p300 and PCAF Act Cooperatively To Mediate Transcriptional Activation from Chromatin Templates by Notch Intracellular Domains In Vitro. Molecular and Cellular Biology *22*, 7812-7819.

Wang, G., Sun, L., Reina, C.P., Song, I., Gabel, C.V., and Driscoll, M. (2019). CED-4 CARD domain residues can modulate non-apoptotic neuronal regeneration functions independently from apoptosis. Scientific Reports *9*, 13315.

Wang, H., Liu, J., Gharib, S., Chai, C.M., Schwarz, E.M., Pokala, N., and Sternberg, P.W. (2017a). cGAL, a temperature-robust GAL4–UAS system for Caenorhabditis elegans. Nature Methods *14*, 145-148.

Wang, H., Liu, J., Yuet, K.P., Hill, A.J., and Sternberg, P.W. (2018). Split cGAL, an intersectional strategy using a split intein for refined spatiotemporal transgene control in *Caenorhabditis elegans*. Proceedings of the National Academy of Sciences *115*, 3900.

Wang, S., Tang, N.H., Lara-Gonzalez, P., Zhao, Z., Cheerambathur, D.K., Prevo, B., Chisholm, A.D., Desai, A., and Oegema, K. (2017b). A toolkit for GFP-mediated tissue-specific protein degradation in *C. elegans*. Development (Cambridge, England) *144*, 2694-2701.

Wang, W., and Struhl, G. (2004). Drosophila Epsin mediates a select endocytic pathway that DSL ligands must enter to activate Notch. Development (Cambridge, England) *131*, 5367-5380.

Wang, W., and Struhl, G. (2005). Distinct roles for Mind bomb, Neuralized and Epsin in mediating DSL endocytosis and signaling in Drosophila. Development (Cambridge, England) *132*, 2883-2894.

Wang, X., Gupta, P., Fairbanks, J., and Hansen, D. (2014). Protein kinase CK2 both promotes robust proliferation and inhibits the proliferative fate in the C. elegans germ line. Developmental biology *392*, 26-41.

Ward, A., Liu, J., Feng, Z., and Xu, X.Z.S. (2008). Light-sensitive neurons and channels mediate phototaxis in C. elegans. Nature Neuroscience *11*, 916-922.

Ward, J.D. (2015). Rapid and Precise Engineering of the Caenorhabditis elegans Genome with Lethal Mutation Co-Conversion and Inactivation of NHEJ Repair. Genetics *199*, 363-377.

Watts, J.S., Harrison, H.F., Omi, S., Guenthers, Q., Dalelio, J., Pujol, N., and Watts, J.L. (2020a). New Strains for Tissue-Specific RNAi Studies in Caenorhabditis elegans. G3 Genes|Genomes|Genetics *10*, 4167-4176.

Watts, J.S., Harrison, H.F., Omi, S., Guenthers, Q., Dalelio, J., Pujol, N., and Watts, J.L. (2020b). New Strains for Tissue-Specific RNAi Studies in *Caenorhabditis elegans*. G3: Genes|Genomes|Genetics *10*, 4167-4176.

Waugh, D.S. (2011). An overview of enzymatic reagents for the removal of affinity tags. Protein expression and purification *80*, 283-293.

Wei, X., Henke, V.G., Strübing, C., Brown, E.B., and Clapham, D.E. (2003). Real-Time Imaging of Nuclear Permeation by EGFP in Single Intact Cells. Biophysical Journal *84*, 1317-1327.

Wei, X., Potter, C.J., Luo, L., and Shen, K. (2012). Controlling gene expression with the Q repressible binary expression system in Caenorhabditis elegans. Nature Methods *9*, 391-395.

Weirauch, Matthew T., Yang, A., Albu, M., Cote, A.G., Montenegro-Montero, A., Drewe, P., Najafabadi, Hamed S., Lambert, Samuel A., Mann, I., Cook, K.*, et al.* (2014). Determination and Inference of Eukaryotic Transcription Factor Sequence Specificity. Cell *158*, 1431-1443.

Wen, C., Metzstein, M.M., and Greenwald, I. (1997). SUP-17, a Caenorhabditis elegans ADAM protein related to Drosophila KUZBANIAN, and its role in LIN-12/NOTCH signalling. Development (Cambridge, England) *124*, 4759-4767.

Weng, A.P., Ferrando, A.A., Lee, W., Morris, J.P., Silverman, L.B., Sanchez-Irizarry, C., Blacklow, S.C., Look, A.T., and Aster, J.C. (2004). Activating Mutations of NOTCH1 in Human T Cell Acute Lymphoblastic Leukemia. Science (New York, NY) *306*, 269-271.

Wilkinson, H.A., Fitzgerald, K., and Greenwald, I. (1994). Reciprocal changes in expression of the receptor lin-12 and its ligand lag-2 prior to commitment in a C. elegans cell fate decision. Cell *79*, 1187-1198.

Wilkinson, H.A., and Greenwald, I. (1995). Spatial and temporal patterns of lin-12 expression during C. elegans hermaphrodite development. Genetics *141*, 513-526.

Wing, C.E., Fung, H.Y.J., and Chook, Y.M. (2022). Karyopherin-mediated nucleocytoplasmic transport. Nature Reviews Molecular Cell Biology.

Wu, G., Lyapina, S., Das, I., Li, J., Gurney, M., Pauley, A., Chui, I., Deshaies Raymond, J., and Kitajewski, J. (2001). SEL-10 Is an Inhibitor of Notch Signaling That Targets Notch for Ubiquitin-Mediated Protein Degradation. Molecular and Cellular Biology *21*, 7403-7415.

Wu, L., Aster, J.C., Blacklow, S.C., Lake, R., Artavanis-Tsakonas, S., and Griffin, J.D. (2000). MAML1, a human homologue of Drosophila Mastermind, is a transcriptional co-activator for NOTCH receptors. Nature Genetics *26*, 484-489.

Xiao, C., Calado, D.P., Galler, G., Thai, T.-H., Patterson, H.C., Wang, J., Rajewsky, N., Bender, T.P., and Rajewsky, K. (2007). MiR-150 Controls B Cell Differentiation by Targeting the Transcription Factor c-Myb. Cell *131*, 146-159.

Xu, D., Farmer, A., Collett, G., Grishin, N.V., and Chook, Y.M. (2012). Sequence and structural analyses of nuclear export signals in the NESdb database. Molecular biology of the cell *23*, 3677-3693.

Yang, Z.-j., Yu, Z.-y., Cai, Y.-m., Du, R.-r., and Cai, L. (2020). Engineering of an enhanced synthetic Notch receptor by reducing ligand-independent activation. Communications Biology *3*, 116.

Yi, Y.-H., Ma, T.-H., Lee, L.-W., Chiou, P.-T., Chen, P.-H., Lee, C.-M., Chu, Y.-D., Yu, H., Hsiung, K.-C., Tsai, Y.-T.*, et al.* (2015). A Genetic Cascade of let-7-ncl-1-fib-1 Modulates Nucleolar Size and rRNA Pool in Caenorhabditis elegans. PLOS Genetics *11*, e1005580.

Yoo, A.S., Bais, C., and Greenwald, I. (2004). Crosstalk between the EGFR and LIN-12/Notch pathways in C. elegans vulval development. Science (New York, NY) *303*, 663-666.

Yoo, A.S., and Greenwald, I. (2005). LIN-12/Notch Activation Leads to MicroRNA-Mediated Down-Regulation of Vav in *C. elegans*. Science (New York, NY) *310*, 1330-1333.

Zacharioudaki, E., and Bray, S.J. (2014). Tools and methods for studying Notch signaling in Drosophila melanogaster. Methods *68*, 173-182.

Zakeri, B., Fierer, J.O., Celik, E., Chittock, E.C., Schwarz-Linek, U., Moy, V.T., and Howarth, M. (2012). Peptide tag forming a rapid covalent bond to a protein, through engineering a bacterial adhesin. Proceedings of the National Academy of Sciences of the United States of America *109*, E690-E697.

Zhang, J., Sun, X., Qian, Y., LaDuca, J.P., and Maquat, L.E. (1998). At Least One Intron Is Required for the Nonsense-Mediated Decay of Triosephosphate Isomerase mRNA: a Possible Link between Nuclear Splicing and Cytoplasmic Translation. Molecular and Cellular Biology *18*, 5272-5283.

Zhang, L., Ward, J.D., Cheng, Z., and Dernburg, A.F. (2015). The auxin-inducible degradation (AID) system enables versatile conditional protein depletion in *C. elegans*. Development (Cambridge, England) *142*, 4374-4384.

Zhang, X., and Greenwald, I. (2011). Spatial Regulation of lag-2 Transcription During Vulval Precursor Cell Fate Patterning in *Caenorhabditis elegans lag-2*. Genetics *188*, 847-858.

Zhang, Z., and Lutz, B. (2002). Cre recombinase-mediated inversion using lox66 and lox71: method to introduce conditional point mutations into the CREB-binding protein. Nucleic Acids Research *30*, e90-e90.

Zheng, C.L., Fu, X.-D., and Gribskov, M. (2005). Characteristics and regulatory elements defining constitutive splicing and different modes of alternative splicing in human and mouse. RNA *11*, 1777-1787.

Zhu, K., Zhou, X., Yan, Y., Mo, H., Xie, Y., Cheng, B., and Fan, J. (2017). Cleavage of fusion proteins on the affinity resins using the TEV protease variant. Protein expression and purification *131*, 27-33.

Appendix A: Limitations of subnuclear SALSA reporters

The nucleolar reporter was constructed and analyzed with the assistance of Matt Johnson.

1. Introduction

In Chapter 3, I used SALSA to show that differences in LIN-12 activity in the α cells can be biased by the relative birth order between the two cells when the time interval between the births is >45 minutes. When the time interval between the α cell births is ≤45 minutes, the LIN-12 activity advantage is random with respect to birth order. This is consistent with the previous data, in which the first-born α cell has a VU fate bias only at birth time intervals >40-45 minutes, but at birth time intervals ≤40-45 minutes the α cell that becomes the VU is random with respect to birth order (Attner et al., 2019). It was also shown that the relative order of the onset of expression of an endogenous HLH-2::GFP reporter in the parents of the α cells indicates which α cell will become the VU, even at short birth time intervals. The model suggests that LIN-12 activity would first appear in the α cell daughter of the parent with initial HLH-2::GFP expression. It was not possible to simultaneously image SALSA and HLH-2::GFP, or a similar endogenous HLH-2::mScarlet reporter, because SALSA uses both nuclear green and red fluorescence in its output. Substituting one of the fluorescent proteins for a blue fluorescent protein was not feasible because exposing *C. elegans* larvae to high intensity or frequent exposure of the BFP excitation wavelength causes developmental arrest and death (Edwards et al., 2008; Ward et al., 2008).

One way to image different reporters in the same fluorescent channel would be to separate the reporters into different subnuclear compartments or regions. Fluorescent proteins can be targeted to the inner nuclear membrane (INM) by tagging them to LEM-2/LEMD2, an integral transmembrane protein embedded in the INM (Brachner et al., 2005). LEM-2 contains

an N-terminal LAP-2-Emerin-MAN1 (LEM) domain that interacts with the chromatin associated protein BAF-1/BANF1 (Brachner and Foisner, 2011), and is functionally redundant in most contexts with other LEM domain-containing proteins such as EMR-1/Emerin (Barkan et al., 2011; Liu et al., 2003). A transgene encoding a LEM-2::mCherry C-terminal fusion with *lem-2* regulatory sequences marks the INM ubiquitously and fully rescues *lem-2(0)*; *emr-1(RNAi)* embryonic lethality (Morales-Martínez et al., 2015). Using LEM-2 to spatially restrict a SALSA reporter to the INM could allow fluorescence from the reporter to be distinguished from nuclear HLH-2 reporter expression.

The nucleolus could also be used to distinguish SALSA reporter fluorescence from nuclear HLH-2 reporter fluorescence. FIB-1/Fibrillarin is a nucleolar methyltransferase that regulates the expression and maturation of rRNA (Grummt, 2013; Rodriguez-Corona et al., 2015; Tessarz et al., 2014). FIB-1::GFP (Lee et al., 2010; Yi et al., 2015) and FIB-1::BFP (de la Cova, unpublished) transgenes are localized strictly to nucleoli, and *fib-1* regulatory sequences drive expression in all cell types. A FIB-1 SALSA reporter would have to be single-color to reserve the other color for the HLH-2 reporter, which also has some nucleolar expression. I describe here three iterations of a SALSA reporter system using LEM-2 and/or FIB-1, and discuss issues with each.

2. Materials and Methods

Strains

All strains were maintained at 20°C on 6 cm NGM plates seeded with *E. coli* OP50. Imaging was done at 25°C. The following strains were used in Appendix A:

GS9320 *lem-2(ar645)[lem-2::mCherry::tcut::gfp]* II; *lin-12(ar640)[lin-12::tevp]* III; *arTi112[ckb-3p::mCherry::h2b::unc-54 3' UTR]* V

GS9810 *arSi125[fib-1p::fib-1::tcut::gfp::nls::unc-54 3' UTR]* I; *lin-12(ar640)* III; *arTi436[rps-27p::lem-1(flexon)::mCherry::unc-54 3' UTR]* V; *arTi237[ckb-3p::Cre(opti)::tbb-2 3' UTR]* X

Strains that contained *lem-2(tcutgfp)[lem-2::tcut::gfp::nls]* were not named or frozen. The strain used here contained *lem-2(tcutgfp)* II; *lin-12(ar640)* III; *jjIs3900[hlh-8p::nls::mCherry::lacZ + myo-2p::mCherry]* IV.

Plasmid construction and genome editing

lem-2(ar645)[lem-2::mCherry::tcut::gfp] was made using CRISPR/Cas9 to insert *mCherry::tcut::gfp* into the endogenous *lem-2* locus. The repair template pJS129 was made using Gibson cloning to insert a 5' homology arm for the *lem-2* coding region amplified from gDNA, GFP amplified from pJS117, and a 3' homology arm for *lem-2* 3' UTR amplified from pBN21 (Morales-Martínez et al., 2015) into the mCherry SEC vector pJJR83 digested with AvrII and SpeI-HF. The Tcut site within the SEC construct was co-opted for use as the Tcut site in the reporter. The sgRNA sequence in pJW1285 was replaced with *lem-2* sgRNA sequences by Gibson cloning to make pJS121 and pJS122. A mix containing pJS129 (50 ng/µl), pJS122 (25 ng/µl), pJS121 (25 ng/µl), and the co-injection markers pCFJ90 (7.5 ng/µl) and pGH8 (10 ng/µl) was injected into the germline of adult N2 hermaphrodites. Genome insertions were identified, homozygosed, and the SEC excised using the standard protocol (Dickinson et al., 2015); the insertion was sequenced for quality assurance.

lem-2(tcutgfp)[lem-2::tcut::gfp::nls] was made using CRISPR/Cas9 to insert *tcut::gfp::nls* into the endogenous *lem-2* locus. To make the repair template pJS141, the vector

pDD282 was digested with AvrII, SpeI-HF, and BglII to remove the GFP. PCR fragments containing the 3' and 5' *lem-2* homology arms from pJS129, the *gfp::nls::unc-54 3' UTR* from pJS110, and a fragment that restores the portion of the SEC were inserted into the digested vector using Gibson cloning. The Tcut site within the SEC construct was co-opted for use as the Tcut site in the reporter. An injection mix containing pJS141 (50 ng/µl), pJS121 (50 ng/µl), and the co-injection markers pCFJ90 (7.5 ng/µl) and pGH8 (10 ng/µl) was injected into the germline of adult N2 hermaphrodites. Genome insertions were identified, homozygosed, the SEC excised, and the insertion sequenced as in *lem-2(ar645)*.

arSi125[fib-1p::fib-1::tcut::gfp::nls::unc-54 3' UTR] was made using CRISPR/Cas9 to generate a single copy-transgene at the LGI locus *ttTi4348.*. The repair template pMJ1 was made using Gibson cloning to insert the PCR fragments *fib-1p::fib-1* amplified from pCC384 and *gfp::nls::unc-54* amplified from pJS110 into pZW111 digested with AvrII and NotI-HF. Overlaps between the Gibson primers were used to generate *tcut* between the fragments. A mix containing pMJ1 (50 ng/µl), pAP582 (50 ng/µl), and the co-injection markers pCFJ90 (2.5 ng/µl) and pGH8 (10 ng/µl) was injected into the germline of adult N2 hermaphrodites. Genome insertions were identified, homozygosed, the SEC excised, and sequenced as in *lem-2(ar645)*.

arTi436[rps-27p::lem-1(flexon)::mCherry::unc-54 3' UTR] was generated by inserting sequence from pMJ2 randomly into the genome using miniMos. To make pMJ2, a PCR fragment containing *rps-27p* amplified from pJS145 and two dsDNA fragments ordered from Genewiz that together contained the 5' end of *lem-2* with the *flexon* were inserted into the vector pMA118 that had been digested with NotI-HF and BstZ17I. An injection mix with pMJ2 (10 ng/µl), pCFJ601 (65 ng/µl), pMA122 (10 ng/µl), and the co-injection markers pCFJ90 (2.5 ng/µl) and pGH8 (10 ng/µl) was injected into the germline of adult GS9215 *lin-12(ar640)* hermaphrodites.

Genomic insertions were identified, homozygosed, and mapped using standard protocol (Frøkjær-Jensen et al., 2014).

Imaging

Prior to imaging, *C. elegans* were mounted onto 3% agar pads and immobilized with 10 mM levamisole. Animals were imaged using a Zeiss AxioObserver Z1 inverted microscope with a 63X, 1.4NA oil immersion objective and a spinning disk. A 488 nm, 100mW laser was used to excite GFP and a 561 nm, 75 mW laser was used to excite mCherry. Z-stacks of GFP and RFP fluorescence were simultaneously captured with a dual-camera system. The parameters used for imaging were: for GS9320, 250 ms exposure, 400 gain, 15% 488 nm laser intensity, 25% 561 nm laser intensity, 500 nm slice interval; for *lem-2(tcutgfp); jjIs3900,* 250 ms exposure, 400 gain, 10% 488 nm and 561 nm laser intensity, 500 nm slice interval; for GS9810, 150 ms exposure, 400 gain, 3% 488 nm laser intensity, 25% 561 nm laser intensity, 300 nm slice interval.

3. Results and Discussion

LEM-2-based reporter

The allele *lem-2(ar645)* expresses LEM-2::mCherry::Tcut::GFP from the endogenous *lem-2* locus. The mCherry INM fluorescence could be used to segment the nuclei of interest, and the INM Red:Green fluorescence ratio could be used to quantify LIN-12::TEVp activity (Fig. 1A). In cells with low LIN-12::TEVp activity, the LEM-2::mCherry::Tcut::GFP reporter would be mostly uncleaved and have a low INM Red:Green ratio, but in cells with high LIN-12::TEVp activity the GFP is cleaved from the INM, increasing the Red:Green ratio along the INM. Fluorescence from HLH-2::mScarlet could be distinguished from the LEM-2 SALSA reporter

because the former would have red fluorescence in the whole nucleus, while the latter would have red fluorescence only at the INM.

To determine the feasibility of using *lem-2(ar645)* as a SALSA reporter, I looked for reporter cleavage in α and β cells in the somatic gonad of animals co-expressing *lem-2(ar645)* and the LIN-12::TEVp switch. I identified somatic gonad nuclei using a red nuclear marker driven by *ckb-3p.* Somatic gonad nuclei without LIN-12::TEVp switch expression had strong green fluorescence distinctly at the INM; although it was difficult to distinguish the INM from the red nuclear marker in the somatic gonad, all cells in other tissues had strong red INM fluorescence, suggesting that the somatic gonad cells did as well (Fig. 1B). The α and β cells retained red INM fluorescence while GFP fluorescence was diffuse throughout the cell, indicating that the reporter was being cleaved by LIN-12::TEVp switch. At the somatic gonad primordium stage, there was evidence of reporter cleavage in VUs, but there was also evidence of cleavage in the the AC, which should no longer have LIN-12 expression or activity at the somatic gonad primordium stage (not shown).

The LEM-2 reporter cleavage in the AC could have been due to either perdurance of cleaved reporter in response to active LIN-12::TEVp prior to specification, or ligand-independent cleavage of the reporter from inactive LIN-12::TEVp. The M lineage would be a better paradigm than the somatic gonad for testing whether inactive LIN-12::TEVp could cleave the LEM-2 reporter because it contains two distinct cell populations that both express LIN-12, but only one has LIN-12 activity. However, the ubiquitous LEM-2 reporter expression made it difficult to distinguish the nuclei of the M lineage without using an additional marker fluorescent marker. The ubiquitous expression also made it difficult to segment nuclei, which would be

necessary to quantify the INM Red:Green ratio; since the cleaved GFP was free to diffuse throughout the cell, there was not another way to robustly quantify reporter cleavage.

To simultaneously address the segmentation issue and determine if LEM-2 reporters are prone to ligand-independent cleavage by inactive LIN-12::TEVp, I established a new LEM-2 SALSA reporter in which the segmentation and reporting units were separated. I used CRISPR/Cas9 to insert *tcut::gfp::nls* at the endogenous *lem-2* locus to create a reporter that I will refer to as *lem-2(tcutgfp)*. Upon cleavage of the LEM-2::Tcut::GFP::NLS reporter by LIN-12::TEVp, the free GFP::NLS should be restricted to the nucleus; thus, LIN-12 activity could be quantified by changes in nuclear GFP fluorescence (Fig. 2A), which is easier to segment and measure than the INM. I established a strain with *lem-2(tcutgfp)* and *lin-12(ar640)* to test whether *lem-2(tcutgfp)* is cleaved specifically by active LIN-12::TEVp. Using a nuclear red fluorescent marker to mark cells of the M lineage, I observed nuclear GFP fluorescence at visually even levels in both the ventral M descendants, which express LIN-12::TEVp and have activity, and the dorsal M descendants, which express LIN-12::TEVp but do not have activity; other cells that do not express LIN-12::TEVp had only INM GFP fluorescence (Fig. 2B).

Between the ligand-independent cleavage of *lem-2(ar645)* in the AC and *lem-2(gfp)* in the dorsal M descendants, it appears that LEM-2 reporters are prone to cleavage by inactive LIN-12::TEVp, and therefore are not suitable for use with SALSA. The ectopic cleavage could be a result of the subcellular location of LEM-2 synthesis. Integral INM proteins are translated on the rough ER before being moved via the ONM to the INM (Holmer and Worman, 2001). It is possible that if LEM-2 reporters can interact with inactive LIN-12::TEVp within the ER prior to each being transported to their respective subcellular locations. An INM-based SALSA reporter may more accurately report LIN-12::TEVp activity if it is tagged to a peripheral INM protein

that is translated in the cytoplasm and transported as a soluble protein into the nucleus before associating with the INM (Lusk et al., 2007), thereby avoiding interaction with LIN-12::TEVp in the ER.

FIB- 1 SALSA reporter

I also designed a nucleolar SALSA reporter with separate segmentation and sensing units. This FIB-1 SALSA reporter uses a *fib-1p::fib-1::tcut::gfp::nls* transgene as the LIN-12::TEVp activity sensing unit (Fig. 3A). In the presence of active LIN-12::TEVp switch, the GFP::NLS would be cleaved from the FIB-1 nucleolar tether, allowing GFP fluorescence to spread from the nucleolus to fill the nucleus. A *lem-2(flexon)::mCherry* marker driven by the strong ubiquitous promoter *rps-27p* would be the sensing unit; there would be strong, red INM fluorescence only in cells in which the *flexon c*assette was excised using a tissue-specific Cre driver. When co-expressed, the LEM-2::mCherry marker would be used to segment the nuclei of interest and the FIB-1::Tcut::GFP::NLS SALSA reporter to quantify LIN-12 activity; neither would interfere with nuclear fluorescence from the HLH-2::mScarlet reporter.

We established a strain expressing the FIB-1 SALSA reporter, the LEM-2::mCherry marker only in the somatic gonad, and LIN-12::TEVp switch. The FIB-1 SALSA reporter had strong, ubiquitous nucleolar GFP fluorescence. However, we did not qualitatively detect any nuclear green fluorescence outside of the nucleolus in the VUs (Fig. 3B), so it appears that the FIB-1 SALSA reporter does not respond to active LIN-12::TEVp switch. It is possible that the cleavage site in the FIB-1::Tcut::GFP::NLS reporter is not accessible to proteolytic activity of nuclear LIN-12::TEVp, either because it is hidden by FIB-1 or complexes that FIB-1 associates with; it is also possible that that active LIN-12::TEVp does not have enough access to the

nucleolus. Lastly, there could be reporter cleavage at levels that were visibly undetectable, but would be picked up by quantitation. It was difficult to quantify GFP fluorescence only in the non-nucleolar areas of the nucleus in cells in which the nucleolus was large or not centered in the nucleus. Thus, we were unable to quantify LIN-12 activity in the somatic gonad using the FIB-1 SALSA reporter. An updated quantification pipeline may allow segmentation and quantification of non-nucleolar areas in small nuclei, but the lack of visual non-nucleolar fluorescence is discouraging for the feasibility of this FIB-1 SALSA reporter.

Appendix A Figures

Figure 1

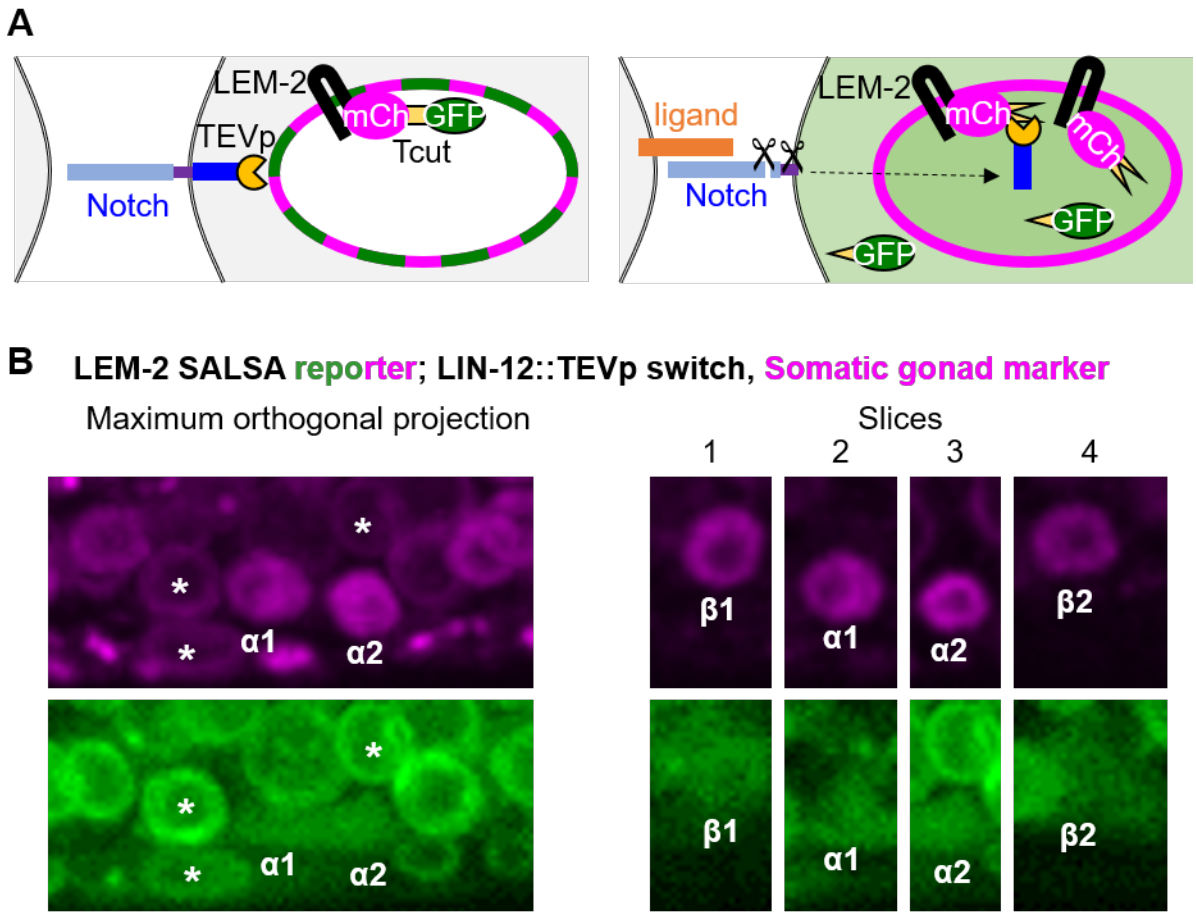

Figure 1. A dual-color LEM-2 SALSA reporter. (A). In the absence of ligand, GFP remains tethered at the inner nuclear membrane (INM) to the segmentation marker LEM-2::mScarlet, resulting in a low INM Red:Green ratio. In the presence of ligand, the Notch::TEVp switch intracellular domain translocates to the nucleus, where it can cleave the GFP from the INM tether and allow it to diffuse throughout the cell, thereby increasing the INM Red:Green ratio. (B) Photomicrographs of the LEM-2 SALSA reporter in an early L2 animal prior to AC/VU specification. A red nuclear histone marker was included to distinguish somatic gonad cells from other LEM-2 reporter-expressing cells. In the maximum orthogonal projection on the left, red and green fluorescence from the LEM-2 SALSA reporter is clearly visible on the INM of cells that do not express LIN-12::TEVp (asterisks). The α cell nuclei have diffuse GFP fluorescence due to expression of the LIN-12::TEVp switch. The β cell nuclei are not distinguishable due to fluorescence from cells in other planes. On the right, each panel is a section of one slice of the Z stack that was used for the maximum projection. The α and β nuclei can be distinguished without interference from nuclei in other planes. The somatic gonad marker obscures the red fluorescence from the LEM-2 reporter at the INM, but diffuse GFP expression in and around each nucleus suggests the GFP is cleaved from the LEM-2 reporter.

Figure 2

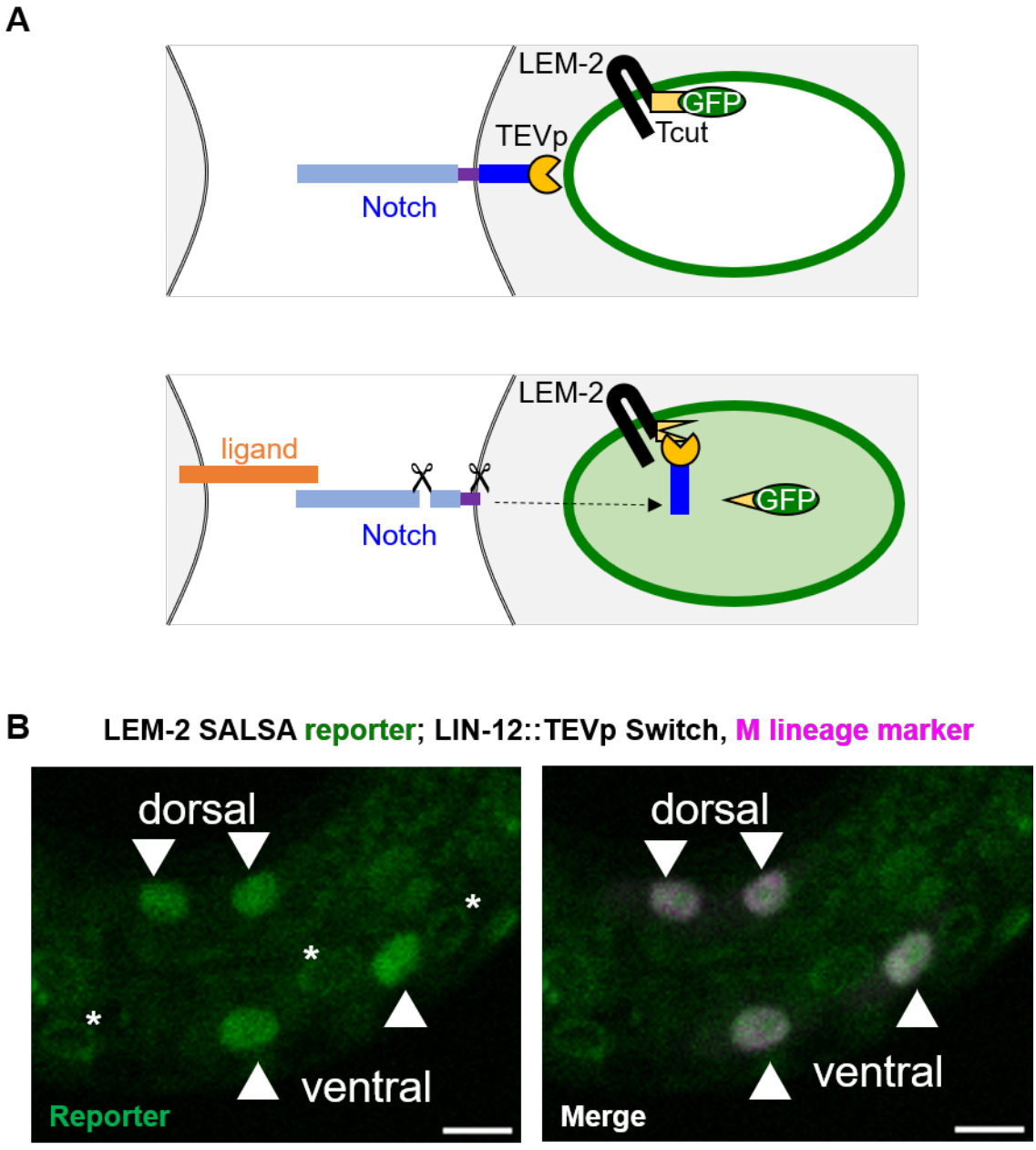

Figure 2. A single-color LEM-2 SALSA reporter. (A) A cartoon of a single-color LEM-2 SALSA reporter. GFP::NLS is tethered directly to LEM-2 via a Tcut site. LIN-12::TEVp switch activity cleaves the Tcut site and releases the GFP::NLS from the INM tether to diffuse throughout the nucleoplasm. This reporter does not have a built-in segmentation marker. (B) Single planes from Z stacks of the M descendants expressing the LEM-2 SALSA reporter. M cell descendants express a red fluorescent nuclear marker. Cells outside of the M lineage have green fluorescence on the INM only (examples indicated by asterisks). Both ventral and dorsal descendants (arrowheads) have nuclear GFP fluorescence, suggesting the reporter is being cleaved.

Figure 3

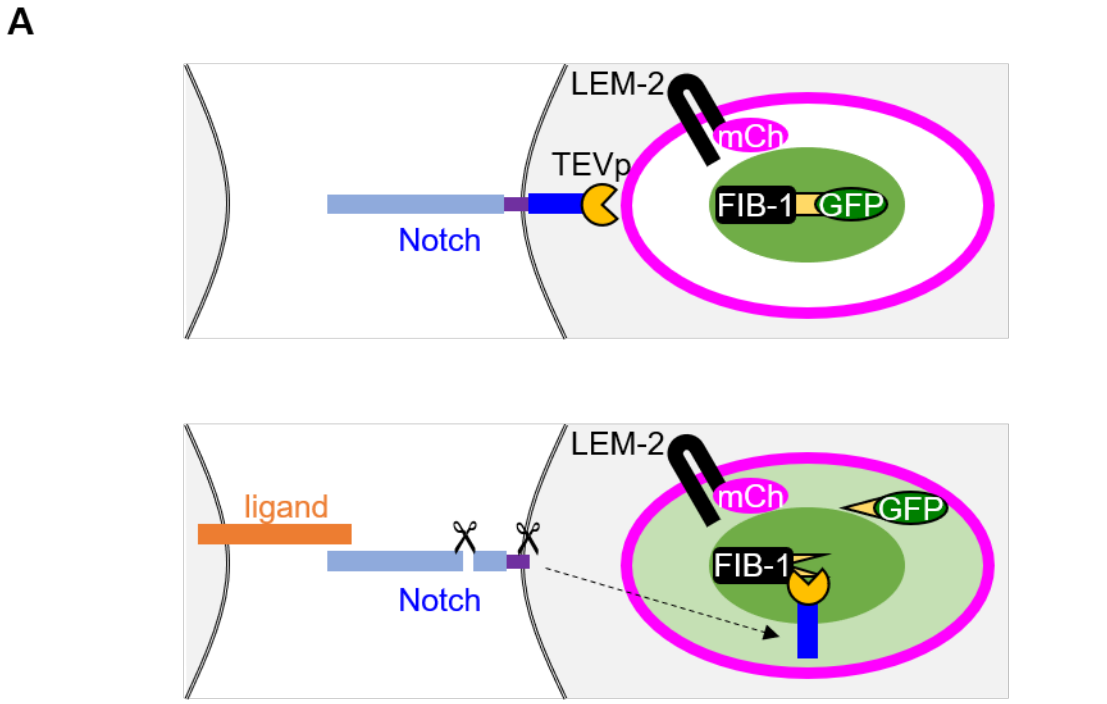

Figure 3. A FIB-1 SALSA reporter. (A) A cartoon of the FIB-1 SALSA reporter. Tissue-specific LEM-2::mCherry is a segmentation marker. In the absence of Notch::TEVp signal transduction, GFP::NLS is tethered to FIB-1 in the nucleolus. Ligand interaction allows the Notch::TEVp intracellular domain to translocate to the nucleus, where it cleaves GFP::NLS from FIB-1, releasing GFP::NLS into the nucleoplasm. (B) A maximum projection of the proximal somatic gonad primordium of a worm co-expressing the FIB-1 reporter and the LIN-12::TEVp switch. Somatic gonad cells are labeled with LEM-2::mCherry. There is strong nucleolar GFP fluorescence in all cells, including the VUs, but not nuclear GFP fluorescence in any cells.

Appendix B: SALSA reporters with Nuclear Export Signals

1. Introduction

As discussed in Chapter 3, the SALSA reporter uses changes in subcellular localization of GFP after cleavage from the nuclear RFP::H2B tether to indicate Notch::TEVp switch activity. However, the current SALSA reporter has some limitations that may decrease the sensitivity or rapidity of the system. First, the free GFP reaches equilibrium across all compartments of the cell; some of the free GFP remains in the nucleus, reducing the dynamic range of the reporter. Second, passive diffusion of GFP across the nuclear envelope is about 100x slower than diffusion within the nucleus or the cytoplasm (Wei et al., 2003). Actively transporting the GFP from the nucleus after reporter cleavage could decrease the level of leftover GFP in the nucleus and the response time of the reporter, thus increasing the sensitivity and speed of readout.

Nuclear Export Signals (NESs) are short peptide sequences that direct active transport of a protein from the nucleus to the cytoplasm. NES sequences are canonically hydrophobic and leucine rich, with a consensus of Φ1-X3-Φ2-X2-Φ3-X-Φ4, where Φ stands for hydrophobic residues such as Leu, Val, Ile, Phe, or Met, and X indicates any residue, with a preference for negatively charged amino acids (Xu et al., 2012). NES sequences direct nuclear export by interacting directly with the karyopherin-exportin XPO-1/CRM1 (Wing et al., 2022). In theory, adding an NES to the GFP would result in active transport out of the nucleus after it is cleaved from the reporter by active nuclear Notch::TEVp, thereby increasing the dynamic range and speed of response of the reporter. In this Appendix, I will describe the fluorescent patterns of SALSA reporters with NES::GFP, and discuss the implications that the findings from testing the NES reporters have on future SALSA reporter adaptations.

2. Materials and Methods

Strains

All strains were maintained at 20°C on 6 cm NGM plates seeded with *E. coli* OP50. All imaging was done at 25°C. The following strains were used in Appendix B:

GS9153 *arTi317[hlh-8p::mek-2nes::gfp::unc-54 3′ UTR]* II

GS9154 *arTi318[hlh-8p::ranbp1nes::gfp::unc-54 3′ UTR]* V

GS9155 *arTi319[hlh-8p::mapkk1nes::gfp::unc-54 3′ UTR]* II

GS9169 *arTi326[hlh-8p::mek-2nes::gfp::tcut::wrmScarlet::h2b::unc-54 3′ UTR]* I

GS9170 *arTi326* I; *lin-12(ar640)[lin-12::tevp]* III

GS9334 *arTi348[lin-31p::mek-2nes::gfp::tcut::wrmScarlet::h2b::unc-54 3′ UTR]* I; *lin-12(ar640)* III

GS9337 *arTi350[lin-31p::hiv-revnes::gfp::tcut::wrmScarlet::h2b::unc-54 3′ UTR]* II; *lin-12(ar640)* III

GS9332 *arTi357[ckb-3p::mek-2nes::gfp::tcut::wrmScarlet::h2b::unc-54 3′ UTR]* V

GS9335 *arTi349[ckb-3p::hiv-revnes::gfp::tcut::wrmScarlet::h2b::unc-54 3′ UTR]* I

The strain containing the transgene *hlh-8p::hiv-revnes::gfp::unc-54 3′ UTR* was not frozen and was lost.

Plasmid construction and genome editing

All transgenes were generated as single-copy, random genomic insertions and mapped using standard mimiMos protocol (Frøkjær-Jensen et al., 2014). Injection mixes contained the plasmid vector (10 ng/µl), pCFJ601 (65 ng/µl), pMA122 (10 ng/µl), and the co-injection markers

pCFJ90 (2.5 ng/µl) and pGH8 (10 ng/µl). All transgenes were established in N2, with the exception of *arTi350*, which was established in GS9215 *lin-12(ar640).*

The transgenes *arTi317, arTi318, arTi319,* and *hlh-8p::hiv-revnes::gfp::unc-54 3' UTR* were generated using plasmid vectors pJS91, pJS94, pJS95, and pJ92, respectively. To make the plasmids, DNA primers encoding the NES sequences were annealed and ligated into pJS89 digested with ApaI and AgeI-HF using T4 ligase.

The transgene *arTi326* was generated using plasmid vector pJS107. The plasmid was generated by Gibson cloning to insert PCR fragments containing *mek-2nes::gfp* amplified from pJS91 and *wrmScarlet::h2b:unc-54 3' UTR* amplified from pJS82 into the miniMos vector pCC346 digested with NotI-HF and AgeI-HF. The *tcut* sequence between the fragments was generated using fragment overlap.

The transgene *arTi348* was generated from pJS115, which was made by inserting *mek-2nes::gfp::tcut::wrmScarlet::h2b::unc-54 3' UTR* amplified from pJS107 into pJS15 (pCC249) digested with AgeI-HF and NotI-HF by Gibson cloning. Similarly, the transgene *arTi357* was generated from pJS113, which was made by Gibson cloning to insert the same fragment without the 3' UTR into pJS110 digested with AgeI-HF and AflII.

arTi349 was generated using pJS117. The plasmid was made using Gibson cloning to insert PCR fragments containing *hiv-revnes::gfp* from pJS101 and *tcut::wrmScarlet::h2b* amplified from pJS113 into the plasmid vector pJS110 digested using AgeI-HF and AflII. The transgene *arTi350* was generated using pJS120, which was made using Gibson cloning to insert PCR fragments containing *hiv-revnes::gfp* amplified from pJS117 and *tcut::wrmScarlet::h2b* amplified from pJS107 into the plasmid vector pJS15 digested with AgeI-HF and NotI-HF.

Imaging

Prior to imaging, *C. elegans* were mounted onto 3% agar pads and immobilized with 10 mM levamisole. GS9153, GS9154, GS9155, *hlh-8p::hiv-revnes::gfp::unc-54 3' UTR*, GS9169, GS9170, GS9332, and GS9334 were imaged using a Zeiss AxioObserver Z1 inverted microscope with a 63X, 1.4NA oil immersion objective and a spinning disk. For GS9153, GS9154, GS9155, and *hlh-8p::hiv-revnes::gfp::unc-54 3' UTR*, a 488 nm, 100mW laser was used to excite GFP at 25% laser power with an exposure time of 350 ms and 400 gain. The 561 nm, 75 mW laser was not used. Z stacks were taken with 500 nm intervals between slices. For GS9169, GS9170, GS9332, and GS9334, Z-stacks of GFP and wrmScarlet fluorescence were simultaneously captured with a dual-camera system. For imaging GS9169, GS9170, and GS9332, the following parameters were used: 350 ms exposure, 15% 488 nm laser intensity, 20% 561 nm laser intensity, 400 gain, 500 nm interval between slices. For GS9334, the exposure time was lowered to 100 ms, and the 488 nm laser intensity was increased to 20%.

GS9335 and GS9337 were imaged using a Zeiss AxioImager D1/D2 with an X-cite 120Q series 120W mercury vapor lamp. GS9335 was imaged using a 63X, 1.4NA oil immersion objective; GS9337 was imaged using a 40x, 1.3NA oil immersion objective. GS9335 was illuminated using 1 second exposure time with the dsRed filters and 300 ms exposure time using the GFP filters. GS9337 was illuminated using 300 ms second exposure time for both dsRed and GFP filter sets.

3. Results and Discussion

Since NES sequences have not been widely used in *C. elegans*, I tested the relative strength of nuclear export for four different NES sequences using NES::GFP transgenes. I chose

to use the NES sequences from HIV-REV and mammalian MAPKK1 because they are leucine rich and commonly used for nuclear export of transgenic proteins in other models (Xu et al., 2012); notably, the HIV-REV sequence has been used for NES::GFP in *C. elegans* (Reinke et al., 2017). I also tested the NES sequence from human RanBP1 because it contains fewer leucine residues, and the NES from MEK-2, the *C. elegans* homolog of MAPKK1. I expressed each NES::GFP construct specifically in the M and SM lineages using the 5' regulatory region *hlh-8p*, and checked in the SM descendants for the extent of GFP exclusion from the nucleus (Fig. 1). All of the NES sequences generated strong visual exclusion of GFP fluorescence from the nucleus, although the MEK-1 and MAPKK1 sequences appeared slightly stronger than the HIV-REV and RanBP1 sequences. Thus, any of the NES sequences could be used for strong nuclear export of NES::GFP after cleavage from the SALSA reporter.

A preliminary test using a MEK-2 NES::GFP::Tcut::wrmScarlet SALSA reporter in the M cell descendants showed promising results (Fig. 2A). In the presence of LIN-12::TEVp, the ventral descendants with LIN-12::TEVp activity had a visibly higher nuclear Red:Green ratio than the dorsal descendants, which do not have activity LIN-12::TEVp activity. When the reporter was expressed in a *lin-12(+)* background without any TEVp present, there was mild cytoplasmic red and green fluorescence in both ventral and dorsal cells, but the reporter was mostly enriched in the nucleus. To test the effect of adding an NES sequence to the SALSA reporter in other tissues with more complex LIN-12 activity patterns, I used the *lin-31p* regulatory sequence to drive expression of reporters fused with either the HIV-REV NES or MEK-2 NES sequence in VPCs in the presence of the LIN-12::TEVp switch (Fig. 2B). There was visibly high nuclear Red:Green ratio and cytoplasmic GFP fluorescence in all of the VPCs including P4.p and P8.p, which do not have LIN-12::TEVp activity, suggesting ligand-

independent cleavage of the NES-tagged reporters in the VPCs. I further tested the reporters with MEK-2 NES and HIV-REV NES in the somatic gonad using the *ckb-3p* driver, this time in the absence of LIN-12::TEVp (not shown). The uncleaved MEK-2 NES reporter was strongly excluded from the nucleus of somatic gonad cells; the HIV-REV NES reporter was slightly enriched in the nucleus but also had high levels of cytoplasmic red and green fluorescence.

The cytoplasmic red and green fluorescence of the NES-tagged reporters in the absence of LIN-12::TEVp indicates that there is intramolecular competition wihin the NES::GFP::Tcut::RFP::H2B reporter between the NES and the histone for subcellular localization. In the presence of LIN-12::TEVp, NES reporter cytoplasmic fluorescence is mostly green and the red fluorescence is almost entirely nuclear, indicating that reporter is being cleaved and allowing NES::GFP and wrmScarlet::H2B localization to be governed separately. Ligand-independent cleavage of the reporter in cells without LIN-12::TEVp signal transduction suggests that reporter localized to the cytoplasm is accessible to TEVp tethered to the membrane; thus, NES-tagged reporters are not ideal reporters of LIN-12::TEVp signaling activity in these contexts. However, the variable nuclear export strength of the NES fusions in different *C. elegans* tissues suggests that in some cell contexts, a balance may be found in which an NES fusion has limited effect on uncleaved reporter, but strongly exports free NES::GFP after cleavage.

Appendix B Figures

Figure 1

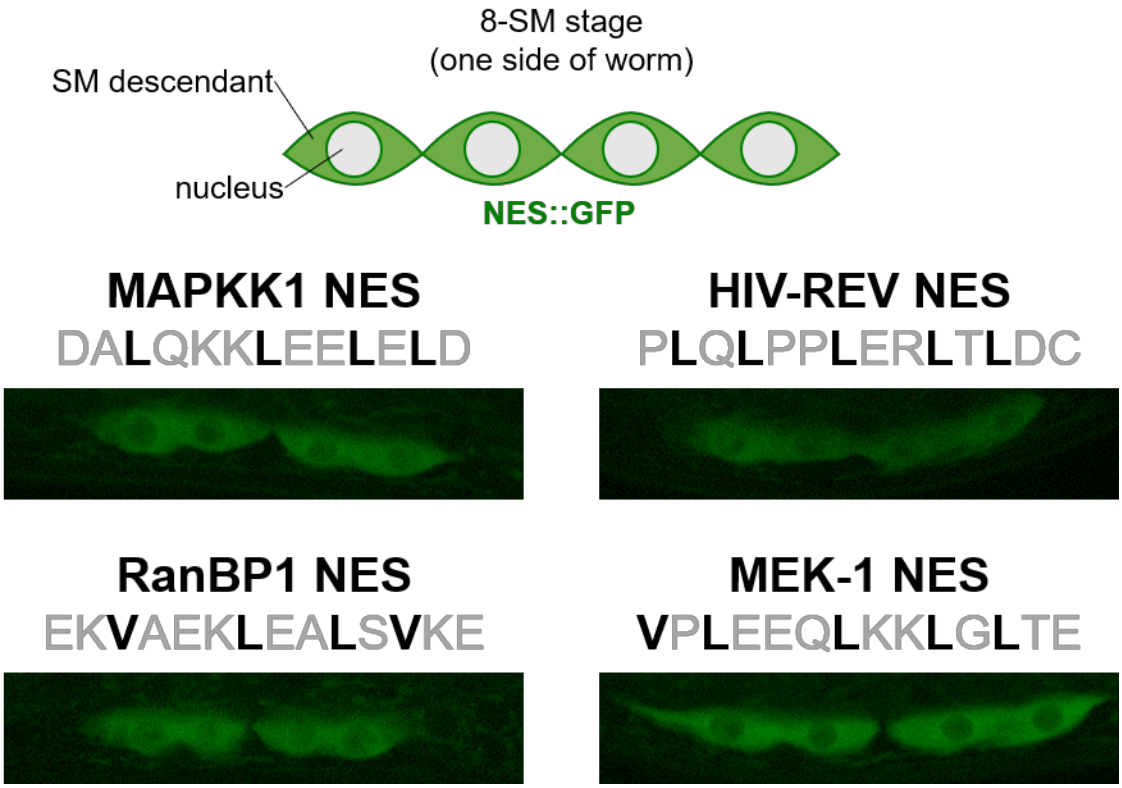

Figure 1. Four different Nuclear Export Signal (NES) sequences strongly export GFP from nucleus. Four NES sequences were fused to GFP to test the relative nuclear export strength of each sequence. The conserved hydrophobic residues of the NES sequences used are bold. NES::GFP expression was driven by the M lineage-specific regulatory region hlh-8p, and visualized at the 8-SM stage, when four SM descendants are located on each the left and right side of the worm. Photomicrographs are of one slice from a Z stack that captures one side of the worm. All NES::GFP fusions had strong nuclear export.

Figure 2

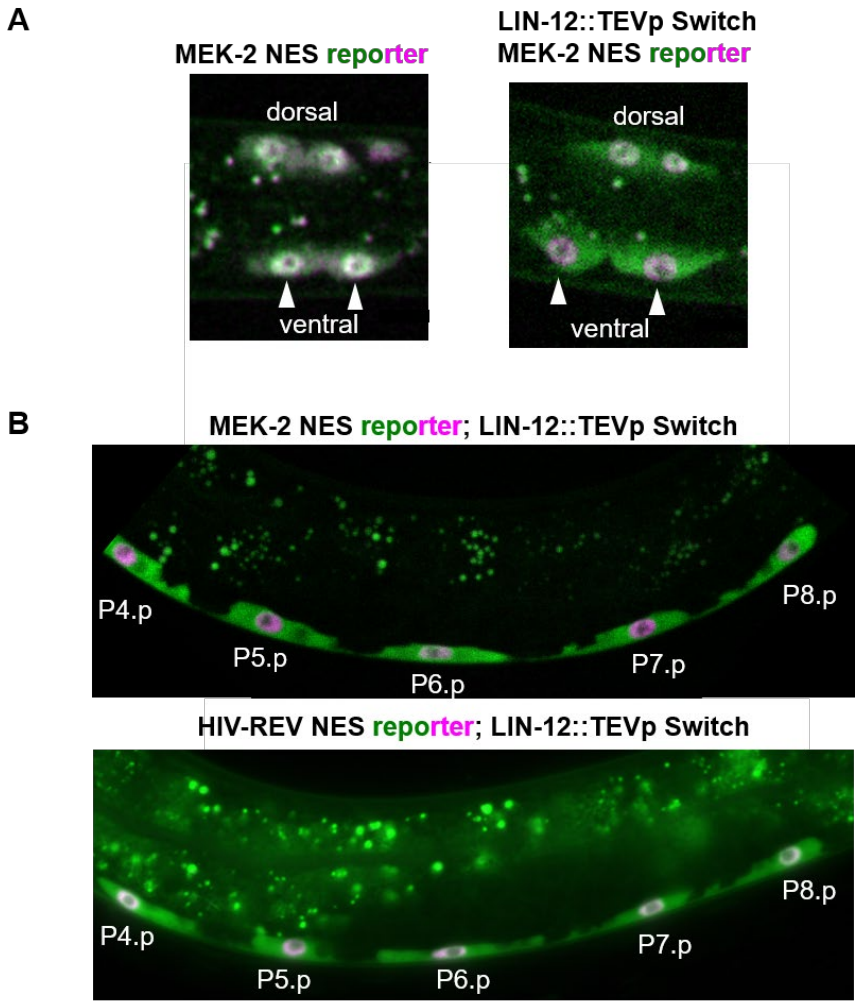

Figure 2. NES reporters in M cell descendants and the VPCs. (A) The MEK-2 NES reporter is strongly cleaved by LIN-12::TEVp in the ventral descendants of the M lineage, but only mildly cleaved in the dorsal descendants. The animals in the photomicrographs are at the 8-M stage, in which the dorsal and ventral M descendants (arrowheads) each have two cells on the left and two cells on the right; hlh-8p drives reporter expression in all of the descendants. The photomicrographs are single slices of Z stacks so that the M cell descendants on one side of the animal are visible. Without the LIN-12::TEVp switch, red and green fluorescence from the MEK-2 NES reporter is visible throughout the cell but mostly enriched in the nucleus. In the presence of the LIN-12::TEVp switch, the ventral cells have an increased nuclear Red:Green ratio; the cytoplasm in the dorsal cells has some green fluorescence but the nuclei have a low nuclear Red:Green ratio. (B) A comparison of NES-reporters in the VPCs at the L2/L3 Pn.p stage. In the presence of LIN-12::TEVp switch, both the MEK-2 NES SALSA reporter and the HIV-REV SALSA reporter have high nuclear Red:Green ratio in all VPCs, regardless of expected LIN-12::TEVp activity patterns. Note that the photomicrographs were taken using different microscopes; they are only illustrative and not to be compared.

Appendix C: Investigation of feedback loops at the *lin-12* and *lag-2* endogenous loci

lin-12(ar624ar646) was generated and analyzed with assistance from Alejandro Garcia Diaz

1. Introduction

In Chapter 3, I discuss how feedback loops amplify small differences in LIN-12 activity in the α cells to ensure robust fate outcomes during the AC/VU decision. LIN-12 activity positively autoregulates its own expression while promoting degradation of the transcriptional activator HLH-2. The loss of HLH-2 expression leads to loss of expression of its targets, including LAG-2. Therefore, the α cell with a LIN-12 activity advantage maintains LIN-12 expression at the cost of HLH-2 and LAG-2 expression and becomes the VU, while the other α cell loses LIN-12 expression but maintains LAG-2 and HLH-2 expression and becomes the AC.

LIN-12 positive autoregulation appears to require *LCS1,* a 67 bp sequence approximately 1.6 kb upstream of the *lin-12* start site (Wilkinson et al., 1994). *LCS1* is required for maintenance, but not initiation, of expression from a *lin-12::lacZ* transcriptional reporter, as well as for rescue of the 2 AC phenotype in a *lin-12(0)* mutant using an extrachromosomal array of sequence from the *lin-12* locus. The presence of a LAG-1 binding site within *LCS1* lends weight to the idea that the sequence is required for LIN-12 positive autoregulation. It is important to note that all data regarding *LCS1* was generated using extrachromosomal arrays, which do not always recapitulate endogenous expression patterns or levels. Furthermore, the *lin-12::lacZ* transcriptional reporter used for the analysis contained the entire *lacZ* coding region, including a stop codon, inserted between the 5' regulatory region and the coding region of a *lin-12* transgene; a *smg-1* background was required for expression since the transcript had a long 3'

UTR that was degraded by nonsense-mediated decay. The requirement for *LCS1* has not been tested in a more native context.

The mechanisms of *lag-2* regulation in the AC/VU decision have also mostly been studied using extrachromosomal arrays and reporters. We do know that HLH-2 is required for expression of an endogenous LAG-2::GFP reporter in the α cells (Attner et al., 2019). A *lag-2* rescuing array containing 3.3 kb of the 5' regulatory region rescues the 2 AC phenotype of *lag-2(ts)* at the restrictive temperature, but not when the HLH-2 homodimer binding sites were mutated (Karp and Greenwald, 2003). The same binding site mutations reduced the penetrance of *lag-2::lacZ* reporter expression in the AC in a *smg-1* background. Interestingly, *lag-2p::gfp* multicopy reporters constructed with only 3 kb of the 5' regulatory region do not have GFP fluorescence in the AC, even with all HLH-2 binding sites intact (Chesney et al., 2009). Promoter bashes of the entire 7.1 kb 5' flanking region of *lag-2* using extrachromosomal array-based reporters indicated that there are sequences crucial for regulating *lag-2* transcription in VPCs about 5.6 kb upstream of the *lag-2* start site, and that these sequences plus about 1 kb of sequence immediately upstream of the *lag-2* start site were sufficient to drive expression of YFP in the AC in some animals (Zhang and Greenwald, 2011). It is unclear which *cis* regulatory regions are sufficient *lag-2* expression, and if HLH-2 is the only factor that regulates *lag-2* expression at the endogenous locus.

To investigate the mechanisms of LIN-12 and LAG-2 regulation in a native context, we used CRISPR/Cas9 to generate 1) an *LCS1* deletion in an endogenous *lin-12::gfp* reporter, and 2) a *lag-2::gfp::sl2::2xnls-tdTomato* allele at the endogenous locus. The *sl2* trans-splice site from the *gpd-2/gpd-3* operon creates separate transcripts from the same gene (Spieth et al., 1993), and is used here to try to distinguish between pre-translational and post-translational regulation. In

this Appendix, I discuss the generation analysis, and limitations of these two alleles, as well as the implications for future analysis of LIN-12 feedback loops in the AC/VU decision.

2. Materials and Methods

Strains

All strains were maintained at 20°C on 6 cm NGM plates seeded with *E. coli* OP50. Imaging was done at 25°C. The following strains were used in Appendix C:

GS9371 *arTi145[ckb-3p::mCherry::h2b::unc-54 3' UTR]* II; *lin-12(ar624ar646)[ΔLCS1::lin-12::gfp]* III

GS9408 *lin-12(ar624ar646)* III; *qyIs50[cdh-3>mCherry::moeABD]* V

GS9003 *lag-2(ar628)[lag-2::gfp::sl2::tdTomato::nls]* V

Plasmid construction and genome editing

lin-12(ar624ar646) was generated using a *dpy-5* co-CRISPR/Cas9 strategy (Kim et al., 2014) to remove the *LCS1* region from *lin-12(ar624)[lin-12::gfp]*. A mix containing a repair ssODN template for an *LCS1* deletion (1000 ng/µl), plasmids containing Cas9 and sgRNA sequences targeting *LCS1* pJSW2 and pJSW5 (25 ng/µl each), and the *dpy-5* sgRNA-containing plasmid pDR91 (25 ng/µl), was injected into the germlines of GS9219 *arTi145; lin-12(ar624)* adult hermaphrodites. Injected animals were placed at 25°C, and Dpy progeny were isolated 4 days post-injection and allowed to lay eggs before being lysed for sequencing. The sequences were analyzed using ICE (Synthego) to determine guide efficiency and edited candidates. An allele was isolated with a 116 bp deletion of *lin-12(ar624)* 5' regulatory region that included the entirety of the *LCS1* sequence. The *dpy-5* mutation was crossed out to make GS9731.

lag-2(ar628) was generated using the repair template pJS51, which was cloned in a two-step Gibson cloning process. First, the intermediate plasmid pJS52 was made by inserting the genomic *lag-2* coding sequence with introns from pXK52 into the GFP SEC bluescript vector pJC41 digested with AvrII, forming the 5' homology arm. Then, the final plasmid pJS51 was made by digesting pJS52 with SpeI-HF, and adding PCR fragments of the *gpd-2/gpd-3 sl2* sequence from pMA108, *2xnls::tdTomato* from pCFJ1209, and 1014 bp of sequence from downstream of the *lag-2* coding region amplified from pXK52 to form the 3' homology arm. The sgRNA plasmid pJS33 was generated using Gibson cloning to replace the sgRNA sequence of pJC33 with a different *lag-2* target sequence. A mix consisting of pJS51 (50 ng/µl), the sgRNA plasmids pJC33 and pJS31 (25 ng/µl each), *Peft-3::Cas9-SV40 NLS::tbb-2 3'UTR* (Friedland et al., 2013) (50 ng/µl), and the co-injection markers pGH8 (10 ng/µl) and pCFJ90 (2.5 ng/µl) was injected into the germlines of adult N2 hermaphrodites. The genome edit was isolated and homozygosed using standard SEC protocol (Dickinson et al., 2015) and checked by sequencing.

Imaging

Prior to imaging, *C. elegans* were mounted onto 3% agar pads and immobilized with 10 mM levamisole. GS9003 was imaged using a Zeiss AxioObserver Z1 inverted microscope with a 63X, 1.4NA oil immersion objective and a spinning disk. A 488 nm, 100mW laser was used to excite GFP and a 561 nm, 75 mW laser was used to excite the RFPs. Both fluorescent channels were set with the following parameters: 350 ms exposure, 400 gain, 15% laser power, and 500 nm intervals between Z slices.

GS9731 was imaged using a Zeiss AxioImager Z1 with a 63X, 1.4NA oil immersion objective and an X-cite 120 series mercury vapor lamp. Exposure times through the GFP filter set was 750 ms, and 500 ms through the DsRed filter.

3. Results and Discussion

Endogenous *LCS1* deletion

We used CRISPR/Cas9 to generate a deletion of the *LCS1* region at the endogenous locus of the LIN-12::GFP reporter *lin-12(ar624)*, which will be referred to here as *ΔLCS1::lin-12::gfp* (Fig. 1A). We expected that deleting the *LCS1* region would reduce LIN-12 expression in the α cells, leading to reduced LIN-12 activity and a 2 AC phenotype; we might also have expected to see other phenotypes associated with loss of LIN-12 function if *LCS1* is also important for LIN-12 expression in other contexts. However, *ΔLCS1::lin-12::gfp* hermaphrodites and males were viable, fertile, and indistinguishable from wild-type at surface level. *ΔLCS1::lin-12::gfp* had no noticeable differences in GFP fluorescence from what is expected from wild-type *lin-12::gfp*; GFP fluorescence was present on the membrane of α and β cells (not shown), was strongly maintained on the membrane of VUs but not the AC (Fig. 1B), and was retained on the membrane and nuclei of VU descendants in expected patterns as somatic gonad development progressed (Fig. 1C).

We found that *ΔLCS1::lin-12::gfp* had a low penetrance 2 AC phenotype (3/61) when looking in L3 larva; however, the cell positioning at this stage made it difficult to be certain of AC fate. Thus, we looked for a 2 AC phenotype in *ΔLCS1::lin-12::gfp* in early to mid L4 larva, when the AC is easier to identify at the apex of the invaginating vulva; we found no 2 AC animals (0/31) at this stage. To further test for AC fate in *ΔLCS1::lin-12::gfp,* we established a

strain with the AC fate marker *cdh-3p::mCherry::moeABD*, which labels the cell membrane of the AC with red fluorescence. No L3 larva had more than one cell expressing the AC fate marker (0/29; Fig. 1D). These data suggest that *ΔLCS1::lin-12::gfp* does not compromise *lin-12* expression enough to affect the AC/VU decision.

While we did not detect any difference in LIN-12::GFP expression or activity when *LCS1* was deleted, the possibility of a small role for *LCS1* in mediating LIN-12 expression cannot be dismissed. *LCS1* falls in the 5' regulatory region of *lin-12*; transcriptional reporters using only the *lin-12* 5' regulatory region do not have high expression levels or a robust *lin-12* expression pattern. It is possible that *LCS1* and other regulatory sequences in the 5' regulatory region act redundantly or complementarily with sequences in other regions of the locus. For example, many *C. elegans* genes have long first introns that contain conserved regulatory sequences (Fuxman Bass et al., 2014); one such gene is LAG-1, which has several conserved LAG-1 binding sites within a "HOT region" that is required for LAG-1::GFP positive autoregulation in response to LIN-12 activity in the gonad (Luo et al., 2020). Indeed, the first three introns of *lin-12* have several LAG-1 binding sites. The *ΔLCS1::lin-12::gfp* data indicates that the intronic regulatory sequences and 5' regulatory sequences are sufficient for endogenous LIN-12 expression without *LCS1*. Separating the intronic regulatory sequences from the start site, as was done in the *lin-12::lacZ* reporter (Wilkinson et al., 1994), may have weakened the relative strength of the intronic sequences and caused reporter expression to rely more heavily on the sequences in the 5' regulatory region. Deleting *LCS1* in the reporter context may have dropped the activating strength of the regulatory regions below the threshold required for maintenance of reporter expression. However, this would not explain the loss of 2 AC rescue from the *lin-12(ΔLCS1)* extrachromosomal array, which maintained the relative positioning of the introns and the start

site (Wilkinson et al., 1994). To further study the transcriptional regulation of *lin-12* during the AC/VU decision, it may be of interest to generate endogenous *lin-12* alleles with the LAG-1 binding sites and regulatory regions mutated independently or in difference combinations; conditional knockout using site-specific recombinase systems could be used to generate spatiotemporal-specific mutations to avoid pleiotropic effects.

Endogenous lag-2 reporter

To investigate *lag-2* regulation at the endogenous locus in the somatic gonad, I used CRISPR/Cas9 to generate a *lag-2::gfp::sl2::2xnls::tdTomato* allele (Fig. 2A). The allele had GFP fluorescence at the membrane of the unspecified α and β cells, DTCs, and AC (Fig. 2B); it also had GFP fluorescence in the head at several stages, in the ventral nerve cord in L1, and in the VPC P6.p and descendants, consistent with *lag-2* transcriptional reporters. There was also bright nuclear tdTomato expression in these cells, although there was tdTomato expression in many cells in which LAG-2 expression has not been observed, including somatic gonad cells other than those expressing LAG-2::GFP (Fig. 2B), as well as VPCs other than P6.p and their descendants. Nuclear tdTomato fluorescence in cells without membrane GFP fluorescence could indicate cells with post-transcriptional regulation of the *lag-2* locus, or it could indicate that the *gpd-2/gpd-3 sl2* sequence drives a basal level of transcription of the downstream *2xnls::tdTomato* gene in the absence of transcription of the upstream *lag-2::gfp.* Thus, we were unable to use this reporter to discern between transcriptional and post-translational regulation of *lag-2.*

Although LAG-2::GFP is expressed brightly and in the expected pattern, it does not retain the native 3' UTR, so it is a less desirable reporter of LAG-2 expression than an

endogenous allele without the *sl2::2xnls-tdTomato.* It is important to keep in mind the possibility of ectopic expression of the downstream gene in an artificial *sl2* operon, although perhaps *sl2* sequences other than *gpd-2/gpd-3* will not have as much ectopic expression.

Appendix C Figures

Figure 1.

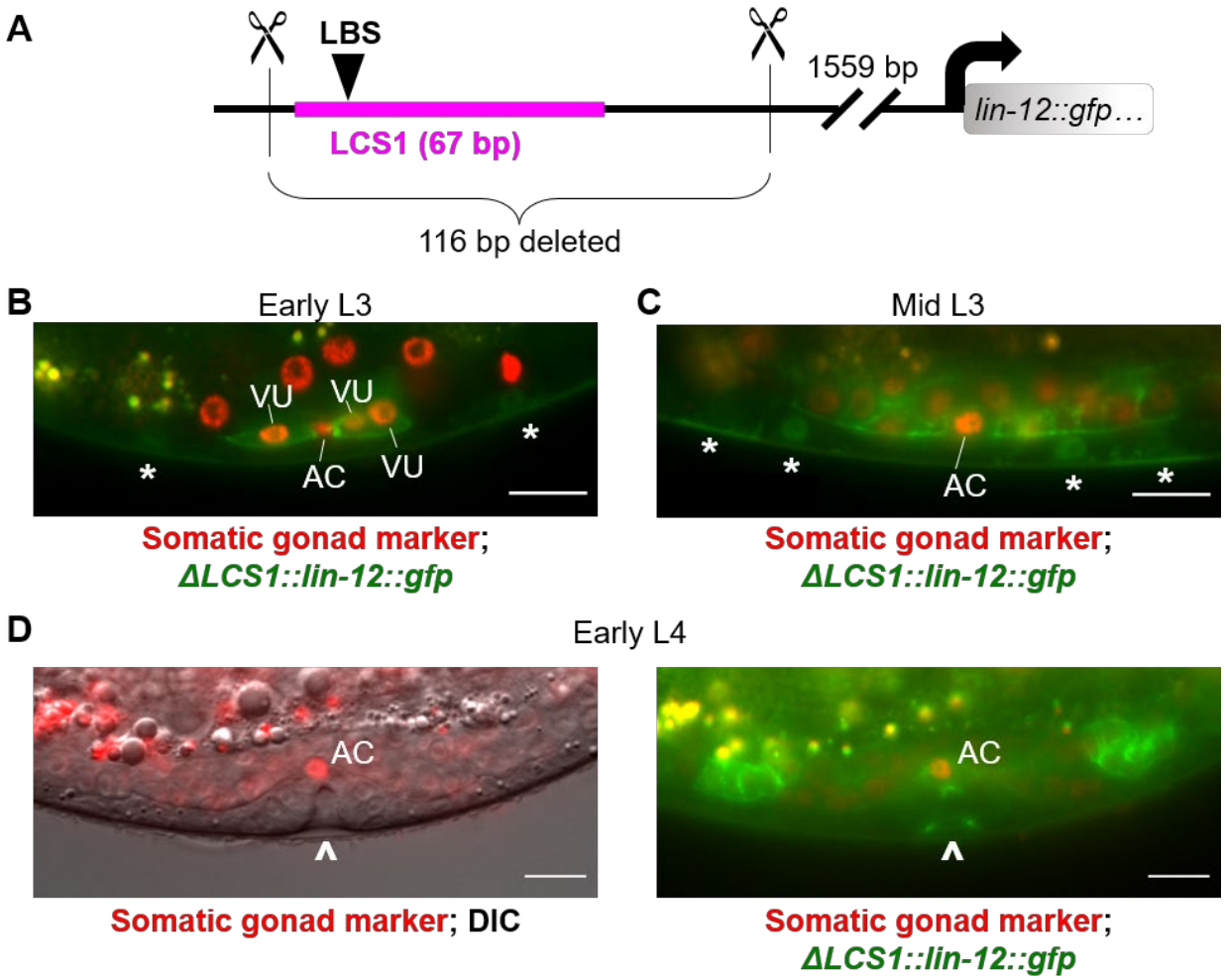

Figure 1. Deletion of LCS1 does not prevent LIN-12::GFP expression in the VUs or compromise AC/VU deletion. (A) A schematic of the lin-12(ar624ar646)[ΔLCS1::lin-12::gfp] regulatory region. The LAG-1 Binding Site (LBS) within the deleted region is shown (B) ΔLCS1::lin-12::gfp in the somatic gonad primordium in early L3. Somatic gonad nuclei are marked with ckb-3p::mCherry::h2b. This picture is of a single plane, so the VUs are not perfectly in frame. Note there is strong GFP fluorescence only at the VU cell membrane, not the AC. Asterisks indicate active nuclear LIN-12::GFP in the VPCs P5.p and P7.p. (C) ΔLCS1::lin-12::gfp in mid L3. Many of the somatic gonad cells have strong GFP fluorescence at the membrane; these are likely VU descendants. P5.px and P7.px are indicated by asterisks; only the proximal cells have active nuclear LIN-12; the distal cells have brighter GFP fluorescence at the membrane. (D) ΔLCS1::lin-12::gfp in early L4. There is one AC present, and LIN-12::GFP fluorescence is still at the membrane of cells near the AC and invaginating vulva (indicated by the carrot), and more distally in the somatic gonad. (B-D) Scale bars are 10 microns.

Figure 2.

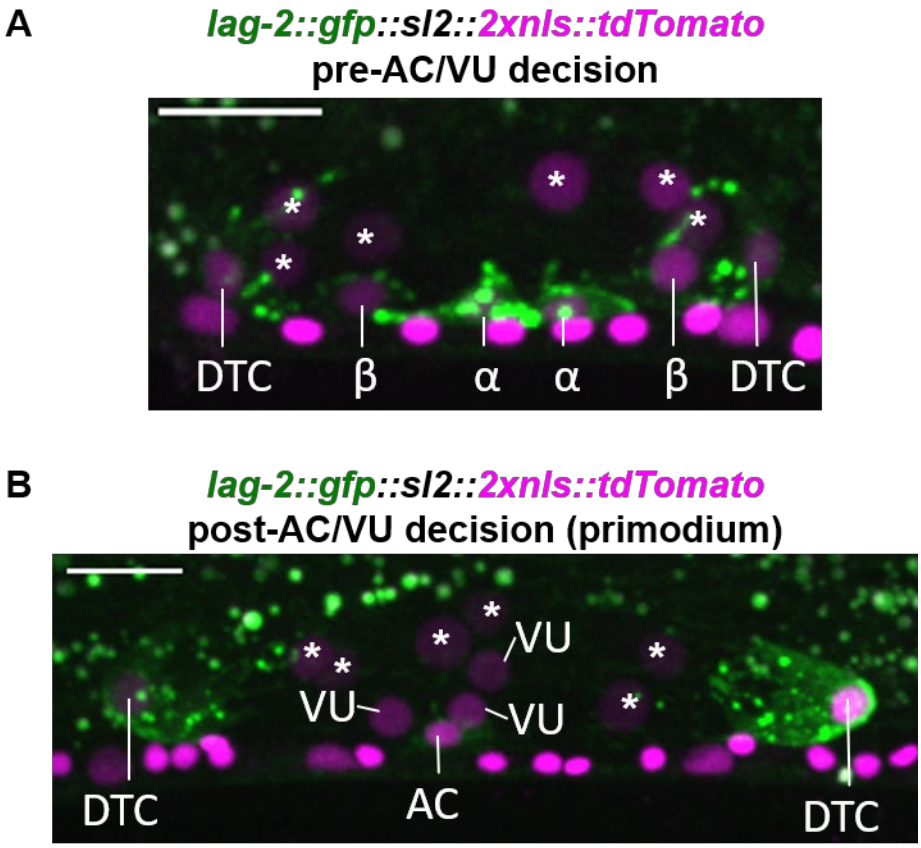

Figure 2. lag-2::gfp::sl2::2xnls::tdTomato endogenous reporter. Photomicrographs are maximum orthogonal projections. (A) Prior to the AC/VU decision, LAG-2::GFP is expressed at the membrane of the α, β, and Distal Tip Cells (DTCs). There is nuclear 2xNLS::tdTomato expression the cells with LAG-2::GFP expression, but there is also tdTomato expression in all other somatic gonad cells (asterisks). (B) At the somatic gonad primordium stage, LAG-2::GFP is expressed in the AC and the DTCs, but not the VUs. Fluorescence from 2xNLS::tdTomato is also present in all of the somatic gonad cells (asterisks). (A-B) Scale bars are 10 microns.